Synthesis and Characterisation of Diblock and Statistical Copolymers Prepared by RAFT Polymerisation in Non-polar Media

Isabella Rose Dorsman

Department of Chemistry

The University of Sheffield

Submitted to the University of Sheffield in fulfilment of the requirements for the award of Doctor of Philosophy

March 2022

Declaration

The work described in this thesis was undertaken at the University of Sheffield under the supervision of Professor Steven P. Armes between October 2017 and March 2022 and has not been submitted, either wholly or in part, for this or any other degree. All the work is the original work of the author, except where acknowledged.

Signature: _____

Isabella Rose Dorsman

March 2022

Acknowledgements

I feel lucky to have received the support of many people throughout the ups and downs of getting to the submission of this Thesis.

I would like to thank my supervisor, Professor Steve Armes, for his scientific ideas, expertise and proof-reading. I would also like to say a special thanks to Dr. Matt Derry for his invaluable guidance, patience and support given at the start of my PhD.

I would like to acknowledge all of the Armes and Spain group members, past and present, who I have got to know during my time in Sheffield. Thank you for welcoming me into the office, answering any scientific and lab-based questions, providing SEM and SAXS analysis and providing great company during conferences, the ski trip and many visits to Interval for PLPs!

I would like to thank my fellow CDT members, from my cohort and the others, for all the support and fun shared experiences over these four years. I would also like to thank Scott Bader Ltd. for sponsoring my PhD. Thank you to Steven, Clive and Vicki for your advice and feedback during our project meetings and for your support during my placement (even if it was during a Pandemic!).

A special thanks to my housemates, Anna, Fran, Gina, Heather and Lily, for first welcoming me to Sheffield and providing moral support and encouragement through the shared challenges of undertaking PhD research.

I would like to thank my family (Mum, Dad, Raphie, Ellie and Mikey) for all their love and support; the past few years have helped me to appreciate the importance of family. Mum and Dad, I dedicate this thesis to you both.

Finally, I would like to say a massive thank you to Charlie. Thank you for your unwavering support, love and encouragement over the past six years. Thank you for helping me to believe that I could do it! I look forward to our next adventures together.

Conferences and Publications

Macro Group Young Researchers Meeting, Dublin, July 2018, **Poster Presentation**

Macro Group Young Researchers Meeting, Kent, July 2019, **Poster Presentation**

The 258th National Meeting & Exposition of the American Chemical Society (ACS), San Diego, August 2019, **Conference Talk**

I. R. Dorsman, M. J. Derry, V. J. Cunningham, S. L. Brown, C. N. Williams and S. P. Armes, Tuning the vesicle-to-worm transition for thermoresponsive block copolymer vesicles prepared *via* polymerisation-induced self-assembly, *Polymer Chemistry*, 2021, **12**, 1224-1235

Abstract

This Thesis focuses on the synthesis and characterisation of methacrylic diblock and statistical copolymers prepared by reversible addition-fragmentation chain transfer (RAFT) polymerisation in non-polar media. First, the thermoresponsive behaviour of poly(stearyl methacrylate)-poly(benzyl methacrylate) [PSMA-PBzMA] diblock copolymer vesicles prepared in mineral oil *via* polymerisation-induced self-assembly (PISA) has been revisited. Such vesicles undergo a vesicle-to-worm transition on heating, which provides an interesting new oil-thickening mechanism (see M. J. Derry, *et al.*, *Angew. Chem.*, 2017, **56**, 1746–1750). In this Thesis, an unexpected reduction in dispersion viscosity occurs when heating vesicles of approximately the same composition above a certain critical temperature. Transmission electron microscopy (TEM) studies indicate rich thermoresponsive behaviour, with vesicles present at 20 °C, worms at 130 °C and spheres at 180 °C, indicating that an unsuspected worm-to-sphere transition occurs after the initial vesicle-to-worm transition. Moreover, statistical copolymerisation of *n*-butyl methacrylate (BuMA) with BzMA when generating the membrane-forming block has been used to tune the critical onset temperature required for the vesicle-to-worm transition. Oscillatory rheology studies confirmed that targeting membrane-forming blocks containing up to 50 mol% BuMA lowered the critical onset temperature required to induce the vesicle-to-worm transition to 109 °C, compared to 167 °C for the reference PSMA-PBzMA vesicles. Small-angle X-ray scattering experiments confirm a vesicle-to-worm transition, with the vesicles initially present at 20 °C being converted into worms when heated above 130 °C. These thermal transitions proved to be irreversible on cooling on normal experimental timescales (hours).

Behenyl methacrylate (BeMA) was synthesised and used to prepare poly(lauryl methacrylate)-poly(behenyl methacrylate) [PLMA-PBeMA] diblock copolymers by thermally-initiated RAFT solution polymerisation at 30% w/w solids in mineral oil at 90 °C. Alternatively, photoiniferter RAFT polymerisation of BeMA was conducted using blue light irradiation at either 32 or 15 °C. Both synthetic protocols achieved high monomer conversions (up to 99%), as determined by ^{1}H NMR spectroscopy, and GPC studies indicated that comparable M_n and $Đ$ values were obtained. Oscillatory rheology studies showed that these diblock copolymers exhibited reversible thermoresponsive behaviour: relatively transparent free-standing gels were formed at or below 20 °C, whereas free-flowing fluids were obtained at higher temperatures. This behaviour is consistent with the crystallisation and melting temperatures (T_c and T_m, respectively) of PLMA-PBeMA, as determined by differential scanning calorimetry (DSC) studies. In principle, such behaviour is consistent with the formation of PBeMA-core cylinders or rods, typically achieved by crystallisation-driven self-assembly (CDSA). However, TEM, dynamic light scattering (DLS) and shear-induced polarised-light imaging (SIPLI) studies did not provide any evidence for the presence of such highly anisotropic nanoparticles. Instead, only ill-defined colloidal aggregates were observed.

Finally, two series of PLMA-PBeMA diblock and P(LMA-*stat*-BeMA) statistical copolymers have been evaluated as additives for the crystal habit modification of a model wax comprising 5.0% w/w *n*-octacosane in *n*-dodecane. DSC studies confirmed that the statistical copolymers exhibited significantly lower T_c and T_m values than the corresponding diblock copolymers of almost identical overall composition. Temperature-dependent turbidimetry studies were conducted for the various wax-copolymer mixtures to determine T_{cool}, the temperature at which zero transmittance was first recorded owing to wax crystallisation. At a constant molar copolymer concentration of 0.26 mM, each of the eight copolymers produced a modest reduction in T_{cool} of approximately 3-5 °C. Scanning electron microscopy (SEM) studies confirmed that the presence of such copolymers led to a reduction in the overall size and/or a higher crystal aspect ratio. Diblock and statistical copolymers were essentially equivalent in their performance as potential wax crystal modifiers. However, the statistical copolymers were easier to prepare and did not suffer from any homopolymer contamination. Moreover, optical microscopy and SEM studies revealed that needle-like crystals were formed instead of platelets when employing BeMA-rich statistical copolymers.

Common Abbreviations

η	Viscosity
η^*	Complex viscosity
λ	Wavelength
AIBN	2,2'-azobisisobutyronitrile
ATRP	Atom transfer radical polymerisation
BeMA	Behenyl methacrylate
BuMA	Butyl methacrylate
BzMA	Benzyl methacrylate
CDB	Cumyl dithiobenzoate
CDSA	Crystallisation-driven self-assembly
CGT	Critical gelation temperature
CMC	Critical micelle concentration
CTA	Chain transfer agent
$Đ$	Dispersity
DLS	Dynamic light scattering
DP	Degree of polymerisation
DSC	Differential scanning calorimetry
FRP	Free-radical polymerisation
G'	Storage modulus
G''	Loss modulus
GPC	Gel permeation chromatography
LAP	Living anionic polymerisation
LMA	Lauryl methacrylate
M_n	Number-average molecular weight
M_w	Weight-average molecular weight
Macro-CTA	Macromolecular chain transfer agent
MWD	Molecular weight distribution

NMP	Nitroxide-mediated polymerisation
NMR	Nuclear magnetic resonance
OM	Optical microscopy
PETTC	4-Cyano-4-(2-phenylethanesulfanylthiocarbonyl)sulfanylpentanoic acid
PDI	Polydispersity index (DLS)
PI-CDSA	Polymerisation-induced crystallisation-driven self-assembly
PISA	Polymerisation-induced self-assembly
PPD	Pour point depressant
PRE	Persistent radical effect
RAFT	Reversible addition-fragmentation chain transfer
RDRP	Reversible deactivation radical polymerisation
RI	Refractive index
SAXS	Small-angle X-ray scattering
SEM	Scanning electron microscopy
SIPLI	Shear-induced polarised light imaging
SMA	Stearyl methacrylate
T21s	*Tert*-butyl peroxy-2-ethylhexanoate
T_c	Crystallisation temperature
T_{cool}	Temperature at which zero transmittance was first recorded owing to wax crystallisation
T_g	Glass transition temperature
T_m	Melting temperature
TEM	Transmission electron microscopy
THF	Tetrahydrofuran
UV	Ultraviolet
WI	Wax inhibitor

Contents

Chapter 1. Introduction

1.1. General Concepts in Polymer Science

The long-chain nature of polymers was first proposed by Staudinger in 1920.[1] The common belief held by the scientific community at the time was that very large covalently bonded molecules could not exist and that polymers must consist of physically-associated aggregates of small molecules.[2,3] Widespread acceptance of Staudinger's idea was not achieved until 1929, following the publication of a series of reactions performed by Carothers.[4] In the present day, it is recognised that a polymer is a long-chain molecule composed of many repeat units, synthesised from monomers. A monomer must have two or more bonding sites, through which each can be linked to other monomers to form the polymer chain.[2]

Polymers are extremely diverse in structure and versatile in terms of their physicochemical properties. Moreover, they are usually cheaper to manufacture than traditional materials such as metals, ceramics or glass. The majority of global polymer production is made up of commodity polymers, such as polyethylene, polypropylene, poly(ethylene terephthalate), polystyrene, poly(vinyl chloride) and polyurethane. Applications of such polymers are vast and include packaging, construction, electrical insulation and appliances, toys, textiles and medical devices.[3]

More recent advances in polymer synthesis and applications have typically involved speciality polymers, which offer bespoke chemical functionality, specific architectures and desirable properties. Such polymers are used in emerging fields such as renewable energy, electric vehicles, targeted drug delivery and 3D printing. Research has also focused on replacing oil-based polymers with more sustainable options. These include bioderived polymers, where biomass from plants is often used as the renewable raw material, for example polylactides. However, there remains a requirement for

favourable economics and superior material properties than those of conventional polymers before these are widely adopted for commercial applications.[5]

Unlike small molecules, polymers do not possess a single unique molecular weight. Instead, all synthetic polymers exhibit a molecular weight distribution (MWD). In principle, information regarding the whole MWD is desirable but in practice it is convenient to characterise the distribution in terms of molecular weight averages. The number-average molecular weight (M_n) and weight-average molecular weight (M_w) are commonly used to describe polymer molecular weight and MWD. The M_n and M_w are defined in **Equations 1.1** and **1.2,** respectively.

$$M_n = \frac{\sum n_i M_i}{\sum n_i} \quad 1.1$$

$$M_w = \frac{\sum w_i M_i}{\sum w_i} = \frac{\sum n_i {M_i}^2}{\sum n_i M_i} \quad 1.2$$

Where n_i is the number of chains containing i repeat units, and M_i is the molecular weight of these chains. The weight fraction of chains with i repeat units is represented by w_i and is equal to the product of $n_i M_i$.

The M_n gives the arithmetic mean molecular weight of a polymer chain, whereas M_w is more biased to the presence of higher molecular weight species. Consequently, M_w is always greater than M_n for any MWD with a finite width, as illustrated in **Figure 1.1**. The mean degree of polymerisation (DP) of a polymer is the mean number of monomer repeat units per chain. Thus, the DP is equal to the M_n divided by the mass of the monomer repeat unit.

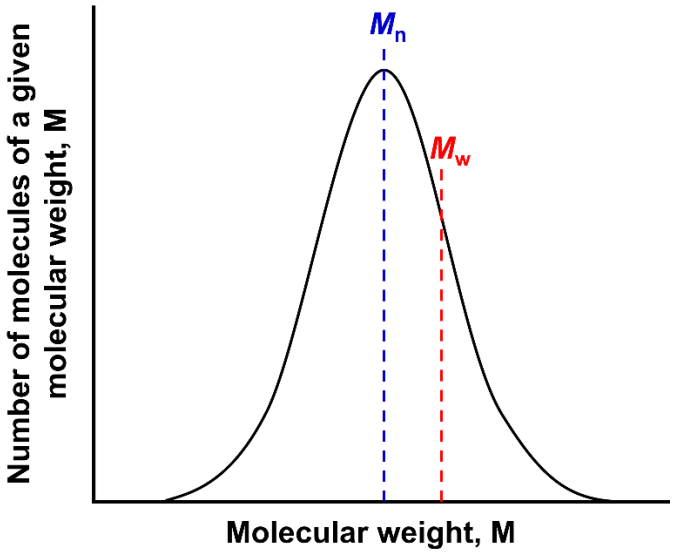

Figure 1.1. Schematic representation of a MWD curve for a typical synthetic polymer indicating the M_n and M_w values on this distribution as defined by Equations 1.1 and 1.2.

The MWD can be represented by polydispersity index (PDI) or, simply, dispersity (*Đ*) as recommended by the International Union of Pure and Applied Chemistry (IUPAC) in 2009, [6] and is defined as:

$$Đ = \frac{M_w}{M_n} \qquad 1.3$$

1.1.1. Polymer Architectures

In its simplest form, a polymer composed of just one type of monomer repeat unit is known as a homopolymer. More complex architectures are available *via* copolymerisation. A copolymer is a polymer derived from two or more types of monomer. There are several important categories of copolymer that differ by their spatial arrangement of the repeat units along the polymer chain. Block, alternating, statistical (for which random copolymers are a specific example) and graft copolymers are the most common categories.[2,3] For simplicity, the schematic representations of the different categories of copolymer shown in **Figure 1.2** are comprised of only two

types of monomer, although certain copolymers can contain three or more species of monomer (e.g. triblock and multiblock copolymers).

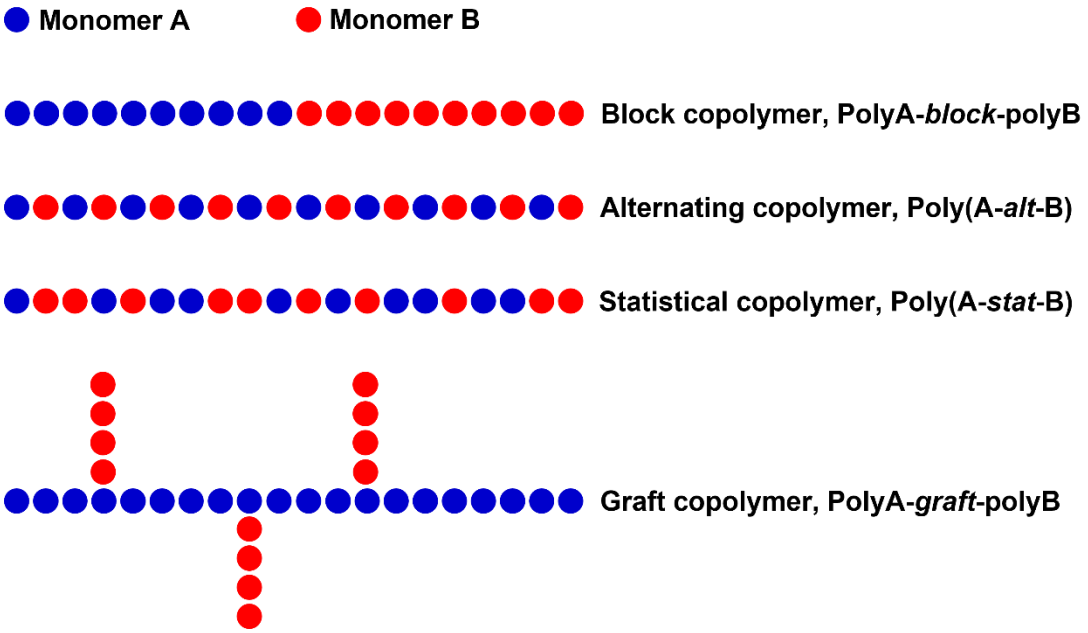

Figure 1.2. Simplified representation of the main types of copolymer architecture and their corresponding nomenclature.

Block copolymers are linear chains in which each monomer repeat unit is present in long sequences (or blocks). Typically, block copolymers are synthesised by polymerisation of monomer A to form a homopolymer, followed by sequential addition of monomer B to prepare the second block. In contrast, alternating copolymers are obtained when equimolar quantities of two monomers are copolymerised together and are distributed in a highly regular alternating fashion in the polymer chain.[2] Statistical copolymers are obtained when irregular propagation occurs which is essentially random, but influenced by the individual comonomer reactivities. Random copolymers are a special type of statistical copolymer in which the distribution of two or more repeat units is truly random. This can be achieved when the probability of adding monomer A to the growing chain-ends is equal to the probability of adding monomer B.[3] Graft copolymers are branched polymers in which

the branches have a different chemical structure to that of the main chain. In the literature, the term *-co-* is used when the type of copolymer is not specified.

Statistical, random and alternating copolymers generally exhibit properties which are intermediate between those of the corresponding homopolymers.[3] A good example of such a property is the glass transition temperature (T_g).[7] In contrast, block and graft copolymers typically exhibit properties that are characteristic of each constituent homopolymer.[3]

In this Thesis, the synthesis and characterisation of AB diblock copolymers, (A-*stat*-B) statistical copolymers and diblock copolymers in which the second block comprises a statistical copolymer is examined.

1.1.2. Crystalline and Amorphous Behaviour of Polymers

The terms *crystalline* and *amorphous* are used to indicate the ordered and unordered regions within a polymer, respectively. Many polymers are *semi-crystalline* and hence simultaneously exhibit characteristics of both crystalline and amorphous solids.[8] Some polymers are completely amorphous (*e.g.* polystyrene) whereas others can possess relatively high crystallinity (*e.g.* linear polyethylene).[3] Fully crystalline polymers are very rare.[8]

Polymers often exhibit two characteristic thermal transitions: the *crystalline melting temperature* (T_m) and the *glass transition temperature* (T_g). The former is the melting temperature of the crystalline domains within a semi-crystalline material, whereas the latter is the temperature at which the polymer switches from a rubbery to a glassy state (often becoming brittle, stiff and rigid).[8] On the molecular level, the T_g corresponds to the onset of significant segmental chain motion.[3,8] Completely amorphous or fully

crystalline polymers only exhibit a T_g or a T_m, respectively. In contrast, typically semi-crystalline polymers exhibit both a T_g and T_m.[3]

A common experimental technique for determining the T_g and T_m of polymers is differential scanning calorimetry (DSC). The change in heat capacity of the polymer is recorded as a function of temperature by measuring the heat flow required to maintain a zero temperature differential between an inert reference material and the sample.[8] An example of a DSC trace for a typical semi-crystalline polymer is displayed in **Figure 1.3**.

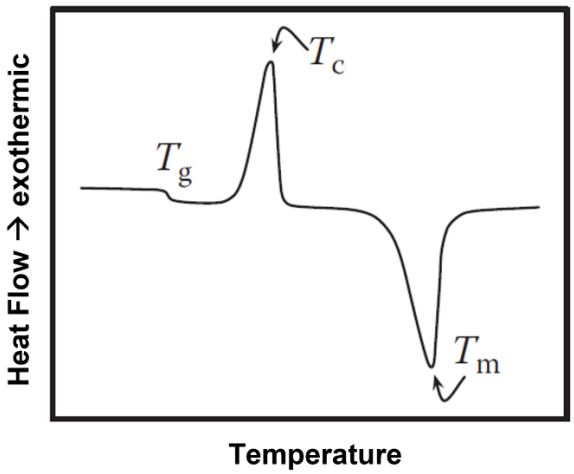

Figure 1.3. Schematic diagram of a typical DSC trace showing the thermal transitions exhibited by a semi-crystalline polymer, where T_g is the glass transition temperature, T_c is the crystallisation temperature and T_m is the melting temperature. Adapted from reference 3.

T_g and T_m are both endothermic events whereas T_c, which is the *crystallisation temperature*, is an exothermic event. The latter transition is the temperature at which the molten amorphous polymer becomes crystalline on cooling.[3]

The T_g and T_m values for a polymer dictate its mechanical properties at any given temperature and hence the temperature range over which the polymer can be used for a given application. For example, polyisoprene, the main component of natural rubber, has a relatively low T_g of -73 °C.[8] This means its chains are highly flexible and mobile

at ambient temperature and hence lightly crosslinked polyisoprene exhibits rubber elasticity.

1.1.3. Polymer Classification

The first attempt to classify polymers was introduced by Carothers in 1929.[4] Two types of polymerisation were identified: condensation or addition. These terms are based on the comparison of the molecular formula of a polymer and that of the monomer(s) from which it is formed. Condensation polymerisations yield polymers with repeat units having fewer atoms than are present in the monomers from which they are formed. This usually arises from chemical reactions which involve the elimination of a small molecule, such as H_2O, HCl or CH_3OH. In contrast, addition polymerisations yield polymers with repeat units having identical molecular formulae to those of the monomers from which they are formed. However, assigning polymers using these classifications is not always straightforward; certain condensation polymerisations have the characteristic features of typical addition polymerisations and vice versa. For example, the synthesis of polyurethanes from diols and diisocyanates is classified as a condensation polymerisation, yet the reaction proceeds without the elimination of any small molecules.[8] An improved classification for polymers, that avoids such confusion and is the preferred classification used today, was introduced by Flory in 1953.[9] Unlike Carothers, Flory chose to distinguish between polymers based on their underlying polymerisation mechanism. Again, there are two types: step or chain polymerisation.

In a step polymerisation, the polymer chains grow stepwise by reactions that can occur between any two molecular species. First, one monomer reacts with another monomer to form dimers. These dimers can then react with another monomer unit or another dimer to produce trimers or tetramers, respectively. Trimers and tetramers can then

react with further monomer, dimers or other trimers and tetramers. Rapid consumption of monomer in the early stages of the reaction is followed by the slow, stepwise build-up of molecular weight throughout the polymerisation. As a result, high molecular weight polymers are not formed until near the end of the polymerisation reaction.

Conversely, chain polymerisations involve addition of individual monomer units to (typically) one end of a growing chain. Chain polymerisations usually require an initiator (or catalyst) to commence the chain growth. Monomer reacts rapidly (one unit at a time) with a reactive end-group on a propagating chain, with regeneration of the active centre after each addition. Chain growth continues until termination occurs, which results in loss of the reactive end-group. Unlike for step polymerisation, high molecular weight polymer chains are obtained even at low monomer conversions. Although cyclic monomers can also be used, chain polymerisation typically involves the polymerisation of vinyl monomers. Chain polymerisation will be exclusively used throughout this Thesis.

1.2. Polymerisation Techniques

1.2.1. Free Radical Polymerisation (FRP)

Free radical polymerisation (FRP) is an example of a chain polymerisation with a radical-based reactive centre. These radicals are generated by an external source, typically by thermal degradation or by photolysis of an initiator. A wide range of functional vinyl monomers can be polymerised in various solvents by FRP. Moreover, radical polymerisations are unaffected by protic impurities, and can be carried out either in the bulk or under solution, dispersion, emulsion or suspension conditions.[10] This versatility has led to FRP being widely used for the industrial manufacture of many vinyl polymers. However, FRP must be conducted under an inert atmosphere as

oxygen acts as a retarder. There are three distinct stages in FRP: initiation, propagation and termination (see **Figure 1.4**).[2,3,8,9,11]

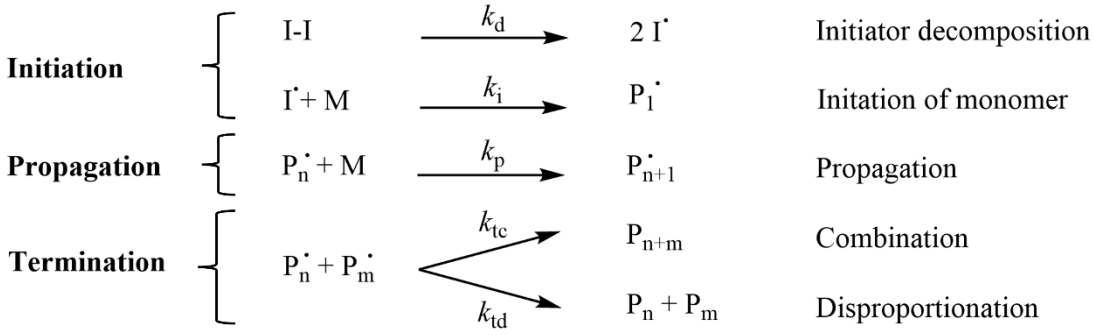

Figure 1.4. Three elementary steps in free radical polymerisation. Adapted from reference 10.

Initiation consists of two steps: (i) generation of free radicals by decomposition of a radical source and (ii) the subsequent initiation of monomer. The first step typically proceeds by homolytic cleavage of an initiator molecule (I-I) to give two primary radicals (I$^{\bullet}$). These radicals then react with a single monomer unit (M) to generate a new active centre (P$_1^{\bullet}$). Homolytic cleavage (or homolysis) in FRP is most commonly induced by thermal decomposition but radicals can also be generated by photolysis. One advantage of photolysis is that the formation of free radicals occurs immediately on irradiation and stops as soon as the light source is removed.[3]

The rate of initiator decomposition is relatively slow compared to the rate of reaction of the primary radicals with monomer ($k_d << k_i$). Therefore, the overall rate of initiation (R_i) is given by **Equation 1.4**, where k_d is the rate constant for decomposition, f is the initiator efficiency and the numerical factor of two denotes that two radicals are generated per initiator molecule. The initiator efficiency is the fractional probability that the primary radical initiates monomer, rather than undergoing side reactions.

$$R_{\mathrm{i}} = \frac{\mathrm{d}[\mathrm{P}_1^{\cdot}]}{\mathrm{dt}} = 2k_{\mathrm{d}}f[\mathrm{I}] \qquad 1.4$$

Following initiation, the radicals react rapidly with many monomer units (propagation rate constant, $k_p \sim 10^2$ - 10^4 M^{-1} s^{-1}).[10,12] As a result, high molecular weight polymer chains are formed in the early stages of the reaction (typically within 5-10% conversion). The rate of propagation (R_p) is assumed to be independent of the polymer chain length and therefore is assumed to be equal for the addition of each monomer unit (see **Equation 1.5**).

$$R_{\mathrm{p}} = -\frac{\mathrm{d}[\mathrm{M}]}{\mathrm{dt}} = k_{\mathrm{p}}[\mathrm{P}_{\mathrm{n}}^{\cdot}][\mathrm{M}] \qquad 1.5$$

Propagation continues until two polymer radicals (denoted as $P_n^{\cdot}$ and $P_m^{\cdot}$) react with each other to form an inactive or 'dead' polymer chain. The two most common termination mechanisms are combination and disproportionation. In the former case, two polymer radicals react together to form one dormant chain with a mean DP equal to the sum of the DPs of the two original polymer radicals. In contrast, disproportionation involves hydrogen abstraction from one polymer radical by a second polymer radical, which results in the formation of two polymer chains bearing a saturated and unsaturated chain-end respectively. The respective rates of these reactions are shown in **Equations 1.6** and **1.7**, where k_{tc} and k_{td} are the rate constants for termination by combination and disproportionation, respectively.

$$R_{\mathrm{tc}} = k_{\mathrm{tc}}[\mathrm{P}_{\mathrm{n}}^{\cdot}][\mathrm{P}_{\mathrm{m}}^{\cdot}] \qquad 1.6$$

$$R_{\mathrm{td}} = k_{\mathrm{td}}[\mathrm{P}_{\mathrm{n}}^{\cdot}][\mathrm{P}_{\mathrm{m}}^{\cdot}] \qquad 1.7$$

The dominant mechanism for termination depends on the monomer type and polymerisation conditions. Typically, polystyrene and polyacrylic radicals terminate by combination, whereas polymethacrylic radicals terminate predominantly by

disproportionation.[3] The overall rate of termination (R_t) is given by **Equation 1.8**, where the rate constant for termination (k_t) is equal to the sum of k_{tc} and k_{td}.

$$R_t = 2k_t[P^{\cdot}]^2 \qquad 1.8$$

The rate of termination is very rapid ($k_t > 10^8$ M^{-1} s^{-1}) compared to that of propagation.[12] Thus, R_t must be much slower than R_p to produce long polymer chains by FRP. Termination is a second-order reaction with respect to radical concentration (see **Equation 1.8**) while propagation is first-order (see **Equation 1.5**). Hence R_t becomes substantially slower than R_p at very low radical concentrations.

Although initiation, propagation and termination are the three most important steps during FRP, various side reactions may also take place. In particular, chain transfer reactions can occur to initiator (I), monomer (M), solvent (S), dormant polymer chains (P_x) or transfer agents (TA) (see **Figure 1.5**).

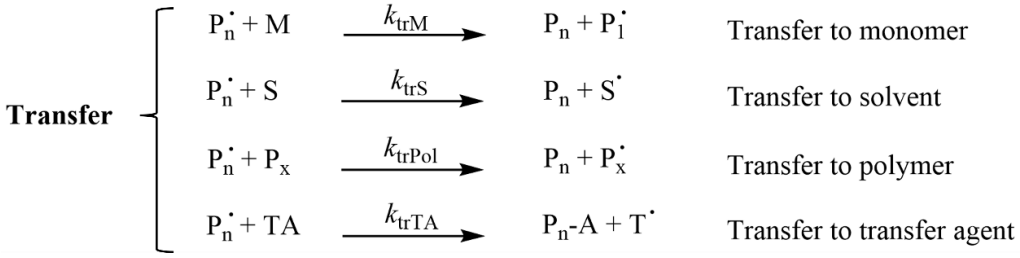

Figure 1.5. Known chain transfer side reactions during free radical polymerisation. Reproduced from reference 10.

Chain transfer does not result in a change in the number of radical species present and therefore does not affect the overall rate of polymerisation (R_{polym}). However, these side reactions can affect the molecular weight and $Đ$ of the final polymer. For example, chain transfer to polymer leads to branching, which leads to an increase in M_w.[13] R_{polym} is only affected by the initiation, propagation and termination steps. To a good first approximation, the overall rate of polymerisation is simply equal to the rate of

propagation. This is because the vast majority of the reacting monomer units are consumed during propagation rather than initiation, particularly for high molecular weight polymers. Quantifying polymer radical concentration is difficult. However, the instantaneous concentration of polymer radicals is small and becomes constant within a very short time scale. Therefore, the steady state approximation can be applied, such that $R_t = R_i$. Combining and rearranging **Equations 1.4** and **1.8** gives an expression for the concentration of polymer radicals [P˙]:

$$[\mathrm{P}^{\cdot}] = \sqrt{\frac{f k_\mathrm{d}[\mathrm{I}]}{k_\mathrm{t}}} \qquad 1.9$$

The expression for [P˙] substituted into **Equation 1.5** gives the overall rate of polymerisation (R_{polym}):

$$R_{\mathrm{polym}} = k_\mathrm{p}[\mathrm{M}]\sqrt{\frac{f k_\mathrm{d}[\mathrm{I}]}{k_\mathrm{t}}} \qquad 1.10$$

The kinetic chain length (D_k) is the mean number of monomer units consumed by each radical and can be calculated using the relative rates of propagation and termination as shown below, given that $R_i = R_t$:

$$D_\mathrm{k} = \frac{R_\mathrm{p}}{R_\mathrm{t}} = \frac{k_\mathrm{p}[\mathrm{M}][\mathrm{P_n}^{\cdot}]}{2k_\mathrm{t}[\mathrm{P_n}^{\cdot}]^2} = \frac{k_\mathrm{p}[\mathrm{M}]}{2\sqrt{f k_\mathrm{d} k_\mathrm{t}[\mathrm{I}]}} \qquad 1.11$$

According to **Equation 1.10**, R_{polym} is proportional to both [M] and $[I]^{1/2}$. Thus, increasing either the monomer or initiator concentration produces a faster rate of polymerisation. However, **Equation 1.11** indicates that D_k (and hence the polymer molecular weight) is dictated by [M] and $[I]^{-1/2}$, with higher molecular weights being achieved when the monomer concentration is increased or the initiator concentration is reduced. For this reason, the production of high molecular weight polymers using FRP can be problematic.

Although FRP is extremely versatile, there are various drawbacks associated with the synthesis of well-defined polymers by this technique. Typically, initiators with relatively long half-lives ($\tau_{1/2}$) are used. Therefore, the rate of initiation is much slower than that for propagation ($R_i << R_p$), which results in the generation of new active centres throughout the polymerisation. Combined with chain termination events and chain transfer side reactions, this invariably leads to the synthesis of polymers with broad MWDs ($Đ$ > 1.50). Moreover, since termination is irreversible in FRP, the relatively short lifetime of the propagating polymer radicals prevents the synthesis of block copolymers and other complex polymer architectures.[12] Fortunately, such shortcomings can be overcome by employing 'living' polymerisation techniques, which offer much greater control over both the MWD and the copolymer architecture (see **Section 1.2.2** below).

1.2.2. Living Anionic Polymerisation (LAP)

Living anionic polymerisation (LAP) is another example of a chain polymerisation. Unlike radical-based FRP, LAP utilises an anionic species for propagation. The first example of LAP was reported in 1956 by Szwarc and co-workers.[14] The anionic polymerisation of styrene was conducted in tetrahydrofuran using a sodium naphthalene complex. A key intrinsic feature of LAP is that the mechanism involves no termination (or transfer) step. Thus, if all protic impurities (*e.g.* water) can be eliminated, then a living polymerisation is obtained.[8] In practice, this means that the monomer(s) and solvent must be rigorously dried prior to the polymerisation, which must be conducted in a thoroughly dry reaction vessel to avoid premature loss of initiator and/or irreversible termination of living polymer chains.

In an ideal anionic polymerisation the rate of initiation is much faster than the rate of propagation ($R_i >> R_p$) so initiation is complete prior to chain growth. Combined with

the absence of any intrinsic termination mechanism, this results in uniform growth of polymer chains. Therefore, a linear evolution of polymer molecular weight (or DP) with monomer conversion is observed for LAP (see **Figure 1.6**). In contrast, high molecular weights are observed at low monomer conversions for FRP.

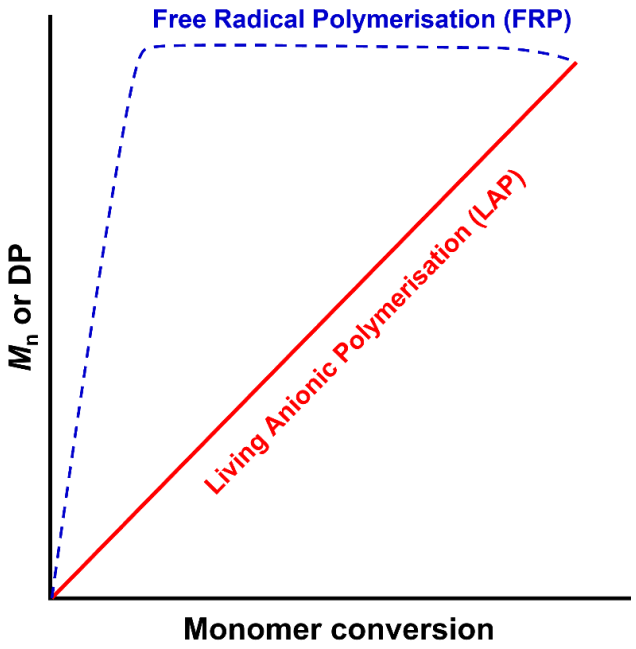

Figure 1.6. Schematic representation of the variation of number-average molecular weight (M_n) or mean degree of polymerisation (DP) with monomer conversion for conventional free radical polymerisation (FRP, blue dashed line) and living anionic polymerisation (LAP, red solid line).

Furthermore, the concentration of propagating species remains constant throughout a living anionic polymerisation. Thus, polymers with very narrow MWDs can be achieved ($Đ < 1.10$).[15]

Moreover, the target DP of a polymer synthesised by LAP can be varied simply by adjusting the monomer/initiator molar ratio (see **Equation 1.12**) where $[M]_0$ is the initial concentration of monomer and $[I]_0$ is the initial concentration of initiator, assuming 100% monomer conversion.[2]

$$\mathrm{DP} = \frac{[\mathrm{M}]_0}{[\mathrm{I}]_0} \qquad 1.12$$

The living character of LAP enables the preparation of well-defined block copolymers *via* sequential monomer addition. However, LAP is limited to monomers that possess electron-withdrawing groups and, owing to the sensitivity of LAP to protic impurities, there are relatively few examples of copolymers being prepared *via* LAP on an industrial scale.[16]

1.2.3. Reversible Deactivation Radical Polymerisation (RDRP)

Reversible deactivation radical polymerisation (RDRP), often known in the literature as controlled radical polymerisation (CRP) or living radical polymerisation (LRP), has become an increasingly popular technique over the past few decades.[17] RDRP combines the control of LAP with the versatility of FRP. It has been used to polymerise a wide range of functional vinyl monomers in a variety of solvents (including protic solvents such as water or lower alcohols).[17–21] Moreover, the polymer chains remain active after all of the monomer has been consumed, therefore block copolymers and complex polymer architectures can be prepared. Importantly, the radical-based chemistry used for RDRP means that this approach is applicable to a much broader range of functional vinyl monomers than LAP.

RDRP techniques afford pseudo-living polymerisations whereby termination is not eliminated, but its probability is significantly suppressed relative to that of propagation. RDRP takes place in the presence of reagents able to reversibly deactivate the propagating polymer radicals and establish a rapid equilibrium between a large proportion of deactivated or ‘dormant’ chains and a small proportion of active growing polymer chains.[12,17,19,20] This serves to reduce the instantaneous concentration of propagating polymer radicals and hence to lower the rate of termination (R_t) relative

to that of propagation (R_p). This is because $R_t \propto [P_n^{\cdot}]^2$, whereas $R_p \propto [P_n^{\cdot}]$. This results in a more controlled polymerisation compared to FRP and produces polymers with relatively narrow MWDs (typically, $Đ \leq 1.2$).[12]

There are two main mechanisms by which a rapid, dynamic equilibrium between active propagating polymer chains and dormant species can be achieved. Firstly, a reversible deactivation/activation mechanism can be employed (**Scheme 1.1**), with examples including nitroxide-mediated polymerisation (NMP)[22] and atom transfer radical-polymerisation (ATRP).[23,24] Alternatively, a reversible chain transfer mechanism can be used (see **Scheme 1.2**), for example in the case of reversible addition-fragmentation chain transfer (RAFT) polymerisation.[25]

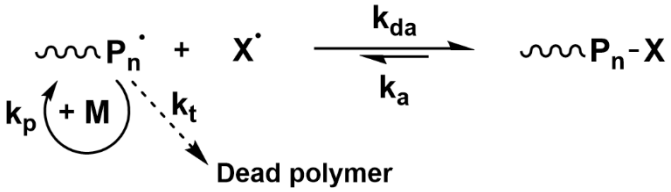

Scheme 1.1. Reversible deactivation/activation of a propagating polymer chain with a capping species, X.[10]

The activation/deactivation process shown in **Scheme 1.1** is based on the persistent radical effect (PRE).[26,27] Typically, the capping species, X, is a stable radical such as a nitroxide (as in NMP) or a halide (as in ATRP). X is also known as a 'persistent' radical. During deactivation, $X^{\cdot}$ reacts with a propagating polymer radical ($P_n^{\cdot}$), with a rate constant of deactivation (k_{da}), to produce a dormant capped polymer species (P_n-X). During activation, the dormant P_n-X is activated thermally (as in NMP) or catalytically (in ATRP), with a rate constant of activation (k_a), to reform the propagating $P_n^{\cdot}$ radicals. Crucially, the equilibrium favours deactivation ($k_{da} > k_a$), meaning that the polymer chains mostly remain in their dormant state, $[P_n^{\cdot}]$ is reduced and termination is suppressed. However, when the polymer chains are in their active

radical form ($P_n^{\cdot}$), then either propagation (k_p) or termination (k_t) can take place. Importantly, $X^{\cdot}$ cannot terminate by reacting with another $X^{\cdot}$ species, which is why it is described as a persistent species. Therefore, termination *via* radical-radical annihilation (by either combination or disproportionation) leads to an irreversible accumulation of $X^{\cdot}$,[12] which shifts the equilibrium in favour of the dormant polymer chains and reduces the instantaneous concentration of the propagating polymer radicals.

An alternative mechanistic pathway to achieve a dynamic equilibrium between active propagating radicals and dormant species involves a reversible transfer process, as shown in **Scheme 1.2**, where k_{exc} is the rate constant for exchange.

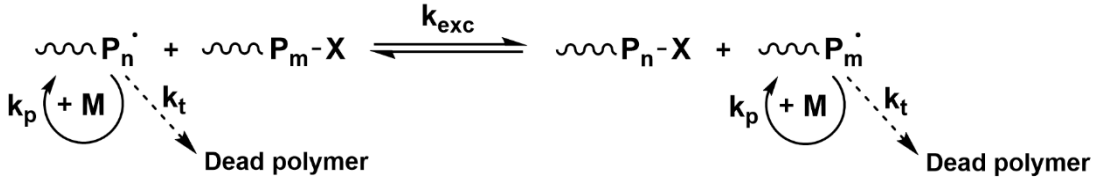

Scheme 1.2. Reversible transfer mechanism of propagating polymer radical chains.[10]

In contrast to the activation/deactivation process, reversible transfer does not involve the persistent radical effect. Instead, it proceeds by a mechanism more similar to that of FRP, where steady-state kinetics are established by relatively slow initiation and fast termination. Control over the polymerisation is facilitated by a chain transfer agent (CTA, or X), which moves from one propagating chain to another. Polymer radicals capped by the CTA (P_n-X) are dormant and unreactive. Importantly, the rate of exchange of the CTA with $P_n^{\cdot}$ must be significantly faster than the rate of propagation ($k_{exc} > k_p$) in order to achieve good control over the target molecular weight and MWD during the polymerisation.[12,28,29] This reversible transfer mechanism is the basis of reversible addition-fragmentation chain transfer (RAFT) polymerisation, which is be discussed in more detail in **Section 1.2.4** below.

1.2.4. Reversible Addition-Fragmentation chain Transfer (RAFT) polymerisation

RAFT polymerisation was first reported in 1998 by Chiefari *et al.*, a CSIRO research team based in Australia.[25] Independently, Zard and co-workers in France reported essentially the same methodology,[30] which was patented by Rhodia and termed MADIX (Macromolecular Design by Interchange of Xanthate) polymerisation.[31,32] Both RAFT polymerisation and MADIX polymerisation are based on the principle of rapid reversible chain transfer, which affords much better control over a radical polymerisation compared to FRP. This is achieved by introducing a thiocarbonythio RAFT chain transfer agent (CTA). As suggested by the name, MADIX polymerisation refers to the use of xanthate-based CTAs.[32] Since the use of dithiobenzoate and trithiocarbonate RAFT CTAs are used exclusively in this Thesis, the polymerisation mechanism for RAFT is discussed in more detail below.

1.2.4.1. The RAFT mechanism

The generally-accepted RAFT polymerisation mechanism involves five key steps, as shown in **Figure 1.7**. In the first step, an external source of radicals is required to initiate the polymerisation. Initiation can then commence as it does in conventional FRP, followed by propagation, to give polymeric radicals ($P_n^{\cdot}$). In the second step, $P_n^{\cdot}$ can propagate either by reaction with further monomer (M) or by reacting reversibly with CTA (1) to produce the radical intermediate (2). This intermediate carbon-centred radical (2) then fragments via β-scission to form a new radical ($R^{\cdot}$) and the stable CTA-capped polymer (3). In the third step, the radical ($R^{\cdot}$) goes on to re-initiate polymerisation to form other propagating species ($P_m^{\cdot}$). The fourth key step in the RAFT mechanism involves the rapid equilibrium between the two active propagating radicals ($P_n^{\cdot}$ and $P_m^{\cdot}$) and their dormant CTA-capped species (3) via the intermediate radical species (4). This is analogous to the general equilibrium for reversible transfer

in **Scheme 1.2**. It is this chain equilibrium step that ensures the 'pseudo-living' character of a RAFT polymerisation by providing equal opportunity for all chains to grow, thus producing polymers with relatively narrow molecular weight distributions. The final step in the RAFT mechanism is termination, where two polymer radicals react together to form an unreactive 'dead' polymer chain. Because termination is suppressed relative to propagation, the CTA groups are retained on the vast majority of polymer chain-ends, therefore RAFT polymerisation enables the synthesis of well-defined block copolymers via sequential monomer addition.[33] Furthermore, the thiocarbonylthio group allows post-polymerisation modifications via a broad range of reactions.[34,35]

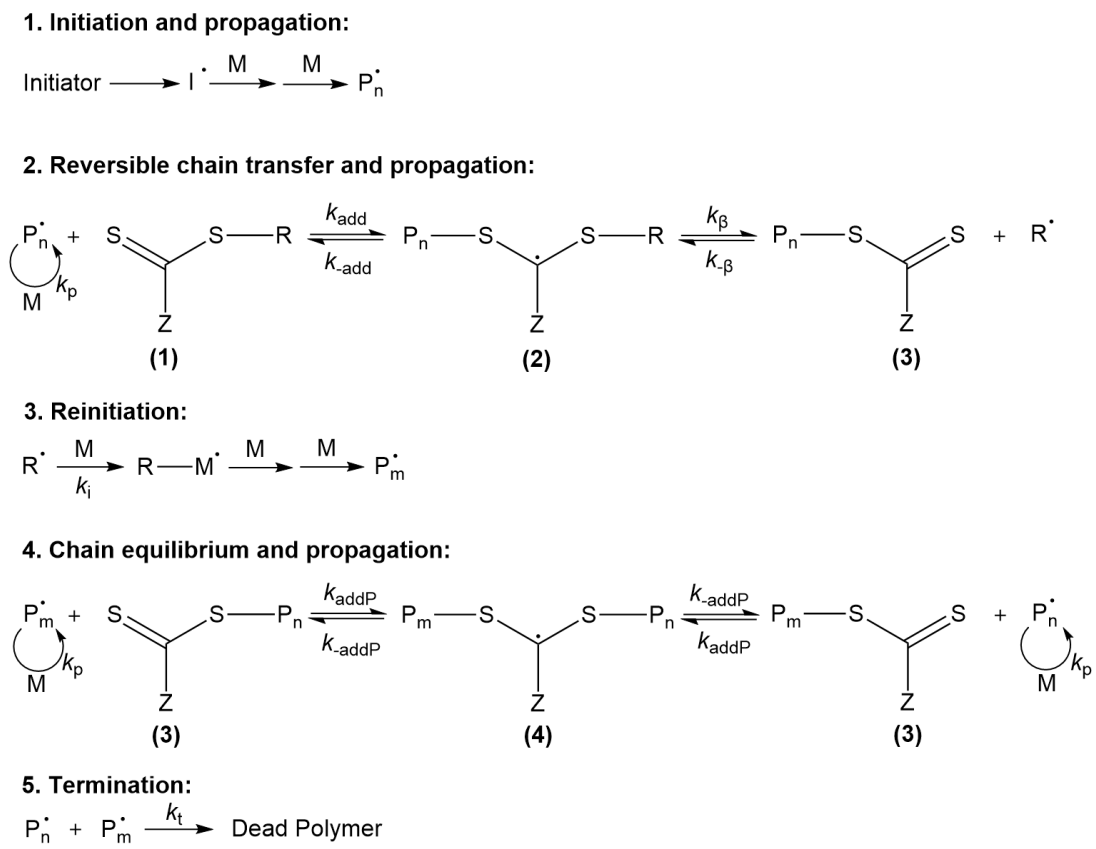

Figure 1.7. The mechanism of RAFT polymerisation.[36]

Consideration of the relative rates involved in the RAFT polymerisation mechanism in **Figure 1.7** is important to understanding the technique. In a well-controlled RAFT

polymerisation, k_{add} and k_{β} are high and $k_{\beta} \geq k_{-add,}$ therefore the dormant species (3) is favoured and R˙ radicals are rapidly produced. If fragmentation is slow, species (2) is more likely to undergo either chain transfer or irreversible radical-radical termination reactions leading to retardation.[29] Fast fragmentation allows the system to reach the main equilibrium (step 4) relatively early in the reaction (*i.e.* at low monomer conversions), which enables equilibrium of the growing chains and results in the formation of polymer chains of low dispersity.[33] It is also important that the leaving group radicals (R˙) efficiently re-initiate the polymerisation in the third step ($k_i > k_p$).[36] Moreover, the chain equilibrium in step 4 must be carefully balanced such that the concentration of dormant species (3) is significantly greater than the concentration of active propagating species, but exchange between active and dormant species is rapid. The intermediate radical (4) should fragment rapidly and give no side reactions (high k_{addP}).[36] In a well-designed RAFT polymerisation, the equilibria described in steps 2 and 4 do not generate or destroy radicals, thus they do not influence rate of polymerisation. Termination events are not eliminated in the RAFT process, but their probability is suppressed relative to propagation.[33]

1.2.4.2. The choice of RAFT Chain Transfer Agent (CTA)

Selection of an appropriate CTA is crucial for achieving a high level of control in a RAFT polymerisation.[37] The generic chemical structure of a RAFT CTA, with its key features highlighted, is illustrated in **Figure 1.8**. In addition to the reactive C=S double bond, the choice of Z- and R-group is important for a well-controlled RAFT polymerisation. The Z-group activates the C=S bond towards radical addition and stabilises intermediate radical species (2) and (4) formed during the polymerisation. The R-group is a good radical leaving group, which enables the formation of stable

CTA-capped polymer chains (3). The R˙ radical is also capable of reinitiating polymerisation.[38]

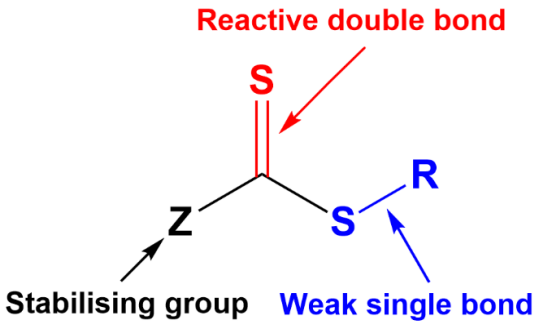

Figure 1.8. Generic chemical structure of a RAFT CTA indicating its key components.

RAFT polymerisation is applicable to an extensive range of functional monomers. Careful selection of the Z- and R-group depends on the type of monomer to be polymerised (see **Figure 1.9**). Most vinyl monomers can be divided into two categories based on their reactivity: (i) 'more activated' monomers (MAMs) and (ii) 'less activated' monomers (LAMs).

MAMs have their vinyl group conjugated to a double bond (e.g., butadiene, isoprene), an aromatic ring (e.g., styrene, vinylpyridine), a carbonyl group (e.g., (meth)acrylates and (meth)acrylamides, maleic anhydride, maleimide), or a nitrile (e.g., acrylonitrile).[21] As a result of this electronic stabilisation (and often steric factors) MAMs produce relatively more stabilised radicals, and therefore require a Z-group to help with the stabilisation of the intermediate radical to favour radical addition on the C=S. Thus, RAFT CTAs with higher transfer coefficients, such as dithiobenzoates (Z = Ph) or trithiocarbonates (Z = *S*-alkyl), are typically selected to control the polymerisation of MAMs.[21]

In contrast, LAMs have a double bond adjacent to oxygen, nitrogen, halogen, sulfur lone pairs, or saturated carbons (e.g., vinyl acetate, *N*-vinyl pyrrolidone, vinyl

chloride, 1-alkenes). Owing to the lack of any radical-stabilising functional group, LAMs produce highly reactive radicals that are relatively poor leaving groups. Therefore, they require a CTA with a Z-group that promotes less stable intermediate radicals (lower transfer coefficients), such as in xanthates (Z = *O*-alkyl) or dithiocarbamates (Z = *N*-alkyl), to favour fragmentation of the propagating radical. If a CTA with a high transfer coefficient, such as a dithiobenzoate, is mistakenly selected for polymerisation of a LAM, the more stable intermediate would act as a radical sink and lead to an uncontrolled polymerisation.[21]

In general, R-groups stabilised by resonance (CN, Ph, and esters) are more active, and thus suitable for the polymerisation of MAMs, than unstabilised R-groups (simple alkyls). Moreover, tertiary alkyl groups are more active than secondary and primary alkyls (see **Figure 1.9**).

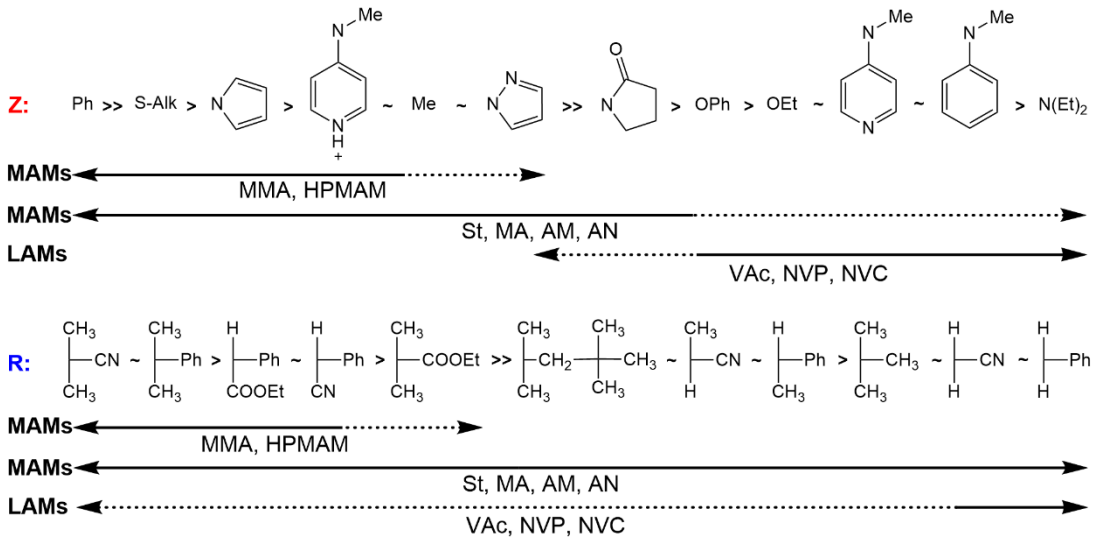

Figure 1.9. Guidelines for the selection of the Z- and R-group of RAFT CTAs (Z-C(=S)S-R) for the polymerisation of various monomers. For Z groups, addition rates decrease and fragmentation rates increase from left to right. For R groups, both transfer coefficients and fragmentation rates decrease from left to right. Solid lines indicate that good control can be achieved, whereas dashed lines indicate that only partial control (e.g. broad MWD or substantial retardation) can be achieved. Abbreviations: MMA = methyl methacrylate, HPMAM = *N*-(2-hydroxypropyl) methacrylamide, St = styrene, MA = methyl acrylate, AM = acrylamide, AN = acrylonitrile, VAc = vinyl acetate, NVP =*N*-vinylpyrrolidone, and NVC = *N*-vinylcarbazole.[21,37]

The RAFT CTAs used for the experimental work performed in this Thesis were 4-cyano-4-(2-phenylethane sulfanylthiocarbonyl)sulfanylpentanoic acid (PETTC) and cumyl dithiobenzoate (CDB), see **Figure 1.10**. Such CTAs are well-documented to be suitable for the polymerisation of methacrylic monomers.[39–43]

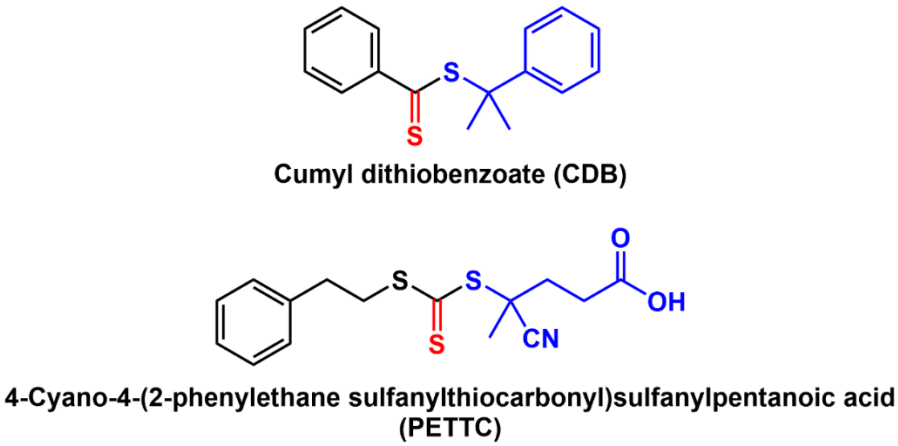

Figure 1.10. The chemical structures of the two RAFT CTAs used in this Thesis.

Although dithiobenzoates have the highest transfer coefficients, trithiocarbonates can offer several advantages. For example, the latter CTAs suffer much less retardation, are more stable with respect to hydrolytic degradation and, typically, can be more readily synthesised.[28] PETTC was synthesised in-house by Andrew Leigh and Dr. Shannon North. CDB was selected as a commercially available dithiobenzoate-based CTA. Previous unpublished work in the Armes group had established that this particular dithiobenzoate was much preferred over PETTC for achieving a well-defined vesicle morphology in the case of poly(stearyl methacrylate)-poly(benzyl methacrylate) [PSMA-PBzMA] diblock copolymer nanoparticles.

It is well-known that RAFT end-groups are gradually lost under monomer starved conditions (*i.e.* at high monomer conversions) as termination becomes more prevalent.[44] For the synthesis of the first block of a diblock copolymer (macro-CTA), polymerisations are typically taken to monomer conversions of 70-80%. In principle,

this should help to avoid such conditions and maintain RAFT end-groups required for subsequent chain extension by monomer to form a second polymer block. In practice, there is published work to suggest this is not essential.[21]

In contrast, the quantitative removal of RAFT end-groups is often desired from diblock copolymers for potential applications.[21] This is because RAFT CTAs are coloured, malodorous and potentially toxic. RAFT end-groups can be readily cleaved *via* thermolysis,[45,46] photolysis,[47,48] or addition of a selective reagent[49–51] to cleave the organosulfur group from soluble polymer chains.

1.2.4.3. The choice of initiator

Although careful selection of the CTA is crucial for a RAFT polymerisation, typically, optimisation of other parameters such as temperature, solvent, initiator choice and [CTA]/[initiator] molar ratio is also required to achieve narrow MWDs and high monomer conversions.

Well-controlled RAFT polymerisations typically require relatively low initiator concentrations (*i.e.* a relatively high [CTA]/[initiator] molar ratio of 5-10).[36] From a practical perspective, the effect of the initiator concentration on the target DP of the polymer chains in a RAFT polymerisation is negligible. Therefore, the target DP can be controlled by varying the relative [M]/[CTA] molar ratio (see **Equation 1.13**), where c is the fractional monomer conversion, $[M]_0$ and $[CTA]_0$ are the initial concentrations of monomer and CTA, respectively.[8]

$$\mathrm{DP} = \frac{c[\mathrm{M}]_0}{[\mathrm{CTA}]_0} \qquad 1.13$$

As already mentioned, an external source of radicals is required for initiation in a RAFT polymerisation. This is because there is no net change in radical concentration during the chain transfer process. Radicals can be generated by using heat, electromagnetic radiation (e.g., light) or redox chemistry.[52–54] Often, radicals are produced from the thermal decomposition of diazo or peroxide chemical initiators. Polymerisations are usually conducted at the temperature that approximately corresponds to the 10-hour half-life ($\tau_{1/2}$ = 10 h) of the initiator to ensure a continuous supply of radicals during the reaction. The RAFT polymerisations reported in this Thesis were performed using a well-known diazo compound, 2,2'-azobisisobutyronitrile (AIBN), and a peroxide initiator, Triganox 21s (T21s), see **Figure 1.11**.

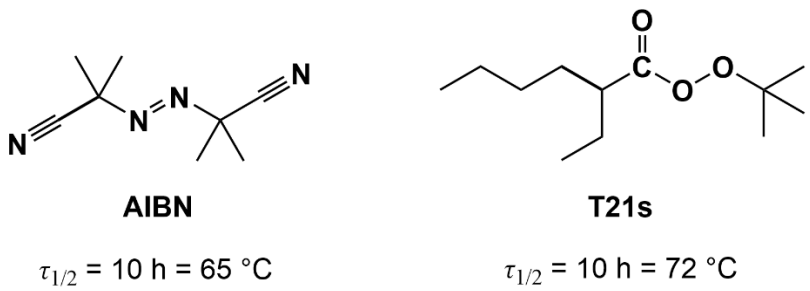

Figure 1.11. Chemical structures and 10-hour half-lives ($\tau_{1/2}$) for the two free radical initiators used in this Thesis.

RAFT polymerisations can also be conducted without the need of a thermally activated azo or peroxide initiator. Instead, radicals can be generated *via* light irradiation using either a photoinitiator (or photocatalyst) or by decomposition of the CTA itself in a photoiniferter mediated RAFT polymerisation (see **Figure 1.12**).[55,56]

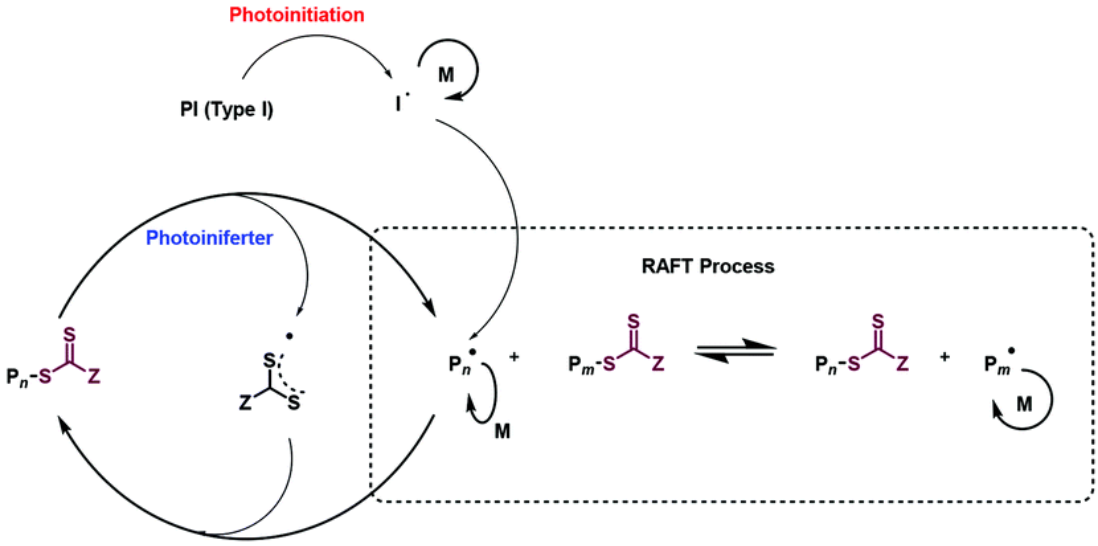

Figure 1.12. RAFT polymerisation mechanisms *via* the photoinitiator or photoiniferter pathways.[55]

There have been many reported examples where the addition of exogenous photoinitiators,[57,58] e.g. diphenyl (2,4,6-trimethylbenzoyl) phosphine oxide [TPO],[55,59] or photocatalysts have been utilised for photoactivation in combination with RDRP techniques.[60–63] Advantages of photoinitiated polymerisation include the possibility of spatiotemporal control and the ability to conduct polymerisations under relatively mild conditions (*i.e.* ambient temperature).[56,64] A further advantage of photoiniferter RAFT is that, as the CTA itself is the radical source, no free catalyst has to be removed after the polymerisation. As it is relevant to some of the work reported in this Thesis, photoiniferter RAFT polymerisation will be discussed in more detail below.

The iniferter concept (a molecule that can act as initiator, transfer-agent and termination agent) was first introduced by Otsu in 1982.[65,66] Photoiniferter RAFT polymerisation does not require an external radical source or photo-catalyst. The thiocarbonylthio unit of a CTA can be activated by either visible,[64,67,68] or UV irradiation.[69–72] The activated species can then react in a β-cleavage process, where the C-S bond between R-group and thiocarbonylthio group is cleaved *via* homolytic bond dissociation. This produces an R$^{\cdot}$ radical and a thiocarbonylthio radical. While the

former is able to initiate a polymerisation reaction, the latter is relatively stable, but reactive enough to deactivate growing chains *via* a reversible (de)activation process.[56,73] As deactivated polymer chains can be reactivated by light, the concentration of polymeric radicals remains relatively constant throughout the polymerisation. This confers an advantage for photoiniferter RAFT over a conventional RAFT polymerisation conducted with an exogeneous radical source, because there is a greater probability of the generation of dead chains in the latter case.[56,73] Indeed, the high livingness associated with photoiniferter RAFT was recently demonstrated by Lehnen *et al.* where multiblock copolymers with up to 20 blocks and a high number of repeating units per block (DP = 25-100), whilst maintaining high precision (M_n = 90.3 kg mol^{-1}; $Đ$ = 1.29) were synthesised using a UV light source.[73] However, irreversible degradation of the CTA end-group under prolonged irradiation can be problematic when producing such multiblock copolymers *via* photoiniferter RAFT. The choice of CTA and irradiation time are both essential for limiting this side reaction.[53,56] Typically, dithioesters seem to suffer most from irreversible degradation under UV light, whereas trithiocarbonates are less problematic.[56,74] Moreover, this side reaction can be avoided if the time scale for polymerisation is faster than that of irreversible chain-end degradation.

The photochemistry of thiocarbonyl (C=S) compounds is different from that of carbonyls (C=O) (see **Figure 1.13**). For the former compounds, the first excited state (the n-π* transition) has a relatively low energy, which corresponds to wavelengths within the visible absorption spectrum. In contrast, the same transition occurs within the UV region for carbonyl compounds. Indeed, the intrinsic colour exhibited by thiocarbonyls (*e.g.* $\lambda \approx 510$ nm for red dithiobenzoates or $\lambda \approx 440$ nm for yellow trithiocarbonates) is the direct result of this n-π* transition.[56] In principle, a

thiocarbonyl compound can be excited using either visible light (spin forbidden n-π* transition) or UV-light (spin allowed π-π* transition). Although the former transition is much weaker, it provides more efficient energy transfer for homolytic bond cleavage, which is beneficial for the initiation of photoiniferter RAFT polymerisations.[56,73,75]

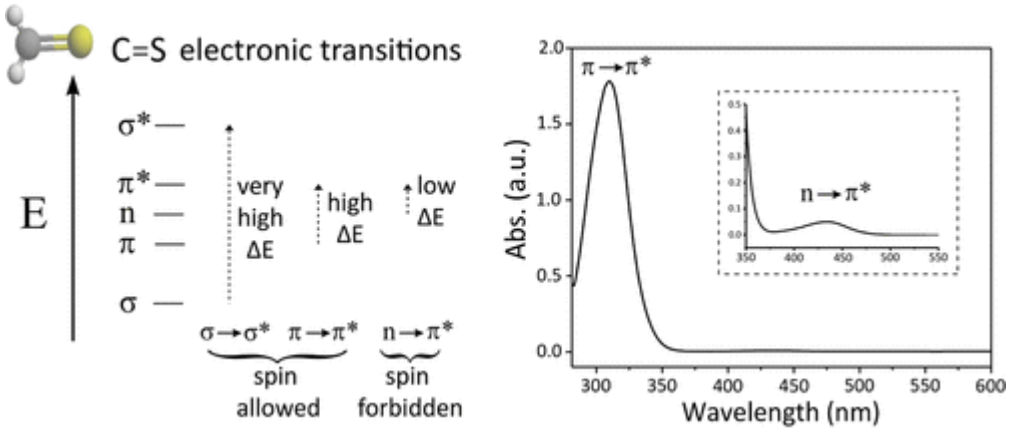

Figure 1.13. Simplified electronic energy level diagram for thiocarbonyl compounds and representative UV-visible absorption spectrum of a trithiocarbonate compound in toluene (0.1 mmol L^{-1}).[67]

The maximum absorption wavelength is influenced by the CTA substituents. This was demonstrated by Cai and co-workers, who recorded UV-visible absorption spectra throughout a RAFT polymerisation conducted using a symmetrical trithiocarbonate.[76] The initial absorption band observed at around 460 nm was blue-shifted to 425 nm soon after initiation, as the tertiary R group of the CTA was replaced by a secondary methacrylic repeat unit. One limitation of using visible light instead of UV light for photoiniferter RAFT is that longer reaction times (hours to days) are typically required.[56] However, Cameron and co-workers demonstrated that visible light-mediated photoiniferter RAFT polymerisations are completed within minutes if a more intense light source is used (*e.g.* 206 W *vs.* <10 W, which is typical for most other reports).[77] In this case, the much faster rate of polymerisation was attributed to both the greater photon flux and a higher polymerisation temperature.

1.2.4.4. Strengths and Weaknesses of RAFT Polymerisation

RAFT polymerisation has been proven to be an effective and versatile synthetic technique; it has been used to prepare a wide range of functional polymers with good control over the target molecular weight, MWD, copolymer architecture and end-group functionality. It is broadly applicable to many monomer classes, including those difficult to polymerise using other RDRP techniques, e.g. methacrylates (which undergo side-reactions during NMP),[78] and acidic monomers without requiring protecting group chemistry (which is an issue for ATRP).[19] However, the RAFT polymerisation of primary or secondary amine-based monomers can be problematic owing to their intrinsic reactivity with thiocarbonylthio compounds. Nonetheless, some success has been reported in this area by carrying out the polymerisation in acidic aqueous solution, whereby protonation of the amine groups prevents deactivation of RAFT end-groups.[79,80]

Moreover, RAFT polymerisation can be conducted in either polar or non-polar solvents over a range of temperatures (usually optimised for the initiator).[81] Desirable end-group functionality can be conferred simply by choosing an appropriate CTA.[21,35] However, CTA-capped polymers exhibit colour, malodour and potential cytotoxicity, which may prevent their use for certain applications. In principle, these problems can be addressed by end-group removal using various chemistries.[34,45,47,82] In practice, the intended application will dictate whether it is actually cost-effective to undertake such post-polymerisation modification. Finally, RAFT polymerisation is an attractive technique for the industrial scale-up of polymer formulations, as it more closely resembles conventional FRP formulations than other RDRP techniques.[83]

1.3. Polymerisation Methods

Vinyl polymerisations can be conducted either in the bulk or using various solvents. The three most relevant physical forms of polymerisation for the work conducted in this Thesis are bulk, solution and dispersion polymerisation. These formulations are discussed in turn below.

1.3.1. Bulk Polymerisation

Bulk polymerisation is conducted in the absence of solvent; the reaction mixture contains only monomer and an initiator (or catalyst). Polymers with minimal contamination are produced by this method. However, the reaction mixture becomes highly viscous at relatively low concentrations, which often makes heat dissipation and stirring difficult.[8]

1.3.2. Solution Polymerisation

In a solution polymerisation, the monomer, initiator and resulting polymer are all soluble in the chosen solvent. The addition of solvent enables more efficient heat dissipation and easier stirring. However, purification of polymer (*i.e.*, by removal of solvent and residual unreacted monomer) can be problematic. Ideally, a solvent is used that is also suitable for the final product, thus eliminating the need for its removal.

1.3.3. Dispersion Polymerisation

In a dispersion polymerisation, an initially *soluble* monomer is polymerised to form an *insoluble* polymer.[84–86] Moreover, all reagents (*i.e.*, monomer(s), initiator, and polymeric stabiliser) are initially soluble in the reaction medium. Upon polymerisation, polymer chains become insoluble (at a critical chain length) which results in particle formation. In the absence of a suitable stabiliser, macroscopic precipitation occurs and the process is known as a precipitation polymerisation.[86]

Traditional dispersion polymerisation formulations utilise conventional FRP. The mechanism for particle formation in a typical FRP-mediated dispersion polymerisation is shown schematically in **Figure 1.14** and is described below.

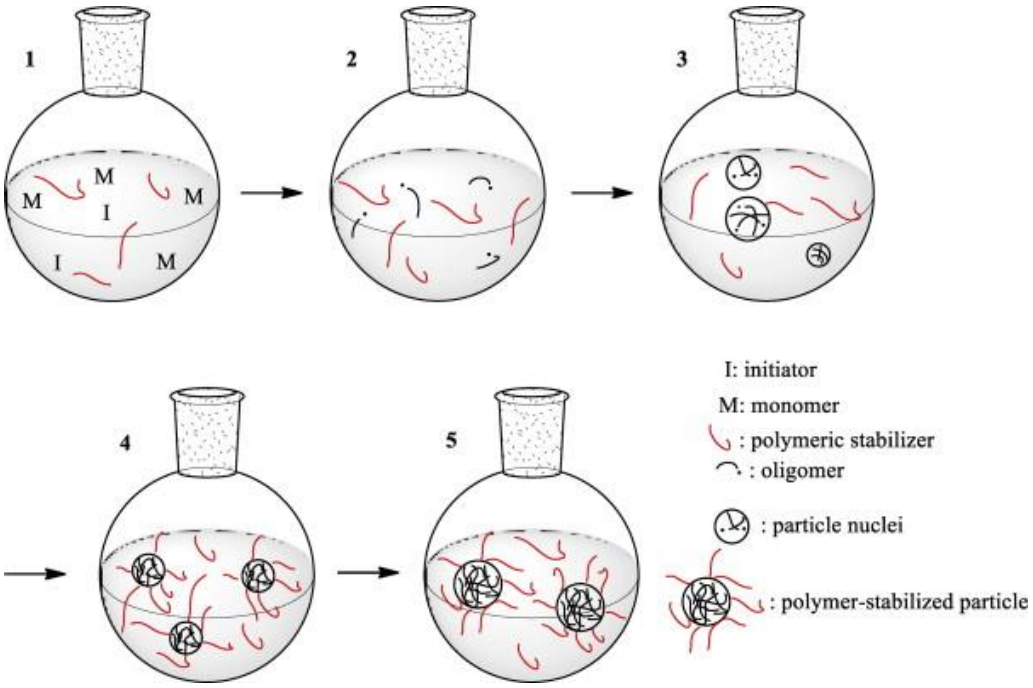

Figure 1.14. Schematic illustration of a FRP-based dispersion polymerisation in either non-polar or polar media showing (1) initial homogeneous phase, (2) initiation and formation of soluble oligomers, (3) precipitation and coagulation into particles, (4) particle stabilisation by polymer adsorption and (5) particle growth.[85]

Firstly, all the reagents are dissolved in the continuous phase (**1**). Next, free radicals are formed on heating the initiator, which then react with monomer in solution to form soluble linear oligomers/polymers (and/or graft copolymers) (**2**). When a certain critical molecular weight is reached, the growing chains are no longer soluble in the continuous phase, hence precipitation occurs and nascent particle nuclei are formed (**3**). The nascent particles aggregate and grow in size. Meanwhile, the soluble polymeric stabiliser chains either physically adsorb or chemically graft onto colloidally unstable particles, thus affording steric stabilisation (**4**). Finally, when all precipitating particles have become sufficiently stable towards aggregation, no new particles are formed and the existing monomer-swollen particles grow until nearly all

the monomer is consumed (**5**).[85] Typically, remarkably uniform spherical particles of 0.1-15 μm diameter can be prepared.[87,88] These colloidally stable particles are often referred to as *latexes*.[85] The final particle size can be tuned by varying parameters such as monomer concentration, polymerisation temperature and concentration of steric stabiliser.[89,90]

The initial development of dispersion polymerisation was carried out in the early 1960s. At Imperial Chemical Industries (ICI), Osmond and Thompson reported the synthesis of latex particles in non-polar media.[91] Since then, dispersion polymerisation of various vinyl monomers has been conducted in aqueous,[92] alcoholic,[93,94] or non-polar media,[85,95] often utilising RDRP techniques including NMP,[96,97]ATRP,[98] or RAFT polymerisation.[99,100]

1.4. Self-Assembly

Self-assembly is important both in Nature, as exemplified by the self-assembly of phospholipids in living cells to form cell membrane bilayers[101] and in everyday life, for example, the self-assembly of small molecule amphiphiles to form micelles in soaps or detergents.

1.4.1. Surfactant self-assembly

One of the most well-understood examples of self-assembly is the micellisation of surfactants. Such amphiphiles reduce the interfacial tension via adsorption at the liquid-liquid, solid-liquid or air-liquid interface. In the case of two immiscible liquids such as oil and water, surfactants can enable the formation of stable emulsions.

Surfactant molecules are composed of two moieties: a hydrophilic head-group and a hydrophobic tail. In aqueous solution, the head-groups become well hydrated, whereas the hydrophobic tails preferentially interact with each other to minimise unfavourable

interactions with the solvent. Self-assembly of surfactant molecules into aggregates (a.k.a. micelles) takes place above a certain concentration, known as the critical micelle concentration (CMC). Below the CMC, surfactants are molecularly dissolved and exist as individual unimers (see **Figure 1.15**). A dynamic equilibrium exists between the micelles and unimers (also referred to as surfactant exchange). The mean residence time for any given surfactant molecule within a micelle varies from ms to μs (depending on the surfactant type, concentration, temperature, pH, salt concentration, etc.). Above the CMC, the number of micelles increase but there remains a background concentration of free surfactant.

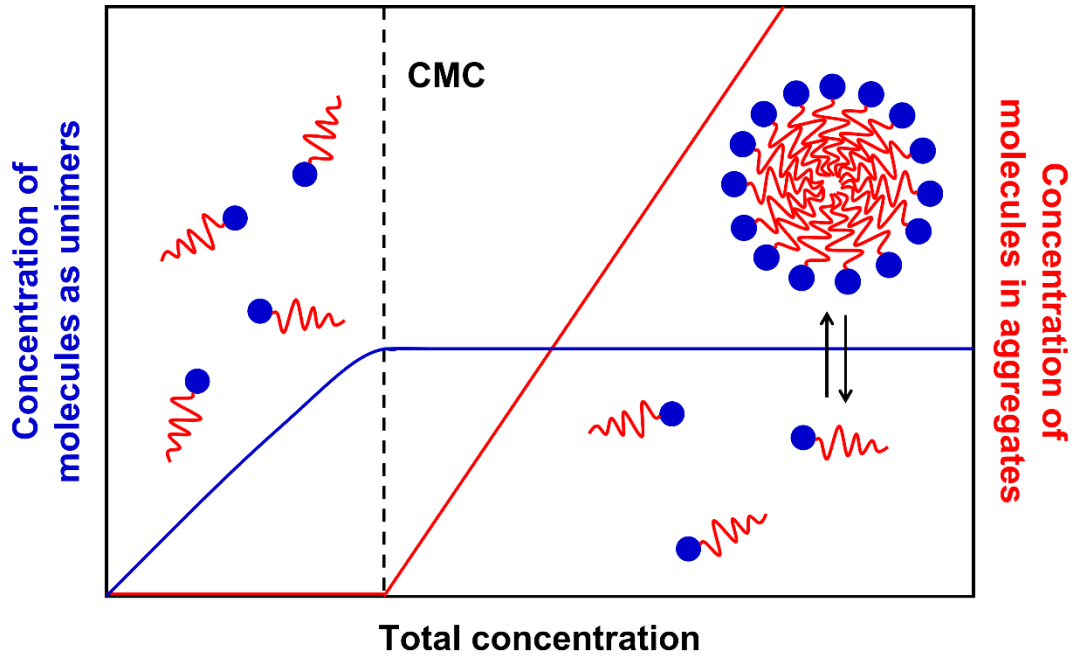

Figure 1.15. Graphical representation of the concentration of surfactant molecules as unimers and the concentration of surfactant molecules in aggregates against the total concentration of the surfactant substrate. The dashed line represents the critical micelle concentration (CMC), above which surfactant molecules self-assemble into aggregates (micelles). A schematic representation of individual surfactant unimers and a micelle is shown, including surfactant exchange between the two.

The driving forces for self-assembly involve both enthalpic and entropic factors, as indicated by the Gibbs equation (see **Equation 1.14**). At room temperature, micelle formation is characterised by a small positive enthalpy change (ΔH_{mix}) and a large positive change in entropy (ΔS_{mix}), therefore self-assembly is energetically favourable and occurs spontaneously ($\Delta G_{mix} < 0$).[102]

$$\Delta G_{\mathrm{mix}} = \Delta H_{\mathrm{mix}} - T\Delta S_{\mathrm{mix}} \qquad 1.14$$

High positive ΔS_{mix} values are surprising: in terms of configurational entropy, aggregation should result in a negative ΔS_{mix}. Moreover, large values of ΔH_{mix} might be expected due to the low solubility of hydrocarbon tails in water resulting in a high enthalpy of solution.[102] To account for the observed behaviour, the interactions of surfactants with water molecules must also be considered.

The enthalpic contribution of surfactant self-assembly comes from the propensity of hydrophobic tails to avoid contact with water molecules, which leads to aggregation and micellisation. The entropic term arises because the tails of surfactant molecules disrupt intermolecular interactions (e.g. hydrogen bonding) between water molecules, which results in a more ordered structure of water molecules locally around the hydrophobic tails. This rearrangement is known as the hydrophobic effect.[103] Such an increase in the overall order of the system is entropically unfavourable. Thus, aggregated structures, such as micelles, are more entropically favoured to limit localised ordering.

Although surfactant self-assembly to form spherical micelles is common in dilute solution, other aggregated structures can also be formed, such as vesicles, bilayers or inverted micelles.[102] The dimensionless packing parameter (P) can be used to describe the preferred surfactant structure (see **Equation 1.15**).[104]

$$P = \frac{V}{a_0 l_c} \qquad 1.15$$

Here P depends on the surface area occupied by the head group (a_0), the volume occupied by the tail group (V) and the effective length of the tail group (l_c) (see **Figure 1.16**).

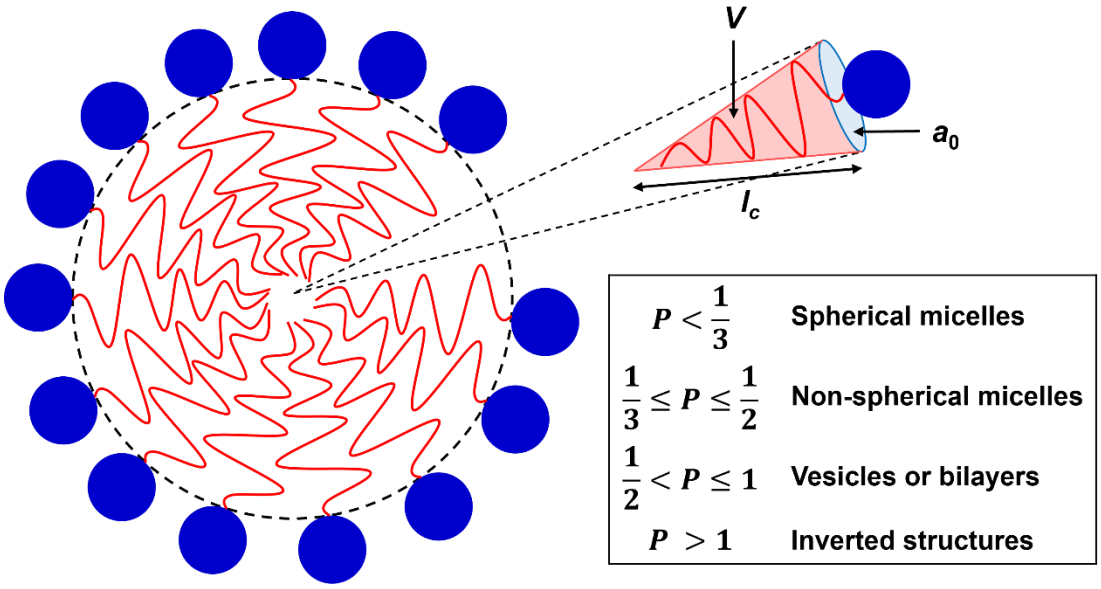

Figure 1.16. Schematic illustration of a spherical micelle with a_0, l_c and V terms labelled for an individual surfactant molecule. Typical values for P for various micelle morphologies are shown.

The packing parameter can be used to rationalise and, in some cases, predict the structure of micelles formed when surfactants self-assemble in aqueous solution.[104] Typical numerical values for P for various morphologies are given in **Figure 1.16**.[104,105]

1.4.2. Block copolymer self-assembly

AB diblock copolymers are high molecular weight analogues of surfactants. In polymer blends containing two or more homopolymers, macrophase separation can occur. In contrast, when two or more chemically distinct polymer chains are covalently linked together, as in the case of a diblock copolymer, microphase separation can result to form nanostructures either in the bulk or in solution.

1.4.2.1. Bulk self-assembly of block copolymers

AB block copolymers comprising immiscible blocks can undergo microphase separation into a variety of nanostructures, including spheres, cylinders, bicontinuous gyroids and lamellae, depending on the precise diblock copolymer composition.[106–108] This spontaneous self-assembly is driven by the free energy cost of contact (incompatibility) between the A and B blocks. This is represented as the Flory-Huggins parameter (χ_{AB}) and varies inversely with temperature. Thus, in principle, the two blocks may become miscible on heating to a sufficiently high temperature. Other factors governing the microphase separation of diblock copolymers are the relative volume fractions of the A and B blocks (f_A and f_B) and the total degree of polymerisation (N).[109]

The degree of microphase separation of diblock copolymers is determined by the segregation product, χN. If χN is sufficiently large, or the temperature of the block copolymer melt is sufficiently low, the incompatibility of the two blocks increases and self-assembly occurs.[107] On the other hand, if χN is relatively low then microphase separation may not occur at all, which is often the case for low molecular weight diblock copolymers.[107]

The self-assembly of diblock copolymers in the bulk has been well studied, both theoretically and experimentally.[109] **Figure 1.17** illustrates the various ordered structures predicted and observed for an AB diblock copolymer as f_A is increased.[109] The initial disordered structure changes to closely packed spheres (CPS) to body-centred cubic spheres (S), through hexagonally packed cylinders (C), and bicontinuous gyroids (G) to lamellae (L) as f_A is increased. Morphological inversion is observed (L-to-G'-to-C'-to-S'-to-CPS'-to-disordered) when the composition is inverted (*i.e.* when $f_A > f_B$).

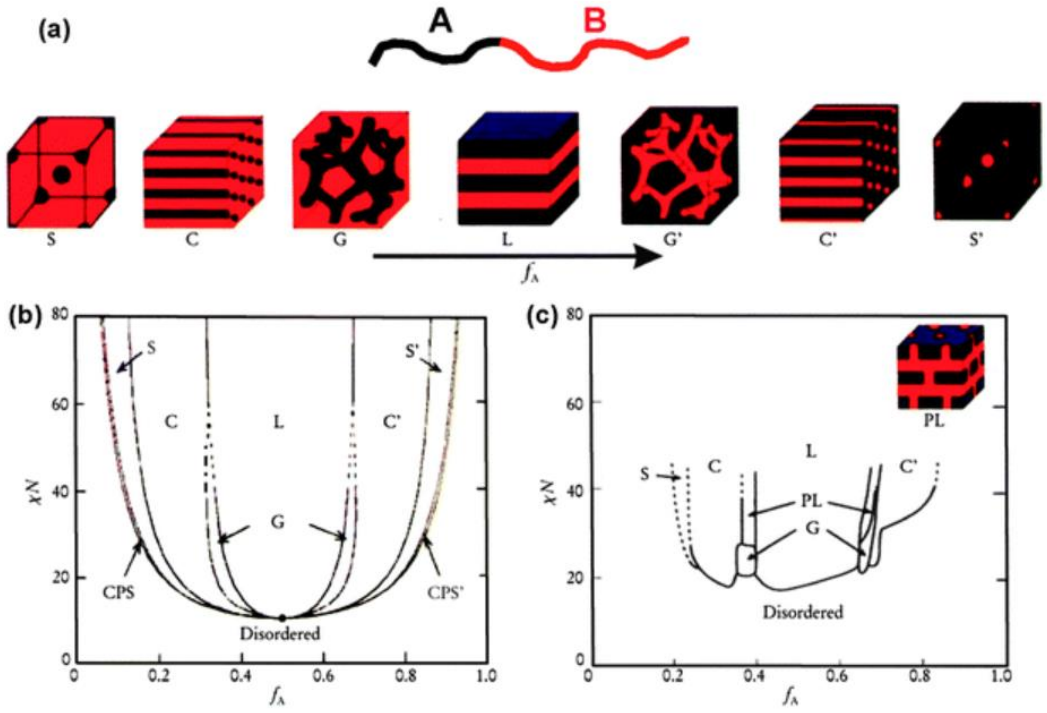

Figure 1.17. (a) AB diblock copolymer morphologies in the bulk where S and S' are body-centred-cubic spheres, C and C' are hexagonally packed cylinders, G and G' are bicontinuous gyroids, and L denotes lamellae. **(b)** Theoretical phase diagram of AB diblock copolymers predicted by self-consistent mean-field theory, depending on the volume fraction of block A (f_A) and the segregation parameter (χN). CPS and CPS' are closely packed spheres. **(c)** Experimental phase diagram of polyisoprene-*block*-polystyrene copolymers, where f_A represents the volume fraction of polyisoprene. PL denotes a perforated lamellae phase.[109]

1.4.2.2. Solution self-assembly of diblock copolymers

Self-assembly of diblock copolymers is more complex in solution than in the bulk: introduction of solvent(s) into the system requires further χ-parameters to represent the additional interactions between the two polymer blocks and the solvent(s).

Various copolymer morphologies are accessible in solution, including spherical micelles, rods, bicontinuous structures, lamellae, vesicles and others.[109] For highly asymmetric amphiphilic diblock copolymers in which the hydrophobic block is much longer than the hydrophilic block, so-called 'crew-cut' aggregates can be formed in aqueous solution.[110–113] In general, the preferred copolymer morphology depends on the nature of the two comonomers, the volume fraction of each block, and the mean DP of each block.

The thermodynamically preferred copolymer morphology is governed by the diblock composition and/or temperature of the system. Often, morphological transitions can be reversed provided that the mobility of polymer chains remains sufficiently high. Morphological transitions are also influenced by kinetics. Given their relatively high molecular weight, chain exchange between block copolymer aggregates and free copolymer chains is comparatively slow compared to the fast exchange between surfactant micelles and free surfactant molecules at thermodynamic equilibrium.[113] Indeed, if the chain mobility of the hydrophobic block is very low, copolymer aggregates can be kinetically frozen or 'trapped' at a specific morphology.[109]

Traditionally, block copolymer self-assembly is achieved by post-polymerisation techniques such as a solvent switch.[112,114] Typically, a diblock copolymer is dissolved in a common solvent, such as DMF, dioxane or THF, which are good solvents for both blocks. Then a selective solvent (e.g. water), which is a non-solvent for hydrophobic

block, is slowly added to the copolymer solution. The resulting aggregates are quenched in an excess of water (to kinetically trap morphologies), before the common solvent is removed by dialysis. Other post-polymerisation techniques include direct hydration (e.g. film rehydration),[115,116] or a pH switch.[117]

1.4.3. Polymerisation-Induced Self-Assembly (PISA)

An attractive alternative to traditional post-polymerisation self-assembly techniques is polymerisation-induced self-assembly (PISA). In a typical PISA synthesis (see **Figure 1.18**), a soluble homopolymer precursor is chain-extended with a second monomer, which forms an insoluble polymer at a critical DP. This drives *in situ* self-assembly to form sterically-stabilised diblock copolymer nanoparticles.[118]

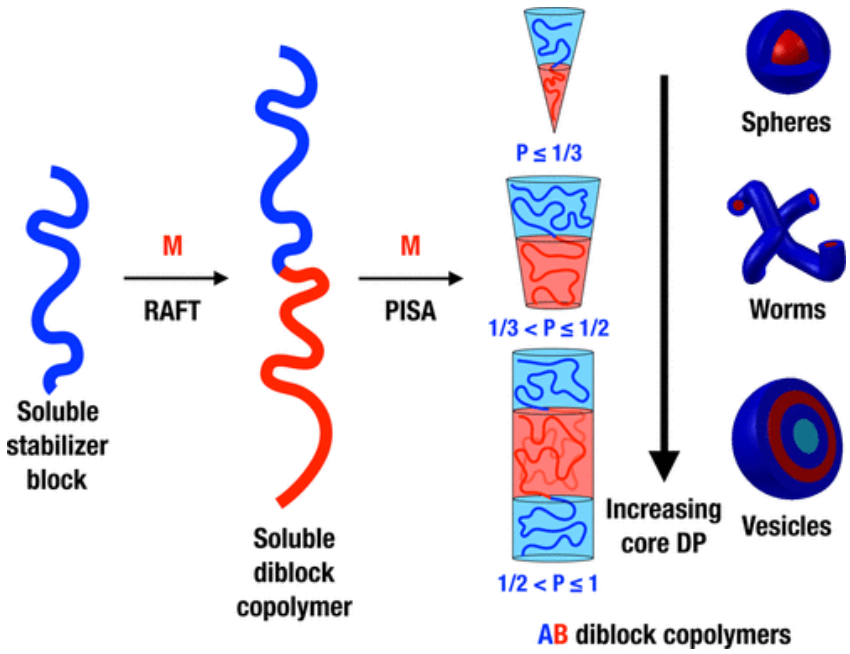

Figure 1.18. Schematic representation of the synthesis of diblock copolymer nanoparticles *via* polymerisation-induced self-assembly (PISA).[118]

The three most common nanoparticle morphologies accessed by PISA are spheres, worms and vesicles.[118,119] The final morphology primarily depends on the relative volume fractions of the two blocks. In principle, increasing the DP of the insoluble structure-directing block (and therefore its effective volume fraction) leads to

increased curvature and higher order morphologies (*e.g.* worms and vesicles).[119] The packing parameter (*P*), as discussed in the context of surfactant self-assembly in **Section 1.4.1** of this Thesis, is a useful concept for rationalising the various morphologies that can be formed by self-assembled diblock copolymers.[120]

In a PISA synthesis, the homopolymer precursor is usually prepared by solution polymerisation. The second block is prepared by either dispersion polymerisation (where the second monomer is initially miscible in the chosen solvent) or emulsion polymerisation (where the second monomer is initially immiscible in the solvent). In principle, PISA syntheses can be conducted *via* either living or pseudo-living polymerisation.[121–125] In practice, the vast majority of the PISA literature is based on RAFT polymerisation (**Section 1.2.4**), which offers exceptional tolerance of monomer functionality and can be conducted directly in many protic solvents, including water and lower alcohols.[119]

PISA offers many advantages over traditional self-assembly methods. PISA has enabled diblock copolymer nanoparticles to be prepared at much higher concentrations (up to 50% w/w solids) than post-polymerisation techniques such as a solvent switch, which are almost invariably conducted in dilute (<1% w/w) solution.[41,126] Moreover, many PISA formulations (especially those performed in aqueous media) exhibit faster polymerisation kinetics, high monomer conversions and lower viscosities than can be achieved *via* solution polymerisation.[118,127,128] Consequently, PISA is a highly attractive method for academic research and is also suitable for the manufacture of diblock copolymer nanoparticles on an industrial scale.

Hydrophilic nanoparticles prepared by RAFT-mediated aqueous PISA have various applications. Spherical nanoparticles can be employed as model emulsifiers for the

production of highly stable oil-in-water Pickering nanoemulsions,[129] or as effective dispersants for crystalline fungicidal microparticles in agrochemical formulations.[130] Soft biocompatible hydrogels formed by diblock copolymer worms can be used as a storage medium for human stem cells,[131] while enzyme-loaded block copolymer vesicles may offer therapeutic applications.[132] There are also several interesting examples of PISA formulations based on RAFT dispersion polymerisation in non-polar media, which will be discussed in more detail in the following Section. In this case, potential applications include tough spherical nanoparticles as boundary lubricants for automotive engine oils,[133] larger spheres as model sterically stabilised particles for analytical centrifugation studies,[134] and worms as rheology modifiers for non-polar oils.[42,135]

1.4.3.1. PISA by RAFT non-polar dispersion polymerisation

The preparation of diblock copolymer nanoparticles by PISA *via* RAFT dispersion polymerisation in non-polar media has been reported by several groups over the past decade. Early work in this area was conducted by Charleux and co-workers, who reported an all-acrylic RAFT non-polar dispersion polymerisation formulation that produced poly(2-ethylhexyl acrylate)-poly(methyl acrylate) [PEHA-PMA] diblock copolymers at 20% w/w in *iso*-dodecane.[136,137] Notably, only spherical nanoparticles were accessed in these studies. Moreover, the dispersion polymerisation of methyl acrylate (MA) with a dithiobenzoate-based PEHA macro-CTA led to strong rate retardation, poor RAFT control ($Đ$ = 6.00 at the highest MA conversion of 85%) and the formation of polydisperse particles (bimodal distribution with PDI = 0.22 by DLS). In contrast, much better RAFT control was achieved for the dispersion polymerisation of MA with a trithiocarbonate-based macro-CTA (100% conversion with a $Đ$ = 1.21

within 4 h) and near-monodisperse nanoparticles were obtained as judged by DLS studies.

An alternative all-acrylic diblock copolymer system was reported by Ratcliffe and co-workers in 2015.[138] In this study, poly(lauryl acrylate)-poly(benzyl acrylate) [PLA-PBzA] diblock copolymer nanoparticles were prepared *via* PISA at concentrations between 5% w/w and 30% w/w solids in *n*-heptane, *n*-dodecane or *iso*-hexadecane. A trithiocarbonate-based PLA precursor was chain-extended with BzA, which resulted in high monomer conversions (>99%) and high blocking efficiencies, as observed by ^{1}H NMR spectroscopy and GPC, respectively. Although the soft, film-forming nature of these low-T_g all-acrylic nanoparticles prevented imaging by conventional TEM studies, selected samples were characterised by vitrification of dilute dispersions in *n*-heptane using cryo-TEM. All three common PISA nanoparticle morphologies (spheres, worms and vesicles) were imaged using this technique (see **Figure 1.19**).

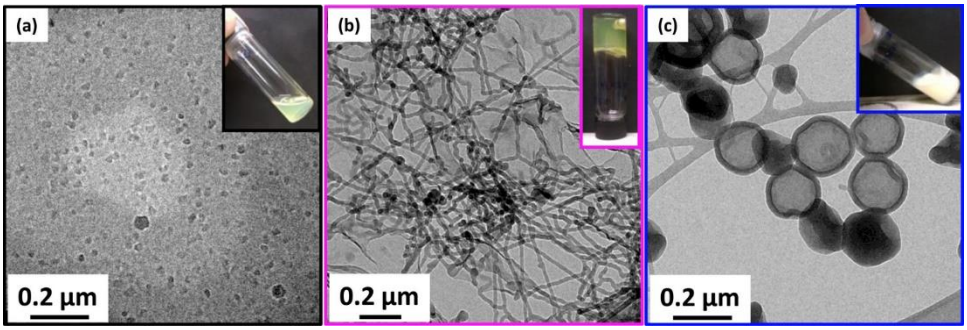

Figure 1.19. Selected cryo-TEM images obtained for diluted dispersions of **(a)** PLA_{14}-$PBzA_{65}$ copolymer prepared at 15% w/w solids in *n*-heptane, **(b)** PLA_{14}-$PBzA_{70}$ copolymer prepared at 20% w/w solids in *n*-heptane, and **(c)** PLA_{14}-$PBzA_{95}$ copolymer prepared at 20% w/w solids in *n*-heptane.[138]

In general, the polymerisation of methacrylic monomers affords better control over the MWD and copolymer morphology compared to their acrylic counterparts, which are more susceptible to chain transfer to polymer.[13] Also, in general, methacrylic

polymers have higher T_g values than poly(acrylates), which enables facile nanoparticle characterisation by conventional TEM imaging.[139] Various literature examples of all-methacrylic diblock copolymer nanoparticles prepared by RAFT dispersion polymerisation in non-polar media are discussed below.

Most PISA syntheses in non-polar media have been conducted in alkanes (*e.g.* *n*-heptane,[133] *n*-dodecane,[140] *n*-tetradecane,[43,141] and *iso*-hexadecane[138]). The preparation of diblock copolymer nanoparticles has also been investigated in more industrially-relevant oils, including synthetic poly(α-olefin),[41] and mineral oil (which is composed of a mixture of alkanes).[41,42,134,135,142–144] The chemical structures of some common oil-soluble methacrylate stabilisers and the corresponding methacrylate monomers used to generate the structure-directing block are illustrated in **Figure 1.20**. Typically, homopolymers comprising lauryl methacrylate ($C_{12}H_{25}$) or stearyl methacrylate ($C_{18}H_{37}$) are employed as the oil-soluble stabiliser block. For a RAFT dispersion polymerisation, the first block must be chain-extended by an oil-soluble monomer, which then forms an oil-insoluble block. These requirements restrict the range of suitable vinyl monomers available. The most commonly reported oil-soluble monomer is benzyl methacrylate (BzMA),[41,42,133–135,140,142,143] but other suitable methacrylate monomers include 3-phenylpropyl methacrylate (PPMA),[141,145] 2,2,2-trifluoroethyl methacrylate (TFEMA),[43] 2-hydroxypropyl methacrylate (HPMA),[144] methyl methacrylate (MMA)[146] and glycidyl methacrylate (GlyMA).[147]

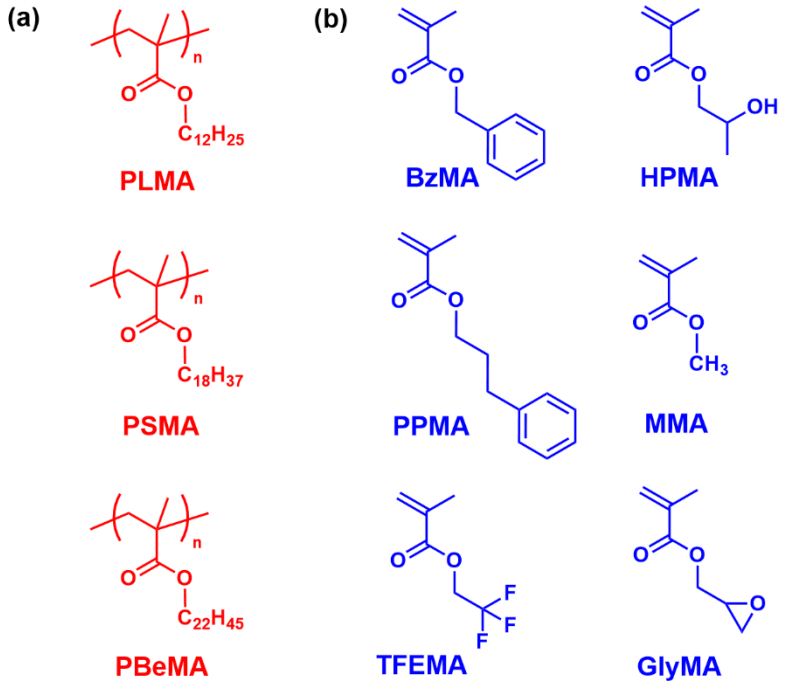

Figure 1.20. (a) Common homopolymers used as oil-soluble stabilising blocks in PISA syntheses *via* RAFT dispersion polymerisation. **(b)** Some examples of oil-miscible methacrylate monomers polymerised *via* RAFT dispersion polymerisation in PISA syntheses to form structure-directing blocks.

An early example of PISA in non-polar media involved the RAFT dispersion polymerisation of benzyl methacrylate, as reported in 2013 by Fielding *et al.*[133] Well-defined poly(lauryl methacrylate)-poly(benzyl methacrylate) [PLMA-PBzMA] diblock copolymer spheres, worms and vesicles were prepared in turn at 20% w/w in *n*-heptane at 90 °C by adjusting the reaction conditions (e.g. the DP of the PLMA block, the target DP for the PBzMA block and the copolymer concentration) (see **Figure 1.21**). High BzMA monomer conversions (>97%) were determined by ^{1}H NMR spectroscopy. GPC analysis confirmed reasonably high blocking efficiencies and relatively low diblock copolymer dispersities ($Đ$ < 1.30) in most cases. This was the first report of higher order morphologies (*e.g.* worms and vesicles) being obtained in a non-polar solvent. A relatively short PLMA macro-CTA (DP = 17) was required to access pure worm-like and vesicular morphologies (see **Figure 1.21c**). A phase diagram was constructed for the $PLMA_{17}$-$PBzMA_x$ diblock copolymer nanoparticles,

where the PBzMA target DP and total solids content were systematically varied and *post mortem* copolymer morphologies were determined by TEM (see **Figure 1.21d**). In this case, the pure worm morphology occupies relatively narrow phase space, which is typical for PISA syntheses.[118] On the other hand, longer PLMA macro-CTAs (DP ≥ 37) invariably resulted in the formation of kinetically-trapped spheres (see **Figure 1.21b**). For this latter series of nanoparticles, the mean diameter increased from 41 to 139 nm as the target DP for the PBzMA core-forming block was increased from 100 to 900.

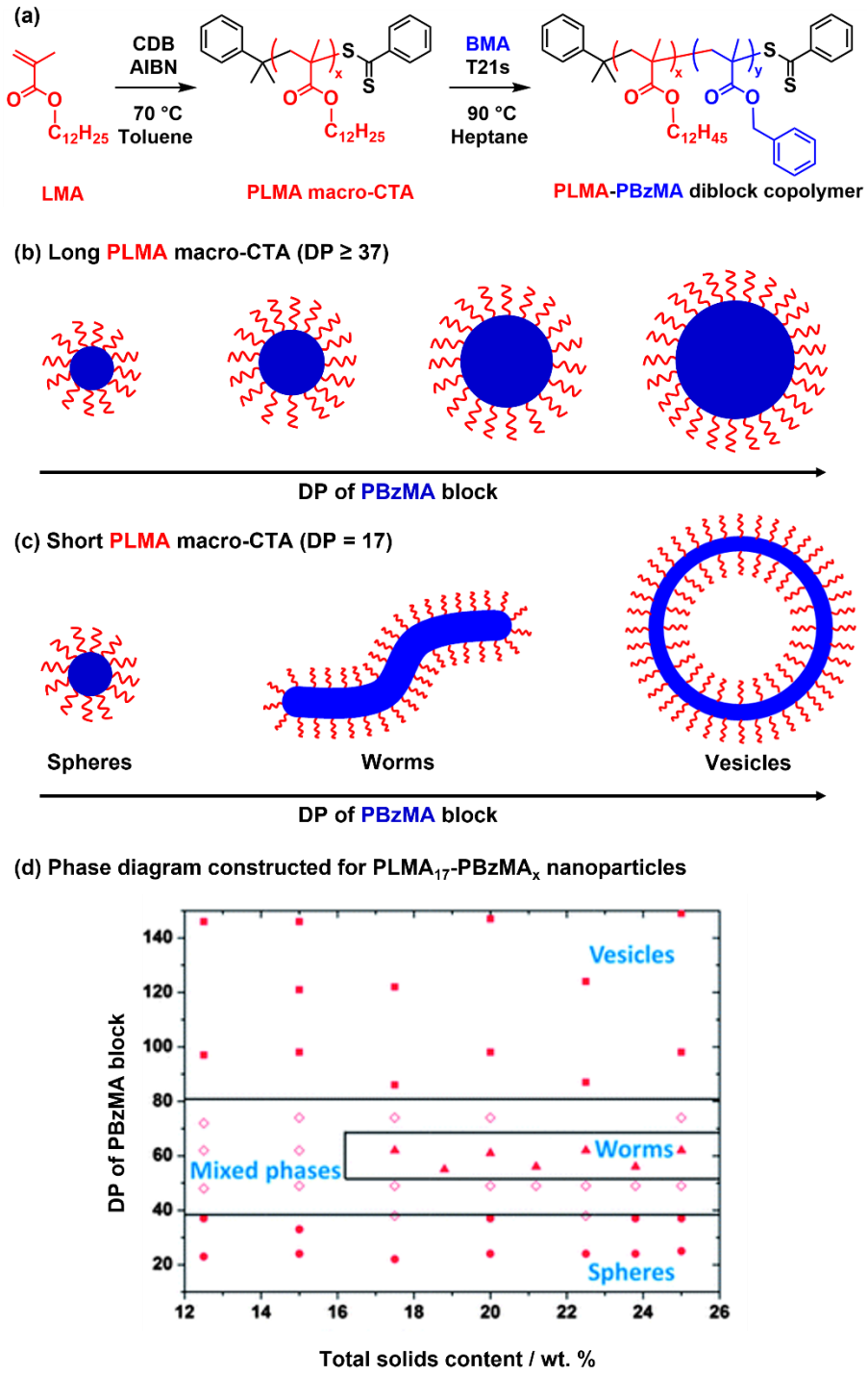

Figure 1.21. (a) RAFT synthesis of poly(lauryl methacrylate) [PLMA] macro-CTA *via* solution polymerisation in toluene at 70 °C, followed by RAFT dispersion polymerisation of benzyl methacrylate (BzMA) in *n*-heptane at 90 °C. **(b)** Schematic representation of the change in size that occurs on increasing the PBzMA target degree of polymerisation when using a relatively long PLMA macro-CTA (DP ≥ 37). **(c)** Schematic representation of the change in morphology that occurs on increasing the PBzMA target degree of polymerisation when using a relatively short PLMA macro-CTA (DP = 17). **(d)** Phase diagram constructed for $PLMA_{17}$-$PBzMA_x$ diblock copolymer nanoparticles, where PBzMA target DP and total solids content were systematically varied and morphologies determined by TEM. Adapted from reference 133.

Fielding and co-workers subsequently reported that PLMA-PBzMA worms prepared in *n*-dodecane exhibited a reversible worm-to-sphere morphological transition on heating.[140] The significantly higher boiling point of *n*-dodecane compared to *n*-heptane facilitates high temperature studies of PLMA-PBzMA nanoparticles and also reduces solvent evaporation. TEM studies confirmed that a worm-to-sphere transition is responsible for the degelation of a 20% w/w $PLMA_{16}$-$PBzMA_{37}$ worm gel that is observed upon heating to 90 °C (see **Figure 1.22**). This is because isotropic spheres interact with each other much less efficiently than highly anisotropic worms, which form a percolating 3D network.[148] Moreover, this thermal transition proved to be reversible at 20% w/w solids, with worms being regenerated on cooling to 20 °C.

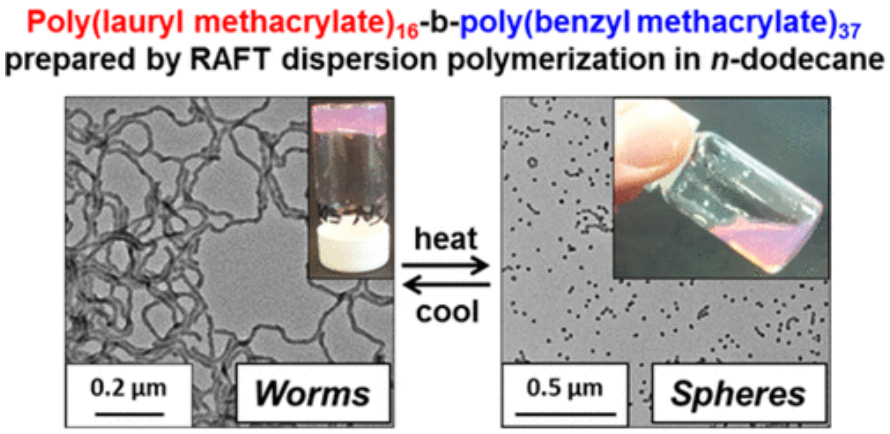

Figure 1.22. The worm-to-sphere transition observed on heating a 20% w/w dispersion of $PLMA_{16}$-$PBzMA_{37}$ worms to 90 °C in *n*-dodecane. TEM imaging indicated reversible behaviour, with worms reforming upon cooling to 20 °C [140]

Variable temperature DLS, rheology and SAXS studies provided comprehensive insight into this thermoresponsive behaviour. Interestingly, it was not necessary to convert all of the worms into spheres in order to induce degelation. Rheology studies indicated that the onset of degelation occurred at approximately 47 °C, whereas pure spheres were only obtained when the original worms were heated up to 160 °C in the SAXS experiment. A gradual reduction in the mean worm contour length, as determined by SAXS, was sufficient to reduce the multiple inter-worm contacts that

cause gelation, which effectively lowers the critical copolymer concentration required for a 3D percolating network.[148] Moreover, variable temperature SAXS and TEM studies indicated that mixtures of worms and spheres were observed at intermediate temperatures. Thus, it was postulated that the dominant mechanism for the worm-to-sphere transition was likely to be sequential budding of spheres from worm ends, rather than random worm scission. It was also demonstrated that the worm-to-sphere transition is essentially irreversible at copolymer concentrations below 5% w/w. Presumably, this is because the formation of worms from the fusion of multiple spheres becomes highly inefficient for dilute dispersions. Similar observations have since been reported for other PISA formulations in non-polar media.[146]

Additionally, in the same study by Fielding and co-workers,[140] variable temperature ^{1}H NMR spectroscopy studies in d_{26}-dodecane revealed partial solvation of the PBzMA block at elevated temperature. If *uniform* plasticisation of the core-forming block had occurred on heating, the increase in effective volume fraction would predict a worm-to-vesicle transition, which does not occur. Instead, the observed worm-to-sphere transition was rationalised by *surface* plasticisation of the PBzMA core-forming block. In this case, the BzMA repeat units nearest to the PLMA stabiliser become solvated: this increases the effective volume fraction of the stabiliser block, which lowers the packing parameter and hence accounts for the observed worm-to-sphere transition.

Similar findings were reported by Lowe and co-workers for poly(stearyl methacrylate)-poly(phenylpropyl methacrylate) [PSMA-PPPMA] nanoparticles in either *n*-octane[145] or *n*-tetradecane.[141] Heating 20-30% w/w dispersions of copolymer worms converted the initial gels to free flowing fluids. A worm-to-sphere transition was confirmed by TEM studies and variable-temperature ^{1}H NMR spectroscopy

studies indicated a higher degree of solvation of the core-forming block with increasing temperature.

Furthermore, the concept of *surface* plasticisation to rationalise the observation of thermoresponsive transitions for various types of diblock copolymer nano-objects has been extended to other PISA formulations. Of particular relevance to this Thesis, a vesicle-to-worm transition was reported by Derry *et al.* on heating a concentrated dispersion of poly(stearyl methacrylate)-poly(benzyl methacrylate) [PSMA-PBzMA] vesicles above 135 °C.[42] **Figure 1.23** illustrates the ingress of hot solvent (mineral oil) into the PBzMA-based membranes. This solvation of the BzMA residues located near the block junction effectively increases the volume fraction of the PSMA stabiliser block and hence reduces the packing parameter, *P*, for the diblock copolymer chains.

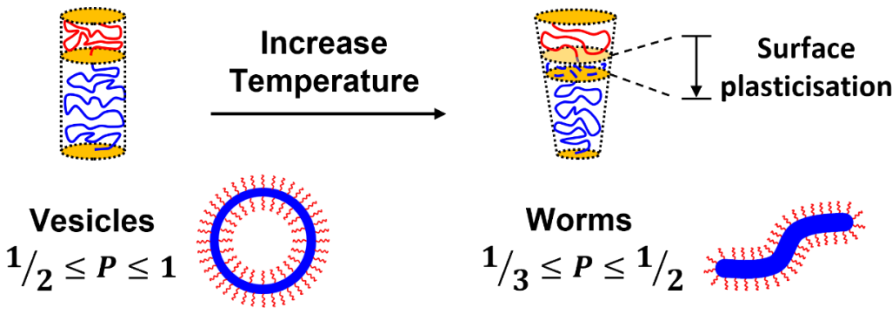

Figure 1.23. Surface plasticisation of the membrane-forming PBzMA block (depicted in blue) on heating the vesicle dispersion above 135 °C results in a vesicle-to-worm transition for $PSMA_{13}$-$PBzMA_{96}$ nanoparticles in mineral oil. Adapted from reference 149.

Derry *et al.* selected PSMA as the stabiliser block because it gave higher blocking efficiencies compared to those achieved when using PLMA.[142] A phase diagram was constructed for $PSMA_{13}$-$PBzMA_x$ nano-objects when targeting PBzMA DPs (x) of 20 to 150 at various copolymer concentrations (5-20% w/w) in mineral oil, with copolymer morphologies being assigned by TEM analysis (see **Figure 1.24**). Like the PLMA-PBzMA PISA formulation discussed earlier, the pure worm morphology occupies a relatively narrow region within the phase diagram.

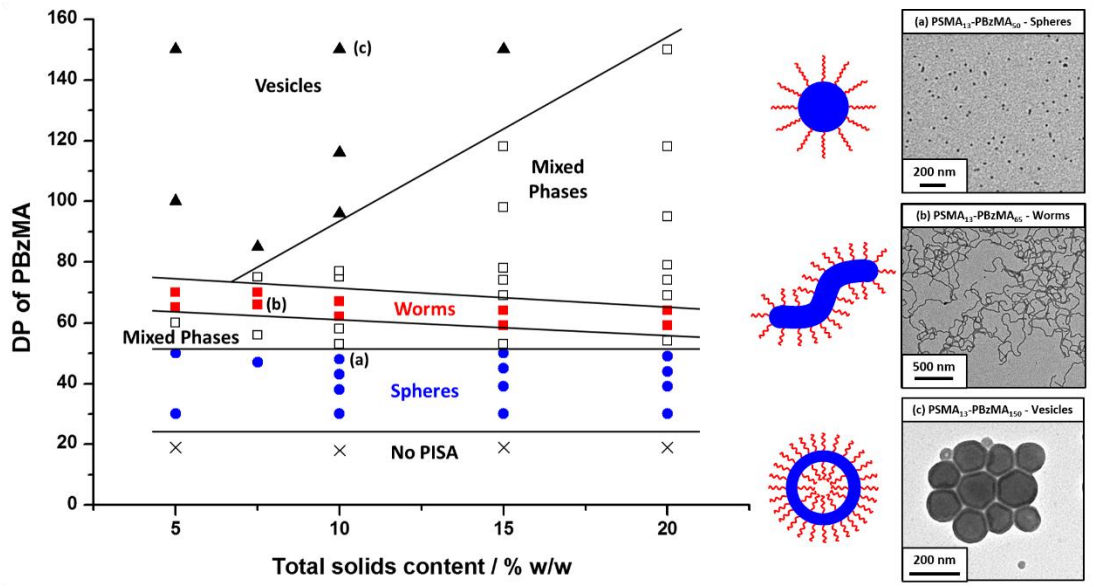

Figure 1.24. Phase diagram constructed for $PSMA_{13}$-$PBzMA_x$ diblock copolymer nanoparticles prepared by RAFT dispersion polymerisation of BzMA in mineral oil at 90 °C. TEM images (a), (b) and (c) correspond to typical examples of the three pure morphologies (spheres, worms or vesicles) respectively.[142]

Moreover, small-angle X-ray scattering (SAXS) was used for the first time to monitor the *in situ* evolution in copolymer morphology that occurrs during the RAFT dispersion polymerisation of BzMA when targeting $PSMA_{13}$-$PBzMA_{150}$ vesicles. The expected gradual evolution of copolymer morphology from spheres to worms to vesicles during PISA was confirmed and approximate 'lifetimes' were assigned to the intermediate pure sphere and worm morphologies. Interestingly, the vesicle membrane thickness increased monotonically with PBzMA DP while overall vesicle dimensions remain essentially constant. The same 'vesicle inward growth' behaviour had been previously reported for an aqueous PISA formulation[150] and this mechanism was verified by Derry *et al.* for the first time for a PISA formulation conducted in non-polar media.

More recently, Derry and co-workers reported the synthesis of poly(behenyl methacrylate)-poly(benzyl methacrylate) [PBeMA-PBzMA] diblock copolymer spheres *via* RAFT-mediated PISA targeting 20% w/w solids in mineral oil at 90 °C.[143]

Interestingly, a turbid, paste-like dispersion was formed on cooling a relatively transparent dispersion of colloidally stable spherical nanoparticles to 20 °C. This thermal transition proved to be fully reversible on heating to 50 °C (see **Figure 1.25**). Various techniques, including turbidimetry, DSC, SAXS and wide-angle X-ray scattering (WAXS), were used to characterise the temperature-dependent behaviour of these diblock copolymer nanoparticles and the sol-gel transition was directly linked to the semi-crystalline nature of the PBeMA stabiliser block. More specifically, the combined SAXS, WAXS and DSC data suggested that the behenyl ($C_{22}H_{45}$) side-chains first formed crystalline nanodomains between adjacent stabiliser chains within individual spherical nanoparticles, followed by crystallisation between neighbouring nanoparticles, with the latter interactions leading to the formation of a *loose fractal network* of strongly interacting spheres.[143]

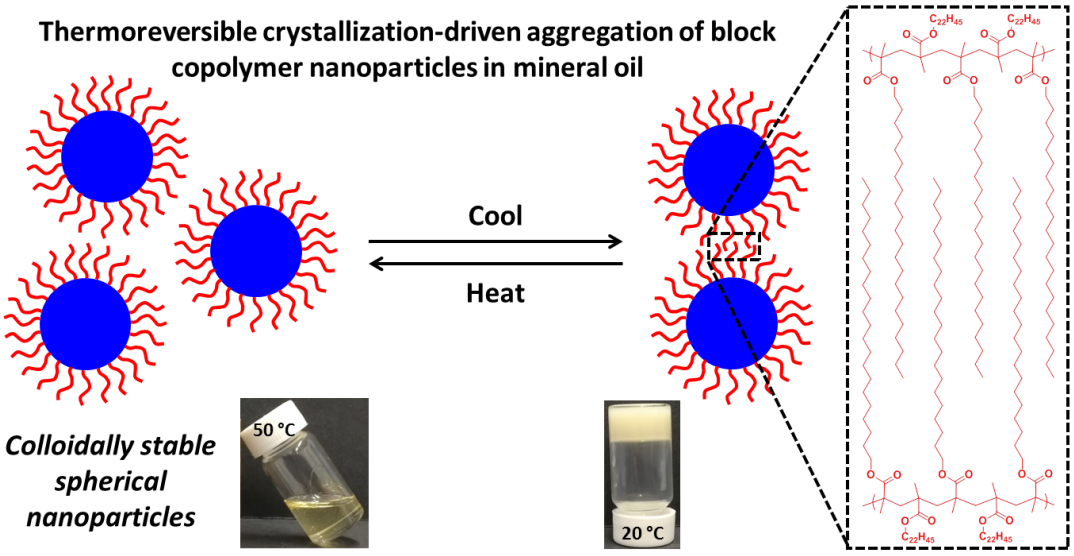

Figure 1.25. Schematic representation of $PBeMA_{37}$-$PBzMA_{100}$ spheres which form a turbid, paste-like dispersion on cooling a relatively transparent dispersion of colloidally stable spherical nanoparticles to 20 °C. The formation of loose mass fractal aggregates *via* crystallisation-driven aggregation between PBeMA chains on neighbouring nanoparticles is also represented.[143]

1.4.4. Crystallisation-Driven Self-Assembly (CDSA)

Crystallisation of polymer chains can also be used to drive block copolymer self-assembly in the bulk or in solution by a post-polymerisation processing technique known as crystallisation-driven self-assembly (CDSA).

In 1998, Manners and co-workers reported that incorporation of a crystallisable core-forming block, poly(ferrocenyldimethylsilane) [PFDMS], enabled the unexpected formation of polydimethylsiloxane-poly(ferrocenyldimethylsilane) [PDMS-PFDMS] cylindrical micelles (not spheres) in *n*-hexane (see **Figure 1.26**).[151] These PFDMS-core nanoparticles were formed after heating in *n*-hexane, which is a selective solvent for PDMS and a precipitant for PFDMS. Remarkably, it was determined that the cylindrical morphology is a direct consequence of the semi-crystalline nature of PFDMS. Changing the second copolymer block to poly(ferrocenylmethylphenylsilane) [PFMPS], which is amorphous, merely resulted in the formation of spherical micelles, as confirmed by TEM studies (see **Figure 1.26**).[152] A diblock copolymer was prepared with the PDMS block replaced by polyisoprene and PIP-PFDMS cylinders were formed in *n*-hexane. Moreover, the semi-crystalline ordered structure of the cylinder cores was confirmed by WAXS studies.[153]

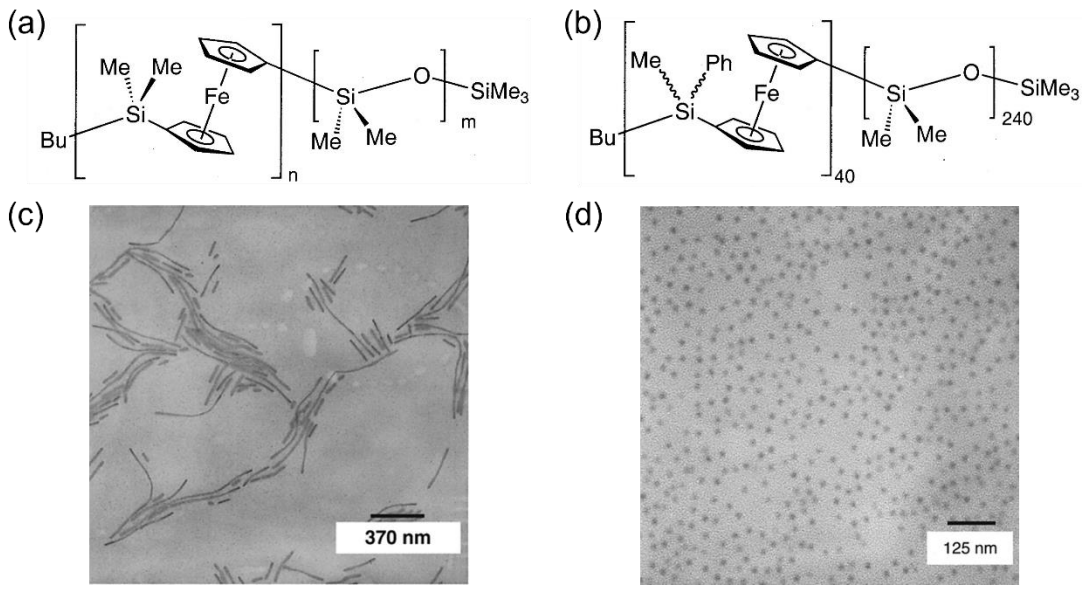

Figure 1.26. The chemical structure of **(a)** a PDMS-PFDMS diblock copolymer, and **(b)** a $PDMS_{240}$-$PFMPS_{40}$ diblock copolymer. TEM micrographs of **(c)** $PDMS_{375}$-$PFDMS_{75}$ cylindrical micelles from an *n*-hexane solution, and **(d)** $PDMS_{240}$-$PFMPS_{40}$ spherical micelles from an *n*-hexane solution. Adapted from reference 152.

PFDMS has become one of the most widely studied core-forming blocks for CDSA. It is been combined with various corona-forming blocks such as polyisoprene (PIP),[154] poly(2-vinylpyridine) (P2VP),[155–157] or poly(methyl methacrylate)[158] for CDSA studies conducted in *n*-alkanes,[154] alcohols,[155] or acetone.[158] PFDMS diblock copolymers have been shown to self-assemble in various selective solvents to produce various micellar morphologies including cylinders,[151,152] tubes,[159,160] fibres,[161] platelets[154] and - if the core-forming block is not crystalline - spheres.[155,158] The PFDMS core is electron-rich, which aids TEM studies by ensuring strong electron contrast without the need for staining.[152,162]

Interestingly, seminal work by Manners, Winnik and co-workers has shown that the termini of PFDMS-containing micelles remain active towards epitaxial growth *via* addition of further copolymer chains, thus providing excellent control over the length of PFDMS-based cylinders.[163,164] Small seed micelles can be generated by ultrasonication of longer cylinders and subsequently used as 'initiators' for so-called

'living' CDSA, which is analogous to the living polymerisation of vinyl monomers.[164] There are two routes to 'living' CDSA: seeded growth or self-seeding (see **Figure 1.27**). The concept of 'living' CDSA has been extended to many other crystallisable core-forming polymers, such as poly(*L*-lactide),[165] poly(ε-caprolactone)[166] and polyethylene.[167] For example, O'Reilly and co-workers reported that poly(ε-caprolactone)-poly(*N*,*N*-dimethylacrylamide) [PCL_{50}-*b*-$PDMA_{180}$] cylinders can be prepared in ethanol *via* 'living' CDSA.[168] In this case, varying the unimer-to-seed ratio led to predictable dimensions. For example, using a unimer/seed ratio of 5.0 produced cylinders with a mean length of approximately 350 nm from 50 nm crystalline seeds. In contrast, near-monodisperse cylinders up to several micrometres in length could be grown using a unimer/seed ratio of 40.

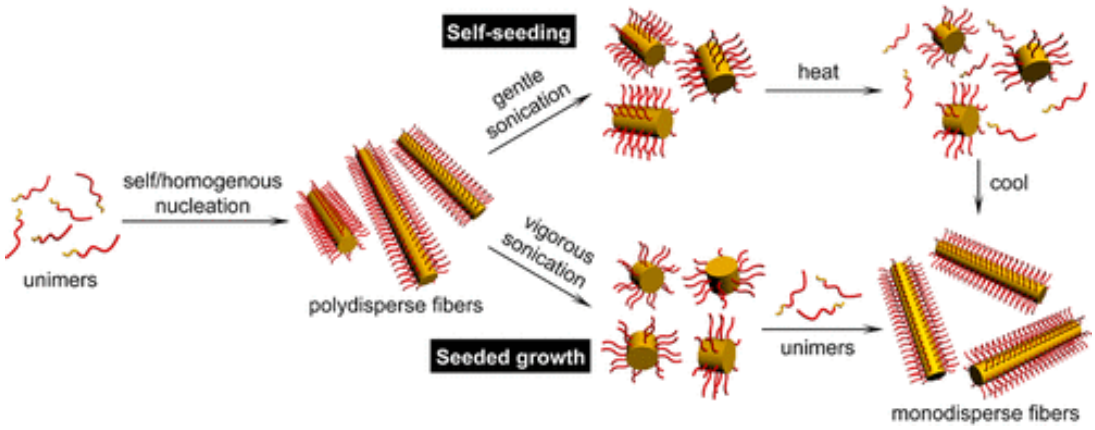

Figure 1.27. Schematic representation of two living CDSA routes: seeded growth (bottom) and self-seeding (top).[169]

The reproducible synthesis of cylinders with controlled length is one advantage of 'living' CDSA over PISA (where controlling the length of worms often remains a challenge).[170,171] Nevertheless, assessing the solvent parameters which are optimal for self-assembly can be challenging in CDSA.[172] PISA remains attractive because it typically involves using cheap commercially available vinyl monomers.

1.5. Thesis Outline

This Thesis will focus exclusively on diblock and statistical copolymers synthesised by either RAFT dispersion or RAFT solution polymerisation in non-polar media. Various methacrylic monomers are polymerised without the need for stringent purification and the resulting copolymers are evaluated for potential industrial applications, such as oil thickeners for personal care products or wax crystal inhibitors/modifiers.

Chapter 2 reports the synthesis of thermoresponsive PSMA-P(BzMA-*stat*-BuMA) diblock copolymer vesicles prepared *via* RAFT-mediated PISA in mineral oil. The effect of varying the target DP and BuMA content of the membrane-forming block on the vesicle-to-worm transition is investigated in the context of an oil-thickening mechanism.

Chapters 3 and 4 explore the synthesis of well-defined PLMA-PBeMA diblock and statistical copolymers. Inspired by the crystallisation-driven aggregation observed for PBeMA-PBzMA diblock copolymer spheres reported by Derry *et al.*,[143] potential polymerisation-induced crystallisation-driven self-assembly (PI-CDSA) formulations utilising PBeMA as a semi-crystalline structure-directing block are explored in Chapter 3. In particular, the RAFT polymerisation of BeMA conducted at 90 °C *via* thermal initiation is directly compared to that at 15 °C using iniferter RAFT polymerisation.

In Chapter 4, two series of PLMA-PBeMA diblock and statistical copolymers are prepared by RAFT solution polymerisation and subsequently investigated as potential wax crystal modifiers for the model wax *n*-octacosane. In particular, the effect of

varying either the target PBeMA DP or the overall copolymer concentration on wax crystal formation is investigated.

1.6. References

1 H. Staudinger, *Ber. Dtsch. Chem. Ges.*, 1920, **53**, 1073–1085.

2 J. M. G. Cowie, *Polymers: Chemistry and Physics of Modern Materials*, Nelson Thornes, Cheltenham, Second Edn., 2001.

3 R. J. Young and P. A. Lovell, *Introduction to Polymers*, CRC Press, Third Edn., 2011.

4 W. H. Carothers, *J. Am. Chem. Soc.*, 1929, **51**, 2548–2559.

5 Y. Zhu, C. Romain and C. K. Williams, *Nature*, 2016, **540**, 354–362.

6 R. F. T. Stepto, *Pure Appl. Chem.*, 2009, **81**, 351–353.

7 T. G. Fox, *Bull. Am. Phys. Soc.*, 1956, **1**, 123.

8 G. Odian, *Principles of Polymerisation*, John Wiley & Sons, Hoboken, Fourth Edn., 2004.

9 P. J. Flory, *Principles of Polymer Chemistry*, Cornell University Press, London, First Edn., 1953.

10 K. Matyjaszewski, Y. Gnanou and L. Leibler, *Macromolecular Engineering: Precise Synthesis, Materials Properties, Applications*, Wiley-VCH, Weinheim, Vol. 1., 2007.

11 P. C. Hiemenz and T. P. Lodge, *Polymer Chemistry*, CRC Press, New York, Second Edn., 2007.

12 W. A. Braunecker and K. Matyjaszewski, *Prog. Polym. Sci.*, 2007, **32**, 93–146.

13 N. M. Ahmad, F. Heatley and P. A. Lovell, *Macromolecules*, 1998, **31**, 2822–2827.

14 M. Szwarc, *Nature*, 1956, **178**, 1168–1169.

15 R. Waack, A. Rembaum, J. D. Coombes and M. Szwarc, *J. Am. Chem. Soc.*, 1957, **79**, 2026–2027.

16 C. M. Bates and F. S. Bates, *Macromolecules*, 2017, 50, 3–22.

17 N. Corrigan, K. Jung, G. Moad, C. J. Hawker, K. Matyjaszewski and C. Boyer, *Prog. Polym. Sci.*, 2020, **111**, 101311.

18 V. Sciannamea, R. Jérôme and C. Detrembleur, *Chem. Rev.*, 2008, 108, 1104–1126.

19 K. Matyjaszewski, *Macromolecules*, 2012, **45**, 4015–4039.

20 J. Nicolas, Y. Guillaneuf, C. Lefay, D. Bertin, D. Gigmes and B. Charleux, *Prog. Polym. Sci.*, 2013, 38, 63–235.

21 S. Perrier, *Macromolecules*, 2017, **50**, 7433–7447.

22 C. J. Hawker, A. W. Bosman and E. Harth, *Chem. Rev.*, 2001, **101**, 3661–3688.

23 J. S. Wang and K. Matyjaszewski, *Macromolecules*, 1995, **28**, 7901–7910.

24 K. Matyjaszewski and J. Xia, *Chem. Rev.*, 2001, **101**, 2921–2990.

25 J. Chiefari, (Bill) Y. K. Chong, F. Ercole, J. Krstina, J. Jeffery, T. P. T. Le, R. T. A. Mayadunne, G. F. Meijs, C. L. Moad, G. Moad, E. Rizzardo and S. H. Thang, *Macromolecules*, 1998, **31**, 5559–5562.

26 H. Fischer, *Chem. Rev.*, 2001, 101, 3581–3610.

27 A. Goto and T. Fukuda, *Prog. Polym. Sci.*, 2004, **29**, 329–385.

28 G. Moad, E. Rizzardo and S. Thang, *Acc. Chem. Res.*, 2008, **41**, 1133–1142.

29 G. Moad, E. Rizzardo and S. H. Thang, *Polymer*, 2008, **49**, 1079–1131.

30 P. Delduc, C. Tailhan and S. Z. Zard, *J. Chem. Soc. Chem. Commun.*, 1988, 308–310.

31 Corpart, P.; Charmot, D.; Zard, S. Z.; Biadatti, T.; Michelet, D., Method for Block Polymer Synthesis by Controlled Radical Polymerisation., WO98/58974, 2000.

32 S. Z. Zard, *Macromolecules*, 2020, **53**, 8144–8159.

33 D. J. Keddie, *Chem. Soc. Rev.*, 2014, **43**, 496–505.

34 H. Willcock and R. K. O'Reilly, *Polym. Chem.*, 2010, **1**, 149–157.

35 G. Moad, E. Rizzardo and S. H. Thang, *Polym. Int.*, 2011, **60**, 9–25.

36 G. Moad, E. Rizzardo and S. H. Thang, *Aust. J. Chem.*, 2009, **62**, 1402–1472.

37 D. J. Keddie, G. Moad, E. Rizzardo and S. H. Thang, *Macromolecules*, 2012, **45**, 5321–5342.

38 Y. K. Chong, J. Krstina, T. P. T. Le, G. Moad, A. Postma, E. Rizzardo and S. H. Thang, *Macromolecules*, 2003, **36**, 2256–2272.

39 M. Semsarilar, E. R. Jones, A. Blanazs and S. P. Armes, *Adv. Mater.*, 2012, **24**, 3378–3382.

40 J. R. Lovett, N. J. Warren, L. P. D. Ratcliffe, M. K. Kocik and S. P. Armes, *Angew. Chemie Int. Ed.*, 2015, **54**, 1279–1283.

41 M. J. Derry, L. A. Fielding and S. P. Armes, *Polym. Chem.*, 2015, **6**, 3054–

3062.

42 M. J. Derry, O. O. Mykhaylyk and S. P. Armes, *Angew. Chemie - Int. Ed.*, 2017, **56**, 1746–1750.

43 E. J. Cornel, S. van Meurs, T. Smith, P. S. O'Hora and S. P. Armes, *J. Am. Chem. Soc.*, 2018, **140**, 12980–12988.

44 C. Barner-Kowollik, *Handbook of RAFT polymerization*, Wiley-VCH: Weinheim, First Edn., 2008.

45 A. Postma, T. P. Davis, G. Moad and M. S. O'Shea, *Macromolecules*, 2005, **38**, 5371–5374.

46 B. Chong, G. Moad, E. Rizzardo, M. Skidmore and S. H. Thang, *Aust. J. Chem.*, 2006, **59**, 755.

47 K. M. Mattson, C. W. Pester, W. R. Gutekunst, A. T. Hsueh, E. H. Discekici, Y. Luo, B. V. K. J. Schmidt, A. J. McGrath, P. G. Clark and C. J. Hawker, *Macromolecules*, 2016, **49**, 8162–8166.

48 R. N. Carmean, C. A. Figg, G. M. Scheutz, T. Kubo and B. S. Sumerlin, *ACS Macro Lett.*, 2017, **6**, 185–189.

49 Z. Wang, J. He, Y. Tao, L. Yang, H. Jiang and Y. Yang, *Macromolecules*, 2003, **36**, 7446–7452.

50 C. P. Jesson, C. M. Pearce, H. Simon, A. Werner, V. J. Cunningham, J. R. Lovett, M. J. Smallridge, N. J. Warren and S. P. Armes, *Macromolecules*, 2017, **50**, 182–191.

51 D. Matioszek, P.-E. Dufils, J. Vinas and M. Destarac, *Macromol. Rapid Commun.*, 2015, **36**, 1354–1361.

52 L. Martin, G. Gody and S. Perrier, *Polym. Chem.*, 2015, **6**, 4875–4886.

53 M. Chen, M. Zhong and J. A. Johnson, *Chem. Rev.*, 2016, **116**, 10167–10211.

54 T. G. McKenzie, Q. Fu, M. Uchiyama, K. Satoh, J. Xu, C. Boyer, M. Kamigaito and G. G. Qiao, *Adv. Sci.*, 2016, **3**, 1500394.

55 N. Zaquen, W. A. A. W. Azizi, J. Yeow, R. P. Kuchel, T. Junkers, P. B. Zetterlund and C. Boyer, *Polym. Chem.*, 2019, **10**, 2406–2414.

56 M. Hartlieb, *Macromol. Rapid Commun.*, 2022, **43**, 2100514.

57 J. Tan, H. Sun, M. Yu, B. S. Sumerlin and L. Zhang, *ACS Macro Lett.*, 2015, **4**, 1249–1253.

58 L. D. Blackman, K. E. B. Doncom, M. I. Gibson and R. K. O'Reilly, *Polym. Chem.*, 2017, **8**, 2860–2871.

59 Y. Shi, H. Gao, L. Lu and Y. Cai, *Chem. Commun.*, 2009, 1368.

60 D. Konkolewicz, K. Schröder, J. Buback, S. Bernhard and K. Matyjaszewski, *ACS Macro Lett.*, 2012, **1**, 1219–1223.

61 B. P. Fors and C. J. Hawker, *Angew. Chemie Int. Ed.*, 2012, **51**, 8850–8853.

62 N. J. Treat, B. P. Fors, J. W. Kramer, M. Christianson, C. Y. Chiu, J. R. De Alaniz and C. J. Hawker, *ACS Macro Lett.*, 2014, **3**, 580–584.

63 J. Xu, K. Jung, A. Atme, S. Shanmugam and C. Boyer, *J. Am. Chem. Soc.*, 2014, **136**, 5508–5519.

64 T. G. McKenzie, L. P. M. Da Costa, Q. Fu, D. E. Dunstan and G. G. Qiao, *Polym. Chem.*, 2016, **7**, 4246–4253.

65 T. Otsu and M. Yoshida, *Die Makromol. Chemie, Rapid Commun.*, 1982, **3**, 127–132.

66 T. Otsu, *J. Polym. Sci. Part A Polym. Chem.*, 2000, **38**, 2121–2136.

67 T. G. McKenzie, Q. Fu, E. H. H. Wong, D. E. Dunstan and G. G. Qiao, *Macromolecules*, 2015, **48**, 3864–3872.

68 J. Xu, S. Shanmugam, N. A. Corrigan and C. Boyer, in *ACS Symposium Series*, 2015, pp. 247–267.

69 J. F. Quinn, L. Barner, C. Barner-Kowollik, E. Rizzardo and T. P. Davis, *Macromolecules*, 2002, **35**, 7620–7627.

70 L. Lu, N. Yang and Y. Cai, *Chem. Commun.*, 2005, 5287.

71 R. Ran, Y. Yu and T. Wan, *J. Appl. Polym. Sci.*, 2007, **105**, 398–404.

72 H. Wang, Q. Li, J. Dai, F. Du, H. Zheng and R. Bai, *Macromolecules*, 2013, **46**, 2576–2582.

73 A.-C. Lehnen, J. A. M. Kurki and M. Hartlieb, *Polym. Chem.*, 2022, Advance Article.

74 D. H. H. Chan, A. A. Cockram, R. R. Gibson, E. L. Kynaston, C. Lindsay, P. Taylor and S. P. Armes, *Polym. Chem.*, 2021, **12**, 5760–5769.

75 J. D. Coyle and H. A. J. Carless, *Chem. Soc. Rev.*, 1972, **1**, 465–480.

76 L. Lu, H. Zhang, N. Yang and Y. Cai, *Macromolecules*, 2006, **39**, 3770–3776.

77 R. W. Lewis, R. A. Evans, N. Malic, K. Saito and N. R. Cameron, *Polym. Chem.*, 2018, **9**, 60–68.

78 R. B. Grubbs, *Polym. Rev.*, 2011, **51**, 104–137.

79 Y. Li, B. S. Lokitz and C. L. McCormick, *Angew. Chemie Int. Ed.*, 2006, **45**, 5792–5795.

80 Z. Deng, H. Bouchékif, K. Babooram, A. Housni, N. Choytun and R. Narain,

J. Polym. Sci. Part A Polym. Chem., 2008, **46**, 4984–4996.

81 M. R. Hill, R. N. Carmean and B. S. Sumerlin, *Macromolecules*, 2015, **48**, 5459–5469.

82 Y. K. Chong, G. Moad, E. Rizzardo and S. H. Thang, *Macromolecules*, 2007, **40**, 4446–4455.

83 M. Destarac, *Polym. Chem.*, 2018, **9**, 4947–4967.

84 K. E. J. Barrett, *Br. Polym. J.*, 1973, **5**, 259–271.

85 A. P. Richez, H. N. Yow, S. Biggs and O. J. Cayre, *Prog. Polym. Sci.*, 2013, **38**, 897–931.

86 P. B. Zetterlund, S. C. Thickett, S. Perrier, E. Bourgeat-Lami and M. Lansalot, *Chem. Rev.*, 2015, **115**, 9745–9800.

87 R. Arshady, *Colloid Polym. Sci.*, 1992, **270**, 717–732.

88 S. Kawaguchi and K. Ito, in *Advances in Polymer Science*, ed. M. Okubo, Springer-Verlag, Berlin, 2005, vol. 175, pp. 299–328.

89 A. J. Paine, *Macromolecules*, 1990, **23**, 3109–3117.

90 K. P. Lok and C. K. Ober, *Can. J. Chem.*, 1985, **63**, 209–216.

91 D. W. J. Osmond, H. H. Thompson, Dispersion Polymerisation, GB893429A, 1962.

92 A. M. I. Ali, P. Pareek, L. Sewell, A. Schmid, S. Fujii, S. P. Armes and I. M. Shirley, *Soft Matter*, 2007, **3**, 1003–1013.

93 S. Shen, E. D. Sudol and M. S. El-Aasser, *J. Polym. Sci. Part A Polym. Chem.*, 1994, **32**, 1087–1100.

94 F. L. Baines, S. Dionisio, N. C. Billingham and S. P. Armes, *Macromolecules*, 1996, **29**, 3096–3102.

95 D. W. J. Osmond and D. J. Walbridge, in *Journal of Polymer Science Part C: Polymer Symposia*, John Wiley & Sons, Ltd, 1970, vol. 30, pp. 381–391.

96 M. Hölderle, M. Baumert and R. Mülhaupt, *Macromolecules*, 1997, **30**, 3420–3422.

97 L. I. Gabaston, R. A. Jackson and S. P. Armes, *Macromolecules*, 1998, **31**, 2883–2888.

98 K. Min and K. Matyjaszewski, *Macromolecules*, 2007, **40**, 7217–7222.

99 J. S. Song and M. A. Winnik, *Macromolecules*, 2006, **39**, 8318–8325.

100 J. Tan, X. Rao, X. Wu, H. Deng, J. Yang and Z. Zeng, *Macromolecules*, 2012, **45**, 8790–8795.

101 S. J. Singer and G. L. Nicolson, *Science*, 1972, **175**, 720–731.

102 J. Eastoe, in *Colloid Science: Principles, Methods and Applications*, ed. T. Cosgrove, John Wiley & Sons Ltd, Chippenham, Second Edn., 2010, pp. 61–89.

103 C. Tanford, *Science*, 1978, **200**, 1012–1018.

104 J. N. Israelachvili, D. J. Mitchell and B. W. Ninham, *J. Chem. Soc. - Faraday Trans.*, 1976, **72**, 1525–1568.

105 R. Nagarajan, *Langmuir*, 2002, **18**, 31–38.

106 E. L. Thomas, D. M. Anderson, C. S. Henkee and D. Hoffman, *Nature*, 1988, **334**, 598–601.

107 F. S. Bates and G. H. Fredrickson, *Annu. Rev. Phys. Chem.*, 1990, **41**, 525–557.

108 F. S. Bates and G. H. Fredrickson, *Phys. Today*, 1999, **52**, 32–38.

109 Y. Mai and A. Eisenberg, *Chem. Soc. Rev.*, 2012, **41**, 5969–5985.

110 L. Zhang and A. Eisenberg, *Science*, 1995, **268**, 1728–1731.

111 L. Zhang, K. Yu and A. Eisenberg, *Science*, 1996, **272**, 1777–1779.

112 L. Zhang and A. Eisenberg, *J. Am. Chem. Soc.*, 1996, **118**, 3168–3181.

113 N. S. Cameron, M. K. Corbierre and A. Eisenberg, *Can. J. Chem.*, 1999, **77**, 1311–1326.

114 L. Zhang and A. Eisenberg, *Polym. Adv. Technol.*, 1998, **9**, 677–699.

115 S. Jain and F. S. Bates, *Science*, 2003, **300**, 460–464.

116 J. R. Howse, R. A. L. Jones, G. Battaglia, R. E. Ducker, G. J. Leggett and A. J. Ryan, *Nat. Mater.*, 2009, **8**, 507–511.

117 V. Bütün, S. . Armes and N. . Billingham, *Polymer*, 2001, **42**, 5993–6008.

118 S. L. Canning, G. N. Smith and S. P. Armes, *Macromolecules*, 2016, **49**, 1985–2001.

119 F. D'Agosto, J. Rieger and M. Lansalot, *Angew. Chemie - Int. Ed.*, 2020, **59**, 8368–8392.

120 A. Blanazs, S. P. Armes and A. J. Ryan, *Macromol. Rapid Commun.*, 2009, **30**, 267–277.

121 G. Delaittre, C. Dire, J. Rieger, J.-L. Putaux and B. Charleux, *Chem. Commun.*, 2009, 2887.

122 X. G. Qiao, M. Lansalot, E. Bourgeat-Lami and B. Charleux, *Macromolecules*, 2013, **46**, 4285–4295.

123 W. M. Wan and C. Y. Pan, *Macromolecules*, 2007, **40**, 8897–8905.

124 J. Wang, Z. Wu, G. Wang and K. Matyjaszewski, *Macromol. Rapid Commun.*, 2019, **40**, 1800332.

125 J. C. Foster, S. Varlas, L. D. Blackman, L. A. Arkinstall and R. K. O'Reilly, *Angew. Chemie Int. Ed.*, 2018, **57**, 10672–10676.

126 V. J. Cunningham, A. M. Alswieleh, K. L. Thompson, M. Williams, G. J. Leggett, S. P. Armes and O. M. Musa, *Macromolecules*, 2014, **47**, 5613–5623.

127 N. J. Warren and S. P. Armes, *J. Am. Chem. Soc.*, 2014, **136**, 10174–10185.

128 A. B. Lowe, *Polymer*, 2016, **106**, 161–181.

129 K. L. Thompson, N. Cinotti, E. R. Jones, C. J. Mable, P. W. Fowler and S. P. Armes, *Langmuir*, 2017, **33**, 12616–12623.

130 D. H. H. Chan, E. L. Kynaston, C. Lindsay, P. Taylor and S. P. Armes, *ACS Appl. Mater. Interfaces*, 2021, **13**, 30235–30243.

131 I. Canton, N. J. Warren, A. Chahal, K. Amps, A. Wood, R. Weightman, E. Wang, H. Moore and S. P. Armes, *ACS Cent. Sci.*, 2016, **2**, 65–74.

132 S. Varlas, J. C. Foster, P. G. Georgiou, R. Keogh, J. T. Husband, D. S. Williams and R. K. O'Reilly, *Nanoscale*, 2019, **11**, 12643–12654.

133 L. A. Fielding, M. J. Derry, V. Ladmiral, J. Rosselgong, A. M. Rodrigues, L. P. D. Ratcliffe, S. Sugihara and S. P. Armes, *Chem. Sci.*, 2013, **4**, 2081–2087.

134 B. R. Parker, M. J. Derry, Y. Ning and S. P. Armes, *Langmuir*, 2020, **36**, 3730–3736.

135 M. J. Derry, O. O. Mykhaylyk and S. P. Armes, *Soft Matter*, 2021, **17**, 8867–8876.

136 L. Houillot, C. Bui, M. Save, B. Charleux, C. Farcet, C. Moire, J.-A. Raust and I. Rodriguez, *Macromolecules*, 2007, **40**, 6500–6509.

137 L. Houillot, C. Bui, C. Farcet, C. Moire, J. A. Raust, H. Pasch, M. Save and B. Charleux, *ACS Appl. Mater. Interfaces*, 2010, **2**, 434–442.

138 L. P. D. Ratcliffe, B. E. McKenzie, G. M. D. Le Bouëdec, C. N. Williams, S. L. Brown and S. P. Armes, *Macromolecules*, 2015, **48**, 8594–8607.

139 S. L. Canning, V. J. Cunningham, L. P. D. Ratcliffe and S. P. Armes, *Polym. Chem.*, 2017, **8**, 4811–4821.

140 L. A. Fielding, J. A. Lane, M. J. Derry, O. O. Mykhaylyk and S. P. Armes, *J. Am. Chem. Soc.*, 2014, **136**, 5790–5798.

141 Y. Pei, L. Thurairajah, O. R. Sugita and A. B. Lowe, *Macromolecules*, 2015, **48**, 236–244.

142 M. J. Derry, L. A. Fielding, N. J. Warren, C. J. Mable, A. J. Smith, O. O. Mykhaylyk and S. P. Armes, *Chem. Sci.*, 2016, **7**, 5078–5090.

143 M. J. Derry, O. O. Mykhaylyk, A. J. Ryan and S. P. Armes, *Chem. Sci.*, 2018, **9**, 4071–4082.

144 C. György, S. J. Hunter, C. Girou, M. J. Derry and S. P. Armes, *Polym. Chem.*, 2020, **11**, 4579–4590.

145 Y. Pei, O. R. Sugita, L. Thurairajah and A. B. Lowe, *RSC Adv.*, 2015, **5**, 17636–17646.

146 C. György, C. Verity, T. J. Neal, M. J. Rymaruk, E. J. Cornel, T. Smith, D. J. Growney and S. P. Armes, *Macromolecules*, 2021, **54**, 9496–9509.

147 P. J. Docherty, M. J. Derry and S. P. Armes, *Polym. Chem.*, 2019, **10**, 603–611.

148 J. R. Lovett, M. J. Derry, P. Yang, F. L. Hatton, N. J. Warren, P. W. Fowler and S. P. Armes, *Chem. Sci.*, 2018, **9**, 7138–7144.

149 M. J. Derry, Polymerisation-Induced Self-Assembly in Non-Polar Media, University of Sheffield, 2016.

150 N. J. Warren, O. O. Mykhaylyk, A. J. Ryan, M. Williams, T. Doussineau, P. Dugourd, R. Antoine, G. Portale and S. P. Armes, *J. Am. Chem. Soc.*, 2015, **137**, 1929–1937.

151 J. Massey, K. Nicole Power, I. Manners and M. A. Winnik, *J. Am. Chem. Soc.*, 1998, **120**, 9533–9540.

152 J. A. Massey, K. Temple, L. Cao, Y. Rharbi, J. Raez, M. A. Winnik and I. Manners, *J. Am. Chem. Soc.*, 2000, **122**, 11577–11584.

153 J. B. Gilroy, P. A. Rupar, G. R. Whittell, L. Chabanne, N. J. Terrill, M. A. Winnik, I. Manners and R. M. Richardson, *J. Am. Chem. Soc.*, 2011, **133**, 17056–17062.

154 L. Cao, I. Manners and M. A. Winnik, *Macromolecules*, 2002, **35**, 8258–8260.

155 H. Wang, M. A. Winnik and I. Manners, *Macromolecules*, 2007, **40**, 3784–3789.

156 S. F. M. Yusoff, M. S. Hsiao, F. H. Schacher, M. A. Winnik and I. Manners, *Macromolecules*, 2012, **45**, 3883–3891.

157 M. S. Hsiao, S. F. M. Yusoff, M. A. Winnik and I. Manners, *Macromolecules*, 2014, **47**, 2361–2372.

158 I. Korczagin, M. A. Hempenius, R. G. Fokkink, M. A. Cohen Stuart, M. Al-Hussein, P. H. H. Bomans, P. M. Frederik and G. Julius Vancso, *Macromolecules*, 2006, **39**, 2306–2315.

159 J. Raez, I. Manners and M. A. Winnik, *J. Am. Chem. Soc.*, 2002, **124**, 10381–10395.

160 D. J. Frankowski, J. Raez, I. Manners, M. A. Winnik, S. A. Khan and R. J. Spontak, *Langmuir*, 2004, **20**, 9304–9314.

161 J. Raez, I. Manners and M. A. Winnik, *Langmuir*, 2002, **18**, 7229–7239.

162 J. A. Massey, K. N. Power, M. A. Winnik and I. Manners, *Adv. Mater.*, 1998, **10**, 1559–1562.

163 X. Wang, G. Guerin, H. Wang, Y. Wang, I. Manners and M. A. Winnik, *Science*, 2007, **317**, 644–647.

164 J. B. Gilroy, T. Gädt, G. R. Whittell, L. Chabanne, J. M. Mitchels, R. M. Richardson, M. A. Winnik and I. Manners, *Nat. Chem.*, 2010, **2**, 566–570.

165 Y. He, J. C. Eloi, R. L. Harniman, R. M. Richardson, G. R. Whittell, R. T. Mathers, A. P. Dove, R. K. O'Reilly and I. Manners, *J. Am. Chem. Soc.*, 2019, **141**, 19088–19098.

166 W. Yu, J. C. Foster, A. P. Dove and R. K. O'Reilly, *Macromolecules*, 2020, **53**, 1514–1521.

167 J. Schmelz, A. E. Schedl, C. Steinlein, I. Manners and H. Schmalz, *J. Am. Chem. Soc.*, 2012, **134**, 14217–14225.

168 M. C. Arno, M. Inam, Z. Coe, G. Cambridge, L. J. Macdougall, R. Keogh, A. P. Dove and R. K. O'Reilly, *J. Am. Chem. Soc.*, 2017, **139**, 16980–16985.

169 H. Qiu, Y. Gao, V. A. Du, R. Harniman, M. A. Winnik and I. Manners, *J. Am. Chem. Soc.*, 2015, **137**, 2375–2385.

170 E. R. Jones, M. Semsarilar, A. Blanazs and S. P. Armes, *Macromolecules*, 2012, **45**, 5091–5098.

171 O. Nahi, O. J. Cayre, Y. Y. Kim, A. J. Smith, N. J. Warren and F. C. Meldrum, *Chem. Commun.*, 2020, **56**, 7463–7466.

172 J. C. Foster, S. Varlas, B. Couturaud, Z. Coe and R. K. O'reilly, *J. Am. Chem. Soc*, 2019, **141**, 2742–2753.

Chapter 2. Tuning the Vesicle-to-Worm Transition for Thermoresponsive Block Copolymer Vesicles Prepared *via* Polymerisation-Induced Self-Assembly

Reproduced in part with permission from [I. R. Dorsman, M. J. Derry, V. J. Cunningham, S. L. Brown, C. N. Williams and S. P. Armes, *Polymer Chemistry*, 2021, **12**, 1224-1235]

2.1. Introduction

Block copolymer self-assembly has been widely studied[1] and offers a diverse range of both potential and practical applications, including thermoplastic elastomers,[2] toughening agents for epoxy resins,[3] the dispersion of diesel soot[4] or pigment particles,[5] drug delivery,[6] and cell culture matrices.[7,8] Traditionally, such self-assembly is achieved in dilute solution (< 1% w/w) using various post-polymerisation processes, such as a solvent switch,[9,10] a pH switch[11,12] or thin film rehydration.[13,14] Over the past ten years, there has been considerable interest in the growing field of polymerisation-induced self-assembly (PISA).[15–19] This technique involves chain extension of a soluble precursor block in a suitable solvent using a second monomer that polymerises to form an insoluble second block, thus producing sterically-stabilised diblock copolymer nanoparticles *in situ*. The final copolymer morphology obtained *via* PISA is primarily dictated by the relative volume fractions of the stabiliser and core-forming blocks, as indicated by the geometric packing parameter (*P*) introduced by Israelachvili and co-workers.[20] The most common copolymer morphologies, in order of increasing *P*, are spheres,[21,22] worms,[23,24] vesicles[25,26] and lamellae.[27,28]

PISA offers three decisive advantages over conventional self-assembly techniques. First, PISA produces nanoparticles directly during synthesis, which means that post-polymerisation processing is not required.[16,18] Second, the rate of polymerisation usually increases significantly after micellar nucleation, which enables very high monomer conversions to be achieved within relatively short reaction times compared to the equivalent solution polymerisations.[29–31] Third, PISA syntheses can be conducted in a wide range of solvents (aqueous,[32] polar[33,34] or non-polar[35–38] solvents,

silicone oils,[39,40] ionic liquids,[41] etc.) at copolymer concentrations of up to 50% w/w.[30,42] Thus, PISA is in principle an attractive technique for industrial scale-up.[43]

PISA has been successfully conducted using reversible-deactivation radical polymerisation (RDRP) techniques such as ATRP[44–46] and NMP.[47–49] However, reversible addition-fragmentation chain transfer (RAFT) polymerisation has been preferred for most PISA syntheses.[15,19,50] RAFT-mediated PISA allows the convenient synthesis of a wide-range of well-defined functional block copolymer nanoparticles in water, lower alcohols or *n*-alkanes.[16,51,52] In this context, RAFT *dispersion* polymerisation is of particular interest since it can provide convenient access to diblock copolymer nano-objects that exhibit thermoresponsive behaviour. For example, block copolymer worms prepared *via* such formulations often exhibit a reversible worm-to-sphere transition when subjected to either heating (if prepared in ethanol[53] or *n*-alkanes[36,37,54]) or cooling (if prepared in aqueous solution).[24,55–57] At sufficiently high copolymer concentration, the initial worms form a soft, free-standing physical gel as a result of multiple inter-worm contacts, which produces a percolating 3D gel network.[58] The worm-to-sphere transition leads to *in situ* degelation, because the non-interacting spheres form a free-flowing dispersion.[54]

Although well-known in the surfactant literature,[59,60] vesicle-to-worm transitions have only recently been demonstrated for block copolymers.[61–67] For example, we reported two examples of a *single* thermoresponsive diblock copolymer prepared by RAFT aqueous dispersion polymerisation that can form spheres, worms or vesicles simply by varying the solution temperature. However, if the structure-directing block is poly(2-hydroxypropyl methacrylate), such thermal transitions can require relatively long time scales.[66] In striking contrast, minimal hysteresis is observed when using a

hydrophobic block comprising mainly poly(4-hydroxybutyl acrylate), which was attributed to the significantly greater mobility of the more flexible acrylic backbone.[67]

Of particular relevance to the present study, Derry *et al.* reported that poly(stearyl methacrylate)-poly(benzyl methacrylate) [PSMA-PBzMA] vesicles prepared by RAFT dispersion polymerisation of BzMA in mineral oil exhibited thermoresponsive behaviour on heating. More specifically, a 10% w/w dispersion of $PSMA_{13}$-$PBzMA_{96}$ vesicles underwent a vesicle-to-worm transition above 135 °C. Variable temperature ^{1}H NMR spectroscopy studies indicated that this change in copolymer morphology was the result of surface plasticisation of the membrane-forming PBzMA block by hot solvent, thereby effectively increasing the effective volume fraction of the stabiliser block and hence reducing the packing parameter for the copolymer chains.[64] In principle, this morphological transition might provide an interesting high temperature oil-thickening mechanism for automotive engine oils or cosmetics formulations.

In the present study, we revisit this PSMA-PBzMA system to examine what happens on heating well above the critical onset temperature required for the vesicle-to-worm transition. Moreover, we investigate whether statistical incorporation of an appropriate comonomer into the membrane-forming block (see **Scheme 2.1**) would enable tuning of the critical onset temperature required for a vesicle-to-worm transition. *n*-Butyl methacrylate (BuMA) was selected as a suitable comonomer. Given the relatively low glass transition temperature (T_g) of poly(*n*-butyl methacrylate),[68] this should enable the critical onset temperature required for the vesicle-to-worm transition to be tuned by statistical copolymerisation of BuMA with BzMA. In contrast, copolymerisation of BzMA with either methyl methacrylate or ethyl methacrylate would raise, rather than lower, the copolymer T_g. Moreover, statistical copolymerisation of lauryl

methacrylate with BzMA is also likely to be problematic because this could result in a soluble second block and hence no self-assembly behaviour.

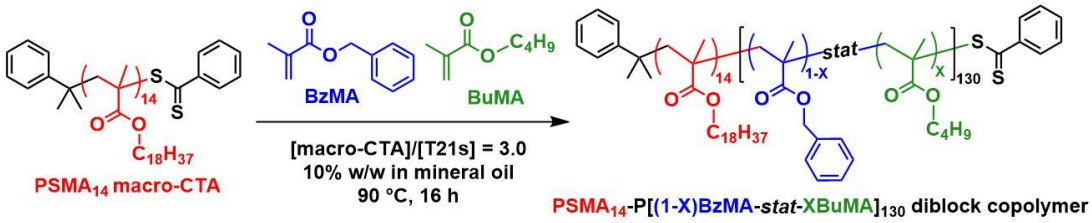

Scheme 2.1. Synthesis of a poly(stearyl methacrylate) (PSMA) diblock copolymer via RAFT dispersion copolymerisation of benzyl methacrylate (BzMA) and *n*-butyl methacrylate (BuMA) targeting 10% w/w solids in mineral oil at 90 °C. (*X denotes the mol fraction of n-butyl methacrylate making up the membrane-forming block (solvent insoluble block), and (1-X) the remaining mol fraction of benzyl methacrylate).*

2.2. Experimental

2.2.1. Materials

All reagents were purchased from Sigma-Aldrich (UK) at the highest possible purity and were used as received unless stated otherwise. *tert*-Butyl peroxy-2-ethylhexanoate (T21s) initiator was purchased from AzkoNobel (The Netherlands). Tetrahydrofuran (THF), *n*-dodecane and toluene were purchased from Fisher Scientific (UK). Deuterated methylene chloride (CD_2Cl_2) was purchased from Goss Scientific (UK). API Group III mineral oil (viscosity = 3.1 cSt at 100 °C) was kindly provided by The Lubrizol Corporation Ltd (Hazelwood, Derbyshire, UK).

2.2.2. Synthesis of poly(stearyl methacrylate)-poly(benzyl methacrylate) [PSMA-PBzMA] diblock copolymer vesicles

The poly(stearyl methacrylate) macromolecular chain transfer agent (PSMA macro-CTA) used in the initial studies reported herein was the same sample as that reported by Derry and co-workers in 2017, hence its synthetic protocol has been previously reported.[64] End-group analysis by ^{1}H NMR spectroscopy indicated a mean degree of polymerisation (DP) of 13. This $PSMA_{13}$ macro-CTA was then used for the synthesis

of $PSMA_{13}$-$PBzMA_{96}$ vesicles at 10% w/w solids in mineral oil *via* RAFT dispersion polymerisation of BzMA as described below. Benzyl methacrylate (BzMA; 0.226 g; 1.28 mmol), T21s initiator (0.555 mg; 2.57 μmol; dissolved at 10.0% v/v in mineral oil) and $PSMA_{13}$ macro-CTA (0.060 g; 12.8 μmol; macro-CTA/initiator molar ratio = 5.0; target PBzMA DP = 100) were dissolved in mineral oil (2.58 g). The reaction mixture was sealed in a 14 mL glass reaction vial and purged with nitrogen gas for 30 min. The deoxygenated solution was then placed in a pre-heated oil bath at 90 °C for 16 h (final BzMA conversion= 97 %; M_n= 19,900 g mol^{-1}, M_w/M_n= 1.10).

2.2.3. Synthesis of poly(stearyl methacrylate) macromolecular chain transfer agent (PSMA macro-CTA)

A second PSMA macro-CTA was synthesised by the RAFT solution polymerisation of stearyl methacrylate using the following protocol. Stearyl methacrylate (SMA; 30.7 g; 90.5 mmol), cumyl dithiobenzoate (CDB; 4.93 g; 18.1 mmol), 2,2'-azobisisobutyronitrile (AIBN; 594 mg; 3.6 mmol; CDB/AIBN molar ratio = 5.0) and toluene (54.2 g) were added to a 250 mL round-bottomed flask. The sealed vessel was purged with nitrogen for 30 min and placed in a pre-heated oil bath at 70 °C for 3.5 h. The resulting PSMA macro-CTA (SMA conversion = 85%; M_n = 6200 g mol^{-1}; M_w = 6900 g mol^{-1}; M_w/M_n = 1.12) was purified by precipitation into excess ethanol (twice). The mean DP of this macro-CTA was calculated to be 14 using ^{1}H NMR spectroscopy by comparing the integrated signals corresponding to the aromatic protons of the dithiobenzoate end-groups with those assigned to the two oxymethylene ester protons of the SMA repeat units. This is close to the mean DP of 13 reported by Derry *et al.*[64]

2.2.4. Synthesis of poly(stearyl methacrylate)-poly(benzyl methacrylate-stat-n-butyl methacrylate) diblock copolymer nanoparticles

A typical PISA synthesis of $PSMA_{14}$-P(0.5BzMA-*stat*-0.5BuMA)$_{130}$ nanoparticles via RAFT dispersion polymerisation at 10% w/w solids was conducted as follows. A 14 mL glass reaction vial was charged with $PSMA_{14}$ macro-CTA (0.060 g; 12.0 μmol) and mineral oil (2.78 g). The reaction mixture was placed in a 70 °C laboratory oven for 2 min to aid dissolution. On cooling to 20 °C, the vial was charged with benzyl methacrylate (BzMA; 0.137 g; 0.778 mmol; 50 mol%), *n*-butyl methacrylate (BuMA; 0.111 g, 0.778 mmol, 50 mol%) and T21s initiator (0.900 mg; 3.99 μmol; dissolved at 10% v/v in mineral oil; macro-CTA/initiator molar ratio = 3.0; target DP = 130). The reaction mixture was sealed and purged with nitrogen gas for 30 min with magnetic stirring. The deoxygenated solution was then placed in a pre-heated oil bath at 90 °C for 16 h (final BzMA conversion = 98%; final BuMA conversion = 92%; M_n = 21,600 g mol^{-1}; M_w/M_n = 1.10).

2.3. Characterisation

2.3.1. ^{1}H Nuclear Magnetic Resonance (NMR) spectroscopy

^{1}H NMR spectra were recorded in either CD_2Cl_2 (to determine the mean DP for the PSMA precursor) or $CDCl_3$ (for all other spectra) using a Bruker AV1-400 MHz spectrometer. Typically 64 scans were averaged per spectrum.

2.3.2. Gel Permeation Chromatography (GPC)

GPC was used to assess (co)polymer molecular weight distributions (MWDs). The GPC set-up comprised two 5 μm (30 cm) mixed C columns and a WellChrom K-2301 refractive index detector operating at 950 ± 30 nm. The THF mobile phase contained 2.0% v/v triethylamine and 0.05% w/v butylhydroxytoluene (BHT) with a toluene

flow-rate marker at a flow rate of 1.0 mL min^{-1}. A series of eleven near-monodisperse poly(methyl methacrylate) (PMMA) standards (M_p values ranging from 800 to 988 000 g mol^{-1}) were used for calibration.

2.3.3. Dynamic Light Scattering (DLS)

DLS studies were performed using a Zetasizer Nano ZS instrument (Malvern Instruments, UK) at a fixed scattering angle of 173°. Copolymer dispersions were diluted to 0.10% w/w using *n*-dodecane prior to light scattering studies at 25 °C. The intensity-average diameter and polydispersity were calculated by cumulants analysis of the experimental correlation function using Dispersion Technology Software version 6.20. Data were averaged over ten runs each of thirty seconds duration.

2.3.4. Transmission Electron Microscopy

TEM studies were conducted using a FEI Tecnai G2 spirit instrument operating at 80 kV and equipped with a Gatan 1k CCD camera. The relatively low glass transition temperature conferred by the *n*-butyl methacrylate comonomer (T_g of PBuMA homopolymer = 20 °C) made imaging more difficult compared to PSMA-PBzMA nano-objects.[64] Prolonged exposure to the high-energy electron beam during TEM studies can cause deformation and/or degradation of the copolymer nano-objects. To aid retention of the original nanoparticle morphology, 0.10% w/w copolymer dispersions were cooled to 3 °C before placing a single droplet onto pre-cooled carbon-coated copper grids and allowing to dry at 3 °C overnight within a laboratory refrigerator.[39] The next day the prepared grids were exposed to ruthenium(VIII) oxide vapor for 7 min at 20 °C prior to analysis. This heavy metal compound acts as a positive stain for the core-forming block to improve electron contrast. Ruthenium(VIII) oxide was prepared as follows: ruthenium(IV) oxide (0.30 g) was added to water (50 g) to form a black slurry; addition of sodium periodate (2.0 g) with

continuous stirring produced a yellow solution of ruthenium(VIII) oxide within 1 min at 20 °C. The 0.10% w/w dispersions of PSMA-PBzMA nano-objects (prepared by dilution using *n*-dodecane) were placed on grids at 20 °C and allowed to dry for 30 min before following the above staining protocol.

In order to study the thermally-induced morphological transitions, a sample vial containing two drops (approximately 30 mg) of a 10% w/w dispersion in mineral oil was placed in a pre-heated oil bath at the desired temperature (e.g. from 130 °C to 180 °C), allowed to equilibrate for 10 min, diluted with n-dodecane (preheated to the same temperature), and then allowed to dry on a grid following the protocol described above.

2.3.5. Oscillatory Rheology

An Anton Paar MCR502 rheometer equipped with a variable temperature Peltier plate and hood and a 50 mm 2° aluminium cone was used for all experiments. The distance between the cone and plate was 207 μm. The storage (*G'*) and loss (*G''*) moduli were measured as a function of temperature at a fixed strain of 1.0% and an angular frequency of 10 rad s^{-1}. The temperature was varied from 20-180-20 °C at a heating/cooling rate of 2 °C min^{-1}.

2.3.6. Shear-Induced Polarised Light Imaging (SIPLI)

The instrument design and general experimental set-up has been previously reported by Mykhaylyk and co-workers.[68] SIPLI experiments were conducted on a 10% w/w dispersion of $PSMA_{14}$-P(0.5BzMA-*stat*-0.5BuMA)$_{130}$ nano-objects in mineral oil at an applied shear rate of 200 s^{-1} on heating from 20 to 180 °C at a rate of 5 °C min^{-1}.

2.3.7. Small Angle X-ray Scattering (SAXS)

SAXS patterns were recorded at a synchrotron source (Diamond Light Source Ltd., Beamline I22, Didcot, Oxfordshire, UK) using monochromatic X-ray radiation (λ = 0.0995 nm, with q ranging from 0.002 to 2.0 nm^{-1}, where $q = 4\pi\sin\theta/\lambda$ is the length of the scattering vector and θ is one-half of the scattering angle) and a Dectris (Dectris AG, Switzerland) Pilatus P3 Hybrid silicon pixel detector. Glass capillaries of 2.0 mm diameter were used as a sample holder and the sample temperature was controlled using a HFSX350-CAP heating/cooling capillary holding stage (Linkam Scientific Instruments Ltd., Tadworth, UK), with 2 min being allowed for thermal equilibration prior to data collection. Scattering data were reduced using standard routines from the beamline[69] and were further analysed using Irena SAS macros for Igor Pro.[70] Water was used for the absolute intensity calibration. Measurements were conducted on a 1.0% w/w dispersion of either $PSMA_{13}$-$PBzMA_{97}$ or $PSMA_{14}$-P(0.5BzMA-*stat*-0.5BuMA)$_{130}$ nano-objects in mineral oil.

2.4. Results and Discussion

2.4.1. Synthesis and characterisation of $PSMA_{13}$-$PBzMA_{97}$ diblock copolymer vesicles

Using the same $PSMA_{13}$ macro-CTA as synthesised by Derry *et al.* and targeting the same diblock copolymer composition as previously reported,[64] $PSMA_{13}$-$PBzMA_{100}$ vesicles were targeted in mineral oil at 10% w/w solids. A BzMA conversion of 97% was achieved within 16 h at 90 °C, as judged by ^{1}H NMR spectroscopy, which agrees well with the 96% conversion achieved after 5 h at 90 °C in the original study. THF GPC analysis showed that the resulting diblock copolymer chains (M_n = 19,900 g mol^{-1}) exhibited a narrow molecular weight distribution

(M_w/M_n = 1.10) and the whole molecular weight distribution curve was well-shifted from that of the $PSMA_{13}$ macro-CTA (see **Figure 2.1**). These data suggest that good RAFT control and a high blocking efficiency was achieved. As expected, TEM studies indicated a predominantly vesicular morphology with a z-average diameter of 133 nm and a polydispersity of 0.09 being obtained by DLS studies (see **Figure 2.2(a)** and **Figure 2.2(c)**, respectively).

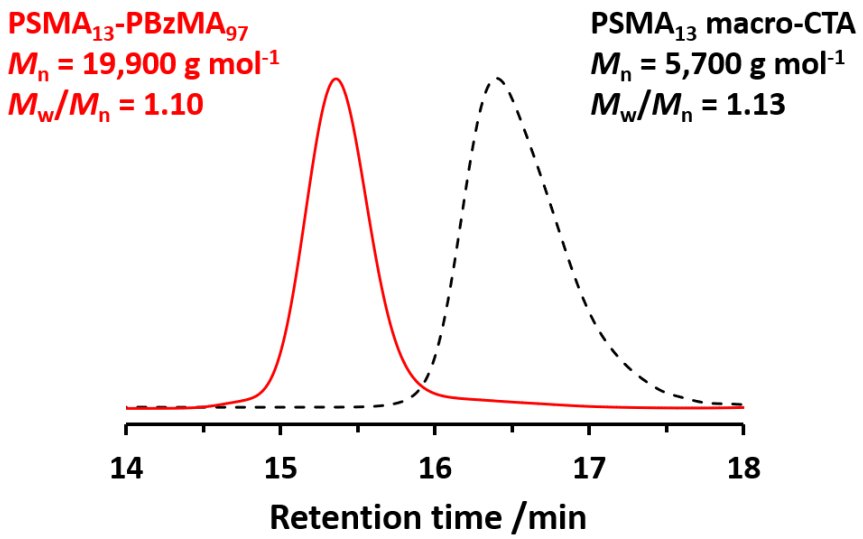

Figure 2.1. THF GPC traces recorded for $PSMA_{13}$-$PBzMA_{97}$ diblock copolymer chains and the corresponding $PSMA_{13}$ macro-CTA precursor.

SAXS studies on a 1% w/w dispersion at 20 °C produced the characteristic pattern expected for vesicles (see **Figure 2.2(a)**): the low q gradient is approximately –2 and there are local minima corresponding to the outer vesicle dimensions at $q \approx 0.005$ Å^{-1} and the vesicle membrane thickness, $T_{membrane}$, at $q \approx 0.05$ Å^{-1}. Fitting this SAXS pattern to a well-known vesicle model[71] gave an overall vesicle diameter, $D_{vesicle}$, of 103 ± 43 nm and a vesicle membrane thickness, $T_{membrane}$, of 9.8 ± 0.4 nm.

These data are in good agreement with TEM and DLS observations and are also close to values reported by Derry and co-workers for $PSMA_{13}$-$PBzMA_{96}$ vesicles characterised by SAXS at 20 °C.[64]

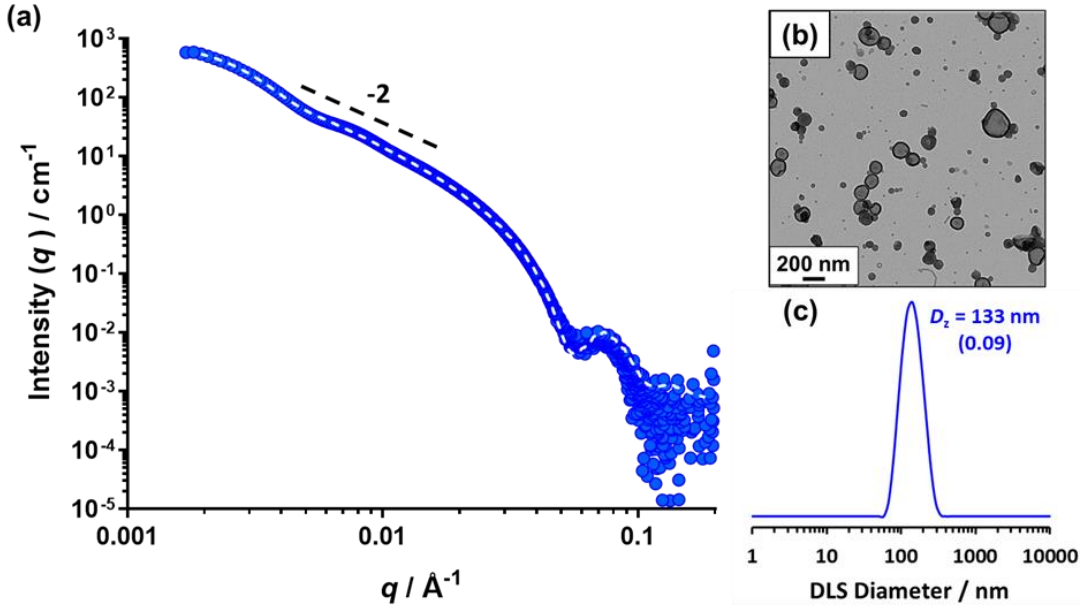

Figure 2.2. (a) Small-angle X-ray scattering (SAXS) pattern recorded for a 1.0% w/w dispersion of $PSMA_{13}$-$PBzMA_{97}$ vesicles in mineral oil at 20 °C. Dashed line to indicate the data fit obtained using the relevant vesicle scattering model. A gradient of –2 shown as a guide to the eye. **(b)** Representative TEM image and **(c)** DLS particle size distribution obtained for a 0.10% w/w dispersion of $PSMA_{13}$-$PBzMA_{97}$ vesicles at 20 °C.

2.4.2. Variable temperature studies of $PSMA_{13}$-$PBzMA_{97}$ diblock copolymer vesicles

The $PSMA_{13}$-$PBzMA_{96}$ vesicles reported by Derry and co-workers[64] exhibited thickening behaviour on heating owing to a vesicle-to-worm transition. However, Derry *et al.* did not explore the effect of heating well above the critical temperature required to induce this morphological transition.

The $PSMA_{13}$-$PBzMA_{97}$ vesicle dispersion prepared in this current study was investigated by oscillatory rheology. A temperature sweep from 20 °C to 190 °C was performed within the linear viscoelastic region (strain amplitude = 1.0 %, angular frequency = 10 rad s^{-1}) at a heating rate of 2 °C min^{-1}. The storage modulus (G') increases by more than five orders of magnitude on heating above 153 °C (see **Figure 2.3**). The cross-over of the storage and loss moduli, also known as the critical gelation

temperature (CGT), is observed at 155 °C, above which the dispersion acts as a viscoelastic gel (since *G'* > *G"*).

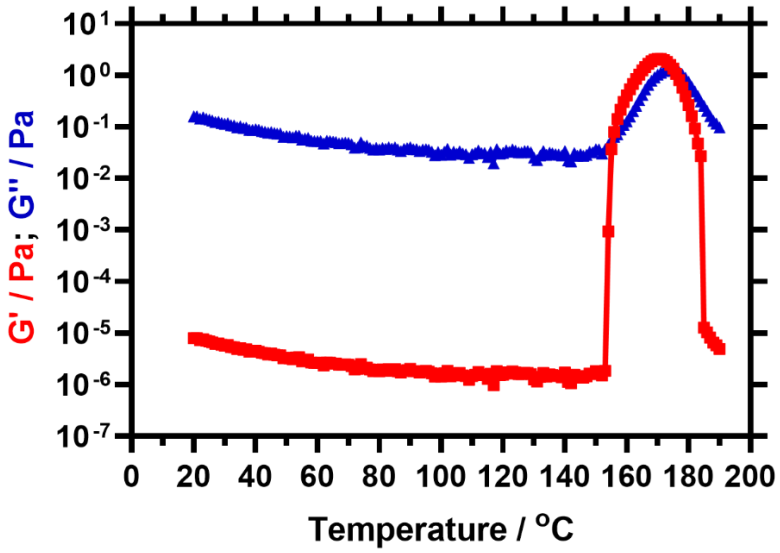

Figure 2.3. Temperature dependence of the storage modulus (*G'*, red squares) and loss modulus (*G"*, blue triangles) observed for a 10% w/w dispersion of $PSMA_{13}$-$PBzMA_{97}$ nano-objects in mineral oil when heating from 20 to 190 °C at 2 °C min^{-1}. This experiment was conducted at 1.0% strain and an angular frequency of 10 rad s^{-1}.

For TEM analysis, 10% w/w $PSMA_{13}$-$PBzMA_{97}$ dispersions were heated to the desired temperature prior to dilution to 0.1% w/w using *n*-dodecane that had been preheated to the same temperature. This sample preparation protocol was adopted to ensure kinetic trapping of the copolymer morphology produced at the designated elevated temperature.[64] The image taken of the sample prepared by this method at 150 °C indicated the presence of worms, thus confirming that the enhanced viscosity measured is the result of a thermally-induced vesicle-to-worm transition (see **Figure 2.4(a)** and **Figure 2.4(b)**). Since the original study by Derry *et al.* in 2017, we have demonstrated that the free-standing gels formed by block copolymer worms at ambient temperature most likely arise from multiple contacts between neighbouring worms, rather than from worm entanglements.[72] The same inter-worm interactions account for the enhanced dispersion viscosity observed in the present study.

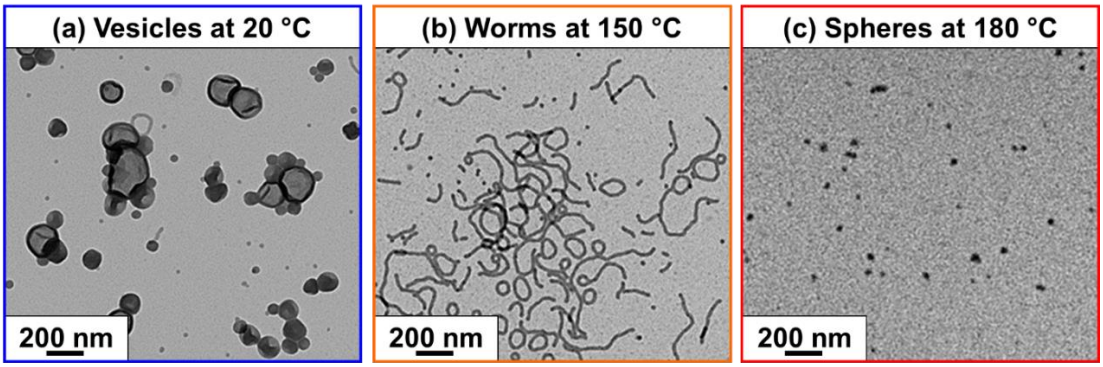

Figure 2.4. Transmission electron micrographs obtained for a 0.1% w/w dispersion of $PSMA_{13}$-$PBzMA_{97}$ nanoparticles showing **(a)** vesicles at 20 °C **(b)** worms at 150 °C and **(c)** spheres at 180 °C.

Interestingly, on further heating to 190 °C, a maximum value in *G'* is observed, followed by a substantial reduction in viscosity. TEM images recorded for a dilute $PSMA_{13}$-$PBzMA_{97}$ dispersion after drying at 180 °C confirm a predominantly spherical morphology under such conditions (see **Figure 2.4(c)**). This indicates a worm-to-sphere transition that is driven by further surface plasticisation of the structure-directing block.[37,54]

This is not the first time that a single diblock copolymer has been shown to exhibit all three common copolymer morphologies (i.e. spheres, worms and vesicles) simply by varying the solution temperature. We have recently published two examples of amphiphilic diblock copolymers that display this behaviour in aqueous solution.[66,67] Moreover, Lodge *et al.*, reported that a dilute solution of polystyrene-polydimethylsiloxane diblock copolymer nano-objects in diethyl phthalate underwent morphology transitions from vesicles to cylinders to spheres on heating.[73]

2.4.3. Synthesis of $PSMA_{14}$-P[(1-X)BzMA-stat-XBuMA]$_{130}$ diblock copolymer nanoparticles

A $PSMA_{14}$ macro-CTA was chain-extended via RAFT dispersion copolymerisation of benzyl methacrylate (BzMA) and *n*-butyl methacrylate (BuMA) to generate a series of $PSMA_{14}$-P[(1-*X*)BzMA-*stat*-*X*BuMA]$_{130}$ diblock copolymer nano-objects in mineral oil at 10% w/w solids (see **Scheme 2.1**).

It is perhaps worth mentioning that the overall target DP of the second insoluble structure-directing block was increased from 100 (as previously targeted for the $PSMA_{13}$-$PBzMA_{97}$ vesicles) up to 130. This was to account for the incorporation of the BuMA monomer (142 g mol^{-1}), which has a lower molecular weight than BzMA (176 g mol^{-1}). Otherwise, the reduction in the relative volume fraction of the structure-directing block would result in a lower packing parameter, *P*, and hence favor a worm morphology.[74]

A kinetic study of the synthesis of $PSMA_{14}$-P(0.5BzMA-*stat*-0.5BuMA)$_{130}$ vesicles via RAFT dispersion copolymerisation of BzMA with BuMA was conducted at 90 °C (see **Figure 2.5**). **Figure 2.5(a)** shows the individual conversion vs. time curves determined for the BzMA and BuMA comonomers respectively during their copolymerisation, as determined by ^{1}H NMR spectroscopy. Initially, up to 100 min, these two comonomers exhibit almost identical reactivities, suggesting a 50/50 random arrangement. On further polymerisation time, up to 200 min, BzMA reacts slightly faster than the BuMA, which is likely due to the relative solubilities of the two monomers in the core/oil (with BuMA more soluble in the oil). As a result, the resultant copolymer is expected to become BzMA rich.

Overall, these two comonomers exhibit comparable reactivities, suggesting a near-random copolymerisation. As shown in **Figure 2.5(b)**, an overall comonomer conversion of 94% was achieved within 6 h and the corresponding semi-logarithmic plot indicated a rate increase after 100 min, which corresponds to an overall comonomer conversion of approximately 40 %. There is likely to be both an effect of nucleation and the relative partitioning of the two monomers between the continuous and dispersed phases, as previously stated. Gel permeation chromatography (GPC) analysis indicated a linear evolution of molecular weight with conversion (**Figure 2.5(c)**). As a result, all RAFT dispersion copolymerisations reported herein were conducted at 90 °C for 16 h to maximise the comonomer conversion.

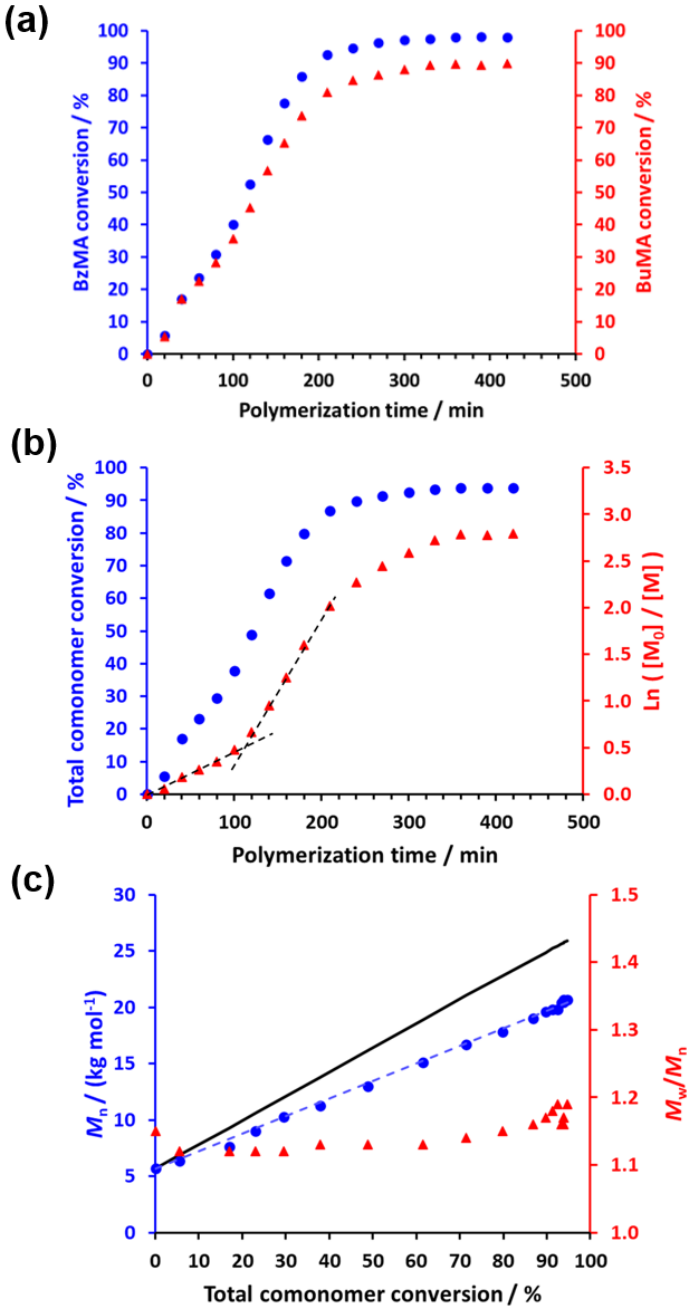

Figure 2.5. (a) BzMA monomer conversion vs. time curve (blue circles) and BuMA monomer conversion vs. time curve (red triangles). **(b)** Overall comonomer conversion vs. time curve (blue circles) and corresponding ln([M]$_0$/[M]) *vs.* time (red triangles) plot. **(c)** Evolution in M_n (blue circles) and M_w/M_n (red triangles) with comonomer conversion during the synthesis of PSMA$_{14}$-P(0.5BzMA-*stat*-0.5BuMA)$_{130}$ nanoparticles via RAFT dispersion copolymerisation of BzMA with BuMA at 90 °C when targeting 10% w/w solids in mineral oil. The theoretical M_n *vs.* overall comonomer conversion relationship is indicated by the black solid line for this series, with the difference being attributed to the GPC calibration error incurred by using poly(methyl methacrylate) standards.

An assigned ^{1}H NMR spectrum recorded for the final reaction mixture in $CDCl_3$ when targeting $PSMA_{14}$-P(0.5BzMA-*stat*-0.5BuMA)$_{130}$ at 10% w/w solids in mineral oil under such conditions is shown in **Figure 2.6**.

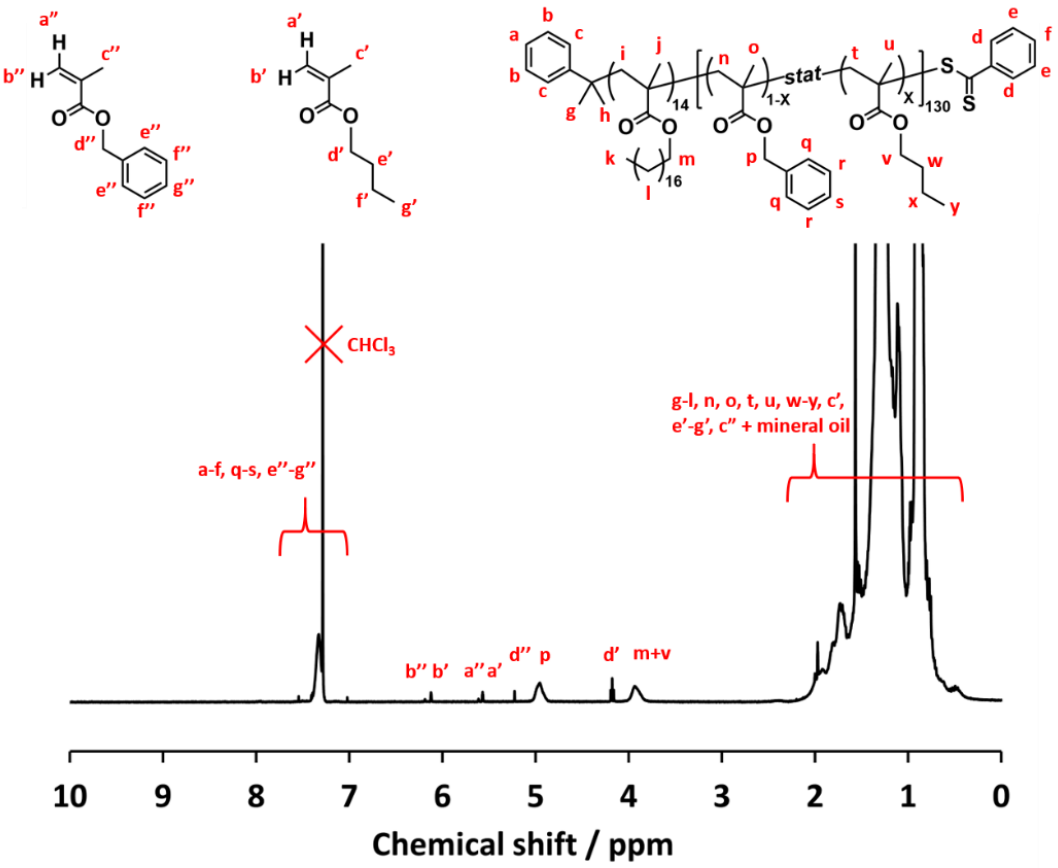

Figure 2.6. Assigned ^{1}H NMR spectrum obtained for the reaction mixture directly after the synthesis of $PSMA_{14}$-P(0.5BzMA-stat-0.5BuMA)$_{130}$ nanoparticles via RAFT dispersion copolymerisation of BzMA with BuMA at 90 °C when targeting 10% w/w solids in mineral oil (in $CDCl_3$).

The mole fraction of BuMA, *X*, was systematically varied, see **Table 2.1**. When targeting BuMA mole fractions of up to 0.70, ≥ 97% BzMA conversion and ≥ 89% BuMA conversion was achieved within 16 h at 90 °C, as judged by ^{1}H NMR spectroscopy. However, somewhat lower comonomer conversions were obtained when targeting a BuMA mole fraction of 0.80 (91% BzMA and 82% BuMA, respectively). The ^{1}H NMR spectra shown in **Figure 2.7** confirm that the structure-

directing block contains a higher proportion of BuMA relative to BzMA when increasing the target BuMA mole fraction from 0.30 to 0.50. THF GPC analysis confirmed that a relatively narrow molecular weight distribution was achieved in all cases ($M_w/M_n \leq 1.16$). Efficient chain extension was confirmed by the unimodal nature of the molecular weight distribution curves observed for such diblock copolymers, which were systematically shifted to higher molecular weight compared to that of the $PSMA_{14}$ precursor, see **Figure 2.8(a)**.

Table 2.1 Summary of Target Mole Fractions of *n*-Butyl Methacrylate, Monomer Conversions, Molecular Weights (M_n), Dispersities (M_w/M_n), Z-average Diameters (D_z), DLS Polydispersity Indices (PDI) and Copolymer Morphologies Obtained for $PSMA_{14}$-P[(1-*X*)BzMA-*stat*-*X*BuMA]$_{130}$ Diblock Copolymer Nano-Objects Prepared at 90 °C for 16 h Targeting 10% w/w Solids and a Core-forming Block DP of 130.

Target mole fraction BuMA (X)	^{1}H NMR[a]		THF GPC[b]		DLS[c]		TEM[d]
	BzMA conv. (%)	BuMA conv. (%)	M_n (g mol^{-1})	M_w/M_n	D_z (nm)	PDI	Predominant Morphology
0.00	97	n/a	23,500	1.09	94	0.07	Vesicles
0.10	97	92	22,000	1.11	112	0.06	Vesicles
0.20	97	90	21,800	1.11	141	0.06	Vesicles
0.30	98	92	21,500	1.12	198	0.24	Vesicles
0.35	98	92	21,300	1.13	208	0.22	Vesicles
0.40	97	91	21,300	1.12	305	0.23	Vesicles
0.45	97	90	20,800	1.11	236	0.21	Vesicles
0.50	98	92	21,600	1.10	318	0.21	Vesicles
0.60	97	89	19,900	1.14	251	0.31	Worms
0.70	97	89	19,800	1.16	113	0.19	Worms
0.80	91	82	16,800	1.14	28	0.09	Spheres

[a]Monomer conversions determined by ^{1}H NMR spectroscopy studies in $CDCl_3$. [b]Determined by THF GPC analysis using a refractive index detector and a series of near-monodisperse PMMA calibration standards. [c]Measurements made after appropriate dilution of the initial dispersion using n-dodecane. [d]Predominant copolymer morphology indicated by TEM analysis of dried copolymer dispersions at 20 °C after staining with ruthenium(VIII) oxide.

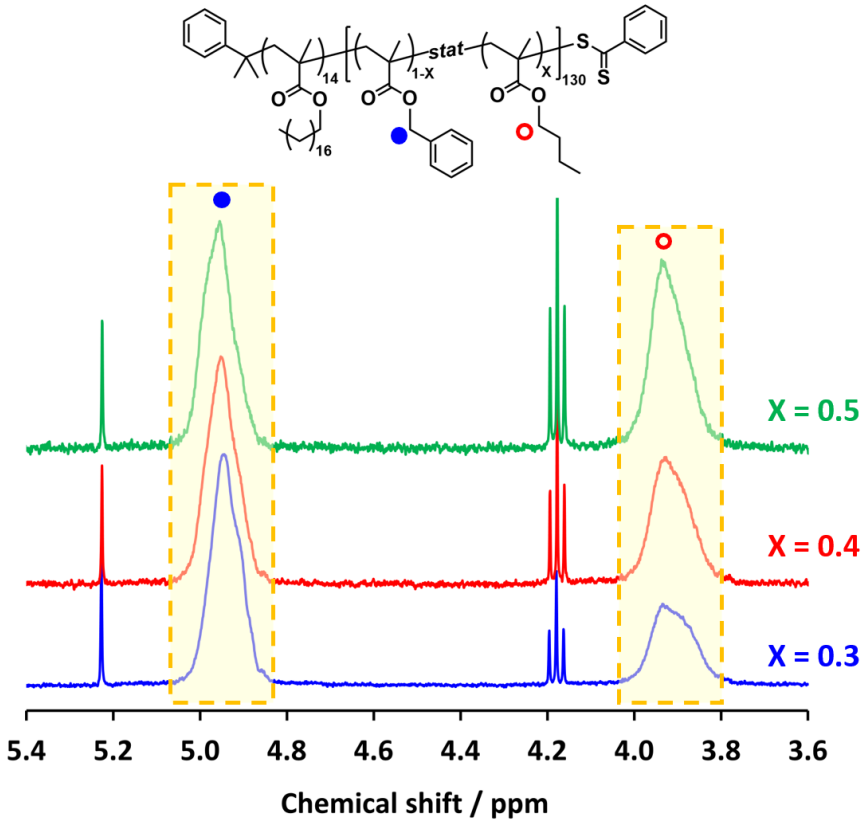

Figure 2.7. ^{1}H NMR spectra showing the relative proportion of BuMA comonomer to BzMA comonomer in the structure-directing block for PSMA$_{14}$-P[(1-X)BzMA-*stat*-XBuMA]$_{130}$ nanoparticles where the target mole fraction, *X*, is equal to 0.3 (blue trace), 0.4 (red trace) and 0.5 (green trace). The broad integral at 3.8 – 4.0 ppm corresponds to the two oxymethylene protons of PBuMA and the integral at 4.8 – 5.1 ppm corresponds to the two oxymethylene protons of PBzMA (see Fig. S3 for the fully assigned ^{1}H NMR spectrum).

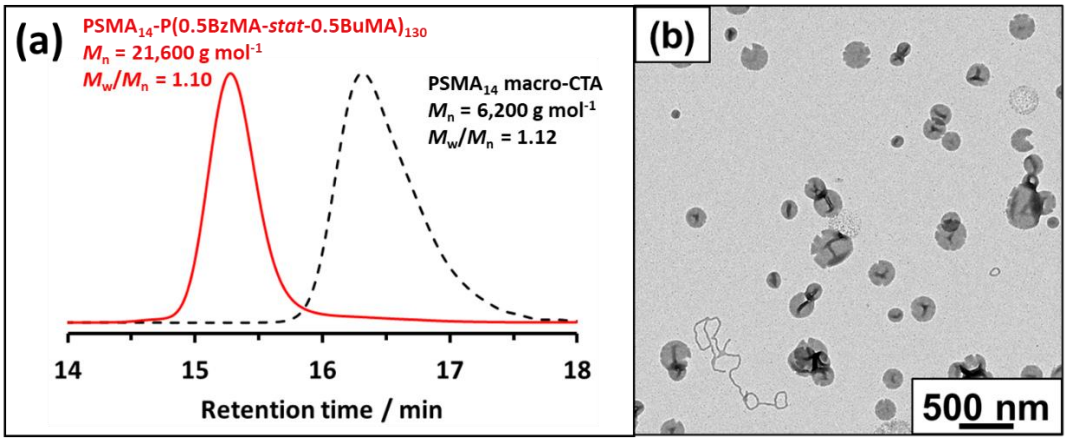

Figure 2.8. (a) THF GPC traces recorded for PSMA$_{14}$-P(0.5BzMA-*stat*-0.5BuMA)$_{130}$ and the corresponding PSMA$_{14}$ macro-CTA precursor. **(b)** representative TEM image recorded for a dried 0.1% w/w dispersion of PSMA$_{14}$-P(0.5BzMA-*stat*-0.5BuMA)$_{130}$ nano-objects at 20 °C showing predominantly vesicles and a few worms.

The predominant morphology for these diblock copolymer nano-objects was determined by TEM analysis (**Figure 2.9**), with DLS providing additional information regarding the particle size distribution. As expected based on the prior study by Derry and co-workers,[64] the $PSMA_{14}$-$PBzMA_{130}$ diblock copolymer formed well-defined vesicles with a number-average diameter of approximately 75 nm as judged by TEM, with DLS reporting a z-average diameter of 94 nm and a polydispersity index of 0.07.

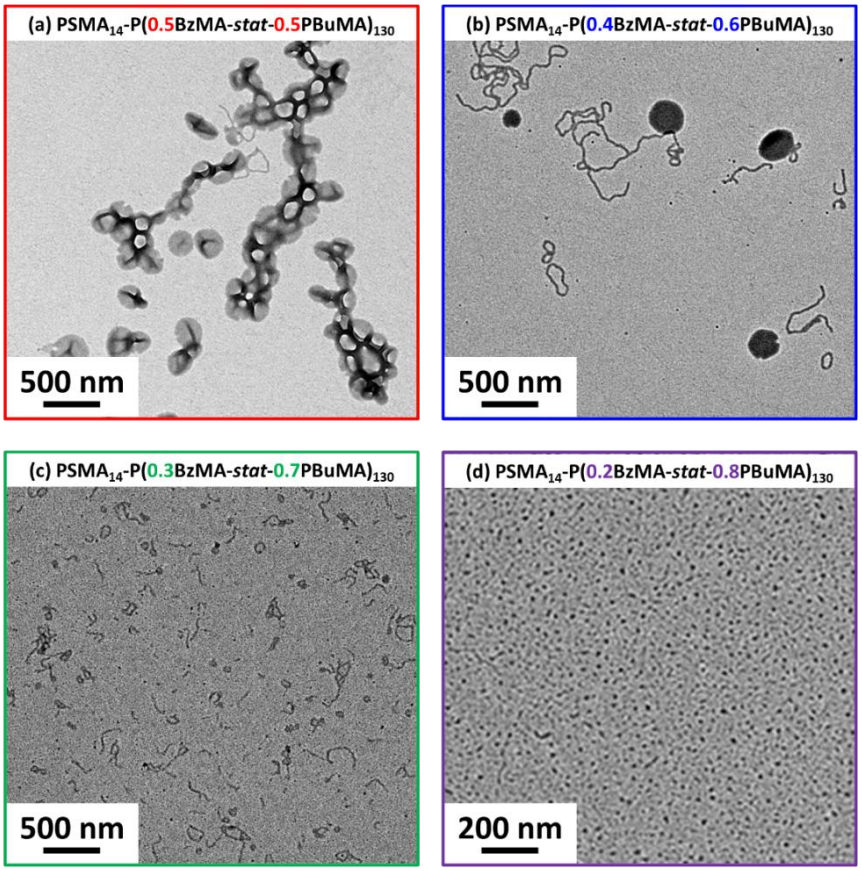

Figure 2.9. Representative TEM images at 20 °C for: **(a)** $PSMA_{14}$-P(0.5BzMA-stat-0.5BuMA)$_{130}$ vesicles (and a few worms), **(b)** $PSMA_{14}$-P(0.4BzMA-stat-0.6BuMA)$_{130}$ vesicles and worms, **(c)** $PSMA_{14}$-P(0.3BzMA-stat-0.7BuMA)$_{130}$ worms and **(d)** $PSMA_{14}$-P(0.8BzMA-stat-0.2BuMA)$_{130}$ spheres.

Introducing up to 45 mol% BuMA comonomer into the core-forming block produced progressively larger, more polydisperse vesicles, as judged by DLS (see **Table 2.1**). At 50 mol% BuMA, TEM (and DLS) studies revealed a mixed phase comprising predominantly vesicles with some worms (see **Figure 2.8(b)**). Moreover, further

increasing the BuMA content up to 60, 70 or 80 mol% produced mixed vesicle and worm, pure worm or spherical morphologies respectively, as judged by TEM. Again, this is because partial replacement of BzMA with the less massive BuMA comonomer reduces the relative volume fraction of the structure-directing block compared to that of the PSMA stabiliser. This lowers the packing parameter, *P*, for the copolymer chains, which in turn favors the worm or sphere morphology.[74]

2.4.4. Variable Temperature Rheology Studies of a Series of PSMA$_{14}$-P[(1-X)BzMA-stat-XBuMA]$_{130}$ Diblock Copolymer Vesicles

A series of five dispersions of PSMA$_{14}$-P[(1-X)BzMA-*stat*-XBuMA)]$_{130}$ vesicles (X = 0.30 to 0.50) were targeted at 10% w/w solids in mineral oil while systematically increasing the BuMA content within the membrane-forming block from 30 to 50 mol%. Each dispersion was characterised by oscillatory rheology and a 10% w/w dispersion of PSMA$_{14}$-PBzMA$_{125}$ vesicles was also evaluated as a reference sample. This target composition was preferred to PSMA$_{14}$-PBzMA$_{130}$ because its temperature-dependent behaviour was partially observable within the 20 °C to 180 °C range that could be accessed in rheology studies (**Figure 2.10(e)**).

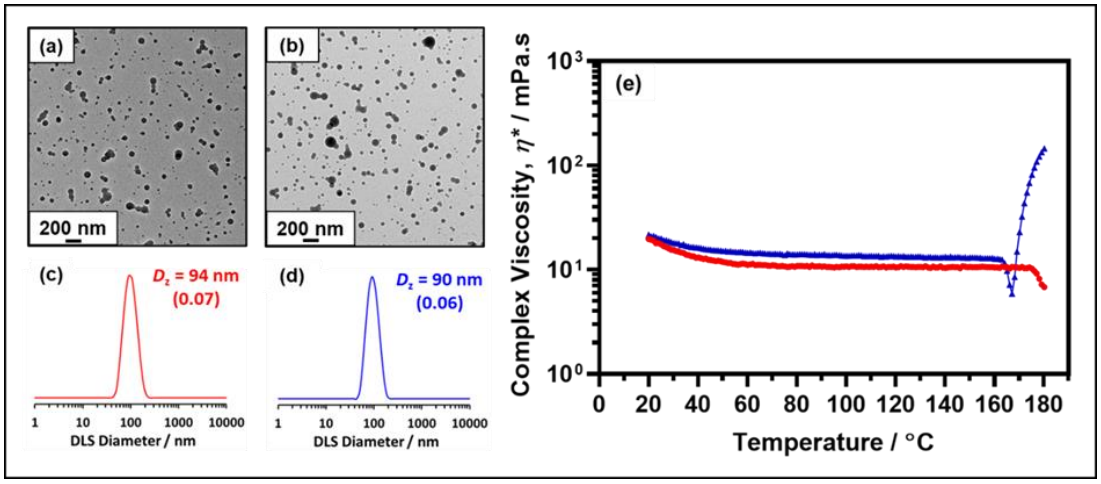

Figure 2.10. Representative TEM images at 20 °C for **(a)** block copolymer vesicles with target composition PSMA$_{14}$-PBzMA$_{130}$ and **(b)** block copolymer vesicles with target composition PSMA$_{14}$-PBzMA$_{125}$. Intensity-average particle diameter distribution obtained by DLS for a

0.10% w/w dispersion of **(c)** $PSMA_{14}$-$PBzMA_{130}$ vesicles and **(d)** $PSMA_{14}$-$PBzMA_{125}$ vesicles. **(e)** Temperature dependence of the complex viscosity (η^*) observed for $PSMA_{14}$-$PBzMA_{130}$ nanoparticles (red circles) and $PSMA_{14}$-$PBzMA_{130}$ nanoparticles (blue triangles) on heating from 20 °C to 180 °C at 2°C min^{-1}. Data were obtained at 1.0 % strain using an angular frequency of 10 rad s^{-1}.

A temperature sweep from 20 °C to 180 °C was performed within the linear viscoelastic region (strain amplitude = 1.0 %, angular frequency = 10 rad s^{-1}) at a heating rate of 2 °C min^{-1}. For all the vesicular dispersions studied, a sharp increase in complex viscosity (η^*) was observed on heating above 100 °C (see **Figure 2.11**). TEM analysis confirmed that, as first reported by Derry *et al.* and further investigated in the present publication for $PSMA_{13}$-$PBzMA_{97}$ vesicles, this enhanced viscosity is the result of a thermally-induced vesicle-to-worm transition.[64]

The data shown in **Figure 2.11** indicate that a series of complex viscosity maxima are observed on further heating. Moreover, the critical temperature required to reach these maximum values can be systematically lowered simply by increasing the relative proportion of BuMA comonomer. Unfortunately, the complex viscosity maximum for the $PSMA_{13}$-$PBzMA_{125}$ reference is not fully observable within the 20 °C to 180 °C range. However, if the *onset temperature* for the upturn in complex viscosity at 167 °C is used for comparative purposes, then targeting a membrane-forming block comprising 50 mol% BuMA lowers this critical temperature by almost 60 °C compared to the $PSMA_{13}$-$PBzMA_{125}$ reference vesicles. An even greater reduction in temperature is observed compared to $PSMA_{13}$-$PBzMA_{130}$ vesicles, for which an onset temperature of approximately 180 °C is predicted (**Figure 2.10**).

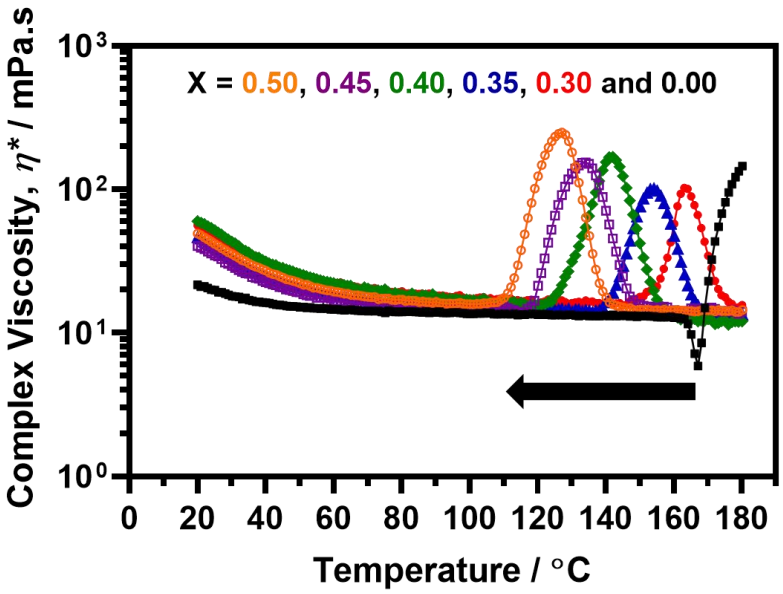

Figure 2.11. Temperature dependence of the complex viscosity (η^*) observed for a series of 10% w/w dispersions of $PSMA_{14}$-P(1-X)BzMA-*stat*-X$BuMA)_{130}$ nano-objects containing varying proportions of BuMA within the membrane-forming block on heating from 20 °C to 180 °C at 2 °C min^{-1}. Data were obtained at 1.0 % strain using an angular frequency of 10 rad s^{-1}. Data obtained for a reference sample of $PSMA_{14}$-$PBzMA_{125}$ vesicles are also shown (black filled squares). Then from right to left, target mole fraction of BuMA in membrane-forming block: 0.30 (red filled circles), 0.35 (dark blue filled triangles), 0.40 (green filled diamonds), 0.45 (purple open squares), and 0.50 (orange open circles).

Indeed, **Figure 2.12** confirms that there is a linear relationship between the critical temperature required to achieve maximum viscosity and the proportion of BuMA comonomer within the membrane-forming block. Strikingly, targeting a copolymer composition comprising 50 mol% BuMA lowered this critical temperature by 30 °C compared to when targeting a copolymer containing 30 mol% BuMA. This suggests that incorporating BuMA comonomer into the vesicle membrane facilitates its enhanced plasticisation by hot solvent (in this case, mineral oil), which in turn enables the vesicle-to-worm transition to occur at lower temperature.

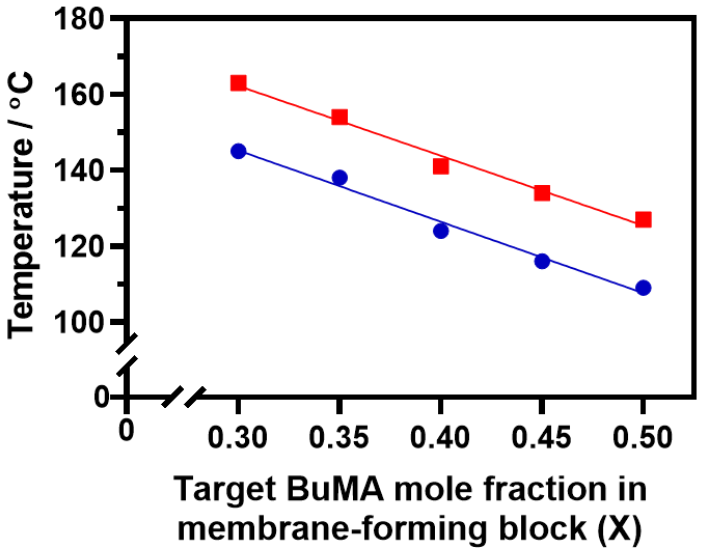

Figure 2.12. Effect of systematically varying the BuMA mole fraction of the membrane-forming block on **(i)** the critical temperature required to achieve maximum complex viscosity (red squares) and **(ii)** the corresponding critical onset temperature for this transition (blue circles) as indicated by oscillatory rheology studies of a series of $PSMA_{14}$-P[(1-X)BzMA-*stat*-XBuMA]$_{130}$ diblock copolymers.

As already noted above for the $PSMA_{13}$-$PBzMA_{97}$ diblock copolymer studied, a substantial *reduction* in complex viscosity is observed for each of the five diblock copolymers on heating well above the critical onset temperature required to induce the vesicle-to-worm transition. This finding is illustrated in **Figure 2.13**, which shows the temperature dependence of the storage modulus (G') and loss modulus (G'') for $PSMA_{14}$-P(0.5BzMA-*stat*-0.5BuMA)$_{130}$. At 20 °C, G'' (6.6 x 10^{-1} Pa) comfortably exceeds G' (3.3 x 10^{-5} Pa), which is typical for a free-flowing dispersion.

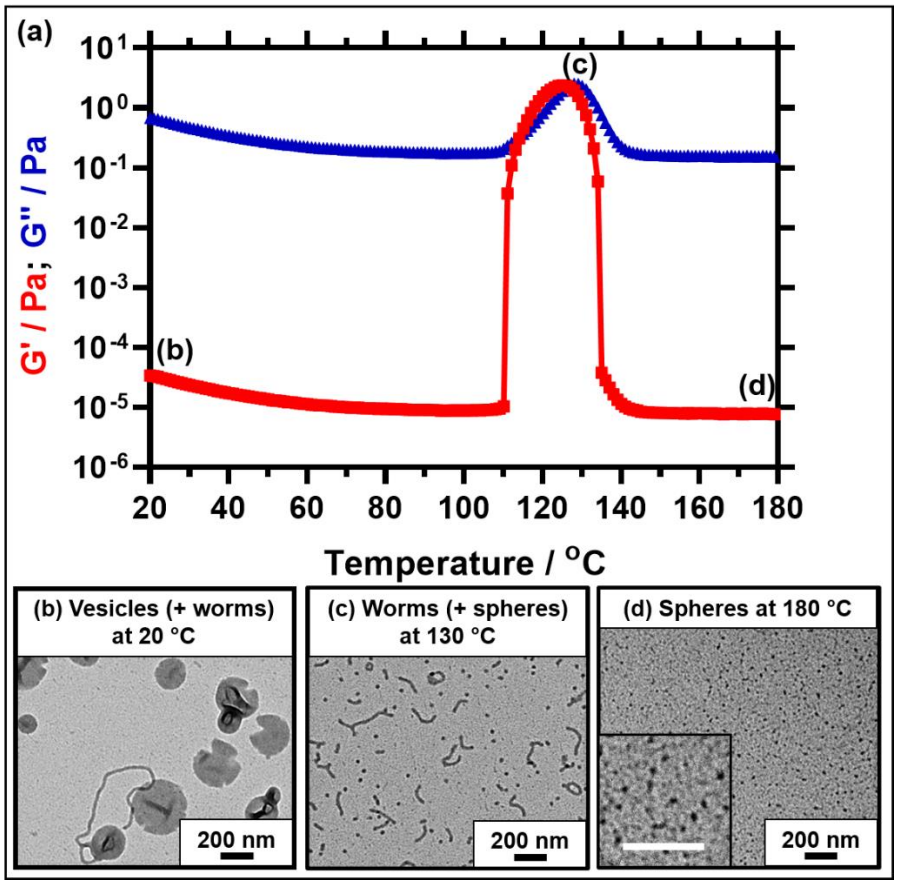

Figure 2.13. Temperature dependence of the storage modulus (*G'*, red squares) and loss modulus (*G''*, blue triangles) observed for a 10% w/w dispersion of $PSMA_{14}$-P(0.5BzMA-*stat*-0.5BuMA)$_{130}$ nano-objects in mineral oil when heating from 20 to 180 °C at 2 °C min^{-1}. This experiment was conducted at 1.0% strain and an angular frequency of 10 rad s^{-1}. Similar rheological data were obtained at a heating rate of 5 °C min^{-1} (data not shown). Representative TEM images recorded after drying 0.10% w/w dispersions of $PSMA_{14}$-P(0.5BzMA-*stat*-0.5BuMA)$_{130}$ nano-objects prepared at **(b)** 20 °C, **(c)** 130 °C and **(d)** 180 °C. All scale bars represent 200 nm.

There is an abrupt increase in G' at 109 °C, with a maximum G' of 2.5 Pa being observed at 128 °C. This latter value is five orders of magnitude greater than that measured at 20 °C and is comparable to the G' of ~ 1 Pa previously reported by Derry et al. for a 10% w/w dispersion of $PSMA_{13}$-$PBzMA_{96}$ nano-objects.[64] The cross-over between the G' and G'' curves occurs at 114 °C, which corresponds to the *critical gelation temperature* (CGT) and is comparable to the critical onset temperature indicated in **Figure 2.11**. G' exceeds G'' between 115 °C and 126 °C, which is characteristic of elastic, solid-like behaviour. On further heating, G' is substantially

reduced to around 8 x 10^{-6} Pa, which is comparable to that recorded at around 100 °C. This suggests that a second morphological transition occurs. Bearing mind the results obtained for the $PSMA_{13}$-$PBzMA_{97}$ system above, the obvious explanation is a worm-to-sphere transition driven by further surface plasticisation of the structure-directing block.[37,54]

Figure 2.13 shows three representative TEM images recorded for copolymer dispersions diluted to 0.1% w/w at 20 °C, 130 °C and 180 °C, as indicated by labels (a), (b) and (c) shown on the corresponding viscosity-temperature plot. At 20 °C, the predominant copolymer morphology is $PSMA_{14}$-P(0.5BzMA-*stat*-0.5BuMA)$_{130}$ vesicles, along with a few worms. Characteristic folds can be observed by TEM, which indicate vesicle collapse under the ultrahigh vacuum conditions required for this imaging technique. Interestingly, the edges of these vesicles have an unusual physical appearance that suggests an embrittlement effect. This may be the result of TEM grid preparation at 3 °C, which is well below the expected T_g for the membrane-forming block (PBuMA T_g = 20 °C; PBzMA T_g = 54 °C).[75] A mixed phase comprising relatively short worms and spheres is observed at 130 °C, while relatively small spheres are visible at 180 °C. These TEM observations are consistent with the rheological data. Further TEM analysis confirmed that these short worms remained stable for at least 1 h at 130 °C. It is also noteworthy that, for the image recorded at 130 °C, the mean worm width is comparable to the sphere diameter. This suggests that the spheres are generated *via* a budding mechanism from worm ends, as postulated by Fielding and co-workers.[54] Moreover, the spheres formed at 180 °C appear to be smaller than those obtained at 130 °C, which suggests a lower aggregation number. This is consistent with studies of thermally-annealed spherical nanoparticles prepared *via* PISA in non-polar media recently reported by Cornel *et al*.[76] This suggests that

these spherical nanoparticles are likely to be in equilibrium with the corresponding molecularly-dissolved copolymer chains at elevated temperature.[4,76,77]

To assess the thermal stability of the copolymer chains above 150 °C, a 10% w/w dispersion in mineral oil was subjected to a 20-180-20 °C thermal cycle and subsequently analysed by GPC using a refractive index detector. The chromatogram recorded for the thermally-annealed copolymer was very similar to that of the original copolymer prior to heating. (see **Figure 2.14**). This indicates that minimal copolymer degradation occurs on heating to 180 °C. Interestingly, GPC analysis of the same copolymer using a UV detector (λ = 302 nm) confirmed that 73% of its RAFT end-groups were removed during this thermal cycle. This is consistent with prior work by Moad and co-workers, who have demonstrated that thermolysis is a viable method for the removal of trithiocarbonate and dithiobenzoate end-groups from methacrylic polymers.[78,79]

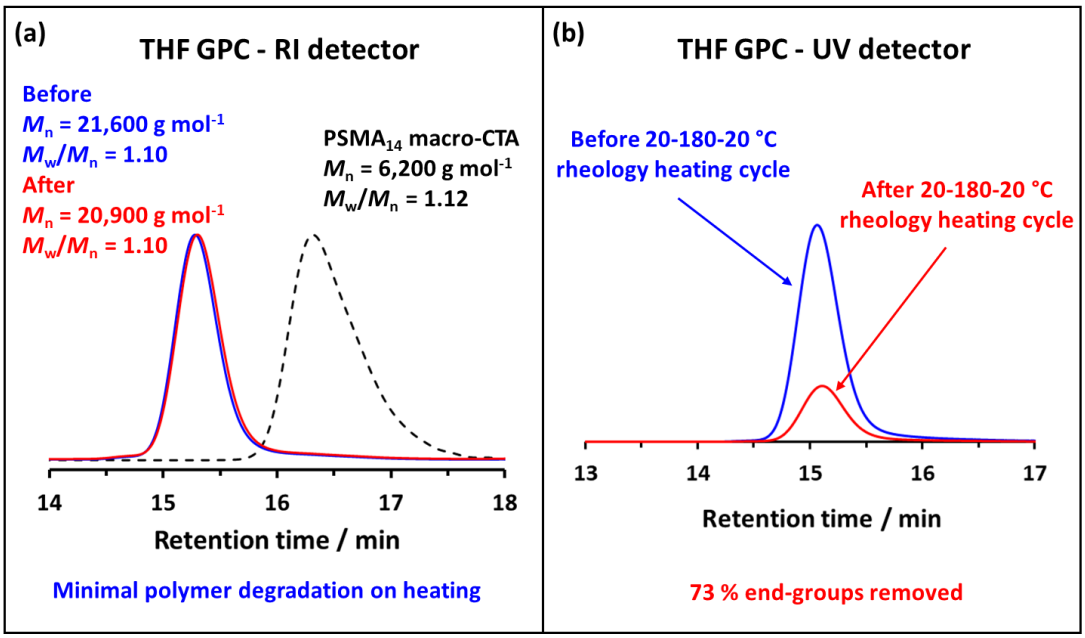

Figure 2.14. THF GPC analysis of PSMA$_{14}$-P(0.5BzMA-*stat*-0.5BuMA)$_{130}$ chains before (blue traces) and after (red traces) subjecting a 10% w/w dispersion of such diblock copolymer nano-objects in mineral oil to a 20-180-20 °C thermal cycle in a rheology experiment. (a) Refractive index (RI) detector with the PSMA$_{14}$ macro-CTA included as a reference. (b) UV detector set at λ = 302 nm.

The relatively low comonomer conversion (92%) achieved for BuMA when targeting PSMA$_{14}$-P(0.5BzMA-*stat*-0.5BuMA)$_{130}$ nano-objects was noted. However, an oscillatory rheology experiment conducted in the presence of an *additional* 8% unreacted BuMA confirmed that this comonomer had minimal effect on the thermal transitions reported herein (see **Figure 2.15**).

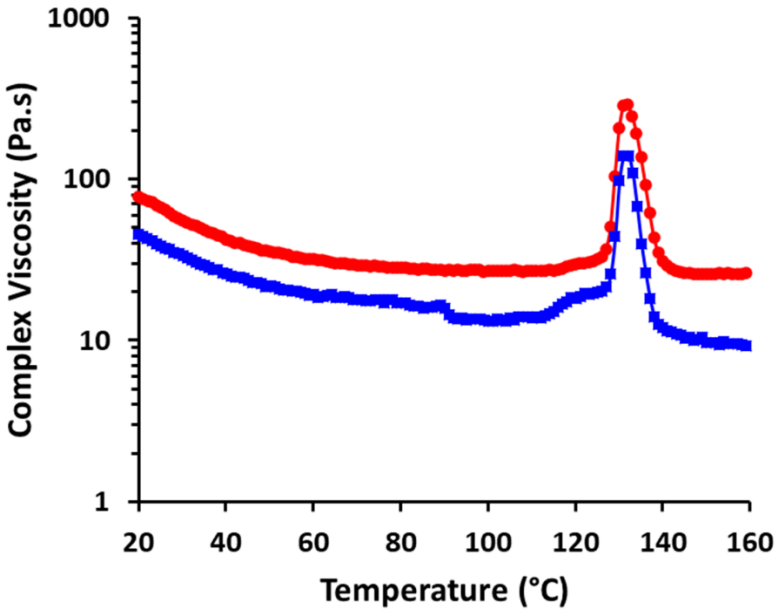

Figure 2.15. Temperature dependence of the complex viscosity (η^*) observed for PSMA$_{14}$-P(0.5BzMA-*stat*-0.5BuMA)$_{130}$ nano-objects on heating from 20 °C to 160 °C. Red circles indicate data obtained for an 'as-synthesised' 10% w/w dispersion of PSMA$_{14}$-P(0.5BzMA-*stat*-0.5BuMA)$_{130}$ nano-objects in mineral oil, (92% BuMA conversion, as determined by ^{1}H NMR spectroscopy). Blue squares indicate data obtained for an equivalent 10% w/w dispersion of PSMA$_{14}$-P(0.5BzMA-*stat*-0.5BuMA)$_{130}$ with post-polymerisation addition of the equivalent of 8% residual BuMA (thus doubling the mass of residual BuMA comonomer that is present). Clearly, the addition of BuMA comonomer has minimal effect on the observed behaviour.

The (ir)reversibility of the thermoresponsive morphological transitions was investigated by cooling a 10% w/w dispersion of PSMA$_{14}$-(0.5PBzMA-*stat*-0.5BuMA)$_{130}$ nano-objects to 20 °C immediately after an initial 20-180 °C heating ramp during the temperature-dependent oscillatory rheology studies. There was a significant increase in both the storage and loss moduli on cooling: G' increased by nine orders of magnitude, resulting in a turbid free-standing

gel (see **Figure 2.16**). TEM images recorded for this dispersion after this 20-180-20 °C thermal cycle indicated a mixture of vesicles and worms, with a significantly higher proportion of the latter nano-objects (see **Figure 2.16(b)** and **Figure 2.16(c)**). Similar observations were made after subjecting $PSMA_{13}$-$PBzMA_{97}$ vesicles to a thermal cycle.

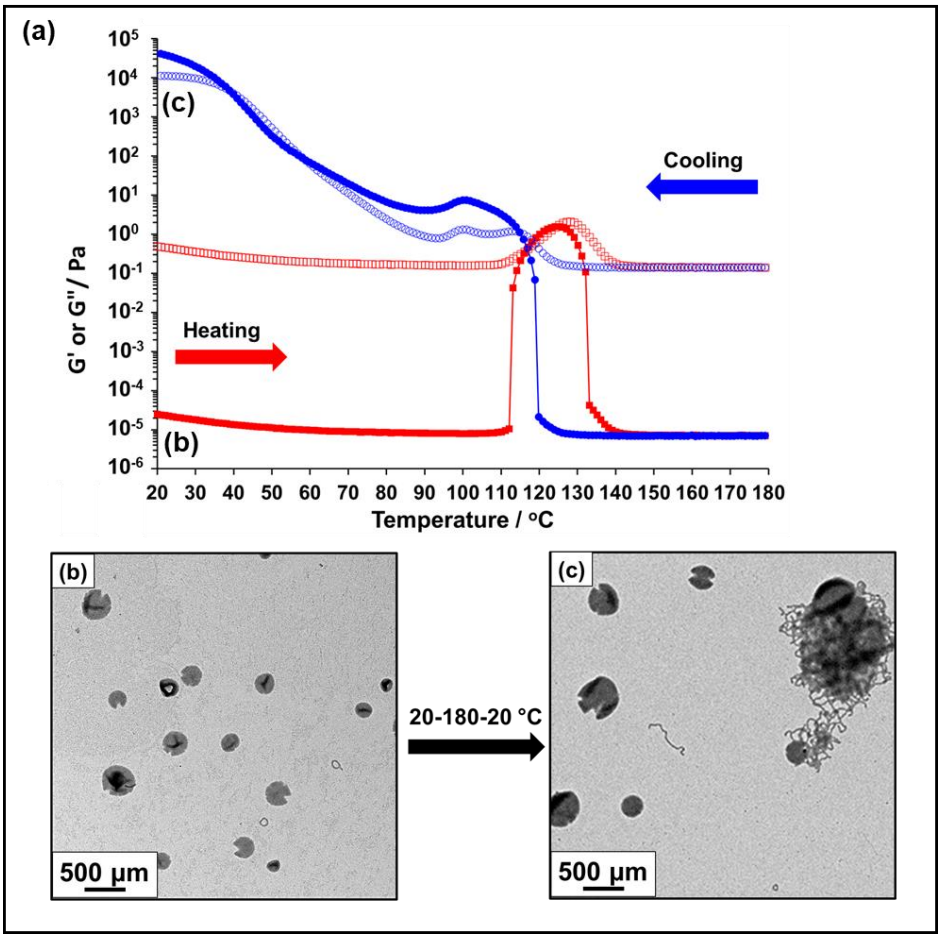

Figure 2.16. (a) Temperature dependence of the storage modulus (*G'*, red filled squares) and loss modulus (*G''*, red empty squares) observed for a 10% w/w dispersion of $PSMA_{14}$-P(0.5BzMA-*stat*-0.5BuMA)$_{130}$ nano-objects in mineral oil when heating from 20 to 180 °C at 2 °C min^{-1}. The storage and loss moduli were also recorded on cooling the sample back down to 20 °C at 2 °C min^{-1} (*G'* = blue filled circles and *G''* = blue empty circles). This experiment was conducted at 1.0% strain and an angular frequency of 10 rad s^{-1}. Representative TEM images recorded after drying 0.10% w/w dispersions of $PSMA_{14}$-P(0.5BzMA-*stat*-0.5BuMA)$_{130}$ nano-objects at 20 °C **(b)** before and **(c)** after the 20-180-20 °C thermal cycle.

2.4.5. Variable Temperature SIPLI Study

These morphological transitions were also examined using Shear-Induced Polarised Light Imaging (SIPLI). This technique combines rotational rheology with a polarised light source and has been recently used to demonstrate the *in situ* alignment of highly anisotropic nano-objects such as block copolymer worms at a certain critical rate of applied shear.[68] **Figure 2.17** shows how the viscosity of a 10% w/w dispersion of $PSMA_{14}$-P(0.5BzMA-stat-0.5BuMA)$_{130}$ nano-objects varies with temperature, along with representative digital images recorded at a constant shear rate at the stated temperatures.

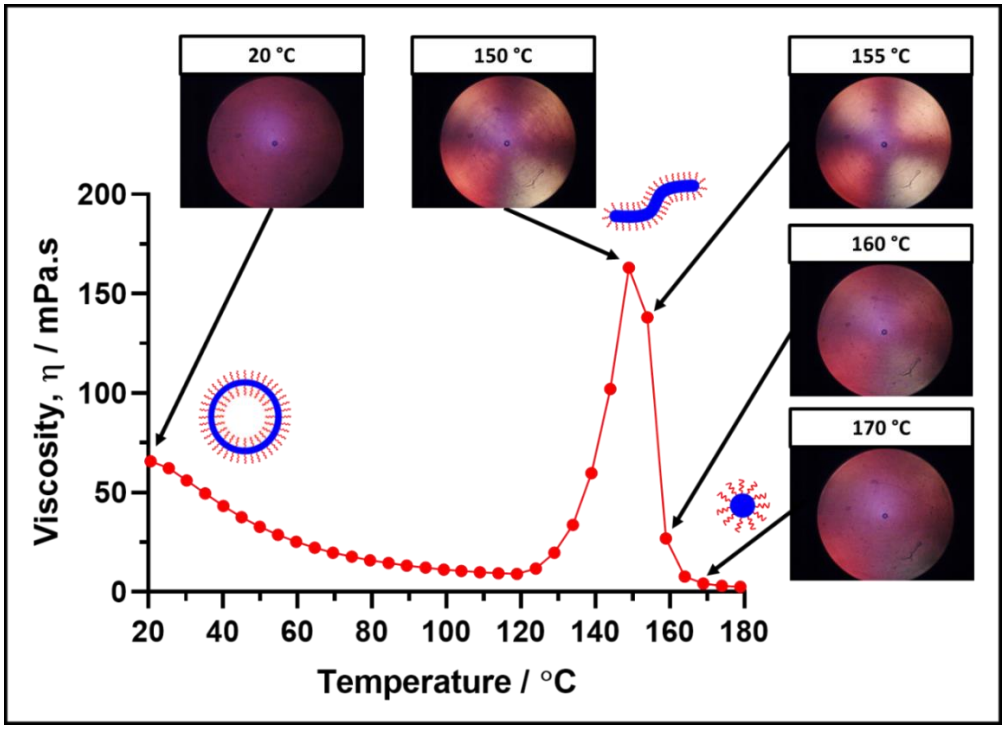

Figure 2.17. Temperature dependence of the dispersion viscosity and corresponding shear-induced polarised light images (SIPLI) recorded for a 10% w/w dispersion of $PSMA_{14}$-P(0.5BzMA-*stat*-0.5BuMA)$_{130}$ nano-objects on heating from 20 to 180 °C at a rate of 5 °C min^{-1}. Experimental conditions: shear rate = 200 s^{-1}, 0.50 mm sample gap.

The polarised light image recorded under constant shear at 20 °C appears dark and featureless because $PSMA_{14}$-P(0.5BzMA-*stat*-0.5BuMA)$_{130}$ forms isotropic vesicles at this temperature. In contrast, a distinctive Maltese cross is observed at the same

shear rate at 150 °C, which indicates the shear-induced alignment of anisotropic worms. This temperature approximately corresponds to that required for the maximum dispersion viscosity. This Maltese cross is also present at 155 °C, but becomes much fainter at 160 °C and has almost completely disappeared at 170 °C. This suggests that the anisotropic worms have been transformed into isotropic spheres at 170 °C.

It is noteworthy that the critical temperatures required to induce vesicle-to-worm and worm-to-sphere transitions suggested in **Figure 2.17** do not match those indicated by the oscillatory rheology data shown in **Figure 2.13**. In fact, these thermally-induced transitions occur at significantly lower temperatures (~20 °C) in the oscillatory rheology experiments. As recently postulated by Byard *et al.* for a similar doubly thermoresponsive diblock copolymer system, it seems likely that continuous applied shear facilitates both thermal transitions.[67] Moreover, a similar explanation has been proposed by Mendes and Menon for the vesicle-to-worm transition exhibited by small molecule surfactants.[59]

2.4.6. Variable Temperature SAXS Studies

SAXS patterns were recorded as a function of temperature for a 1.0% w/w dispersion of $PSMA_{14}$-P(0.5BzMA-*stat*-0.5BuMA)$_{130}$ vesicles originally prepared at 10% w/w solids (see **Figure 2.18**).

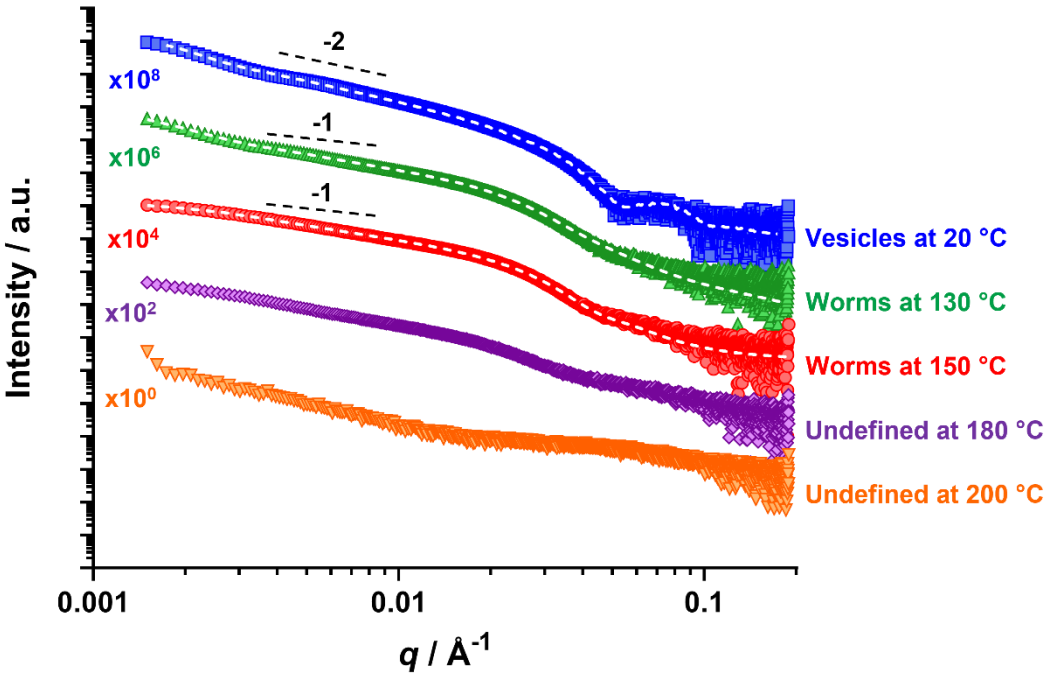

Figure 2.18. Representative SAXS patterns and data fits obtained for $PSMA_{14}$-P(0.5BzMA-*stat*-0.5BuMA)$_{130}$ vesicles at 20 °C (blue squares), $PSMA_{14}$-P(0.5BzMA-*stat*-0.5BuMA)$_{130}$ worms at 130 °C (green triangles) and at 150 °C (red circles). Dashed lines indicate the data fits obtained using the relevant scattering model. Gradients of –2 and -1 shown as a guide to the eye. The patterns recorded at 180 °C (purple diamonds) and 200 °C (orange upside-down triangles) could not be satisfactorily fitted using any of the scattering models presented herein.

The low *q* gradient in such *I(q)* vs. *q* plots (where *I(q)* is the scattering intensity and *q* is the scattering vector) is characteristic of the predominant copolymer morphology.[80] Thus the pattern recorded at 20 °C has a low *q* gradient of approximately –2 and can be satisfactorily fitted using an appropriate vesicle model.[71] In contrast, patterns recorded at 130 °C and 150 °C exhibit low *q* gradients of approximately –1 and can be satisfactorily fitted using a worm-like micelle model,[81] (the former pattern requires

incorporation of a unified fit to account for the slight upturn at low *q*,[82–84] which is an indication of worm branching). Thus, SAXS studies confirm the vesicle-to-worm transition for this statistical block copolymer system, which is consistent with TEM and SIPLI observations. However, SAXS patterns recorded at 180 °C and 200 °C could not be fitted using either spherical micelle or worm-like micelle models (see **Figure 2.18**). In this case, it seems likely that the worm-to-sphere transition was not observed because the time allowed for thermal equilibrium was too short. Moreover, the scattering pattern recorded at 200 °C shows some indication of dissolved chains at high *q*, however the full pattern could not be fitted using a dissolved chain model. Further experiments would be required to confirm this hypothesis but this is beyond the scope of the current study.

2.5. Conclusions

The thermoresponsive behaviour of $PSMA_{13}$-$PBzMA_{97}$ vesicles prepared by RAFT-mediated PISA at 10% w/w in mineral oil was revisited. Temperature-dependent rheology studies indicated a sharp reduction in the dispersion viscosity on heating above the critical temperature required for the previously reported vesicle-to-worm transition.[64] This is attributed to a subsequent worm-to-sphere transition owing to further surface plasticisation of the membrane-forming PBzMA block, which is supported by the TEM observation of spherical nanoparticles for this copolymer dispersion after heating to 180 °C.

Furthermore, the PISA synthesis of $PSMA_{14}$-$P(BzMA\text{-}\textit{stat}\text{-}BuMA)_{130}$ vesicles was achieved via RAFT dispersion copolymerisation of BuMA with BzMA when targeting 10% w/w solids in mineral oil. Introducing BuMA comonomer into the membrane-forming block significantly lowered the critical temperature required to induce a

vesicle-to-worm transition from 167 °C to 109 °C, as determined by oscillatory rheology. This morphological transition was confirmed by TEM, SIPLI and SAXS studies. A five-fold increase in *G′* was observed above the critical temperature, which is comparable to that previously reported for $PSMA_{13}$-$PBzMA_{96}$ vesicles.[64] In principle, lowering this critical temperature should enable a wider range of oil-thickening applications to be explored. In practice, higher final comonomer conversions are certainly desirable prior to commercial exploitation. However, we note that residual comonomer appears to have minimal effect on the behaviour of these thermoresponsive block copolymer nano-objects.

The thermal transitions reported herein proved to be irreversible on cooling within normal experimental timescales (hours). Moreover, the 10% w/w $PSMA_{14}$-$P(0.5BzMA\text{-}stat\text{-}0.5BuMA)_{130}$ dispersion exhibited a significantly greater viscosity after a 20-180-20 °C thermal cycle compared to the original vesicle dispersion. TEM analysis of the annealed dispersion revealed a mixture of worms and vesicles at 20 °C. It is perhaps noteworthy that such irreversibility may be advantageous for certain applications if a permanent thickening effect is desired.

2.6. References

1 Y. Mai and A. Eisenberg, *Chem. Soc. Rev.*, 2012, **41**, 5969–5985.

2 M. Matsuo, T. Ueno, H. Horino, S. Chujyo and H. Asai, *Polymer*, 1968, **9**, 425–436.

3 J. Liu, Z. J. Thompson, H. J. Sue, F. S. Bates, M. A. Hillmyer, M. Dettloff, G. Jacob, N. Verghese and H. Pham, *Macromolecules*, 2010, **43**, 7238–7243.

4 D. J. Growney, O. O. Mykhaylyk and S. P. Armes, *Langmuir*, 2014, **30**, 6047–6056.

5 S. Creutz, R. Jérôme, G. M. P. Kaptijn, A. W. Van Der Werf and J. M. Akkerman, *J. Coatings Technol.*, 1998, **70**, 41–46.

6 Y. Geng, P. Dalhaimer, S. Cai, R. Tsai, M. Tewari, T. Minko and D. E. Discher, *Nat. Nanotechnol.*, 2007, **2**, 249–255.

7 K. A. Simon, N. J. Warren, B. Mosadegh, M. R. Mohammady, G. M. Whitesides and S. P. Armes, *Biomacromolecules*, 2015, **16**, 3952–3958.

8 I. Canton, N. J. Warren, A. Chahal, K. Amps, A. Wood, R. Weightman, E. Wang, H. Moore and S. P. Armes, *ACS Cent. Sci.*, 2016, **2**, 65–74.

9 L. Zhang and A. Eisenberg, *Science*, 1995, **268**, 1728–1731.

10 P. L. Soo and A. Eisenberg, *J. Polym. Sci. Part B Polym. Phys.*, 2004, **42**, 923–938.

11 V. Bütün, S. . Armes and N. . Billingham, *Polymer*, 2001, **42**, 5993–6008.

12 F. Liu and A. Eisenberg, *J. Am. Chem. Soc.*, 2003, **125**, 15059–15064.

13 D. R. Arifin and A. F. Palmer, *Biomacromolecules*, 2005, **6**, 2172–2181.

14 J. R. Howse, R. A. L. Jones, G. Battaglia, R. E. Ducker, G. J. Leggett and A. J. Ryan, *Nat. Mater.*, 2009, **8**, 507–511.

15 B. Charleux, G. Delaittre, J. Rieger and F. D'Agosto, *Macromolecules*, 2012, **45**, 6753–6765.

16 S. L. Canning, G. N. Smith and S. P. Armes, *Macromolecules*, 2016, **49**, 1985–2001.

17 D. Le, D. Keller and G. Delaittre, *Macromol. Rapid Commun.*, 2019, **40**, 1800551.

18 N. J. W. Penfold, J. Yeow, C. Boyer and S. P. Armes, *ACS Macro Lett.*, 2019, **8**, 1029–1054.

19 C. Liu, C.-Y. Hong and C.-Y. Pan, *Polym. Chem.*, 2020, **11**, 3673–3689.

20 J. N. Israelachvili, D. J. Mitchell and B. W. Ninham, *J. Chem. Soc. - Faraday Trans.*, 1976, **72**, 1525–1568.

21 E. J. Cornel, S. van Meurs, T. Smith, P. S. O'Hora and S. P. Armes, *J. Am. Chem. Soc.*, 2018, **140**, 12980–12988.

22 O. J. Deane, O. M. Musa, A. Fernyhough and S. P. Armes, *Macromolecules*, 2020, **53**, 1422–1434.

23 S. J. Byard, M. Williams, B. E. McKenzie, A. Blanazs and S. P. Armes, *Macromolecules*, 2017, **50**, 1482–1493.

24 N. J. W. Penfold, J. R. Whatley and S. P. Armes, *Macromolecules*, 2019, **52**, 1653–1662.

25 C. Gonzato, M. Semsarilar, E. R. Jones, F. Li, G. J. P. Krooshof, P. Wyman, O. O. Mykhaylyk, R. Tuinier and S. P. Armes, *J. Am. Chem. Soc.*, 2014, **136**, 11100–11106.

26 R. R. Gibson, E. J. Cornel, O. M. Musa, A. Fernyhough and S. P. Armes, *Polym. Chem.*, 2020, **11**, 1785–1796.

27 P. Yang, L. P. D. Ratcliffe and S. P. Armes, *Macromolecules*, 2013, **46**, 8545–8556.

28 X. Wang, J. Zhou, X. Lv, B. Zhang and Z. An, *Macromolecules*, 2017, **50**, 7222–7232.

29 A. Blanazs, J. Madsen, G. Battaglia, A. J. Ryan and S. P. Armes, *J. Am. Chem. Soc.*, 2011, **133**, 16581–16587.

30 M. J. Derry, L. A. Fielding and S. P. Armes, *Polym. Chem.*, 2015, **6**, 3054–3062.

31 E. R. Jones, M. Semsarilar, P. Wyman, M. Boerakker and S. P. Armes, *Polym. Chem.*, 2016, **7**, 851–859.

32 C. J. Ferguson, R. J. Hughes, D. Nguyen, B. T. T. Pham, R. G. Gilbert, A. K. Serelis, C. H. Such and B. S. Hawkett, *Macromolecules*, 2005, **38**, 2191–2204.

33 W.-M. Wan, C.-Y. Hong and C.-Y. Pan, *Chem. Commun.*, 2009, 5883.

34 W. M. Wan, X. L. Sun and C. Y. Pan, *Macromolecules*, 2009, **42**, 4950–4952.

35 L. A. Fielding, M. J. Derry, V. Ladmiral, J. Rosselgong, A. M. Rodrigues, L. P. D. Ratcliffe, S. Sugihara and S. P. Armes, *Chem. Sci.*, 2013, **4**, 2081–2087.

36 Y. Pei, O. R. Sugita, L. Thurairajah and A. B. Lowe, *RSC Adv.*, 2015, **5**, 17636–17646.

37 Y. Pei, L. Thurairajah, O. R. Sugita and A. B. Lowe, *Macromolecules*, 2015, **48**, 236–244.

38 E. Guégain, C. Zhu, E. Giovanardi and J. Nicolas, *Macromolecules*, 2019, **52**, 3612–3624.

39 M. J. Rymaruk, S. J. Hunter, C. T. O'Brien, S. L. Brown, C. N. Williams and S. P. Armes, *Macromolecules*, 2019, **52**, 2822–2832.

40 M. J. Rymaruk, C. T. O'Brien, S. L. Brown, C. N. Williams and S. P. Armes, *Macromolecules*, 2020, **53**, 1785–1794.

41 Q. Zhang and S. Zhu, *ACS Macro Lett.*, 2015, **4**, 755–758.

42 V. J. Cunningham, A. M. Alswieleh, K. L. Thompson, M. Williams, G. J. Leggett, S. P. Armes and O. M. Musa, *Macromolecules*, 2014, **47**, 5613–5623.

43 M. Destarac, *Polym. Chem.*, 2018, **9**, 4947–4967.

44 G. Wang, M. Schmitt, Z. Wang, B. Lee, X. Pan, L. Fu, J. Yan, S. Li, G. Xie, M. R. Bockstaller and K. Matyjaszewski, *Macromolecules*, 2016, **49**, 8605–8615.

45 K. Wang, Y. Wang and W. Zhang, *Polym. Chem.*, 2017, **8**, 6407–6415.

46 M. Obeng, A. H. Milani, M. S. Musa, Z. Cui, L. A. Fielding, L. Farrand, M. Goulding and B. R. Saunders, *Soft Matter*, 2017, **13**, 2228–2238.

47 C. Dire, S. Magnet, L. Couvreur and B. Charleux, *Macromolecules*, 2009, **42**, 95–103.

48 A. Darabi, A. R. Shirin-Abadi, J. Pinaud, P. G. Jessop and M. F. Cunningham, *Polym. Chem.*, 2014, **5**, 6163–6170.

49 A. Darabi, P. G. Jessop and M. F. Cunningham, *Macromolecules*, 2015, **48**, 1952–1958.

50 M. Lansalot and J. Rieger, *Macromol. Rapid Commun.*, 2019, **40**, 1800885.

51 X. Wang and Z. An, *Macromol. Rapid Commun.*, 2019, **40**, 1800325.

52 F. D'Agosto, J. Rieger and M. Lansalot, *Angew. Chemie - Int. Ed.*, 2020, **59**, 8368–8392.

53 Y. Pei, N. C. Dharsana, J. A. Van Hensbergen, R. P. Burford, P. J. Roth and A. B. Lowe, *Soft Matter*, 2014, **10**, 5787–5796.

54 L. A. Fielding, J. A. Lane, M. J. Derry, O. O. Mykhaylyk and S. P. Armes, *J. Am. Chem. Soc.*, 2014, **136**, 5790–5798.

55 A. Blanazs, R. Verber, O. O. Mykhaylyk, A. J. Ryan, J. Z. Heath, C. W. I. Douglas and S. P. Armes, *J. Am. Chem. Soc.*, 2012, **134**, 9741–9748.

56 R. Verber, A. Blanazs and S. P. Armes, *Soft Matter*, 2012, **8**, 9915–9922.

57 J. Tan, Y. Bai, X. Zhang and L. Zhang, *Polym. Chem.*, 2016, **7**, 2372–2380.

58 J. R. Lovett, M. J. Derry, P. Yang, F. L. Hatton, N. J. Warren, P. W. Fowler and S. P. Armes, *Chem. Sci.*, 2018, **9**, 7138–7144.

59 E. Mendes and S. V. G. Menon, *Chem. Phys. Lett.*, 1997, **275**, 477–484.

60 H. M. L. Davies and J. R. Manning, *J. Am. Chem. Soc.*, 2006, **128**, 1060–1061.

61 N. J. Warren and S. P. Armes, *J. Am. Chem. Soc.*, 2014, **136**, 10174–10185.

62 J. R. Lovett, N. J. Warren, S. P. Armes, M. J. Smallridge and R. B. Cracknell, *Macromolecules*, 2016, **49**, 1016–1025.

63 R. Deng, Y. Ning, E. R. Jones, V. J. Cunningham, N. J. W. Penfold and S. P. Armes, *Polym. Chem.*, 2017, **8**, 5374–5380.

64 M. J. Derry, O. O. Mykhaylyk and S. P. Armes, *Angew. Chemie - Int. Ed.*, 2017, **56**, 1746–1750.

65 R. Deng, M. J. Derry, C. J. Mable, Y. Ning and S. P. Armes, *J. Am. Chem. Soc.*, 2017, **139**, 7616–7623.

66 L. P. D. Ratcliffe, M. J. Derry, A. Ianiro, R. Tuinier and S. P. Armes, *Angew. Chemie Int. Ed.*, 2019, **58**, 18964–18970.

67 S. J. Byard, C. T. O'Brien, M. J. Derry, M. Williams, O. O. Mykhaylyk, A. Blanazs and S. P. Armes, *Chem. Sci.*, 2020, **11**, 396–402.

68 O. O. Mykhaylyk, N. J. Warren, A. J. Parnell, G. Pfeifer and J. Laeuger, *J. Polym. Sci. Part B Polym. Phys.*, 2016, **54**, 2151–2170.

69 B. R. Pauw, A. J. Smith, T. Snow, N. J. Terrill and A. F. Thünemann, *J. Appl. Crystallogr.*, 2017, **50**, 1800–1811.

70 J. Ilavsky and P. R. Jemian, *J. Appl. Crystallogr.*, 2009, **42**, 347–353.

71 J. Bang, S. Jain, Z. Li, T. P. Lodge, J. S. Pedersen, E. Kesselman and Y. Talmon, *Macromolecules*, 2006, **39**, 5583.

72 J. R. Lovett, M. J. Derry, P. Yang, F. L. Hatton, N. J. Warren, P. W. Fowler and S. P. Armes, *Chem. Sci.*, 2018, **9**, 7138–7144.

73 S. Abbas, Z. Li, H. Hassan and T. P. Lodge, *Macromolecules*, 2007, **40**, 4048–4052.

74 K. E. B. Doncom, L. D. Blackman, D. B. Wright, M. I. Gibson and R. K. O'Reilly, *Chem. Soc. Rev.*, 2017, **46**, 4119–4134.

75 W. A. Lee and R. A. Rutherford, in *Polymer Handbook*, eds. J. Brandrup and E. H. Immergut, Wiley, Second Edn., 1975, pp. 111–147.

76 E. J. Cornel, G. N. Smith, S. E. Rogers, J. E. Hallett, D. J. Growney, T. Smith, P. S. O'Hora, S. Van Meurs, O. O. Mykhaylyk and S. P. Armes, *Soft Matter*, 2020, **16**, 3657–3668.

77 E. J. Cornel, P. S. O'Hora, T. Smith, D. J. Growney, O. O. Mykhaylyk and S. P. Armes, *Chem. Sci.*, 2020, **11**, 4312–4321.

78 A. Postma, T. P. Davis, G. Moad and M. S. O'Shea, *Macromolecules*, 2005, **38**, 5371–5374.

79 B. Chong, G. Moad, E. Rizzardo, M. Skidmore and S. H. Thang, *Aust. J. Chem.*, 2006, **59**, 755.

80 O. Glatter and O. Kratky, *Small Angle X-ray Scattering*, Academic Press, London, vol. 130., 1982.

81 J. S. Pedersen, *J. Appl. Crystallogr.*, 2000, **33**, 637–640.

82 G. Beaucage and D. W. Schaefer, *J. Non. Cryst. Solids*, 1994, **172**–**174**, 797–805.

83 G. Beaucage, *J. Appl. Crystallogr.*, 1995, **28**, 717–728.

84 G. Beaucage, *J. Appl. Crystallogr.*, 1996, **29**, 134–146.

Chapter 3. Synthesis of Poly(lauryl methacrylate)-Poly(behenyl methacrylate) Diblock Copolymers *via* RAFT Solution Polymerisation in Mineral Oil

3.1. Introduction

Solution-phase self-assembly of wholly amorphous diblock copolymers has been widely studied and used to prepare nanoparticles for potential applications in many fields, including biomedicine, biomaterials and catalysis.[1,2] Traditionally, the preparation of diblock copolymer micelles is a multi-step process involving (i) polymerisation, (ii) purification and (iii) self-assembly. Furthermore, a well-known limitation is that such nanoparticles are typically obtained at low copolymer concentration (< 1 % w/w solids). In contrast, polymerisation-induced self-assembly (PISA) enables diblock copolymer nanoparticles to be formed *in situ* as the growing second block becomes insoluble in the chosen reaction medium.[3–5] Moreover, PISA can be conducted at high copolymer concentration (10-50% w/w solids), which makes this approach particularly attractive for industrial scale-up.[4] The main copolymer morphologies (*i.e.* spheres, worms and vesicles) can be accessed via PISA. However, the reaction conditions for a pure worm phase are often difficult to identify because this morphology typically occupies relatively narrow phase space.[4,6]

In contrast, crystallisation-driven self-assembly (CDSA) is a technique known for accessing anisotropic nano-objects, such as cylinders or "rods", using diblock copolymers comprised of a solvophilic block and a semi-crystalline block.[6] In conventional CDSA, self-assembly is induced by the crystallisation of the core-forming block in a selective solvent. In practice, this can involve a solvent switch where dissolution of the diblock copolymer in a common solvent is followed by the slow addition of a selective solvent for the corona-forming block. An alternative method is by heating and subsequently cooling a solution of diblock copolymer in a solvent that is good for both blocks at elevated temperature, but which becomes

selective on cooling.[7] For example, Manners and co-workers used semi-crystalline poly(ferrocenyldimethylsilane) to prepare long cylindrical rodlike micelles by heating a polydimethylsiloxane-poly(ferrocenyldimethylsilane) [PDMS-PFDMS] diblock copolymer in either *n*-hexane or *n*-decane (each a solvent selective for PDMS and a precipitant for PFDMS) at 80 °C.[8] Interestingly, when prepared above the melting temperature, T_m, of PFDMS (ca. 120-145 °C), spherical particles were formed. Thus suggesting that crystallisation of the core-forming block is the driving force for the formation of cylindrical rods below the T_m. To summarise, the two-dimensional folded crystalline lamella of a micelle with a semi-crystalline core stabilises lower curvature structures such as cylindrical micelles.[6]

As expected, the diblock copolymer composition dictates the final copolymer morphology in CDSA. For example, polyisoprene-poly(ferrocenyldimethylsilane) [PIP_{320}-$PFDMS_{53}$] self-assembles to form cylindrical rods in PIP-selective hexanes. In contrast, PIP_{30}-$PFDMS_{60}$ forms tape-like platelets.[9] Typically, cylindrical rods are formed when the corona/core block ratio lies between 5:1 and 10:1.[8–11] Lower block ratios (typically $\leq$ 3:1) usually favour the formation of platelets.[9,12,7] Moreover, hollow tubular structures have been reported by Winnik and co-workers when using a PDMA/PFDMS block ratio of 12:1.[13] In contrast, in PISA syntheses, typically a short corona-forming block and relatively long core-forming block is required to access the worm morphology.[4,14,15] However, in practice, the copolymer morphology in a PISA synthesis is also influenced by other factors, such as the copolymer concentration, the chemical nature of each block and the polymerisation temperature.[16–19]

Control over the length of cylindrical nano-objects prepared by CDSA has been achieved via a seeded-growth approach.[20,21] Although this approach, termed 'living' CDSA, offers a high level of morphological control, it is a multi-step post-

polymerisation process conducted at low concentration (typically < 0.5 % w/w solids). Recently, PISA has been combined with CDSA in a process termed polymerisation-induced crystallisation-driven self-assembly (PI-CDSA). The first example of PI-CDSA was reported in 2017 by Boott *et al.*, as shown in **Figure 3.1.**[22]

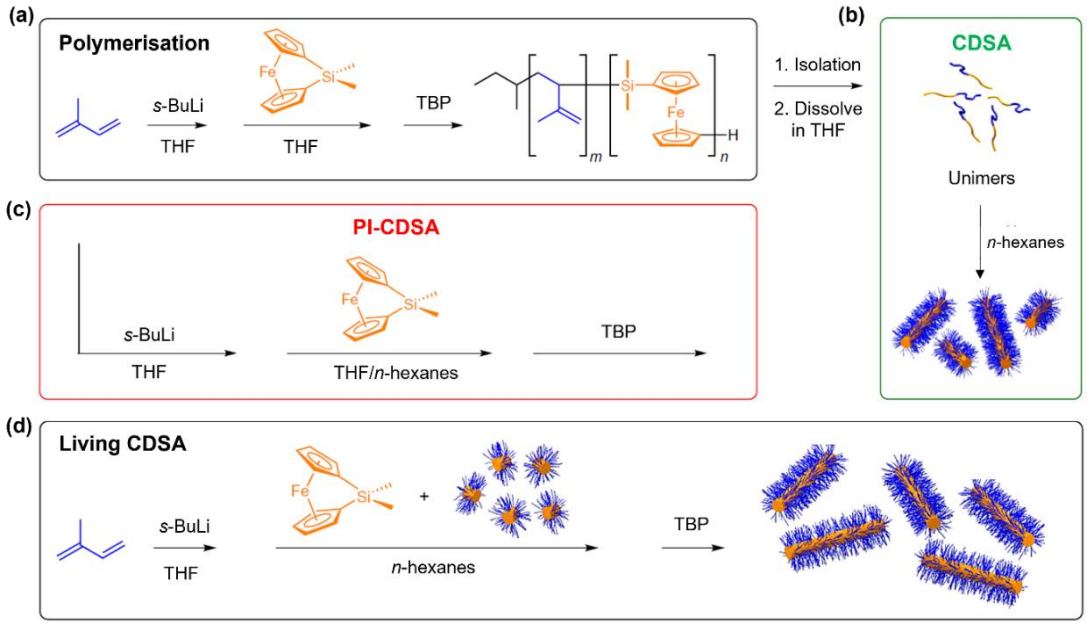

Figure 3.1. Schematic representations of the preparation of polyisoprene-poly(ferrocenyldimethylsilane) [PIP-PFDMS] cylinders. **(a)** Preparation of PIP-PFDMS diblock copolymer by sequential living anionic polymerisation in THF, followed by **(b)** multi-step post-polymerisation solution processing of the PIP-PFDMS diblock copolymers using CDSA protocols in *n*-hexanes. **(c)** By combining established PISA and CDSA techniques polydisperse PIP-PFDMS cylinders can be prepared at high percentage solids (up to 25% w/w solids) in a THF/*n*-hexane solvent mixture by PI-CDSA. **(d)** Preparation of near-monodisperse PIP-PFDMS cylinders *via* a seeded growth mechanism at 10% w/w solids in THF/*n*-hexane solvent mixture by living PI-CDSA. TBP, 4-*tert*-butylphenol, was used as a quenching agent. Adapted from reference 22.

The preparation of PIP-PFDMS cylindrical rods was achieved over a range of block ratios and at up to 25% w/w solids. Self-assembly was able to occur *in situ* via a one-pot approach, whereby the PFDMS block is polymerised in a THF/*n*-hexane solvent mixture (10-20 % v/v THF) instead of neat THF as for conventional CDSA.[22] Polydisperse µm-sized cylinders were prepared by this one-pot approach, which was termed PI-CDSA. Moreover, performing seeded growth enabled the facile preparation

of monodisperse cylinders with enhanced length control via living PI-CDSA. Over the past five years, the scope of PI-CDSA has been broadened to include other PFDMS-based block copolymers,[23] ring-opening metathesis polymerisation (ROMPI-CDSA),[24] and also ring-opening PI-CDSA.[25]

Recently, the synthesis of poly(behenyl methacrylate)-poly(benzyl methacrylate) [PBeMA-PBzMA] diblock copolymer nanoparticles via RAFT-mediated PISA in mineral oil was reported by Derry *et al*.[26] Such sterically-stabilised nanoparticles remained colloidally stable at the synthesis temperature of 90 °C but became flocculated pastes on cooling to ambient temperature owing to crystallisation of the $C_{22}H_{45}$ pendent side-chains on the PBeMA stabiliser chains, which occurred both within the individual nanoparticles and also between neighbouring nanoparticles. Such crystallisation proved to be fully reversible: heating to 50 °C led to complete redispersion of the flocculated nanoparticles as judged by turbidimetry and small-angle X-ray scattering (SAXS) studies.

The aim of this Chapter was to investigate whether poly(lauryl methacrylate)-poly(behenyl methacrylate) [PLMA-PBeMA] diblock copolymer nanoparticles could be prepared using PI-CDSA (see **Scheme 3.1**). In contrast to the prior study by Derry and co-workers,[26] PBeMA is used as the semi-crystalline *core-forming* block, rather than as the steric stabiliser. As discussed above, we targeted cylindrical rods by aiming to prepare highly asymmetric diblock copolymers comprising a long corona-forming block and a short core-forming block. In principle, melting of the crystalline core-forming block cores within the 20-50 °C range should lead to a change in the rheology of such dispersions as the rods become much more flexible, which should lead to a significant reduction in their mean persistence length.

Such thermoresponsive behaviour may offer potential thickening applications (e.g. in cosmetics and personal care formulations).

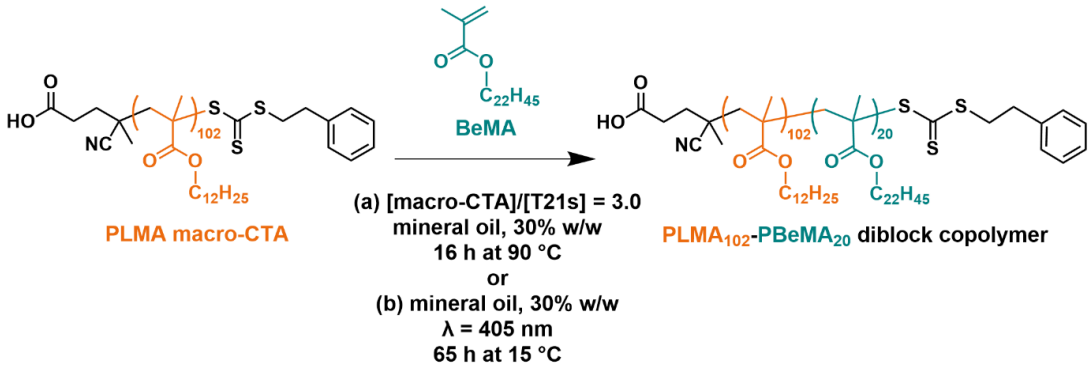

Scheme 3.1. Synthesis of a poly(lauryl methacrylate)-poly(behenyl methacrylate) ($PLMA_{102}$-$PBeMA_{20}$) diblock copolymer *via* RAFT solution polymerisation of BeMA at 30% w/w solids in mineral oil **(a)** by thermal initiation with T21s at 90 °C or **(b)** by photoiniferter polymerisation (λ = 405 nm) at 15 °C.

3.2. Experimental

3.2.1. Materials

All reagents purchased were used as received, unless stated otherwise. Behenyl alcohol (1-docosanol; $C_{22}H_{45}$-OH; 98%), methacryloyl chloride (≥ 97%), triethylamine (TEA), *n*-hexane, and $CDCl_3$ were all purchased from Sigma-Aldrich (UK). Lauryl methacrylate (LMA; 96%) was also purchased from Sigma Aldrich and filtered through basic alumina prior to use in order to remove inhibitor. Toluene, methanol, ethanol and *n*-dodecane (>99%) were purchased from Fisher Scientific (UK). 2,2′-Azoisobutyronitrile (AIBN) was obtained from Molekula (UK) and *tert*-butyl peroxy-2-ethylhexanoate (T21s, >97%) was purchased from AkzoNobel (The Netherlands). Tetrahydrofuran (HPLC grade) was purchased from VWR Chemicals and used in the purification of the PLMA macro-CTA. Anhydrous THF was obtained in-house from a Grubbs solvent purification system and used for the in-house synthesis of the behenyl methacrylate. CD_2Cl_2 was purchased from Goss Scientific (UK). 4-

Cyano-4-(2-phenylethane sulfanylthiocarbonyl)sulfanylpentanoic acid (PETTC, >99%) was synthesised according to the literature.[27] Behenyl methacrylate (BeMA, >99%) and API Group III mineral oil (viscosity = 3.1 cSt at 100 °C) were kindly provided by The Lubrizol Corporation Ltd (Hazelwood, Derbyshire, UK). In addition, behenyl methacrylate, technical grade, was also supplied by BASF (Ludwigshafen, Germany).

3.2.2. Synthesis of behenyl methacrylate (BeMA)

Behenyl methacrylate was synthesised by reacting behenyl alcohol with a 50 mol% excess of methacryloyl chloride in THF, in the presence of triethylamine. A similar protocol was reported for the synthesis of propargyl methacrylate by Ghasdian *et al*.[28] A 500 mL two-neck flask was fitted with a rubber septum and dropping funnel and purged with nitrogen. To this flask was added anhydrous THF (125 mL), behenyl alcohol (51.1 g 0.157 mol) and triethylamine (68.8 mL, 49.9 g, 0.493 mol) and the resulting reaction mixture was stirred at 23 °C. The flask was then placed in an ice bath at 0 °C with continuous stirring. Methacryloyl chloride (22.9 mL, 24.5 g, 0.235 mol) was added dropwise to the reaction mixture via the dropping funnel over 30 min. After stirring for 1 h, anhydrous THF (60.0 mL) was added to facilitate more efficient stirring. The reaction mixture was stirred for 20 h and allowed to warm up to ambient temperature over this period. The resulting viscous white solution was exposed to air to produce a cloudy yellow solution, which was treated with basic alumina to remove unreacted methacryloyl chloride, methacrylic acid and triethylamine hydrochloride salt. The purified product was filtered under vacuum to afford a white solid, which was dissolved in *n*-hexane, washed with sodium bicarbonate solution (pH 9) and then passed through a silica column to remove any

remaining impurities. Then the THF and *n*-hexane were removed under reduced pressure and the residue was dried overnight in a vacuum oven at 30 °C.

Behenyl methacrylate was obtained as a white solid (26.3 g, 66.6 mmol, 42% yield). Elemental microanalysis: C, 79.35%; H, 12.48%. $C_{26}H_{50}O_2$ requires C, 79.12; H, 12.77%. ^{1}H NMR (400 MHz, $CDCl_3$, 20 °C): δ = 0.88-0.93 (t, 3H, -$COOCH_2CH_2(CH_2)_{19}C\boldsymbol{H}_3$), 1.22-1.44 (m, 38H, -$COOCH_2CH_2(C\boldsymbol{H}_2)_{19}CH_3$), 1.64-1.74 (m, 2H, -$COOCH_2C\boldsymbol{H}_2(CH_2)_{19}CH_3$), 1.97 (s, 3H, HHC=C$\boldsymbol{H}_3$COO-), 4.13-4.20 (t, 2H, -$COOC\boldsymbol{H}_2CH_2(CH_2)_{19}CH_3$), 5.57 (s, 1H, $\boldsymbol{H}_2C=CH_3$-, cis), 6.12 (s, 1H, $\boldsymbol{H}_2C=CH_3$-, trans). ^{13}C NMR (100 MHz, $CDCl_3$, 20 °C): 167.8, 136.7, 125.3, 64.9, 32.0, 29.7, 29.3, 28.6, 26.0, 22.7, 18.4, 14.2.

3.2.3. Synthesis of poly(lauryl methacrylate) (PLMA) macromolecular chain transfer agent (macro-CTA)

A typical synthesis of a PLMA macro-CTA was conducted as follows. A 250 mL round-bottomed flask was charged with lauryl methacrylate (LMA; 52.3 g; 206 mmol), 4-cyano-4-(2-phenylethane sulfanylthiocarbonyl)sulfanylpentanoic acid (PETTC; 0.50 g; 1.47 mmol; [LMA]/[PETTC] = 140), 2,2′-azobisisobutyronitrile (AIBN; 48.0 mg; 292 μmol; [PETTC]/[AIBN] molar ratio = 5.07) and toluene (52.8 g; total solids content = 50% w/w). The sealed reaction vessel was purged with nitrogen for 30 min and then placed in a pre-heated oil bath at 70 °C. The LMA polymerisation was allowed to proceed for 3.5 h at this temperature. ^{1}H NMR spectroscopy (see **Figure 3.2**) was used to determine an LMA monomer conversion of 56% using **Equations 3.1-3.3** by comparing the integrated monomer vinyl protons (*a'* and *b'*) with the integrated oxymethylene signals (*f'* and *m*) assigned to LMA monomer and PLMA homopolymer.

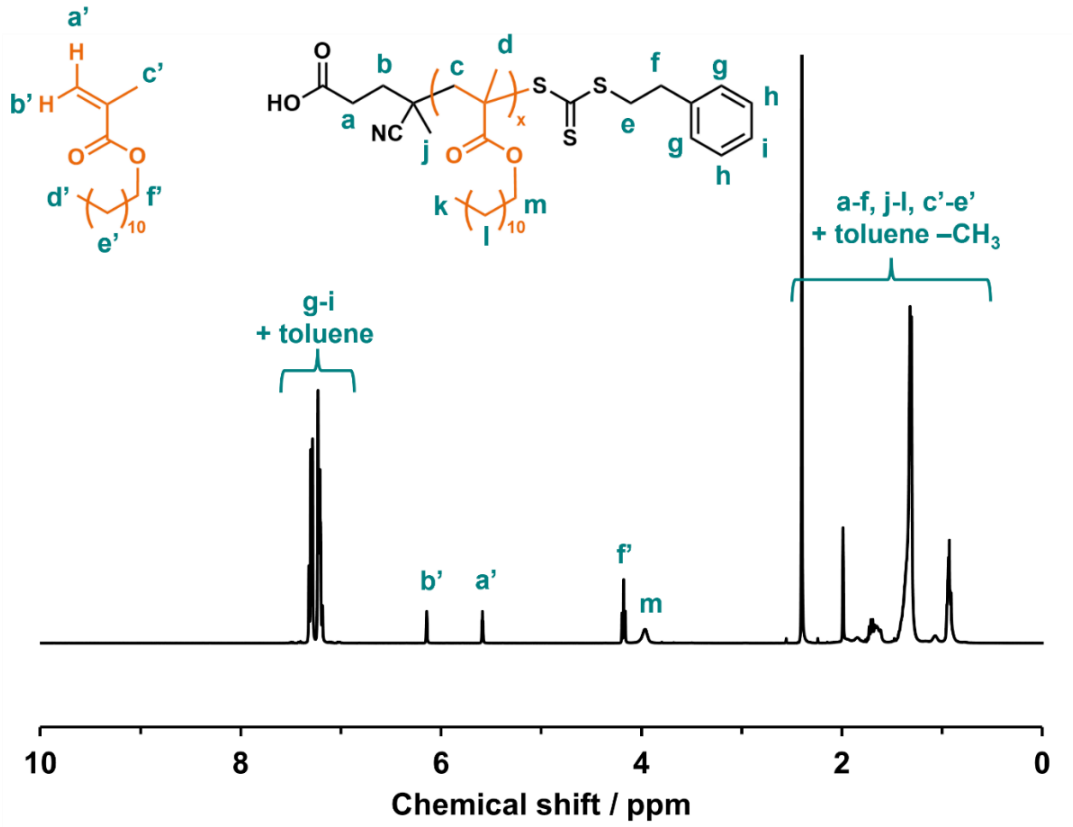

Figure 3.2. Assigned ^{1}H NMR spectrum ($CDCl_3$) recorded for a crude PLMA precursor (target DP = 140, LMA conversion = 56%).

$$I_m = [Integral\ (a' + b')] = 2H \quad 3.1$$

$$I_p = [Integral\ (m + f')] - I_m \quad 3.2$$

$$LMA\ conversion\ (\%) = \left[1 - \frac{I_m}{I_m + I_p}\right] x\ 100\% \quad 3.3$$

The crude product was purified by precipitation (three times) into excess methanol and then dried under vacuum. The mean degree of polymerisation (DP) of the purified macro-CTA was determined via end-group analysis by analysing its ^{1}H NMR spectrum recorded in CD_2Cl_2 **(see Figure 3.3)**. A mean DP of 102 was calculated by comparing the integrated signals corresponding to the aromatic protons of the trithiocarbonate-based end-group at 7.1-7.4 ppm with those assigned to the two oxymethylene ester protons of the LMA repeat units at 3.7-4.2 ppm (**Equations 3.4-**

3.5). THF GPC analysis indicated a PMMA-equivalent number-average molecular weight, M_n, of 20.7 kg mol^{-1} (for comparison, M_n NMR = 26.3 kg mol^{-1}) and dispersity, $Đ$, of 1.19.

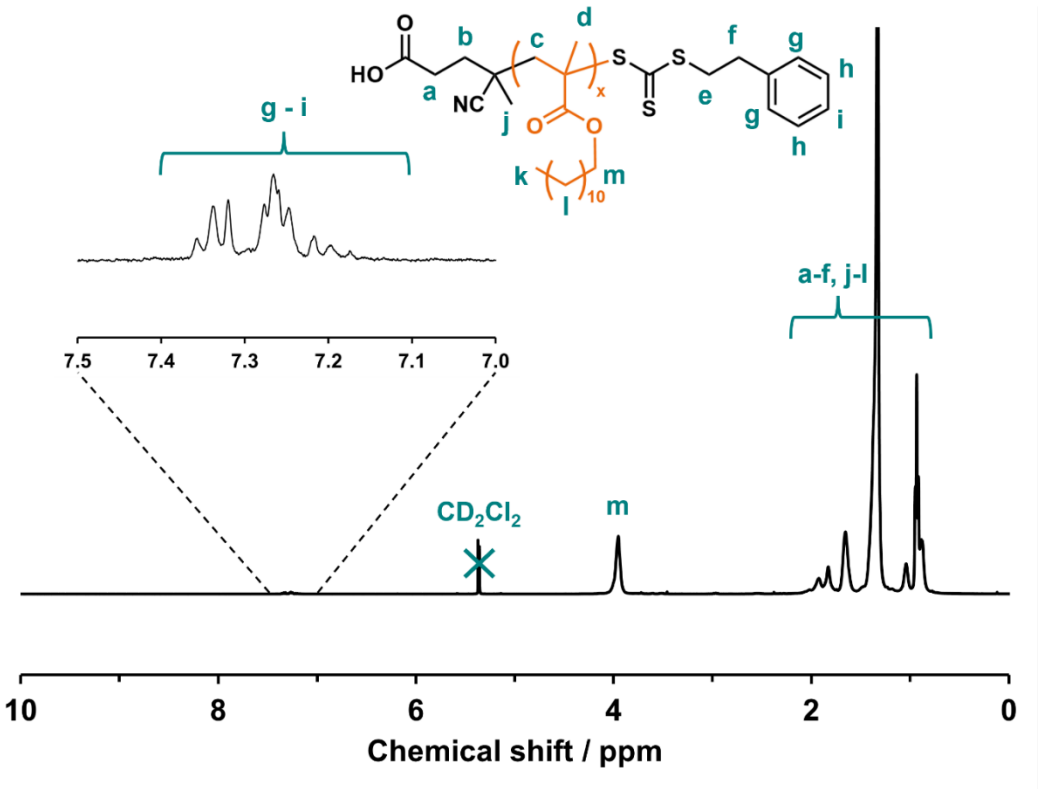

Figure 3.3. Assigned ^{1}H NMR spectrum (CD_2Cl_2) obtained for the purified $PLMA_{102}$ macro-CTA.

$$[Integral\ (g\ +\ h\ +\ i)]\ =\ 5\text{H} \qquad 3.4$$

$$PLMA\ DP = \frac{[Integral\ (m)]}{2} \qquad 3.5$$

3.2.4. Synthesis of poly(lauryl methacrylate)-poly(behenyl methacrylate) [$PLMA_{102}$-$PBeMA_x$] diblock copolymers by thermally-initiated RAFT solution polymerisation at 90 °C

The protocol for the synthesis of a $PLMA_{102}$-$PBeMA_{20}$ diblock copolymer via RAFT solution polymerisation of BeMA at 30% w/w solids in mineral oil is representative

for all of the diblock copolymers prepared by thermal initiation in this Chapter and was conducted as follows. $PLMA_{102}$ (0.333 g; 12.7 μmol), BeMA (0.100 g; 253 μmol), and mineral oil (0.920 g) were weighed into a glass vial and heated in an oven at 70 °C to aid dissolution. A sample (one droplet, approx. 20 mg) of the reaction solution was extracted for use as a 'zero time' reference point for determination of the BeMA conversion by ^{1}H NMR spectroscopy. After cooling the remaining solution to 20 °C, T21s initiator was added (101 μl; 4.21 μmol; 1.0% v/v in mineral oil; [$PLMA_{102}$]/[T21s] molar ratio = 3.0) along with a magnetic stirrer bar and this reaction mixture was purged with nitrogen gas for 30 min. The sealed sample vial was then immersed in a pre-heated oil bath set at 90 °C and the reaction mixture was stirred for 16 h (final BeMA conversion = 97%; M_n = 25.5 kg mol^{-1}; $Đ$ = 1.17).

BeMA conversions were determined via ^{1}H NMR spectrocopy using **Equations 3.6 - 3.9**. In this case, an additional spectrum was recorded at zero time to distinguish between the new oxymethylene signals originating from the PBeMA block and those assigned to the PLMA precursor (see **Figure 3.4**).

$$I_m = [Integral\ (a + b)] = 2H \tag{3.6}$$

$$\text{PLMA } I_p = [Integral\ (c' + d')] - I_m \tag{3.7}$$

$$\text{PBeMA } I_p = \{[Integral\ (c + c' + d')] - I_m\} - PLMA\ I_p \tag{3.8}$$

$$BeMA\ conversion\ (\%) = \left[1 - \frac{I_m}{I_m + PBeMA\ I_p}\right] x\ 100\% \tag{3.9}$$

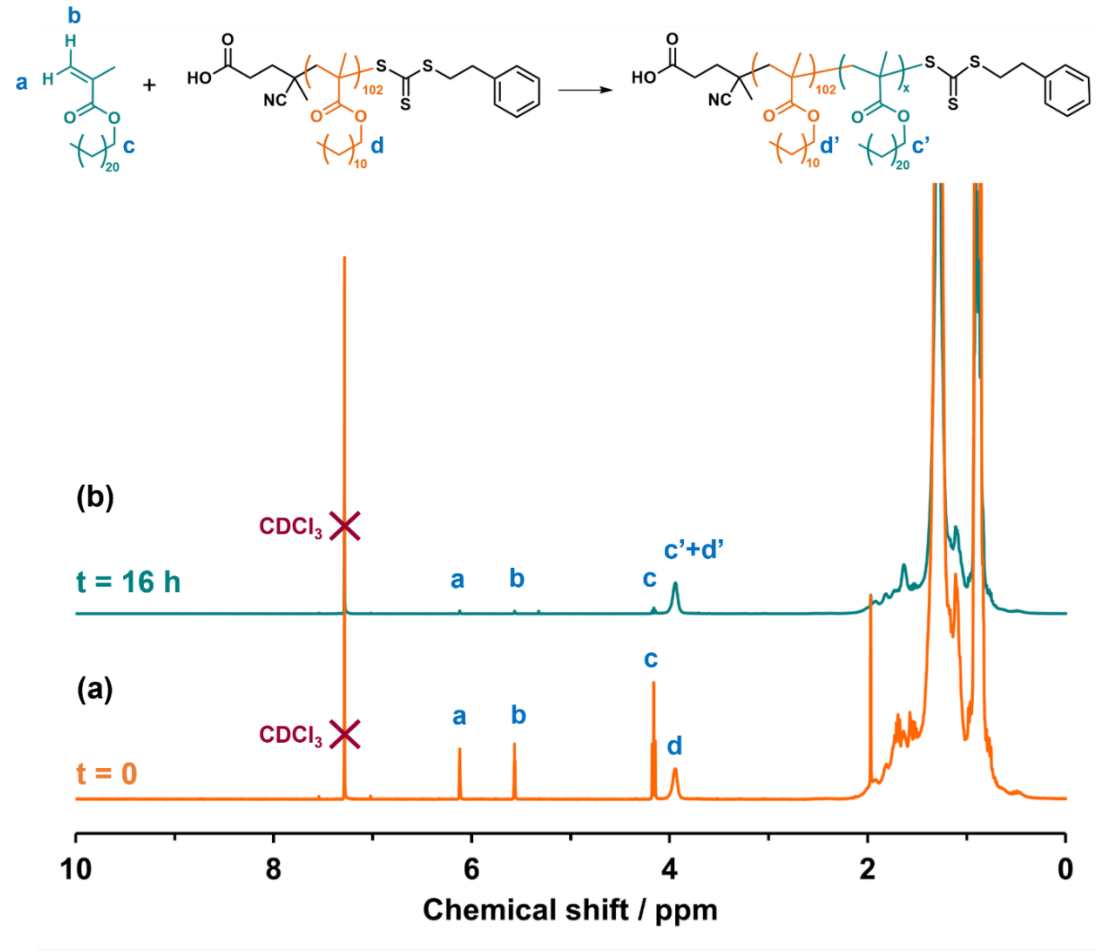

Figure 3.4. Assigned ^{1}H NMR spectra ($CDCl_3$) recorded for **(a)** the reaction mixture at zero time (t = 0) containing a $PLMA_{102}$ precursor and BeMA monomer and **(b)** the same reaction mixture after polymerisation for 16 h to form a $PLMA_{102}$-PBeMA diblock copolymer (BeMA conversion = 97%).

3.2.5. Synthesis of poly(lauryl methacrylate)-poly(behenyl methacrylate) [$PLMA_{102}$-$PBeMA_{20}$] diblock copolymers by photoiniferter RAFT solution polymerisation at 32 °C

A typical synthesis of a $PLMA_{102}$-$PBeMA_{20}$ diblock copolymer at 30% w/w solids in mineral oil via photoiniferter RAFT solution polymerisation at ambient temperature was conducted as follows. $PLMA_{102}$ (0.337 g; 12.8 μmol), BeMA (0.101 g; 256 μmol), and mineral oil (1.021 g) were weighed into a glass reaction vial and heated in an oven at 70 °C to aid dissolution. One droplet (approx. 20 mg) of the reaction solution was taken for use as a reference point (t = 0) for determination of the BeMA conversion

by ^{1}H NMR spectroscopy. A thermocouple was inserted into the reaction mixture along with a magnetic stirrer bar and this reaction mixture was purged with nitrogen gas for 30 min. The sealed sample vial was placed inside a glass beaker containing violet LED lights (λ = 395 nm) wrapped around the inside wall and was stirred for 16 h at 32 °C (final BeMA conversion > 99%; M_n = 26.1 kg mol^{-1}; $Đ$ = 1.19). For photoiniferter polymerisation syntheses conducted at lower temperature, a more sophisticated set-up was used which consisted of violet LED lights (λ = 405 nm, 0.37 mW cm^{-2}) inside a jacketed vessel connected to a thermostat-controlled water bath, as described by Gibson et al.[29]

3.3. Characterisation

3.3.1. ^{1}H NMR spectroscopy

^{1}H NMR spectra were recorded in either CD_2Cl_2 (to determine the mean DP for the PLMA precursor) or $CDCl_3$ (for all other spectra) using a Bruker Avance AVIII 400 MHz spectrometer. Typically, 64 scans were averaged per spectrum.

3.3.2. ^{13}C NMR spectroscopy

^{13}C (DEPTQ) NMR spectra were acquired at 100 MHz using a Bruker Avance AVIII 400 MHz spectrometer. All spectra were recorded in $CDCl_3$ with between 128 and 10,240 scans being averaged per spectrum.

3.3.3. Gas Chromatography – Mass Spectrometry (GC-MS)

Mass spectrometry analysis was conducted using an Agilent 7200 Accurate-Mass Q-TOF instrument connected to a gas chromatograph equipped with an Agilent DB-5MS-UI 30 m x 0.25 mm x 0.25 μm column. The carrier gas was helium at a pressure of 9.47 psi. The injection volume was 1.0 μL and the flow rate was 1.2 ml min^{-1}.

Samples were analysed using the electron impact (EI) scan mode over the 40-900 m/z range.

3.3.4. Elemental Microanalysis

Microanalyses were determined using an Elementar vario MICRO cube analyser.

3.3.5. Melting Point Analysis

The melting point of behenyl methacrylate monomer was determined using a Stuart SMP50 Automatic Melting point instrument. Samples were equilibrated at 35 °C and then heated at a rate of 1.0 °C min^{-1}. Three samples were run using glass capillaries and the mean melting point was calculated.

3.3.6. FT-IR Spectroscopy

FT-IR spectra were recorded for both behenyl methacrylate and the behenyl alcohol precursor using a Thermo Scientific Nicolet iS10 spectrometer equipped with a Diamond ATR Golden Gate accessory. The spectral resolution was 4 cm^{-1} and 32 scans were averaged per spectrum.

3.3.7. Differential Scanning Calorimetry (DSC)

DSC studies were performed using a TA Instruments Discovery DSC instrument equipped with TZero low-mass aluminium pans and hermetically-sealed lids. BeMA monomer was equilibrated at 60 °C for 5 min before two consecutive thermal cycles (from 60 °C to 0 °C to 60 °C) were performed at a constant cooling/heating rate of 10.0 °C min^{-1}. PLMA-PBeMA diblock copolymers were equilibrated at 60 °C for 5 min prior to two consecutive thermal cycles (from 60 °C to 0 °C to 60 °C) performed at a constant cooling/heating rate of 2.0 °C min^{-1}. Two cycles were performed to eliminate any thermal history.

3.3.8. Gel Permeation Chromatography (GPC)

GPC was used to assess molecular weight distributions. The GPC set-up comprised two 5 μm (30 cm) Agilent Mixed C columns and a WellChrom K-2301 refractive index detector operating at 950 ± 30 nm. The THF eluent contained 2.0% v/v triethylamine and 0.05% w/v butylhydroxytoluene (BHT) with a toluene flow-rate marker at a flow rate of 1.0 mL min^{-1}. A series of eleven near-monodisperse poly(methyl methacrylate) (PMMA) standards (M_p values ranging from 800 to 988 000 g mol^{-1}) were used for calibration.

3.3.9. Dynamic Light Scattering (DLS)

DLS studies were performed using a Zetasizer Nano ZS instrument (Malvern Instruments, UK) at a fixed scattering angle of 173°. Copolymer dispersions were diluted to 0.10% w/w using *n*-dodecane, either in a refrigerator at 5 °C or on the bench at ~20 °C, prior to light scattering studies at either 5 °C or 20 °C. The z-average diameter and DLS polydispersity were calculated by cumulants analysis of the experimental correlation function using Dispersion Technology Software version 6.20. Data were averaged over ten runs each of thirty seconds duration.

3.3.10. Transmission Electron Microscopy (TEM)

TEM studies were conducted using a FEI Tecnai G2 spirit instrument operating at 80 kV and equipped with a Gatan 1k CCD camera. Copolymer dispersions were diluted to 0.10% w/w using *n*-dodecane either in a refrigerator at 5 °C or on the bench at ~20 °C. For sample preparation at 5 °C, a single droplet was placed onto a pre-cooled carbon-coated copper grid and allowed to dry at 5 °C overnight within a refrigerator. For sample preparation at 20 °C, a single droplet was placed onto a carbon-coated copper grid and allowed to dry for 30 min. The resulting grids were exposed to ruthenium(VIII) oxide vapor for 7 min at 20 °C prior to analysis. This heavy metal

compound acts as a positive stain for the core-forming block to improve electron contrast. Ruthenium(VIII) oxide was prepared as follows: ruthenium(IV) oxide (0.30 g) was added to water (50 g) to form a black slurry; addition of sodium periodate (2.0 g) with continuous stirring produced a yellow solution of ruthenium(VIII) oxide within 1 min at 20 °C.

3.3.11. Oscillatory rheology

An Anton Paar MCR502 rheometer equipped with a variable temperature Peltier plate and hood and a 50 mm 2° aluminium cone was used for all experiments. The distance between the cone and plate was 207 μm. The storage (G') and loss (G") moduli were measured as a function of temperature at a fixed strain of 1.0% and an angular frequency of 10 rad s^{-1}. The sample was equilibrated at 60 °C for 5 min before performing a thermal cycle from 60 to 10 to 60 °C at a constant cooling/heating rate of 2.0 °C min^{-1}.

3.3.12. Shear-Induced Polarised Light Imaging (SIPLI)

The instrument design and general experimental set-up has been previously reported by Mykhaylyk and co-workers.[30,31] SIPLI experiments were conducted on a 30% w/w solution of $PLMA_{102}$-$PBeMA_{20}$ diblock copolymer in *n*-dodecane at an applied shear rate of 1.0 s^{-1} during a temperature ramp experiment from 50 to 10 to 50 °C conducted at a constant cooling/heating rate of 2.0 °C min^{-1}.

3.4. Results and Discussion

3.4.1. Synthesis of behenyl methacrylate (BeMA)

Preliminary work was conducted using a small batch of BeMA monomer (originally synthesised by Dr. D. Knobloch at The Lubrizol Corporation and kindly provided to the Armes group) that remained after a prior study performed by Derry and co-

workers.[26] For subsequent experiments, a new source of BeMA monomer was required to conduct the majority of the experimental work reported in this Thesis. Initially, BeMA monomer was supplied by BASF (Ludwigshafen, Germany). However, GC-MS analysis indicated that this technical grade batch contained a mixture of C_{18}, C_{20} and C_{22} side-chains (see **Figure 3.5b**), rather than solely C_{22} side-chains observed for the original Lubrizol-sourced BeMA batch (see **Figure 3.5a**). The BASF-sourced BeMA monomer turned out to be unsuitable for further studies because it exhibited inferior crystallisation behaviour. This was confirmed by melting point analysis: a melting point of 29.1 ± 0.2 °C was determined for the impure BeMA batch obtained from BASF, whereas a melting point of 45.6 ± 0.2 °C was obtained for the pure batch originating from Lubrizol. Moreover, a significant difference in the melting and crystallisation temperatures (T_m and T_c, respectively) was observed by DSC studies conducted at a cooling rate of 10 °C min^{-1}. These thermal transitions correspond to the loss or appearance of crystalline structure in the sample. The Lubrizol-sourced BeMA exhibited a T_c at 35 °C on cooling from 60 °C, whereas a much broader peak was observed for the BASF-sourced monomer with a significantly lower T_c of 25 °C (see **Figure 3.5c** and **Figure 3.5d**). It is perhaps worth noting the presence of two second, smaller peaks in the DSC traces for BeMA obtained from Lubrizol: one for crystallisation and one for melting (labelled T_c^* and T_m^* in **Figure 3.5c**). It is likely that these correspond to a conformational order/disorder transition on cooling/heating.[32,33]

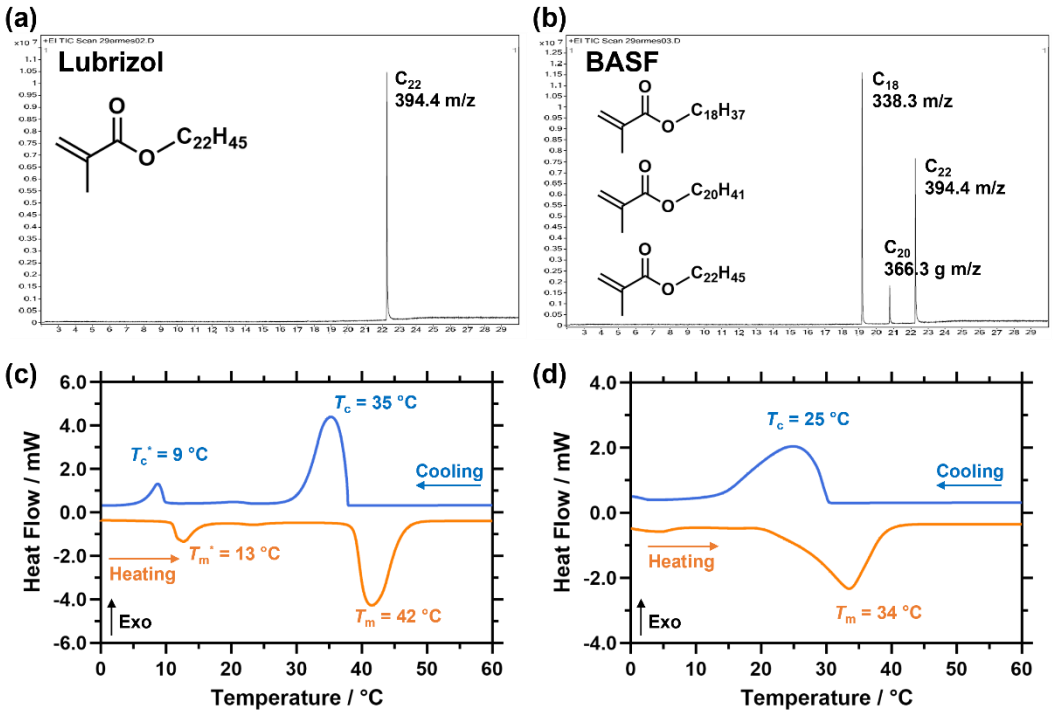

Figure 3.5. GC-MS spectra recorded for BeMA monomer provided **(a)** by Lubrizol and **(b)** by BASF. Differential scanning calorimetry (DSC) curves recorded at a constant cooling/heating rate of 10 °C min^{-1} for BeMA monomer provided **(c)** by Lubrizol and **(d)** by BASF.

Behenyl methacrylate was synthesised in-house by reacting behenyl alcohol (1-docosanol) with excess methacryloyl chloride in THF in the presence of triethylamine (TEA), see **Scheme 3.2**.

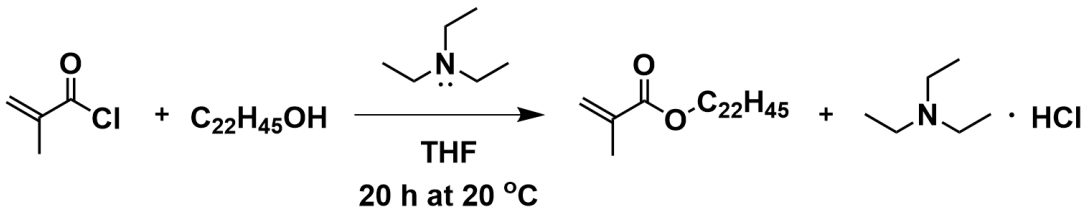

Scheme 3.2. Synthesis of behenyl methacrylate (BeMA) by reacting behenyl alcohol with excess methacryloyl chloride in THF in the presence of triethylamine (TEA).

TEA was dried in a round-bottomed flask over activated molecular sieves and the behenyl alcohol precursor was dried in a vacuum oven overnight to remove any residual moisture prior to esterification. The reaction mixture was stirred for 20 h

under an N_2 atmosphere in a sealed vessel. The crude product was washed with basic alumina to remove any unreacted methacryloyl chloride, methacrylic acid and triethylamine hydrochloride salt. The product was then dissolved in *n*-hexane, washed with mildly alkaline aqueous solution (pH 9), and passed through a silica column to remove any remaining impurities, prior to drying in a vacuum oven for 24 h. A white crystalline powder was obtained and successful purification was confirmed by ^{1}H NMR and ^{13}C NMR. **Figure 3.6** shows ^{1}H NMR spectra of both the crude reaction mixture and the final BeMA product after purification. The labelled proton signals corresponding to impurities present in the crude reaction mixture in spectrum (a) are absent in spectrum (b) recorded for the purified BeMA monomer.

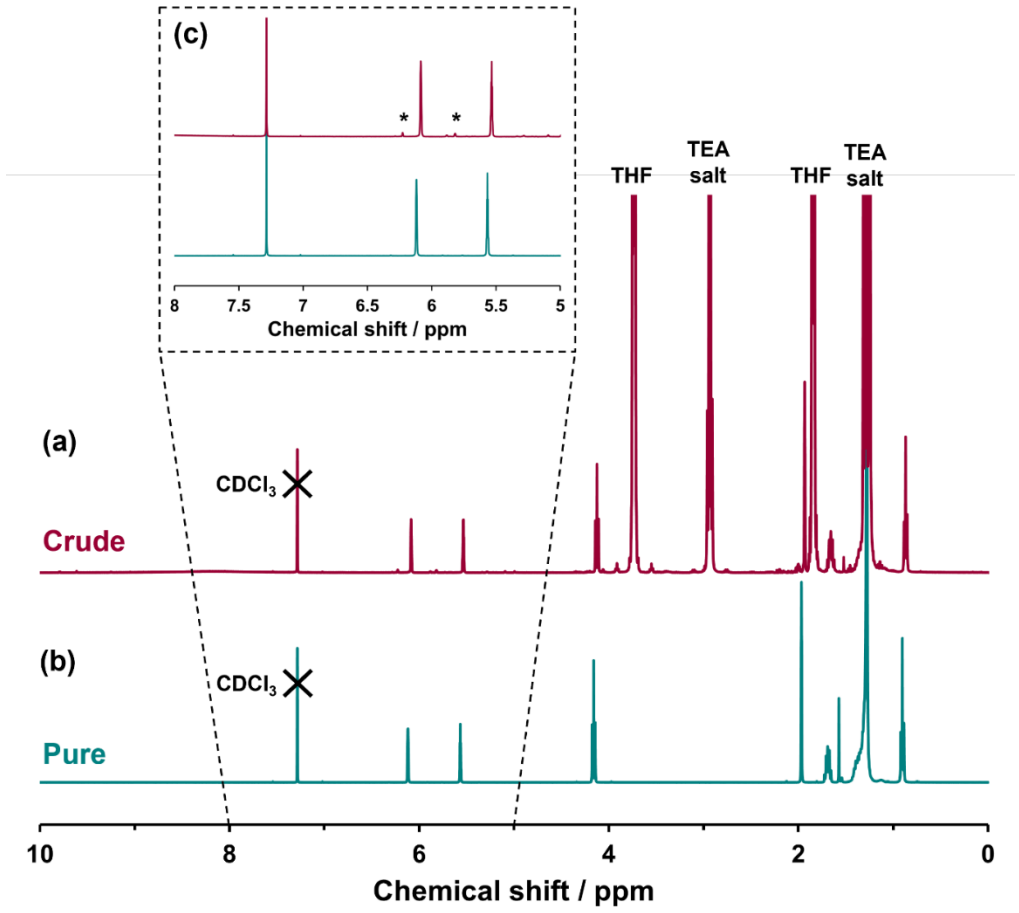

Figure 3.6. ^{1}H NMR spectra recorded in $CDCl_3$ for **(a)** the crude product obtained after in-house synthesis of behenyl methacrylate with labelled proton signals corresponding to impurities and **(b)** purified behenyl methacrylate, confirming removal of such impurities. (c) Partial spectra show the presence of ghost vinyl proton signals (*****) corresponding to unreacted

methacryloyl chloride and/or methacrylic acid for the crude reaction mixture, but not for the purified monomer.

Figure 3.7 and **Figure 3.8** show the assigned NMR spectrum for the purified BeMA monomer, along with the spectrum for the original batch of BeMA provided by Lubrizol, for ^{1}H and ^{13}C NMR respectively. Clearly, in both cases, these two spectra are almost identical.

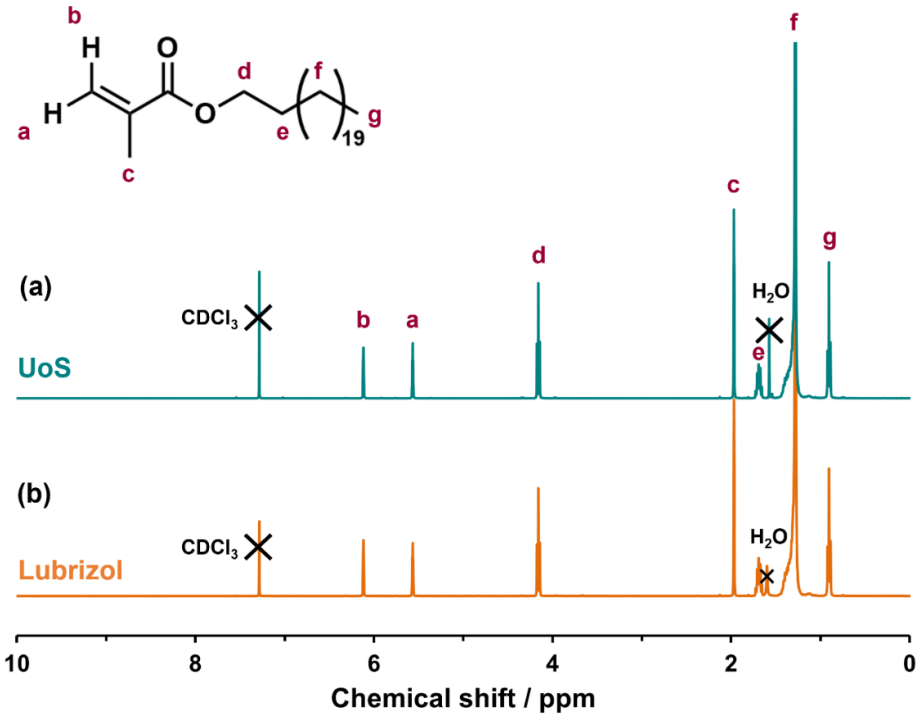

Figure 3.7. Assigned ^{1}H NMR spectra in $CDCl_3$ of **(a)** behenyl methacrylate synthesised in-house at UoS (after purification) and **(b)** behenyl methacrylate provided by The Lubrizol Corporation.

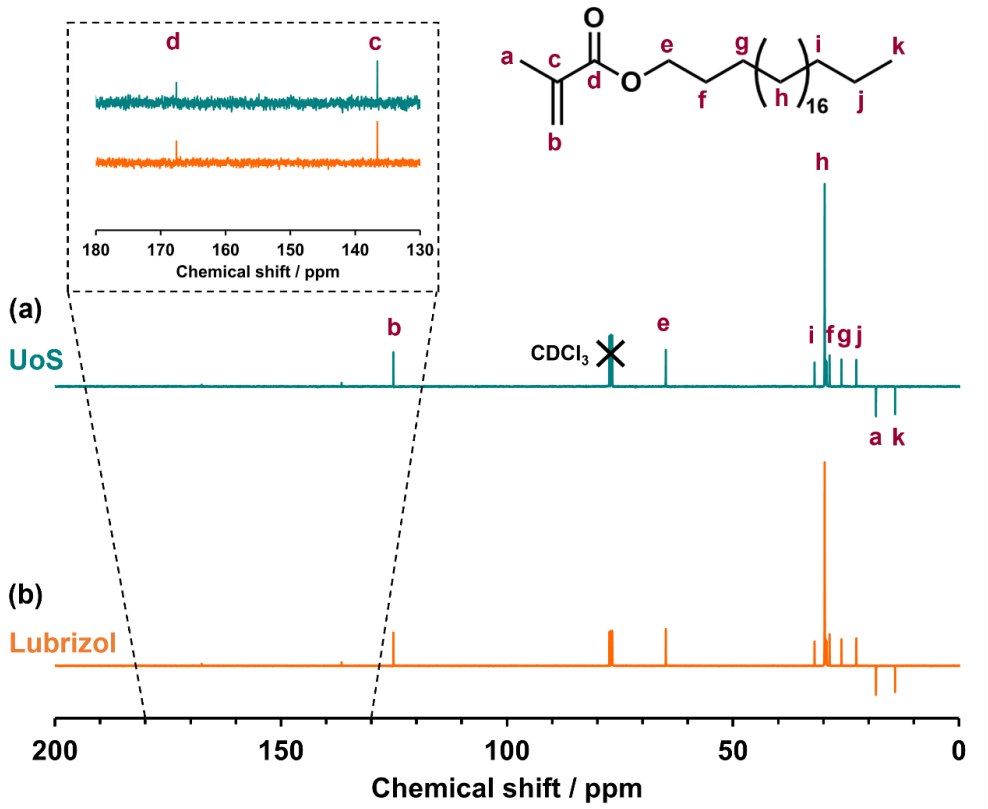

Figure 3.8. Assigned ^{13}C NMR spectra in $CDCl_3$ of **(a)** behenyl methacrylate synthesised in-house at UoS (after purification) and **(b)** behenyl methacrylate provided by The Lubrizol Corporation.

In addition to ^{1}H and ^{13}C NMR spectroscopy, the in-house synthesised BeMA monomer was also characterised by elemental microanalysis, GC-MS, melting point analysis, and FT-IR spectroscopy. The original Lubrizol-sourced BeMA batch was also analysed for comparison. For the in-house synthesised BeMA batch, elemental microanalysis indicated 79.35% C and 12.48% H, which are close to the theoretical values for $C_{26}H_{50}O_2$ of 79.12% and 12.77%, respectively. In comparison, the Lubrizol batch contained 79.31% C and 13.06% H. GC-MS analysis revealed a single peak corresponding to 394.4 m/z, which is identical to the Lubrizol-sourced BeMA chromatogram (see **Figure 3.9**). For comparison, the absolute mass of BeMA is 394.381 m/z. Overall purity was estimated to be more than 99% for both batches. Melting point analysis indicated almost identical data (m.p. = 45.7 ± 0.1 °C for the in-house synthesised batch *vs.* m.p. = 45.6 ± 0.2 °C for the Lubrizol batch).

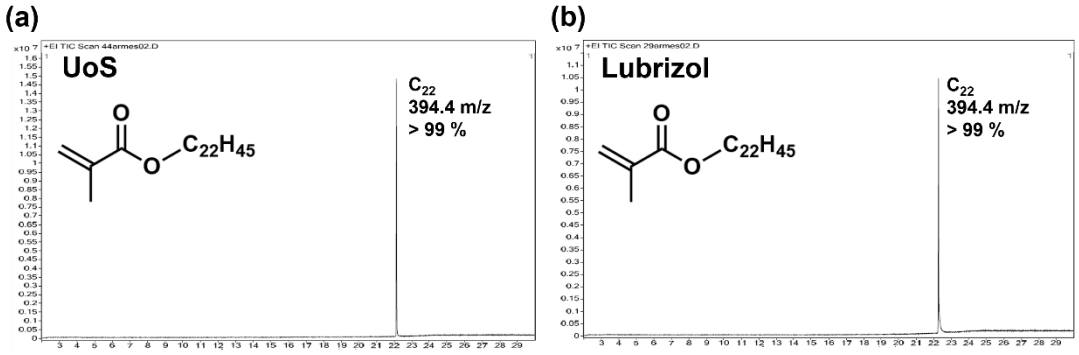

Figure 3.9. GC-MS spectra recorded for **(a)** in-house synthesised behenyl methacrylate and **(b)** Lubrizol-sourced behenyl methacrylate.

FT-IR spectroscopy provided qualitative evidence for successful synthesis of the desired behenyl methacrylate from behenyl alcohol (see **Figure 3.10**). The O-H stretch at around 3340 cm^{-1} observed in the spectrum recorded for the behenyl alcohol precursor **(a)** is absent in the spectra recorded for **(b)** the in-house synthesised behenyl methacrylate and **(c)** the Lubrizol batch**.** In the latter two spectra, the strong 1710 cm^{-1} band is assigned to the ester carbonyl stretch and a 1635 cm^{-1} band is ascribed to the C=C stretch of the vinyl group.[34]

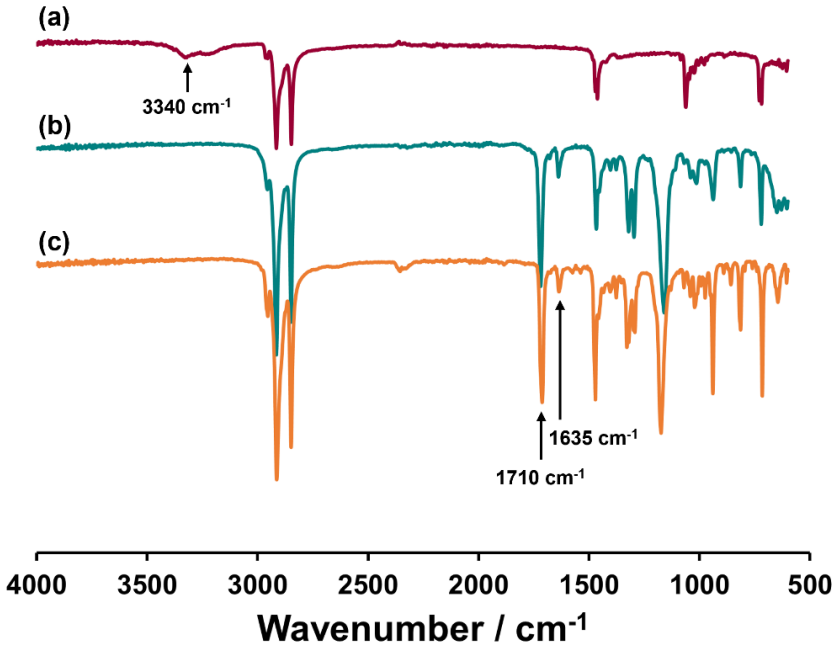

Figure 3.10. FT-IR spectra recorded for **(a)** behenyl alcohol, **(b)** in-house synthesised behenyl methacrylate and **(c)** Lubrizol-sourced behenyl methacrylate.

In summary, the behenyl methacrylate monomer prepared in-house is of comparable purity to that of the original Lubrizol batch employed by Derry *et al*,[26] as confirmed by ^{1}H and ^{13}C NMR spectroscopy, elemental microanalysis, GC-MS, melting point analysis and FT-IR spectroscopy.

3.4.2. Synthesis of PLMA macro-CTA

A $PLMA_{102}$ macro-CTA precursor was prepared via RAFT solution polymerisation of LMA at 50% w/w solids in toluene at 70 °C using PETTC as a RAFT chain transfer agent (CTA) (see **Scheme 3.3**). This polymerisation was quenched at 56 % conversion to produce a mean DP of 102. Quenching the polymerisation well below full conversion avoids monomer-starved conditions and hence aids retention of the trithiocarbonate end-groups.[35,36] This is desirable for high blocking efficiencies in the subsequent synthesis of PLMA-PBeMA diblock copolymers. THF GPC analysis of

this $PLMA_{102}$ macro-CTA indicated an M_n of 20.7 kg mol^{-1} and a relatively narrow molecular weight distribution ($Đ$ = 1.19).

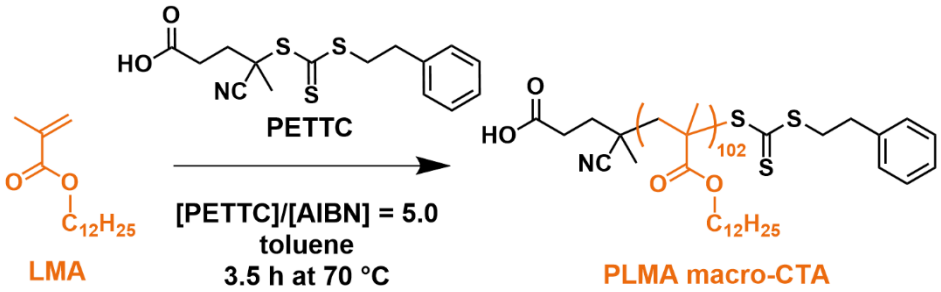

Scheme 3.3. Synthesis of a poly(lauryl methacrylate) (PLMA) macro-CTA by RAFT solution polymerisation of LMA at 50% w/w solids in toluene at 70 °C.

3.4.3. Preliminary Study: Synthesis of PLMA-PBeMA diblock copolymers

Preliminary experiments were conducted to assess the feasibility of chain-extending this $PLMA_{102}$ macro-CTA with BeMA. An initial series of three $PLMA_{102}$-$PBeMA_x$ diblock copolymers targeting a PBeMA DP (x) of 20, 40 or 60, were synthesised via RAFT solution polymerisation of BeMA at 90 °C at 30% w/w solids in mineral oil (see **Scheme 3.4**). Given its relatively high molar mass (394.7 g mol^{-1}), BeMA monomer has a relatively low molar concentration for a given mass concentration compared to most other common methacrylic monomers, e.g. methyl methacrylate (molar mass = 100.1 g mol^{-1}). Thus, 30% w/w solids was chosen to ensure that a high BeMA monomer conversion could be obtained, while still providing conditions under which, on cooling post-polymerisation, self-assembly might be expected to occur (PISA syntheses have been shown to work well at up to 50 % w/w solids in non-polar media).[37]

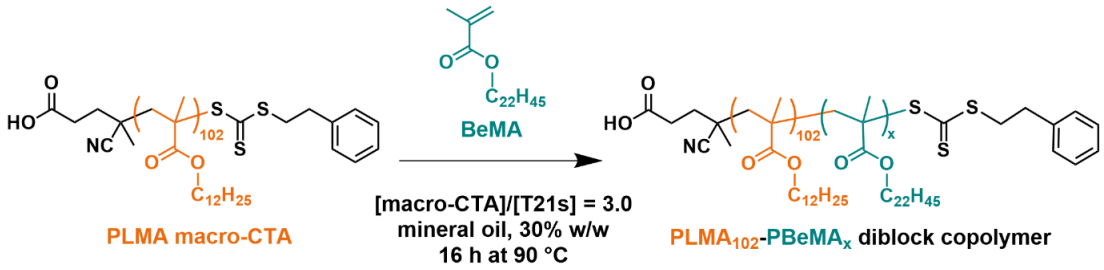

Scheme 3.4. Synthesis of poly(lauryl methacrylate)-poly(behenyl methacrylate) (PLMA-PBeMA) diblock copolymers *via* RAFT solution polymerisation at 30% w/w solids in mineral oil at 90 °C.

A relatively high BeMA conversion of 96% was achieved when targeting PBeMA DP 20 (see **Table 3.1**). However, the final BeMA conversion was reduced to 92% and 59% when targeting of DPs 40 and 60, respectively. THF GPC analysis of the three diblock copolymers using a RI detector showed narrow MWDs and a clear shift in molecular weight was observed relative to the corresponding $PLMA_{102}$ precursor (see **Figure 3.11**). In subsequent experiments, a target DP of 20 was selected for the PBeMA block, which corresponds to a PLMA/PBeMA molar ratio of approximately 5:1. Similar corona/core molar ratios have been reported to be important for producing 1D cylindrical rods by CDSA by Manners and co-workers.[8,9,22]

Table 3.1. Summary of PBeMA target DPs, GPC molecular weights and dispersities for a series of $PLMA_{102}$-$PBeMA_x$ diblock copolymers prepared at 30% w/w solids in mineral oil at 90 °C.

PBeMA target DP	BeMA conv.[a] / %	M_n[b] / kg mol^{-1}	$Đ$[b]
20	96	26.4	1.16
40	92	29.9	1.16
60	59	28.8	1.18

[a]Determined by ^{1}H NMR. [b]Determined by THF GPC against poly(methyl methacrylate) standards.

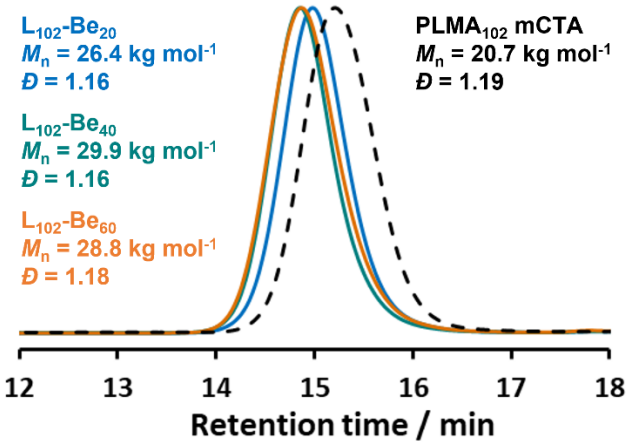

Figure 3.11. THF GPC curves recorded when targeting $PLMA_{102}$-$PBeMA_x$ diblock copolymers, where x = 20, 40 or 60, using a refractive index (RI) detector and a $PLMA_{102}$ macro-CTA reference for comparison.

3.4.4. Synthesis of $PLMA_{102}$-$PBeMA_{20}$ diblock copolymers by either thermally initiated RAFT polymerisation at 90 °C or photoiniferter RAFT polymerisation at 32 °C

A $PLMA_{102}$-$PBeMA_{20}$ diblock was targeted via RAFT polymerisation of BeMA at 30% w/w solids in mineral oil using an organic peroxide initiator (T21s) at 90 °C, see **Scheme 3.5a** and **Figure 3.12a**. ^{1}H NMR spectroscopy studies indicated that 97% BeMA conversion was achieved after 16 h. The visual appearance of the reaction mixture at 90 °C was a clear, pale-yellow fluid (see **Figure 3.12b**). This indicates that the PBeMA block remains soluble under such conditions, which is consistent with prior studies by Derry *et al.*[26] Thus this formulation is an example of RAFT solution polymerisation, rather than PISA.

The same $PLMA_{102}$-$PBeMA_{20}$ diblock copolymer was targeted via photoiniferter RAFT polymerisation at 30% w/w solids in mineral oil at 32 ± 1 °C using violet light (λ = 395 nm) instead of a chemical initiator, see **Scheme 3.5b**. It was hypothesised that such a reaction temperature might be sufficiently low enough for the PBeMA block to crystallise and produce diblock copolymer nanoparticles by CDSA and/or

PISA based on reported work by Derry *et al.*[26] In this published work, DSC studies on a $PBeMA_{37}$ homopolymer determined a melting temperature (T_m) of 59 °C in the solid state and a T_m of 43 °C for a 20% w/w solution in mineral oil. This reaction was conducted within a 2 L glass beaker in which an adhesive violet LED strip was stuck on the internal glass walls (see **Figure 3.12d**). A similar reaction vessel has been previously used within the Armes group for photoiniferter RAFT polymerisations. A Raspberry Pi-controlled thermocouple was used to monitor the temperature of the reaction mixture, which measured 32 ± 1 °C. After 16 h of continuous LED light irradiation, ^{1}H NMR spectroscopy studies indicated that more than 99% BeMA conversion was achieved. The final reaction solution was a clear, pale fluid at 32 °C (see **Figure 3.12e**). Again, this suggested that solution polymerisation had occurred, rather than PISA. This is somewhat surprising given the reaction temperature was below that of the T_m measured for a $PBeMA_{37}$ homopolymer.

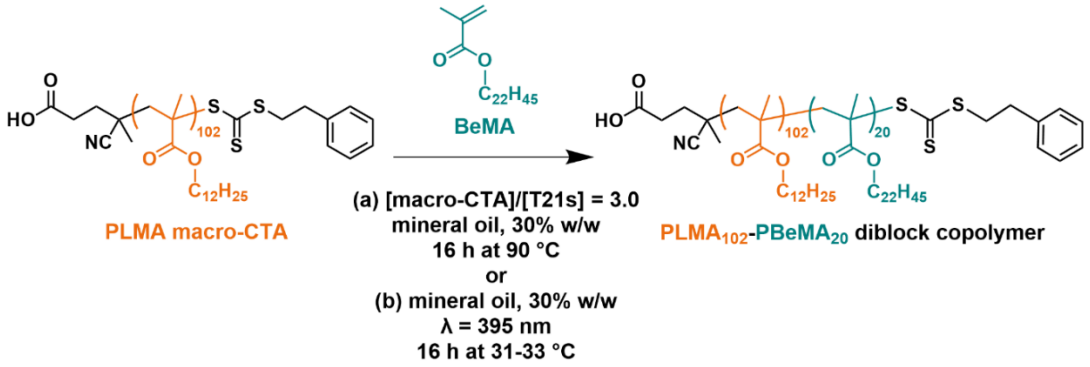

Scheme 3.5. Synthesis of a poly(lauryl methacrylate)-poly(behenyl methacrylate) ($PLMA_{102}$-$PBeMA_{20}$) diblock copolymer *via* RAFT solution polymerisation at 30% w/w solids in mineral oil **(a)** by thermal initiation with T21s at 90 °C or **(b)** by photoiniferter polymerisation (λ = 395 nm) at 32 °C.

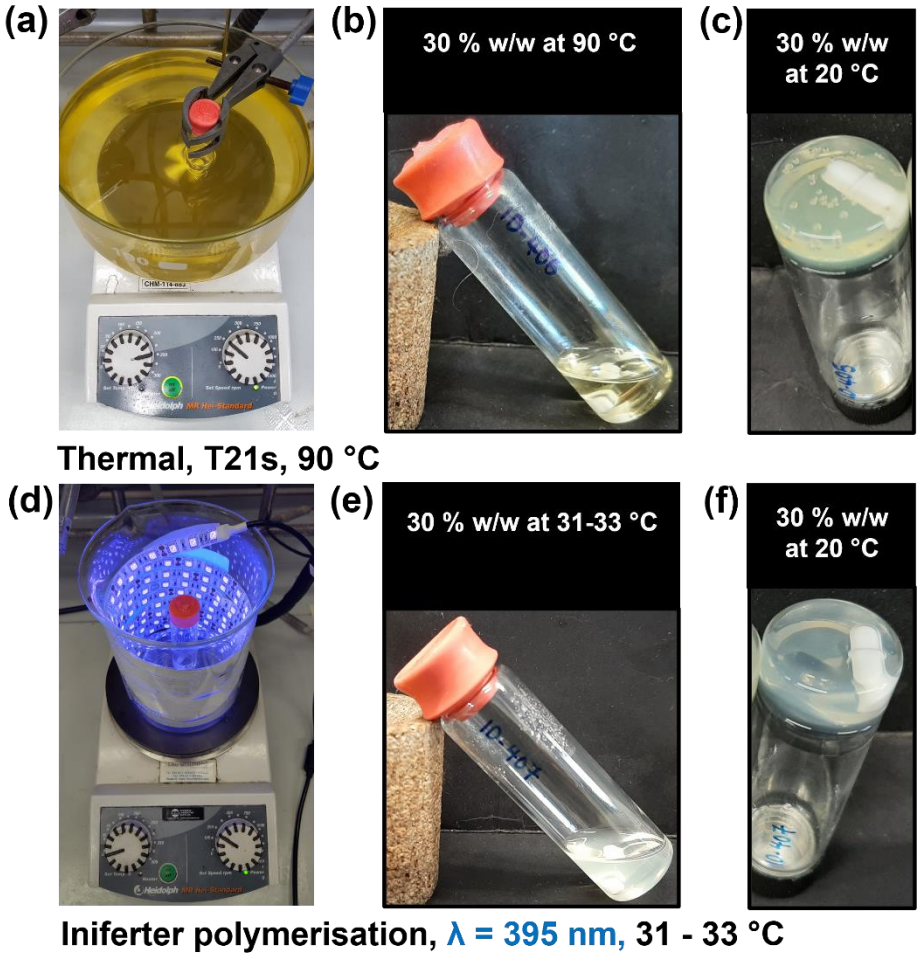

Figure 3.12. Digital photographs recorded when targeting the synthesis of a $PLMA_{102}$-$PBeMA_{20}$ diblock copolymer at 30% w/w solids in mineral oil: **(a)** the reaction setup for thermally-initiated polymerisation in an oil bath at 90 °C, and the concentrated solution **(b)** immediately after synthesis at 90 °C and **(c)** after cooling to 20 °C. Digital photographs, for the synthesis of $PLMA_{102}$-$PBeMA_{20}$ diblock copolymers at 30% w/w in mineral oil, showing **(d)** the reaction setup for photoiniferter polymerisation using violet light (λ = 395 nm) at 32 °C, and the concentrated solution **(e)** immediately after synthesis at 32 °C and **(f)** after cooling to 20 °C.

Each $PLMA_{102}$-$PBeMA_{20}$ diblock copolymer was characterised by THF GPC using a refractive index detector. An M_n of 25.5 kg mol^{-1} ($Đ$ = 1.17) was obtained for the thermally-initiated copolymer and an M_n of 26.3 kg mol^{-1} ($Đ$ = 1.18) was observed for the copolymer produced via iniferter polymerisation (see **Figure 3.13a**). In each case, the PLMA precursor exhibited a high blocking efficiency. Clearly, photoiniferter polymerisation enables a slightly higher conversion to be achieved with comparable MWD control under significantly milder reaction conditions compared to thermal

initiation at 90 °C using a chemical initiator. The effectiveness of photoiniferter RAFT polymerisation under relatively mild conditions has been well-documented.[38–41]

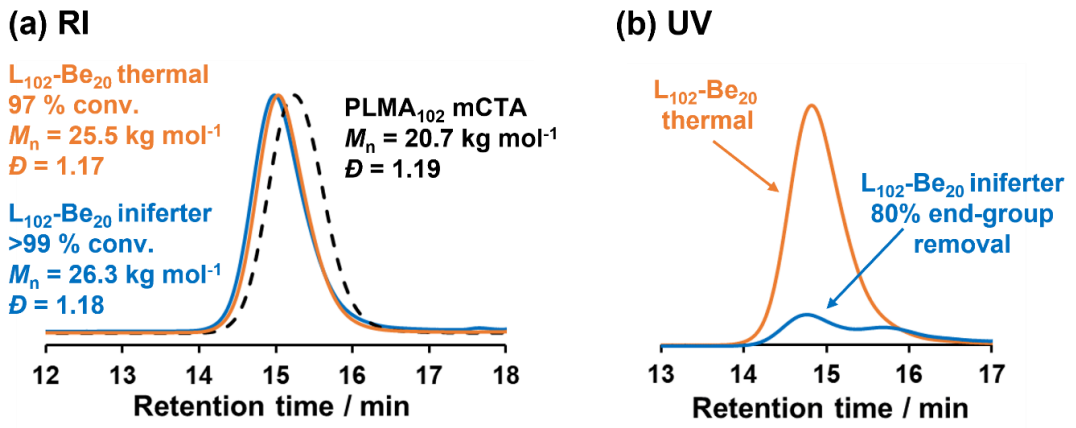

Figure 3.13. THF GPC curves recorded when targeting a $PLMA_{102}$-$PBeMA_{20}$ diblock copolymer via either thermally-initiated RAFT polymerisation at 90 °C or photoiniferter RAFT polymerisation at 32 °C: **(a)** using a refractive index (RI) detector and a $PLMA_{102}$ macro-CTA reference for comparison, and **(b)** a UV detector set to the absorption wavelength of the trithiocarbonate end-group (λ = 298 nm). In the latter case, exposure to violet light irradiation for 16 h leads to degradation of most of the trithiocarbonate end-groups. In contrast, the majority of the trithiocarbonate end-groups are retained during thermally-initiated polymerisation at 90 °C.

One important consequence of using the photoiniferter RAFT polymerisation protocol was the *in situ* removal of most of the RAFT trithiocarbonate end-groups. The final copolymer was discernibly less yellow and had a stronger malodour than that prepared by thermally-initiated polymerisation at 90 °C. THF GPC analysis using a UV detector (λ = 298 nm) confirmed that 80% of the RAFT end-groups had been removed during the polymerisation (relative to the UV GPC curve recorded for the same diblock copolymer prepared at 90 °C), see **Figure 3.13b**. Removal of trithiocarbonate RAFT end-groups during prolonged exposure to violet light has been recently reported by Gibson *et al.*[29] and Chan and co-workers.[42] Given that such RAFT end-groups may need to be removed for certain applications, such *in situ* degradation could be regarded as a potential advantage.[43,44] Moreover, given the comparable RI GPC M_n values observed for the two synthesis protocols, RAFT end-group degradation must occur

after completion of the photoiniferter polymerisation, rather than during the chain growth phase. Otherwise, a significantly higher M_n value (and a much higher $Đ$ value) would be expected.

On cooling to 20 °C, both $PLMA_{102}$-$PBeMA_{20}$ diblock copolymer solutions formed relatively transparent free-standing gels at 30% w/w solids (see **Figure 3.12c** and **Figure 3.12f**). Variable-temperature rheology experiments were conducted on the 30% w/w $PLMA_{102}$-$PBeMA_{20}$ diblock copolymer solution in mineral oil prepared by photoiniferter RAFT polymerisation at 32°C (>99% PBeMA conversion), see **Figure 3.14b**. The sample was loaded onto the heating plate and equilibrated at 60 °C for 5 min, before being subjected to a 60 °C to 10 °C to 60 °C thermal cycle at a constant cooling/ heating rate of 2.0 °C min^{-1}. A copolymer of equivalent composition prepared by thermally-initiated RAFT polymerisation at 90 °C (97% PBeMA conversion) was also analysed for comparison, see **Figure 3.14a**.

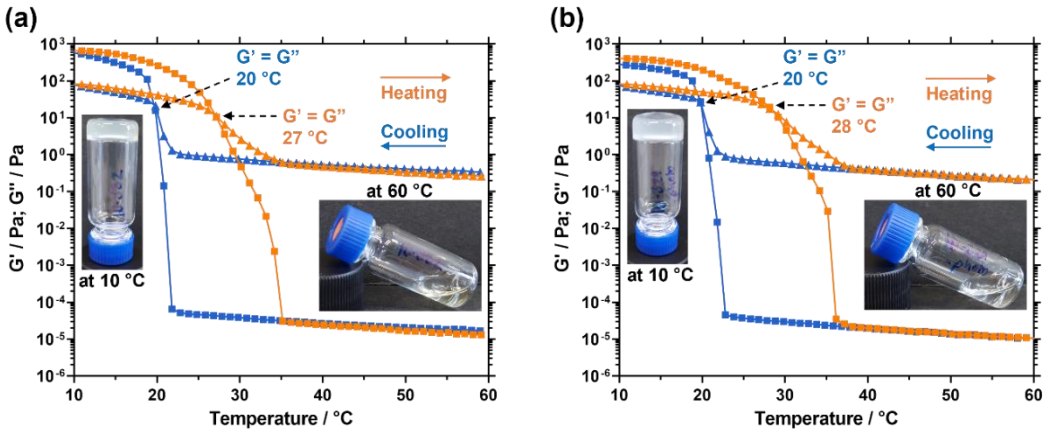

Figure 3.14. Temperature dependence of the storage modulus (G', squares) and loss modulus (G", triangles) obtained for $PLMA_{102}$-$PBeMA_{20}$ at 30% w/w solids in mineral oil on heating from 10 °C to 60 °C (orange symbols) and on cooling from 60 °C to 10 °C (blue symbols) at a constant cooling/heating rate of 2.0 °C min^{-1}: **(a)** prepared by thermal initiation at 90 °C and **(b)** prepared by photoiniferter polymerisation at 32 °C, Data were recorded at 1.0% strain amplitude using an angular frequency of 10 rad s^{-1}.

On heating from 10 °C to 26 °C, each 30% w/w dispersion exhibits solid-like properties, with the storage modulus (*G'*) being larger than the loss modulus (*G"*). The solid-to-liquid transition is defined by the crossover in the *G'* and *G"* curves observed above 27-28 °C. Above this temperature, both samples exhibit fluid-like properties (G" >> G'), as illustrated by the digital photographs recorded at 60 °C. On cooling from 60 °C to 10 °C, the liquid-like properties of both samples are initially retained before reverting to their original solid-like state below the crossover at 20 °C. This is often referred to as the critical gelation temperature (CGT).[45] In this case, significant hysteresis occurs; the CGT during the heating cycle (27-28 °C) is appreciably higher than that observed during the cooling cycle (20 °C). For comparison, Derry *et al.* reported that a relatively transparent, free-flowing, concentrated dispersion of non-interacting PBeMA-PBzMA spheres at 50 °C formed a turbid, paste-like dispersion on cooling to 20 °C as a result of macroscopic precipitation driven by the PBeMA stabiliser block, which becomes insoluble below 26 °C and forms crystalline microdomains.[26] Some hysteresis, as observed in **Figure 3.14**, is expected for a first-order phase transition, i.e. the melting and crystallisation of the PBeMA block. Crystallisation is a kinetically controlled process and depends on nucleation, whereas melting is thermodynamically controlled. Therefore, the crystallisation temperature is often lower than the melting temperature.

In principle, this thermoresponsive rheological behaviour is consistent with a worm-to-sphere (or perhaps worm-to-chain) transition occurring on heating. This is comparable to the worm-to-sphere transition reported by Fielding *et al.* for a dispersion of PLMA-PBzMA diblock copolymer worms in *n*-dodecane on heating from 20 °C to 50 °C.[46] If CDSA had occurred as well as PISA, then such behaviour might be more accurately described as a rod-to-sphere or a rod-to-chain transition.

According to the prior study by Derry *et al.*, the synthesis of $PLMA_{102}$-$PBeMA_{20}$ at 90 °C must be an example of a RAFT solution polymerisation. This is because the PBeMA chains are soluble in mineral oil at this elevated temperature. Thus, molecularly-dissolved diblock copolymer chains are formed, instead of sterically-stabilised nanoparticles. However, CDSA could in principle occur when such a reaction solution is allowed to cool from 90 °C to 20 °C. In principle, a genuine RAFT dispersion polymerisation (possibly also involving CDSA) might be achievable if a photoiniferter RAFT polymerisation was conducted at a suitable reaction temperature such that the BeMA monomer is soluble but the growing PBeMA chains become insoluble (and perhaps also undergo *in situ* crystallisation).

Both $PLMA_{102}$-$PBeMA_{20}$ diblock copolymers were diluted from 30% w/w to 0.1% w/w using *n*-dodecane as a diluent at either 5 °C or 20 °C prior to DLS and TEM analysis. Dilution at 5 °C was achieved with the aid of a refrigerator and DLS studies were performed at this temperature to encourage *in situ* crystallisation of the PBeMA block. However, z-average diameters of 173 nm and 188 nm (with a DLS PDI of 0.14 in each case) were observed at 5 °C and 20 °C for the diblock copolymer prepared via thermally-initiated RAFT polymerisation at 90 °C, see **Figure 3.15a**. Moreover, the derived count rate of 7,500 kcps determined at 5 °C was comparable to that observed at 20 °C (6,400 kcps), suggesting little or no change in particle size and morphology. Disappointingly, TEM studies merely indicated the presence of ill-defined, irregularly-shaped structures of less than 300 nm for dilute dispersions dried at either 5 °C (see **Figure 3.15b**) or 20 °C (**Figure 3.15c**). Certainly, there is no evidence of well-defined worms or rods, which makes the formation of relatively transparent gels at or below 20 °C rather perplexing.

For $PLMA_{102}$-$PBeMA_{20}$ prepared by photoiniferter RAFT polymerisation at 32 °C, DLS analysis also indicated the presence of colloidal structures with z-average diameters exceeding 400 nm at both 5 °C and 20 °C (see **Figure 3.15d**). Again, a slightly higher derived count rate was observed for the dispersion at 5 °C (8,400 kcps) compared to that at 20 °C (7,200 kcps). Ill-defined, irregularly-shaped structures of up to ~1 μm can be observed by TEM after drying 0.1% w/w dispersions at 5 °C (see **Figure 3.15e**) and at 20 °C (see **Figure 3.15f**). Clearly, TEM analysis of these two $PLMA_{102}$-$PBeMA_{20}$ diblock copolymers provides no evidence for the presence of diblock copolymer nano-objects with either a worm or rod morphology. Indeed, it is very difficult to understand how such relatively large, ill-defined morphologies could possibly result in the formation of relatively transparent gels at ambient temperature. Given that TEM would normally be expected to undersize relative to DLS, the cumulative evidence suggests some sort of drying artefact.

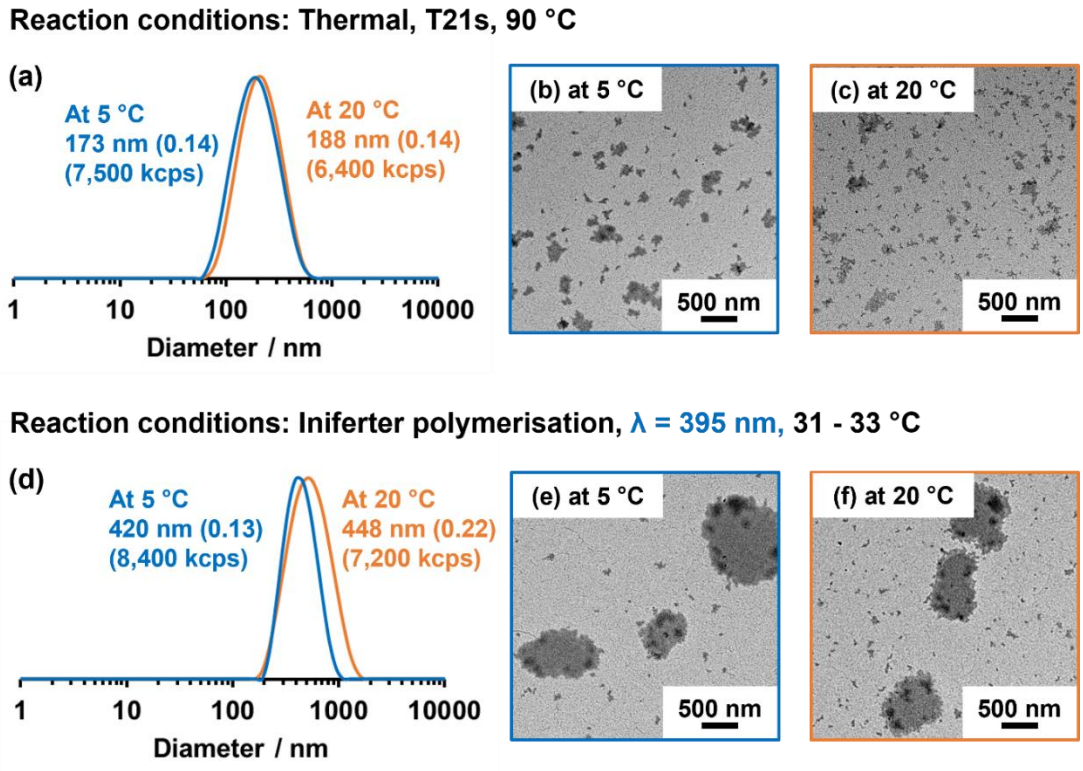

Figure 3.15. Characterisation of a $PLMA_{102}$-$PBeMA_{20}$ diblock copolymer prepared at 30% w/w solids in mineral oil by thermally-initiated RAFT polymerisation at 90 °C, followed by

dilution to 0.1% w/w using *n*-dodecane at either 5 °C or 20 °C. **(a)** Intensity-average particle size distributions obtained by DLS and corresponding TEM images for grids prepared at **(b)** 5 °C and **(c)** 20 °C. Characterisation of a $PLMA_{102}$-$PBeMA_{20}$ diblock copolymer prepared at 30% w/w solids in mineral oil by photoiniferter RAFT polymerisation at 32°C, followed by dilution to 0.1% w/w using *n*-dodecane at either 5 °C or 20 °C. **(d)** Intensity-average particle size distributions obtained by DLS and corresponding TEM images for grids prepared at **(e)** 5 °C and **(f)** 20 °C.

Nevertheless, according to Manners and co-workers, a corona/core block ratio of 5:1 should produce cylindrical rods via CDSA.[8,9,11] Thus, shear-induced polarised light imaging (SIPLI) was used to analyse the $PLMA_{102}$-$PBeMA_{20}$ diblock copolymer prepared via photoiniferter RAFT polymerisation at 32 °C (see **Figure 3.16**). This characterisation technique combines rotational rheology with plane-polarised light imaging: anisotropic particles become aligned at some critical shear rate, which leads to the appearance of a characteristic Maltese cross motif.[30,31,47–49] At 50 °C, the free-flowing copolymer solution has a relatively low viscosity of around 0.1 Pa s. On cooling, a marked increase in viscosity occurs below 18 °C, reaching 20 Pa s at 10 °C. At the latter temperature, the sample forms a weak free-standing gel under zero shear. On returning to 50 °C, the viscosity is gradually reduced to around 0.1 Pa and a free-flowing solution is obtained. The onset temperature for the sharp increase in viscosity indicated by this SIPLI experiment is consistent with that determined by temperature-dependent oscillatory rheology (CGT ≥ 20 °C). Uniformly dark images (*i.e.* no discernible Maltese cross) were observed between 50 °C and 10 °C (see **Figure 3.16a-c** for selected images recorded at 50 °C, 18 °C and 10 °C). The absence of this characteristic motif confirms no shear-induced alignment owing to the absence of any anisotropic nanoparticles (worms or rods).

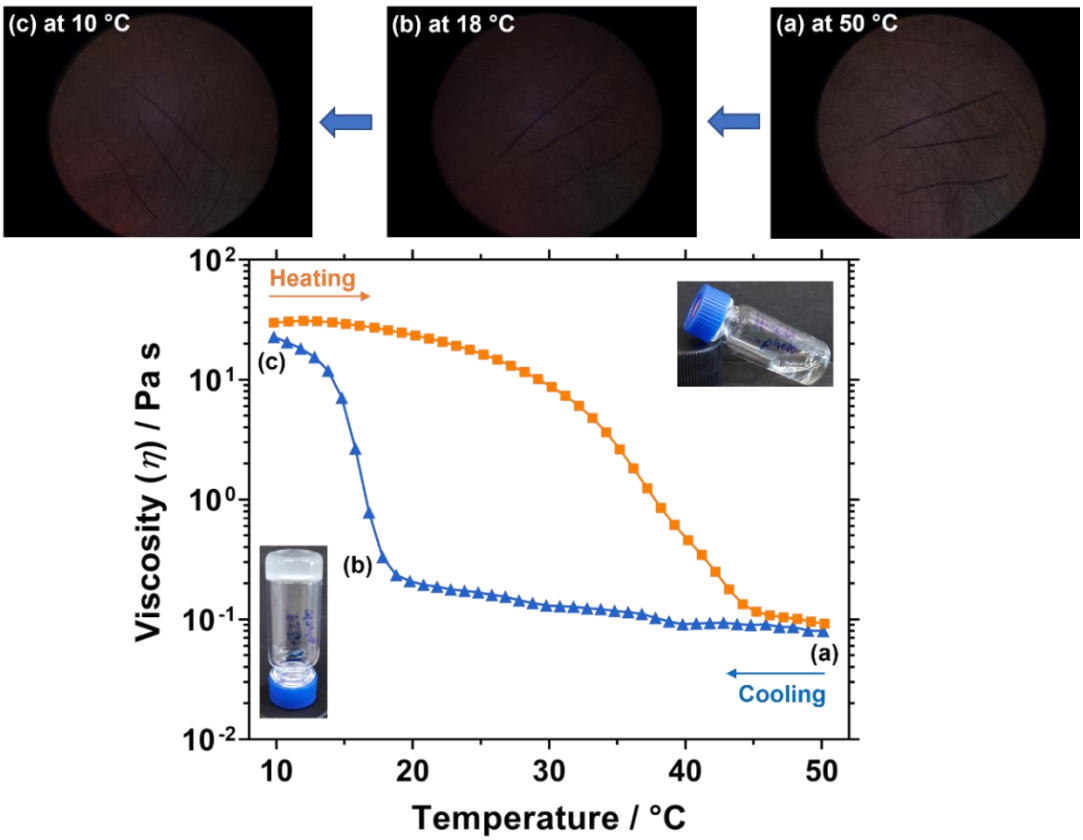

Figure 3.16. Viscosity-temperature plot and shear-induced polarised light images (SIPLI) recorded for a 30 % w/w solution of a $PLMA_{102}$-$PBeMA_{20}$ diblock copolymer (prepared *via* photoiniferter RAFT polymerisation) obtained during a thermal cycle from 50 °C to 10 °C to 50 °C at a constant cooling/heating rate of 2 °C min^{-1} and a fixed shear rate of 1.0 s^{-1}. SIPLI images were recorded at **(a)** 50 °C and then on cooling to **(b)** 18 °C and **(c)** 10 °C. The absence of any Maltese cross indicates that no shear-induced alignment occurs for this sample.

3.4.5. Synthesis of $PLMA_{102}$-$PBeMA_{20}$ diblock copolymers via photoiniferter RAFT polymerisation at 15 °C

In principle, nanoparticle formation via (PI-)CDSA should be most likely to occur at a temperature at which the growing semi-crystalline PBeMA chains become insoluble in the reaction mixture while the PLMA macro-CTA and BeMA monomer remain soluble. A DSC study of the $PLMA_{102}$-$PBeMA_{20}$ diblock copolymer synthesised via RAFT solution polymerisation at 90 °C indicated a crystallisation temperature (T_c) of 20 °C and a melting temperature (T_m) of 30 °C (see **Figure 3.17b**). These results are reasonably consistent with the oscillatory rheology measurements, whereby a CGT of around 20 °C and a critical degelation temperature of approximately 28 °C were

determined for the same diblock copolymer (see **Figure 3.14b**). A sample of BeMA monomer at 6% w/w in mineral oil was also analysed by DSC for comparison (see **Figure 3.17a**). In principle, the optimum reaction temperature for *in situ* PI-CDSA should occur below the T_c of the diblock copolymer observed in mineral oil on cooling, but above the T_c of BeMA (*i.e.* between 2 °C and 20 °C) to ensure solubility of this monomer. Thus, the photoiniferter RAFT polymerisation conducted at 32 °C described above actually corresponds to solution polymerisation conditions.

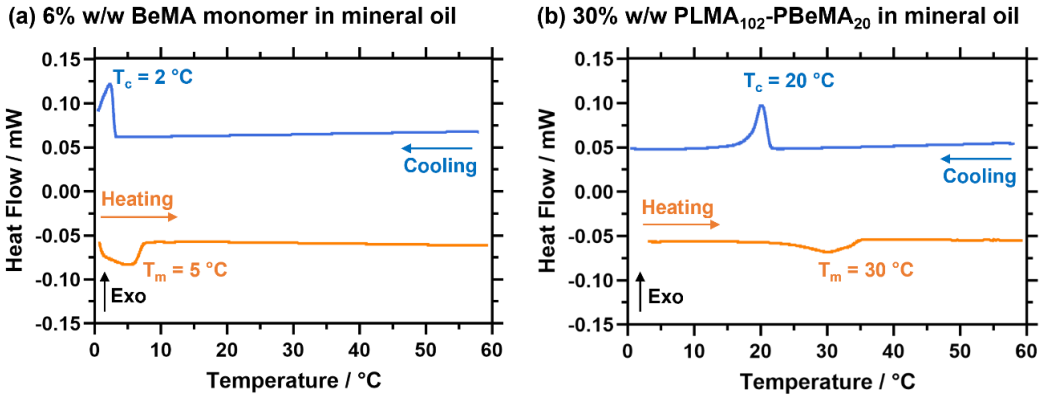

Figure 3.17. DSC experiments conducted at a constant cooling/heating rate of 2.0 °C min^{-1} for **(a)** a 30% w/w solution of behenyl methacrylate (BeMA) monomer in mineral oil and **(b)** 30% w/w solution of a $PLMA_{102}$-$PBeMA_{20}$ diblock copolymer in mineral oil.

Prior to polymerisation, a simple solubility test was conducted to assess the temperature-dependent solubility of BeMA in the reaction mixture. The reaction mixture was first heated at 60 °C until a transparent solution was obtained, then this solution was cooled in a glass cuvette at 5 °C intervals (with 5 min being allowed for thermal equilibration at each temperature). The visual appearance of the reaction mixture was observed at each temperature to judge its solubility. The reaction mixture remained a transparent solution on cooling to 10 °C (see **Figure 3.18a**). After holding for 5 min at 5 °C, a turbid suspension is formed as the BeMA monomer reached its crystallisation temperature and became insoluble (see **Figure 3.18b**). This is consistent with the DSC data (see **Figure 3.17**), where the BeMA monomer became

insoluble below its T_c of 2 °C. The 3 °C difference in solubility temperature for these two methods may be simply the result of the differing cooling rates. Alternatively, the presence of the $PLMA_{102}$ macro-CTA in the reaction mixture could account for this difference: the DSC experiment was conducted on a model system comprising 6% w/w BeMA in mineral oil.

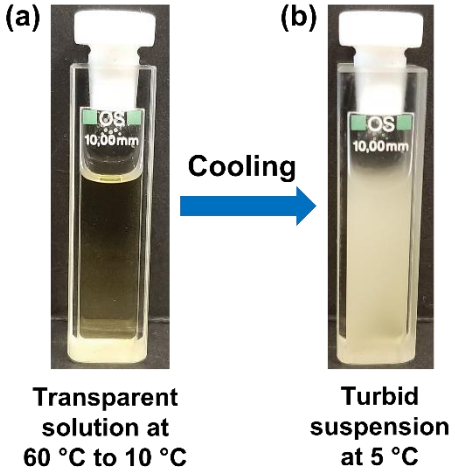

Figure 3.18. Digital photographs recorded for the reaction mixture prior to the BeMA polymerisation when targeting a $PLMA_{102}$-$PBeMA_{20}$ diblock copolymer: **(a)** the transparent reaction solution that is observed from 60 °C to 10 °C and **(b)** the turbid suspension that is formed at 5 °C.

Informed by the DSC and BeMA solubility studies, the synthesis of $PLMA_{102}$-$PBeMA_{20}$ diblock copolymer was conducted at 15 °C at 30% w/w solids in mineral oil via photoiniferter RAFT polymerisation (see **Scheme 3.6**). This reaction temperature was selected because it lies between the T_m of the BeMA monomer and the T_m for the target diblock copolymer. Hence such reaction conditions should afford the best opportunity for the desired PI-CDSA synthesis.

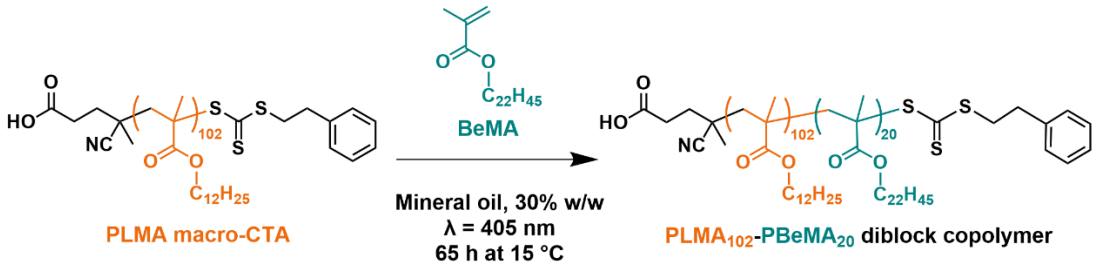

Scheme 3.6. Synthesis of a poly(lauryl methacrylate)-poly(behenyl methacrylate) ($PLMA_{102}$-$PBeMA_{20}$) diblock copolymer *via* RAFT solution polymerisation of BeMA at 30% w/w solids in mineral oil by photoiniferter polymerisation (λ = 405 nm) at 15 °C.

A glass vial containing the reaction mixture was placed in a water-jacketed Schlenk tube wrapped in blue LED light strips (λ = 405 nm, 0.37 mW cm^{-2}) with the recirculating water temperature set to 13 °C (see **Figure 3.19a**). Under these conditions, the average temperature of the reaction mixture over the 65 h reaction period was 14.8 °C, as determined using a Raspberry Pi thermocouple (see **Figure 3.19b**). This experimental setup is identical to that employed by Gibson *et al.* and Chan and co-workers for the RAFT end-group removal from diblock copolymer nanoparticles at elevated temperature.[29,42]

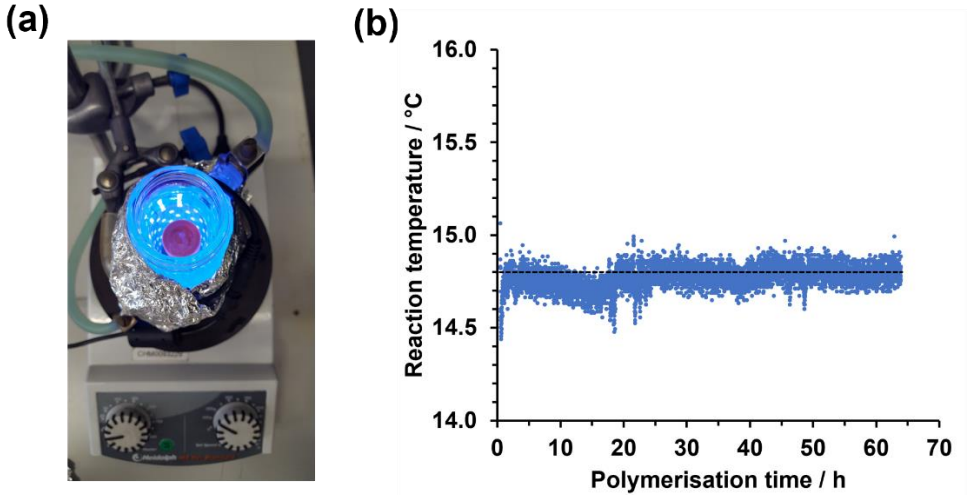

Figure 3.19. (a) Digital photograph showing the reaction setup comprising a water-jacketed Schlenk tube wrapped in blue LED light strips (λ = 405 nm, 0.37 mW cm^{-2}) for the synthesis of $PLMA_{102}$-$PBeMA_{20}$ at 30% w/w in mineral oil by photoiniferter RAFT polymerisation at 15 °C **(b)** The corresponding reaction temperature *vs.* polymerisation time plot. Temperature recorded every 30 s using a Raspberry Pi thermocouple inserted into the reaction mixture (blue data points). Dashed line corresponds to the mean temperature (14.8 °C) recorded over the 65 h polymerisation.

A BeMA monomer conversion of 96% was achieved after 65 h at 15 °C as judged by ^{1}H NMR spectroscopy studies. This polymerisation was repeated at 40% w/w solids in mineral oil and a BeMA conversion of 98% was achieved after 65 h at 15 °C. The final reaction mixture obtained at 15 °C when targeting 30% w/w solids is a slightly turbid, viscous fluid (see **Figure 3.20a**). In contrast, the reaction mixture obtained at 40% w/w solids is a free-standing gel at the same temperature (see **Figure 3.20b**).

Comparable M_n values and relatively narrow molecular weight distributions ($Đ$ = 1.22) were obtained for both copolymers as judged by THF GPC using a refractive index detector and a clear shift in molecular weight was observed relative to the corresponding $PLMA_{102}$ precursor (see **Figure 3.20c**). UV GPC analysis (λ = 298 nm) indicated either 82% or 74% loss of the original trithiocarbonate end-groups for $PLMA_{102}$-$PBeMA_{20}$ prepared at 30% w/w and 40% w/w solids, respectively (see **Figure 3.20d**). These losses are comparable to the 80% end-group removal observed for the photoiniferter RAFT polymerisation conducted at 32 °C for 16 h. Presumably, the much longer irradiation time compensates for the lower reaction temperature.

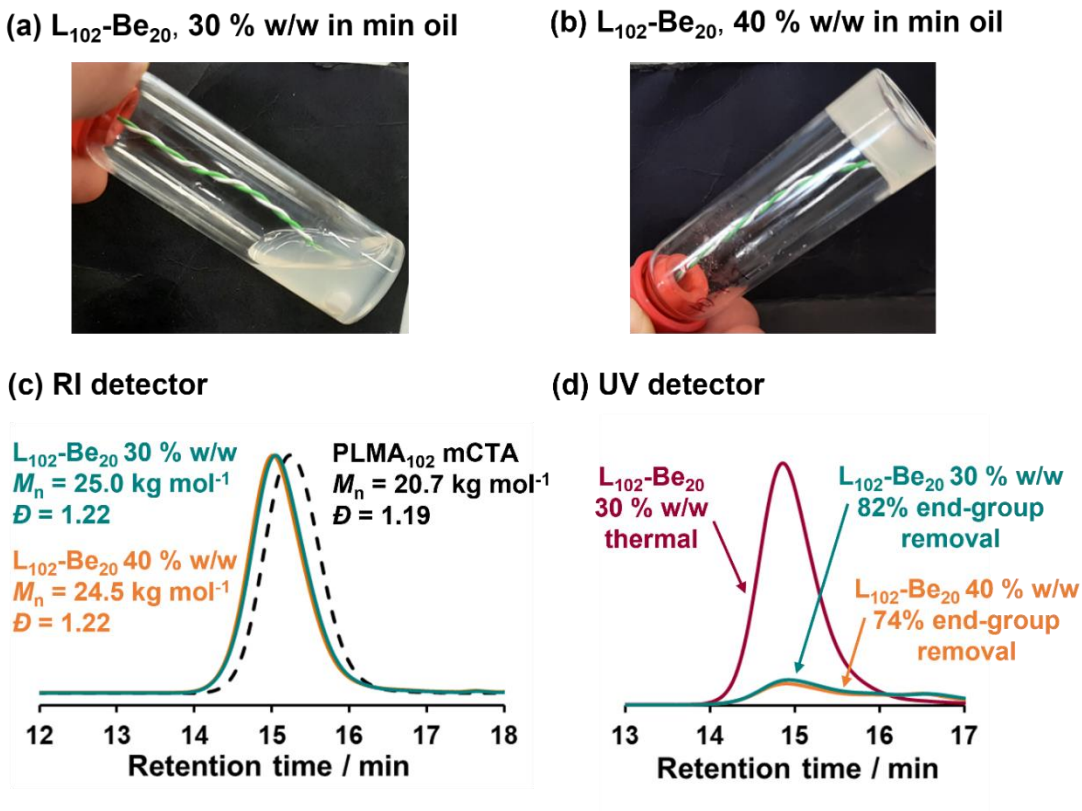

Figure 3.20. Digital photographs recorded immediately after targeting the synthesis of a $PLMA_{102}$-$PBeMA_{20}$ diblock copolymer *via* photoiniferter RAFT polymerisation at 15 °C in mineral oil at **(a)** 30% w/w solids (free-flowing fluid) and **(b)** 40% w/w solids (free-standing gel). THF GPC curves recorded for such $PLMA_{102}$-$PBeMA_{20}$ diblock copolymers **(c)** using a refractive index (RI) detector (with $PLMA_{102}$ precursor as reference) and **(d)** using a UV detector (λ = 295 nm) [N.B. the calculated extent of RAFT end-group removal is calculated relative to that of a $PLMA_{102}$-$PBeMA_{20}$ diblock copolymer prepared *via* thermal initiation at 90 °C].

Each reaction mixture was diluted to 0.1% w/w solids using *n*-dodecane as the diluent at either 5 °C or 20 °C prior to analysis by DLS and TEM. $PLMA_{102}$-$PBeMA_{20}$ diblock copolymers prepared by RAFT solution polymerisation at either 90 °C or 32 °C – for which conditions no PI-CDSA can occur – were used as reference materials (see **Figure 3.15**). As discussed above, the $PLMA_{102}$-$PBeMA_{20}$ diblock copolymer prepared by photoiniferter RAFT polymerisation at 15 °C was considered to offer the best possible chance of nanoparticle formation via PI-CDSA. DLS analysis of 0.1% w/w $PLMA_{102}$-$PBeMA_{20}$ in *n*-dodecane at 20 °C indicated z-average diameters of 111 nm (PDI = 0.39) and 226 nm (PDI = 0.28) for syntheses conducted at 30% w/w

solids and 40% w/w/ solids, respectively (see **Figure 3.21a** and **Figure 3.21d**). In both cases, significantly larger particles and higher derived count rates were obtained at 5 °C Disappointingly, TEM analysis only indicated an ill-defined morphology comprising irregularly-shaped colloidal particles at both 20 °C (see **Figure 3.21b** and **Figure 3.21e**) and 5 °C (see **Figure 3.21c** and **Figure 3.21f**).

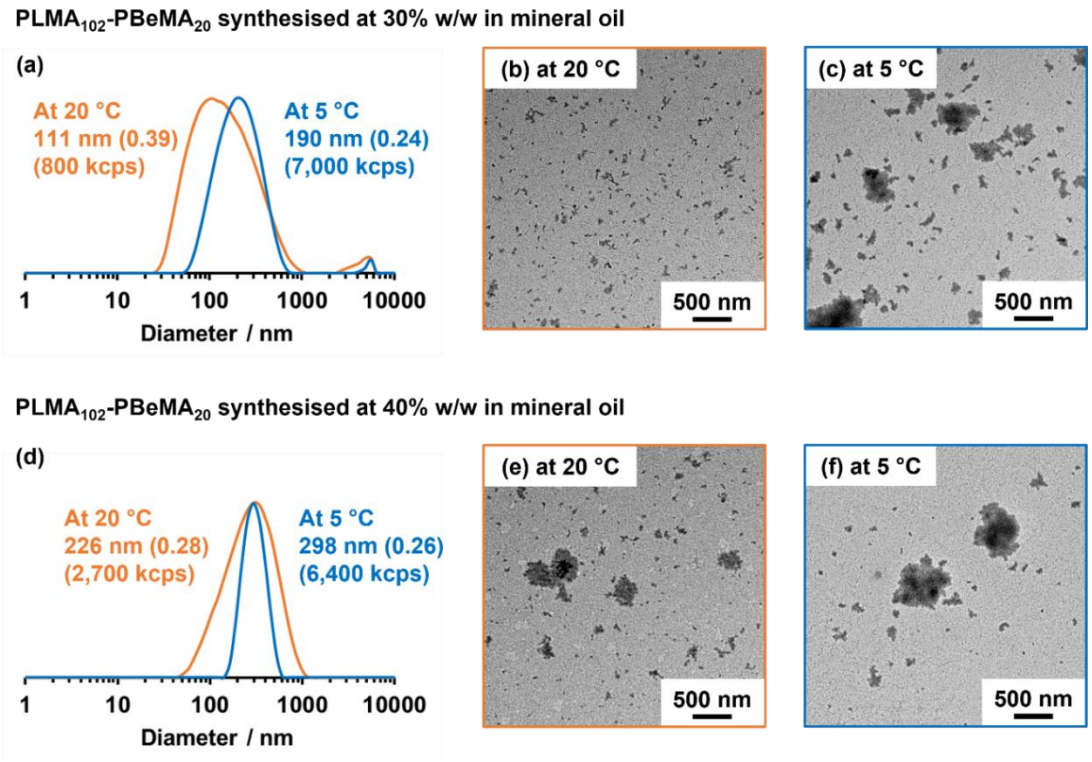

Figure 3.21. Characterisation of a $PLMA_{102}$-$PBeMA_{20}$ diblock copolymer prepared at 30% w/w solids in mineral oil by photoiniferter RAFT polymerisation at 15 °C, followed by dilution to 0.1% w/w using *n*-dodecane at either 5 °C or 20 °C. **(a)** Intensity-average particle size distributions obtained by DLS and corresponding TEM images for grids prepared at **(b)** 5 °C and **(c)** 20 °C. Characterisation of a $PLMA_{102}$-$PBeMA_{20}$ diblock copolymer prepared at 40% w/w solids in mineral oil by photoiniferter RAFT polymerisation at 15 °C, followed by dilution to 0.1% w/w using *n*-dodecane at either 5 °C or 20 °C. **(d)** Intensity-average particle size distributions obtained by DLS and corresponding TEM images for grids prepared at **(e)** 5 °C and **(f)** 20 °C.

In summary, DLS and TEM analysis of $PLMA_{102}$-$PBeMA_{20}$ diblock copolymers prepared at 15 °C (*i.e.* below the T_c of the PBeMA block) indicated similar results to those obtained for $PLMA_{102}$-$PBeMA_{20}$ diblock copolymers prepared at higher temperatures (*i.e.* above the T_c of the PBeMA block). Thus there is no evidence to

suggest that PI-CDSA occurs under the conditions explored in this study. Moreover, given the known insolubility of PBeMA in mineral oil at around 20 °C, it is surprising that conventional PISA does not occur under such conditions. One possible explanation is that the enthalpy of polymerisation leads to an effective reaction temperature that is higher than 20 °C. However, temperature data from a Raspberry Pi thermocouple during the reaction which shows that the temperature does not exceed 15.1 °C over the 65 h reaction period, shows that this is not the case. Alternatively, it is feasible that the desired anisotropic nanoparticles are formed at high copolymer concentrations but then undergo dissociation when subjected to high dilution using *n*-dodecane. In this context, a similarly problematic PISA formulation has just been reported by Beattie and co-workers.[50] However, SIPLI observations at 30% w/w show no evidence of anisotropic particles. In principle, investigating alternative (polar) non-solvents for the PBeMA block such as *iso*-propyl alcohol (IPA) should promote self-assembly.

3.5. Conclusions

In summary, a semi-crystalline BeMA monomer has been prepared from behenyl alcohol and methacrylic acid. The purified product exhibits comparable NMR spectra and elemental microanalyses to that obtained for the original BeMA batch supplied by Lubrizol. Moreover, GC-MS data, melting points and FT-IR spectra are also in good agreement. The in-house synthesised BeMA monomer was used to prepare $PLMA_{102}$-$PBeMA_{20}$ diblock copolymers at 30% w/w solids in mineral oil by RAFT solution polymerisation at 90 °C using a thermal initiator and by photoiniferter RAFT polymerisation using violet light irradiation at 32 °C. Up to 99% BeMA conversion was achieved despite the relatively low molar concentration of this monomer.

Photoiniferter RAFT polymerisation resulted in the loss of approximately 80% of the trithiocarbonate end-groups within 16 h at 32 °C, which resulted in a strong malodor for the final reaction mixture. However, GPC analysis indicated that comparable M_n and $Đ$ values were obtained for both synthetic protocols, which suggests that RAFT end-group removal must occur after, rather than during, the BeMA polymerisation. Such $PLMA_{102}$-$PBeMA_{20}$ diblock copolymers exhibited reversible thermoresponsive behaviour: relatively transparent free-standing gels were formed at or below 20 °C, whereas free-flowing fluids were obtained at higher temperatures. Oscillatory rheology studies indicate that G' increased by more than five orders of magnitude on cooling a 30% w/w solution of $PLMA_{102}$-$PBeMA_{20}$ diblock copolymer in mineral oil from 60 °C to 10 °C. In principle, such behaviour is consistent with the formation of PBeMA-core rods or worms. However, TEM, DLS and SIPLI studies did not provide any evidence for the presence of such highly anisotropic nanoparticles. Instead, only ill-defined colloidal aggregates were observed.

DSC analysis has been used to identify the crystallisation temperature of the $PLMA_{102}$-$PBeMA_{20}$ diblock copolymer (T_c = 20 °C). Accordingly, photoiniferter RAFT polymerisation of BeMA has been conducted at 15 °C to evaluate the feasibility of nanoparticle formation via *in situ* polymerisation-induced crystallisation-driven self-assembly (PI-CDSA) at 15 °C. Intriguingly, a relatively transparent free-standing gel can be obtained at 40% w/w solids. Unfortunately, TEM and DLS analysis of the diluted reaction mixture again provided no evidence for the formation of $PLMA_{102}$-$PBeMA_{20}$ rods or worms.

Nevertheless, there remains considerable scope to expand the range of reaction temperatures for photoiniferter RAFT polymerisation while also investigating a wider range of non-solvents for the PBeMA block. Although well-defined nanoparticles

could not be obtained via (PI-)CDSA, similar PLMA-PBeMA diblock copolymers to those reported herein were subsequently evaluated as an additive for wax crystal modification, as described in Chapter 4.

3.6. References

1 Y. Mai and A. Eisenberg, *Chem. Soc. Rev.*, 2012, **41**, 5969–5985.

2 M. Karayianni and S. Pispas, *J. Polym. Sci.*, 2021, **59**, 1874–1898.

3 B. Charleux, G. Delaittre, J. Rieger and F. D'Agosto, *Macromolecules*, 2012, **45**, 6753–6765.

4 S. L. Canning, G. N. Smith and S. P. Armes, *Macromolecules*, 2016, **49**, 1985–2001.

5 C. Liu, C.-Y. Hong and C.-Y. Pan, *Polym. Chem.*, 2020, **11**, 3673–3689.

6 J. C. Foster, S. Varlas, B. Couturaud, Z. Coe and R. K. O'reilly, *J. Am. Chem. Soc*, 2019, **141**, 2742–2753.

7 L. MacFarlane, C. Zhao, J. Cai, H. Qiu and I. Manners, *Chem. Sci.*, 2021, **12**, 4661–4682.

8 J. A. Massey, K. Temple, L. Cao, Y. Rharbi, J. Raez, M. A. Winnik and I. Manners, *J. Am. Chem. Soc.*, 2000, **122**, 11577–11584.

9 L. Cao, I. Manners and M. A. Winnik, *Macromolecules*, 2002, **35**, 8258–8260.

10 I. Korczagin, M. A. Hempenius, R. G. Fokkink, M. A. Cohen Stuart, M. Al-Hussein, P. H. H. Bomans, P. M. Frederik and G. Julius Vancso, *Macromolecules*, 2006, **39**, 2306–2315.

11 D. A. Rider and I. Manners, *Polym. Rev.*, 2007, **47**, 165–195.

12 S. F. M. Yusoff, M. S. Hsiao, F. H. Schacher, M. A. Winnik and I. Manners, *Macromolecules*, 2012, **45**, 3883–3891.

13 J. Raez, I. Manners and M. A. Winnik, *J. Am. Chem. Soc.*, 2002, **124**, 10381–10395.

14 A. Blanazs, A. J. Ryan and S. P. Armes, *Macromolecules*, 2012, **45**, 5099–5107.

15 L. A. Fielding, M. J. Derry, V. Ladmiral, J. Rosselgong, A. M. Rodrigues, L. P. D. Ratcliffe, S. Sugihara and S. P. Armes, *Chem. Sci.*, 2013, **4**, 2081–2087.

16 S. Sugihara, A. Blanazs, S. P. Armes, A. J. Ryan and A. L. Lewis, *J. Am. Chem. Soc.*, 2011, **133**, 15707–15713.

17 A. A. Cockram, T. J. Neal, M. J. Derry, O. O. Mykhaylyk, N. S. J. Williams, M.

W. Murray, S. N. Emmett and S. P. Armes, *Macromolecules*, 2017, **50**, 796–802.

18 J. C. Foster, S. Varlas, B. Couturaud, J. R. Jones, R. Keogh, R. T. Mathers and R. K. O'Reilly, *Angew. Chemie Int. Ed.*, 2018, **57**, 15733–15737.

19 F. D'Agosto, J. Rieger and M. Lansalot, *Angew. Chemie - Int. Ed.*, 2020, **59**, 8368–8392.

20 X. Wang, G. Guerin, H. Wang, Y. Wang, I. Manners and M. A. Winnik, *Science*, 2007, **317**, 644–647.

21 J. B. Gilroy, T. Gädt, G. R. Whittell, L. Chabanne, J. M. Mitchels, R. M. Richardson, M. A. Winnik and I. Manners, *Nat. Chem.*, 2010, **2**, 566–570.

22 C. E. Boott, J. Gwyther, R. L. Harniman, D. W. Hayward and I. Manners, *Nat. Chem.*, 2017, **9**, 785–792.

23 A. M. Oliver, J. Gwyther, C. E. Boott, S. Davis, S. Pearce and I. Manners, *J. Am. Chem. Soc.*, 2018, **140**, 18104–18114.

24 Y. Sha, M. A. Rahman, T. Zhu, Y. Cha, C. W. McAlister and C. Tang, *Chem. Sci.*, 2019, **10**, 9782–9787.

25 P. J. Hurst, A. M. Rakowski and J. P. Patterson, *Nat. Commun.*, 2020, **11**, 1–12.

26 M. J. Derry, O. O. Mykhaylyk, A. J. Ryan and S. P. Armes, *Chem. Sci.*, 2018, **9**, 4071–4082.

27 M. J. Rymaruk, K. L. Thompson, M. J. Derry, N. J. Warren, L. P. D. Ratcliffe, C. N. Williams, S. L. Brown and S. P. Armes, *Nanoscale*, 2016, **8**, 14497–14506.

28 N. Ghasdian, M. A. Ward and T. K. Georgiou, *Chem. Commun.*, 2014, **50**, 7114–7116.

29 R. R. Gibson, E. J. Cornel, O. M. Musa, A. Fernyhough and S. P. Armes, *Polym. Chem.*, 2020, **11**, 1785–1796.

30 O. O. Mykhaylyk, *Soft Matter*, 2010, **6**, 4430–4440.

31 O. O. Mykhaylyk, P. Chambon, C. Impradice, J. P. A. Fairclough, N. J. Terrill and A. J. Ryan, *Macromolecules*, 2010, **43**, 2389–2405.

32 Y. Kim, H. L. Strauss and R. G. Snyder, *J. Phys. Chem.*, 1989, **93**, 7520–7526.

33 H. Yoshida, *J. Therm. Anal. Calorim.*, 1999, **57**, 679–685.

34 B. Kaczmarczyk, B. Morejko-Buz and A. Stolarzewicz, *Anal. Bioanal. Chem.*, 2001, **370**, 899–903.

35 P. Cacioli, D. G. Hawthorne, R. L. Laslett, E. Rizzardo and D. H. Solomon, *J.*

Macromol. Sci. Part A - Chem., 1986, **23**, 839–852.

36 M. Rodlert, E. Harth, I. Rees and C. J. Hawker, *J. Polym. Sci. Part A Polym. Chem.*, 2000, **38**, 4749–4763.

37 M. J. Derry, L. A. Fielding and S. P. Armes, *Polym. Chem.*, 2015, **6**, 3054–3062.

38 J. Xu, K. Jung, A. Atme, S. Shanmugam and C. Boyer, *J. Am. Chem. Soc.*, 2014, **136**, 5508–5519.

39 T. G. McKenzie, Q. Fu, E. H. H. Wong, D. E. Dunstan and G. G. Qiao, *Macromolecules*, 2015, **48**, 3864–3872.

40 T. G. McKenzie, L. P. M. Da Costa, Q. Fu, D. E. Dunstan and G. G. Qiao, *Polym. Chem.*, 2016, **7**, 4246–4253.

41 M. Hartlieb, *Macromol. Rapid Commun.*, 2022, **43**, 2100514.

42 D. H. H. Chan, A. A. Cockram, R. R. Gibson, E. L. Kynaston, C. Lindsay, P. Taylor and S. P. Armes, *Polym. Chem.*, 2021, **12**, 5760–5769.

43 A. Postma, T. P. Davis, G. Moad and M. S. O'Shea, *Macromolecules*, 2005, **38**, 5371–5374.

44 H. Willcock and R. K. O'Reilly, *Polym. Chem.*, 2010, **1**, 149–157.

45 R. Verber, A. Blanazs and S. P. Armes, *Soft Matter*, 2012, **8**, 9915–9922.

46 L. A. Fielding, J. A. Lane, M. J. Derry, O. O. Mykhaylyk and S. P. Armes, *J. Am. Chem. Soc.*, 2014, **136**, 5790–5798.

47 C. Holland, F. Vollrath, A. J. Ryan and O. O. Mykhaylyk, *Adv. Mater.*, 2012, **24**, 105–109.

48 O. O. Mykhaylyk, A. J. Parnell, A. Pryke and J. P. A. Fairclough, *Macromolecules*, 2012, **45**, 5260–5272.

49 O. O. Mykhaylyk, N. J. Warren, A. J. Parnell, G. Pfeifer and J. Laeuger, *J. Polym. Sci. Part B Polym. Phys.*, 2016, **54**, 2151–2170.

50 D. L. Beattie, O. J. Deane, O. O. Mykhaylyk and S. P. Armes, *Polym. Chem.*, 2022, **13**, 655–667.

Chapter 4. Synthesis of Crystallisable Poly(lauryl methacrylate)-Poly(behenyl methacrylate) Block and Statistical Copolymers and their Application as Wax Crystal Modifiers

4.1. Introduction

The formation of insoluble paraffinic wax crystals in oil at sub-ambient temperature is a long-standing problem that causes pipeline blockages in cold climates.[1,2] This is an important issue for both crude oil transportation and the delivery of diesel fuel to automotive engines.[3–6] The onset temperature at which these *n*-paraffins exceed their solubility limit and precipitate in the form of waxes is often denoted as the 'wax appearance temperature' (WAT) or cloud point temperature.[6,7] Such deposits consist of lamellar crystals that form random, interlocking structures containing occluded crude oil.[8] These crystals form a 3D network, where as little as 2% w/w solid wax is required for gelation.[9,10] Below the WAT, the temperature at which the oil no longer flows under static conditions is known as the pour point temperature (PPT).[7,11]

In principle, the precipitation of wax crystals can be suppressed by the addition of suitable oil-soluble copolymers, which are known as 'wax inhibitors' (WIs) or 'pour point depressants' (PPDs), or more broadly as 'wax crystal modifiers'.[6,12] A wide range of copolymers and various architectures have been evaluated in this context. These include polyethylene-polybutene[8,13–15] or polyethylene-poly(ethylene-*stat*-propylene) diblock or statistical copolymers,[16,17] ethylene-vinyl acetate (EVA)[18–21] or (meth)acrylic[22,23] statistical copolymers and maleic anhydride-based alternating (or statistical) copolymers (see **Figure 4.1**).[4,5,24] In each case, one comonomer is designed to interact with the paraffinic wax while the other comonomer remains solvated and hence confers steric stabilisation. Ideally, the minimum temperature at which wax crystals are formed is lowered below the relevant working temperature for the oil, so there is no precipitation. Alternatively, the wax crystal habit is modified such that the size and shape of the wax crystals do not lead to pipeline blockages. Most studies

report a reduction in crystal size in the presence of wax inhibitors,[19,25–29] and thus a lower critical gelation concentration (CGC).

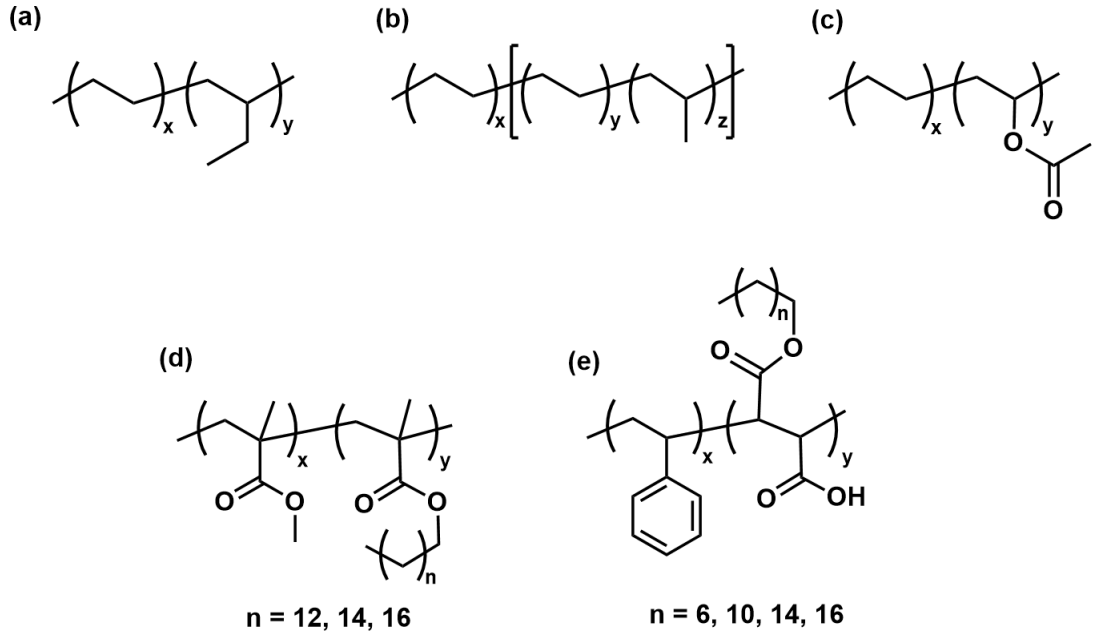

Figure 4.1. Chemical structures of example copolymers evaluated in the literature for wax crystal modification, which include **(a)** polyethylene-*co*-polybutene, **(b)** polyethylene-poly(ethylene-*stat*-propylene), **(c)** poly(ethylene-*stat*-vinyl acetate), **(d)** poly(methyl methacrylate-*stat*-alkyl methacrylate) and **(e)** mono-ester of poly(styrene-*co*-maleic anhydride).

Although some studies report no significant change in the WAT in the presence of wax inhibitors,[5,30–32] the addition of a PPD typically lowers the WAT.[25,33–35] Sjöblom and co-workers reported a reduction in the WAT from approximately 20 °C without any PPD to 15-19 °C for five different PPDs tested, when using DSC to study a 5% w/w macrocrystalline wax in toluene at a PPD concentration of 1000 ppm.[25] This was attributed to a change in the solubility equilibrium as a result of the formation of solute complexes.[36] A change in crystal morphology was also reported. Optical microscopy studies indicated that the wax crystals formed in the absence of any PPD exhibited a mixed needle and plate morphology, whereas those formed in the presence

of the most effective PPD (a commercial carboxylate-based polymer) had a smaller, more compact structure.

In 2015 Binks and co-workers conducted a series of experiments using three model waxes (*n*-eicosane, *n*-tetracosane or *n*-hexatriacontane, *i.e.* $C_{20}H_{42}$, $C_{24}H_{50}$ or $C_{36}H_{74}$).[37] Assuming a thermodynamically ideal solution, the temperature dependence for wax solubility was predicted for *n*-heptane or toluene, which served as model non-polar aliphatic and aromatic solvents respectively. For a given wax concentration, the PPT corresponds to that at which a critical volume fraction of wax crystals has precipitated. Close to this temperature, the wax crystals typically comprise irregular platelets that form a 3D network (see **Figure 4.2a**). Addition of a suitable PPD copolymer typically reduced the size and axial ratio (thickness *h* / diameter *d*) of the wax crystals, as shown in **Figure 4.2b**, which in turn increased the critical volume fraction of wax crystals required to form a 3D network (and hence block a pipeline). Moreover, PPD performance was correlated with the difference between the wax and the polymer solubility boundary temperatures for four different copolymers. More specifically, the pour-point reduction for formulations containing 20% wax by mass proved to be most effective when the critical solubility temperature of the PPD copolymer in a given solvent was approximately 15 °C below that of the target wax–solvent system. In principle, this empirical approach provided a useful method for the rapid identification of next-generation PPD copolymers.

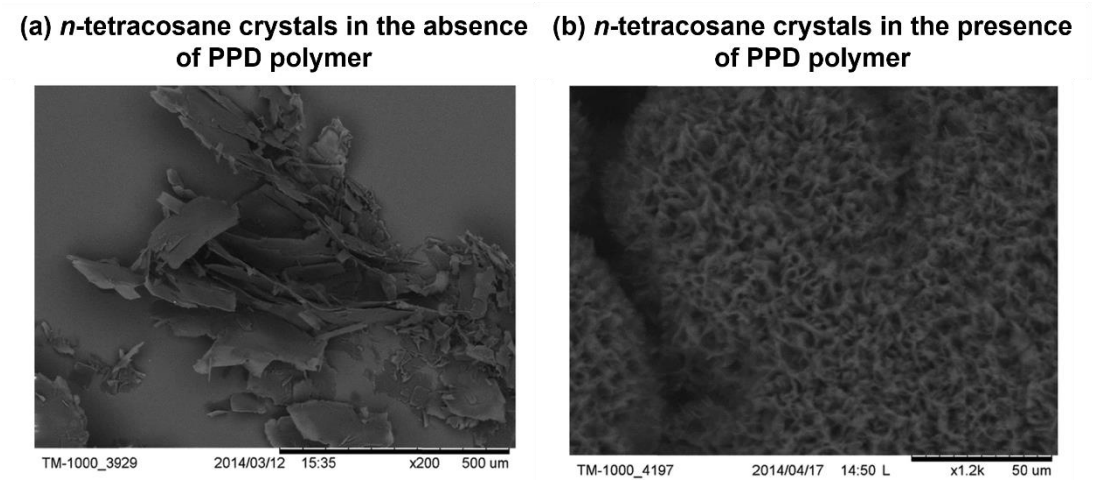

Figure 4.2. Examples of SEM images of extracted wax crystals. **(a)** *n*-tetracosane crystal platelets extracted from a 20% w/w solution in toluene in the absence of PPD polymer. **(b)** relatively small *n*-tetracosane crystals extracted from a 20% w/w solution in toluene with 1% w/w PPD polymer.

The synthesis of well-defined poly(lauryl methacrylate)-poly(behenyl methacrylate) [PLMA-PBeMA] diblock copolymers *via* RAFT solution polymerisation has been discussed in Chapter 3 of this Thesis. Prior research suggests that poly(*n*-alkyl methacrylates) with pendant *n*-alkyl groups comprising 20-30 carbon atoms are potential wax crystal inhibitiors.[30,37] A recent review article by Chi *et al.* on controlling paraffin deposition in production lines noted that effective wax crystal modifiers typically contained paraffin-like crystalline segments.[6] Such PPD polymers can co-crystallise with and hence influence the formation and structure of wax crystal networks.

Given this encouraging precedent, we decided to evaluate the performance of a range of BeMA-based copolymers for wax crystal modification. Accordingly, we prepared two series of well-defined diblock and statistical copolymers using BeMA as the crystallisable ($C_{22}H_{45}$) component and lauryl methacrylate (LMA) as the oil-soluble ($C_{12}H_{25}$) component (see **Scheme 4.1**). All copolymers were prepared via RAFT solution polymerisation to ensure that relatively narrow molecular weight distributions

were obtained. For wax crystal modification studies, *n*-octacosane ($C_{28}H_{58}$) was employed as a model wax and the non-polar solvent was *n*-dodecane.

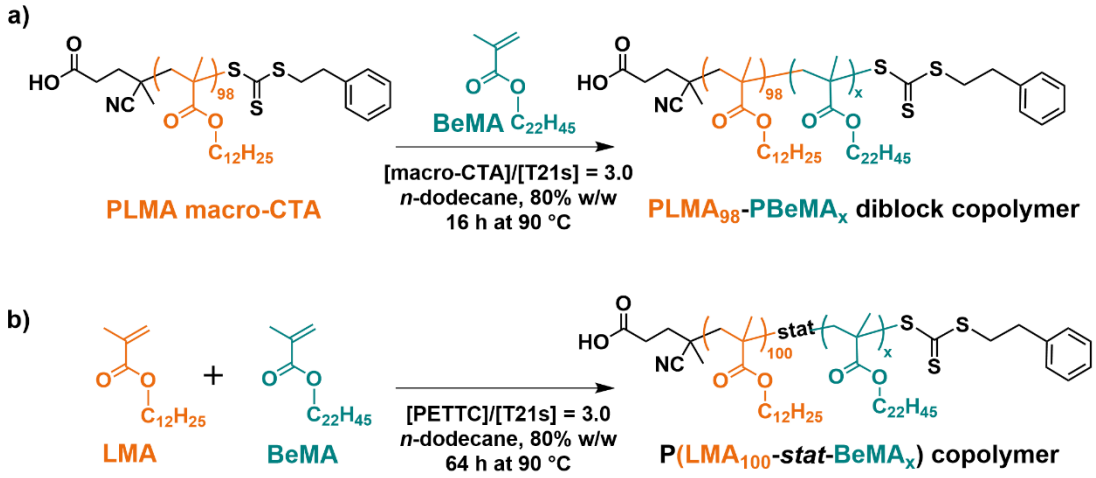

Scheme 4.1. Synthesis of **(a)** poly(lauryl methacrylate)-poly(behenyl methacrylate) [PLMA-PBeMA] diblock copolymers and **(b)** poly(lauryl methacrylate-*stat*-behenyl methacrylate) [P(LMA-*stat*-BeMA)] statistical copolymers by RAFT solution polymerisation at 80% w/w solids in *n*-dodecane at 90 °C.

4.2. Experimental

4.2.1. Materials

All reagents purchased were used as received, unless stated otherwise. $CDCl_3$ was purchased from Sigma-Aldrich (UK). Lauryl methacrylate (LMA; 96%) was also purchased from Sigma Aldrich and filtered through basic alumina prior to use to remove inhibitor. Toluene, methanol, and *n*-dodecane (>99%) were purchased from Fisher Scientific (UK). 2,2′-Azoisobutyronitrile (AIBN) initiator was obtained from Molekula (UK) and tert-butyl peroxy-2-ethylhexanoate (T21s; >97%) initiator was purchased from AkzoNobel (The Netherlands). CD_2Cl_2 was purchased from Goss Scientific (UK). 4-Cyano-4-(2-phenylethane sulfanylthiocarbonyl)sulfanylpentanoic acid (PETTC; >99%) was synthesised according to the literature.[38] The synthesis of behenyl methacrylate (BeMA) is reported in Chapter 3 of this Thesis.

4.2.2. Synthesis of poly(lauryl methacrylate) (PLMA) macromolecular chain transfer agent (macro-CTA)

The synthesis of a PLMA macro-CTA was conducted as follows. A 250 mL round-bottomed flask was charged with lauryl methacrylate (LMA; 52.5 g; 206 mmol), 4-cyano-4-(2-phenylethane sulfanylthiocarbonyl)sulfanylpentanoic acid (PETTC; 0.50 g; 1.47 mmol; target degree of polymerisation, DP = 140), 2,2′-azobisisobutyronitrile (AIBN; 47.9 mg; 292 µmol; [PETTC]/[AIBN] molar ratio = 5.0) and toluene (53.0 g; total solids content = 50% w/w). The sealed reaction vessel was purged with nitrogen for 30 minutes and then placed in a pre-heated oil bath at 70 °C. The polymerisation was allowed to proceed for 3.5 h at this temperature. ^{1}H NMR spectroscopy (see **Figure 4.3**) was used to determine an LMA monomer conversion of 57% using **Equations 4.1-4.3** by comparing the integrated monomer vinyl protons (*a'* and *b'*) with the integrated oxymethylene signals (*f'* and *m*) assigned to LMA monomer and PLMA homopolymer.

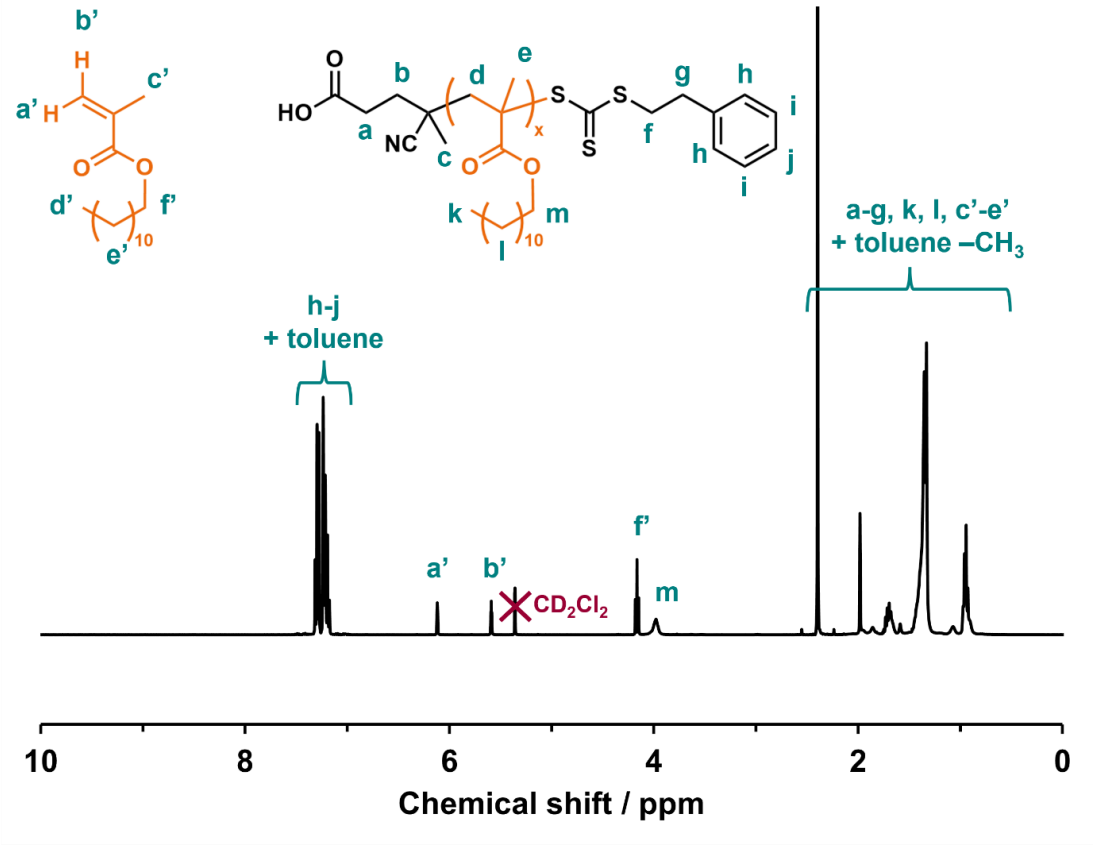

Figure 4.3. Assigned ^{1}H NMR spectrum (CD_2Cl_2) obtained for the reaction mixture directly after the synthesis of a PLMA macro-CTA (target DP = 140. 57% LMA conversion).

$$I_m = [Integral\ (a' + b')] = 2H \tag{4.1}$$

$$I_p = [Integral\ (m + f')] - I_m \tag{4.2}$$

$$LMA\ conversion\ (\%) = \left[1 - \frac{I_m}{I_m + I_p}\right] x\ 100\% \tag{4.3}$$

The crude product was purified by precipitating three times into excess methanol and then dried under vacuum. The mean degree of polymerisation (DP) of the purified macro-CTA was determined via end-group analysis by analysing its ^{1}H NMR spectrum recorded in CD_2Cl_2 (see **Figure 4.4**). A DP of 98 was calculated by comparing the integrated signals corresponding to the aromatic protons of the trithiocarbonate-based end-group at 7.2-7.4 ppm with those assigned to the two

oxymethylene ester protons of the LMA repeat units at 3.8-4.2 ppm (**Equations 4.4-4.5**). THF GPC analysis indicated a PMMA-equivalent number-average molecular weight, M_n, of 18.0 kg mol^{-1} (for comparison, $M_{n\ NMR}$ = 25.3 kg mol^{-1}) and dispersity, $Đ$, of 1.20. A mean DP of 99 was determined using the molar extinction coefficient of 31.64 ± 0.27 mol^{-1} dm^3 cm^{-1} calculated by Dr. E. J. Cornel for the PETTC RAFT agent (see **Figure 4.5**) and **Equations 4.6** and **4.7**.

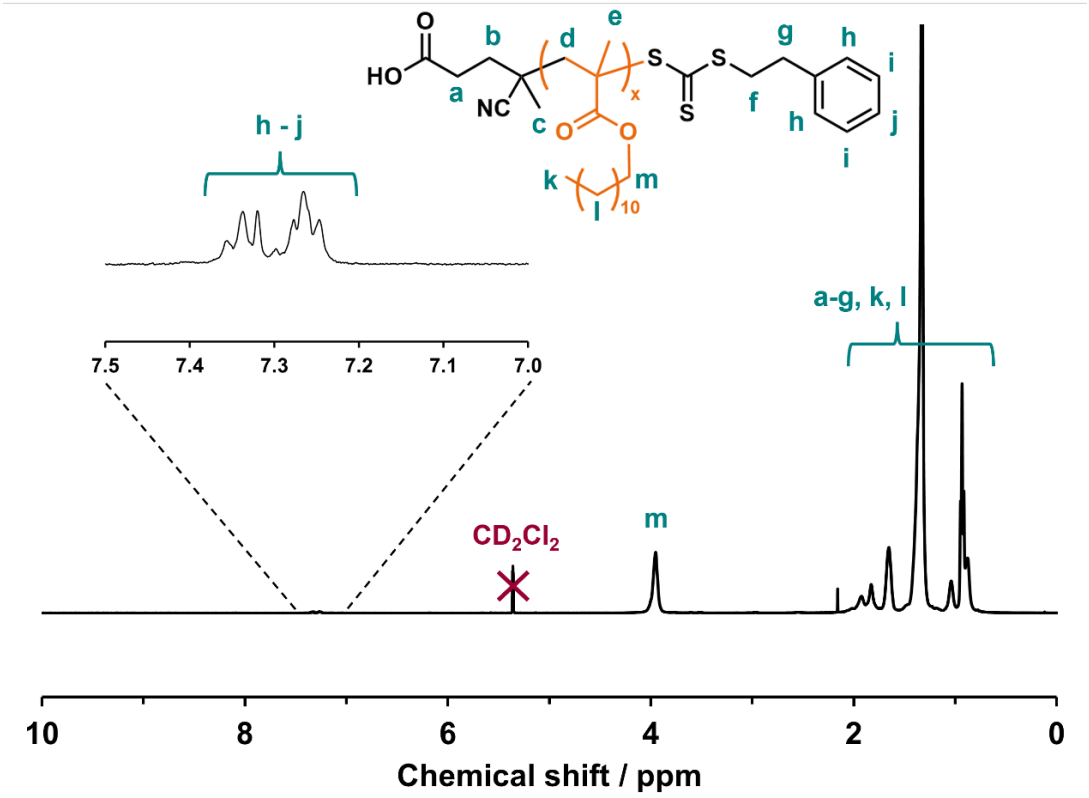

Figure 4.4. Assigned ^{1}H NMR spectrum obtained for the purified $PLMA_{98}$ macro-CTA (in CD_2Cl_2).

$$[Integral\ (h\ +\ i\ +\ j)]\ =\ 5\text{H} \tag{4.4}$$

$$PLMA\ DP\ =\ \frac{[Integral\ (m)]}{2} \tag{4.5}$$

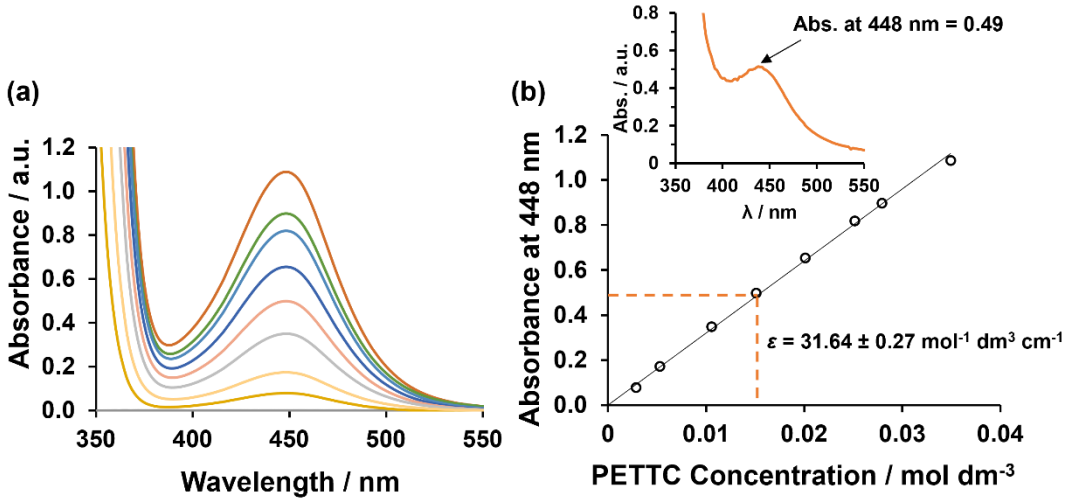

Figure 4.5. (a) Absorbance *vs.* wavelength traces recorded for a series of PETTC solutions in toluene ranging from 2.9 to 35 mmol dm^{-3} and **(b)** Beer-Lambert linear calibration plot used to calculate the molar extinction coefficient of PETTC (ε = 31.64 ± 0.27 mol^{-1} dm^3 cm^{-1} at λ = 448 nm). Insert shown of absorbance *vs.* wavelength trace recorded for a 389 g dm^{-3} PLMA macro-CTA solution in toluene with absorbance peak maximum at λ = 448 nm recorded at 0.49. Determination of the PETTC concentration of this PLMA sample (1.55 x 10^{-2} mol dm^{-3}) shown by orange dashed line.

$$MW\ PLMA\ /\ (g\ mol^{-1})\ =\ \frac{[PLMA]/\ (g\ dm^{-3})}{[PETTC]/\ (mol\ dm^{-3})} \tag{4.6}$$

$$PLMA\ DP\ =\ \frac{MW\ PLMA}{MW\ LMA} \tag{4.7}$$

4.2.3. Synthesis of poly(lauryl methacrylate)-poly(behenyl methacrylate) [$PLMA_{98}$-$PBeMA_x$] diblock copolymers by RAFT solution polymerisation

The protocol for the synthesis of the $PLMA_{98}$-$PBeMA_{60}$ diblock copolymer via RAFT solution polymerisation at 80% w/w solids in *n*-dodecane is representative for all of

the block copolymers used in this study and was conducted as follows. $PLMA_{98}$ (1.45 g; 57.0 μmol), BeMA (1.36 g; 3.45 mmol), and *n*-dodecane (0.672 g) were weighed into a glass vial and heated in an oven at 70 °C to aid dissolution. An aliquot (one droplet, approx. 20 mg) of the reaction solution was taken for use as a 'zero time' reference point for determination of the BeMA conversion by ^{1}H NMR spectroscopy. After cooling the remaining solution to 20 °C, T21s initiator was added (4.14 mg; 19.2 μmol; 10.0% v/v in *n*-dodecane; $[PLMA_{98}]/[T21s]$ molar ratio = 3.0) along with a magnetic stirrer bar and this reaction mixture was purged with nitrogen gas for 30 min. The sealed sample vial was then immersed in a pre-heated oil bath set at 90 °C and the reaction mixture was stirred for 16 h (final BeMA conversion = 98%; M_n = 33.2 kg mol^{-1}; $Đ$ = 1.25). The resulting diblock copolymer was purified to remove residual BeMA by precipitation into excess ethanol at 35 °C (twice), and then dried under vacuum.

BeMA conversions were determined via ^{1}H NMR spectroscopy using **Equations 4.8-4.11**. In this case, an additional spectrum was recorded at zero time to distinguish between the new oxymethylene signals originating from the PBeMA and those assigned to the PLMA precursor (see **Figure 4.6**).

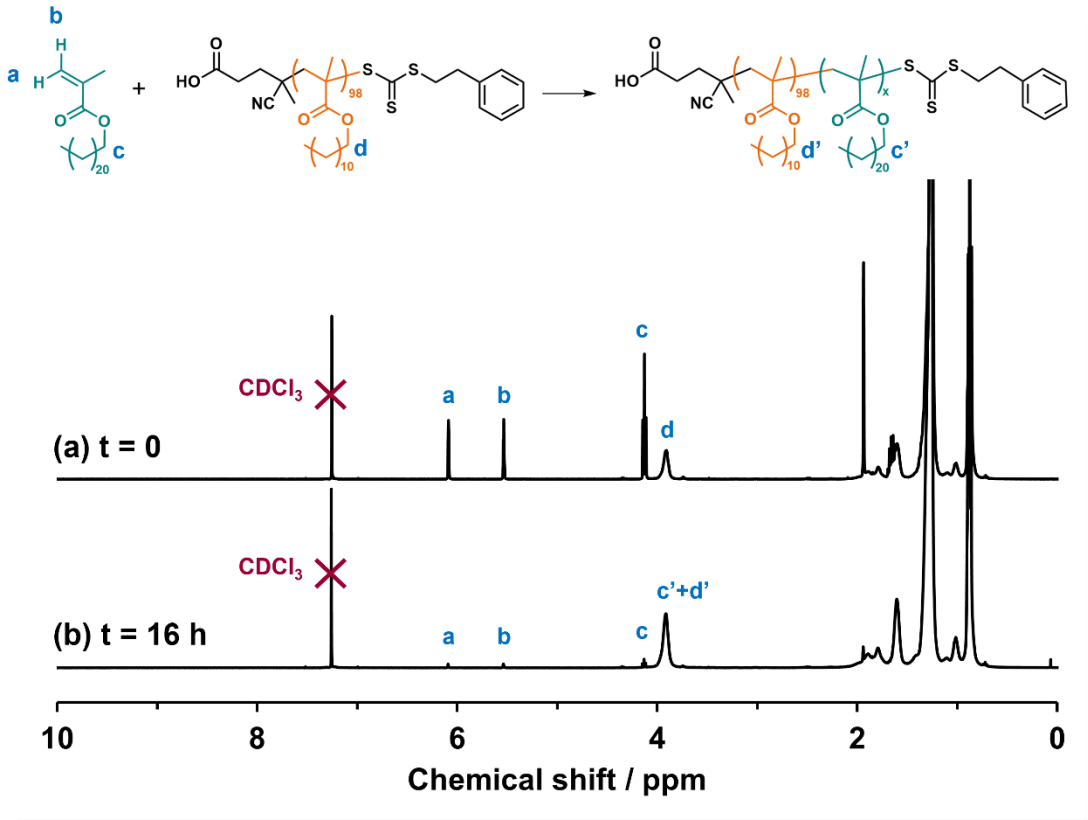

Figure 4.6. Assigned ^{1}H NMR spectra ($CDCl_3$) recorded for **(a)** the reaction mixture at zero time (t=0) containing a $PLMA_{98}$ precursor and BeMA monomer and **(b)** the same reaction mixture after polymerisation for 16 h to form a $PLMA_{98}$-$PBeMA_x$ diblock copolymer.

$$I_m = [Integral\ (a + b)] = 2H \quad (4.8)$$

$$\text{PLMA } I_p = [Integral\ (c' + d')] - I_m \quad (4.9)$$

$$\text{PBeMA } I_p = \{[Integral\ (c + c' + d')] - I_m\} - PLMA\ I_p \quad (4.10)$$

$$BeMA\ conversion\ (\%) = \left[1 - \frac{I_m}{I_m + PBeMA\ I_p}\right] x\ 100\% \quad (4.11)$$

4.2.4. Synthesis of poly(lauryl methacrylate-stat-behenyl methacrylate) [P(LMA$_{100}$-stat-BeMA$_x$)] statistical copolymers by RAFT solution polymerisation

The protocol for the synthesis of P(LMA$_{100}$-*stat*-BeMA$_{60}$) via RAFT solution polymerisation at 80% w/w solids in *n*-dodecane is representative of all the statistical

copolymers used in this study and was conducted as follows. PETTC (25.0 mg, 73.6 μmol; total target DP = 160), LMA (1.87 g, 7.36 mmol), BeMA (1.74 g, 4.42 mol), *n*-dodecane (0.40 g) and T21s initiator (5.31 mg, 24.5 μmol; 10.0% v/v in *n*-dodecane; [PETTC]/[T21s] molar ratio = 3.0) was added to a 10 mL round-bottomed flask along with a magnetic stirrer bar and this reaction mixture was purged with nitrogen for 30 min. The sealed flask was then immersed into a pre-heated oil bath set at 90 °C and the reaction mixture was stirred for 64 h (final comonomer conversion = 99%; M_n = 39.6 kg mol^{-1}; $Đ$ = 1.24). The copolymer was purified by precipitation into ethanol at 35 °C (twice) to remove residual LMA and BeMA, and then dried under vacuum.

4.2.5. Preparation of wax-copolymer solutions

n-Octacosane (0.188 g; 5.0 % w/w), *n*-dodecane (3.53 g) and each polymer in turn (0.26 mM) were weighed into a glass vial and heated in a 70 °C oven to aid dissolution. The resulting solutions were then transferred into glass cuvette cells via syringe for variable temperature turbidimetry measurements. A fixed molar copolymer concentration of 0.26 mM (equivalent to 1.0 % w/w $PLMA_{98}$-$PBeMA_{10}$) was used for initial wax crystal modification experiments, which ensured that the number of copolymer chains remained constant. Thus the copolymer concentrations expressed in weight per cent varied from 1.0 % w/w to 1.7 % w/w. For the $PBeMA_{37}$ and $PLMA_{98}$ homopolymers, 0.26 mM corresponded to 0.5 % w/w and 0.9 % w/w, respectively. Subsequently, the molar copolymer concentration was varied from 0.06 to 1.03 mM (i.e. a factor of four lower or higher than the initial 0.26 mM value).

4.3. Characterisation

4.3.1. ^{1}H NMR spectroscopy

^{1}H NMR spectra were recorded in either CD_2Cl_2 (to determine the mean DP for the PLMA precursor) or $CDCl_3$ (for all other spectra) using a Bruker AV1-400 MHz spectrometer. Typically, 64 scans were averaged per spectrum.

4.3.2. UV-visible absorption spectroscopy

UV-visible absorption spectra were recorded by Dr. E. J. Cornel between 200 and 800 nm using a PC-controlled UV-1800 spectrophotometer at 25 °C and a 1.0 cm path length quartz cell. A Beer–Lambert calibration curve was constructed using a series of eight PETTC solutions in toluene with the PETTC concentration ranging from 2.9×10^{-3} mol dm^{-3} to 3.5×10^{-2} mol dm^{-3}. The absorption maximum at 448 nm assigned to the n-π transition of the trithiocarbonate group was used to construct this calibration plot. The absorbance of a solution of the $PLMA_{98}$ macro-CTA in toluene at known concentration (389 g dm^{-3}) was recorded and the mean DP calculated using **Equations 4.6** and **4.7**.

4.3.3. Gel Permeation Chromatography (GPC)

GPC was used to assess (co)polymer molecular weight distributions. The GPC set-up comprised two 5 μm (30 cm) Agilent Mixed C columns and a WellChrom K-2301 refractive index detector operating at 950 ± 30 nm. The THF eluent contained 2.0% v/v triethylamine and 0.05% w/v butylhydroxytoluene (BHT) with a toluene flow-rate marker at a flow rate of 1.0 mL min^{-1}. A series of eleven near-monodisperse poly(methyl methacrylate) (PMMA) standards (M_p values ranging from 800 to 988 000 g mol^{-1}) were used for calibration.

4.3.4. Differential Scanning Calorimetry (DSC)

DSC studies were performed using a TA Instruments Discovery DSC instrument equipped with TZero low-mass aluminium pans and hermetically-sealed lids. All (co)polymer samples were equilibrated at 90 °C for 5 min before two consecutive thermal cycles (from 90 °C to -90 °C to 90 °C) were performed at a constant cooling/heating rate of 10.0 °C min^{-1}. Two cycles were performed to eliminate any thermal history.

4.3.5. Turbidimetry

Turbidimetry measurements were performed using an Agilent Technologies Cary 300 UV-visible spectrophotometer. Absorbance (A) *vs.* temperature data were recorded at 650 nm, then converted to % transmittance using the formula $\%T = 10^{(2-A)}$. Wax-copolymer mixtures were equilibrated at 50 °C for 5 min before three consecutive thermal cycles (from 50 °C to 0 °C to 50 °C) were performed at a constant cooling/heating rate of 1 °C min^{-1}. T_{cool} was taken as the temperature required for 0 % transmittance on cooling, averaged over the three cooling cycles. During the third thermal cycle, each wax-copolymer mixture was heated from 0 °C to 20 °C at 1 °C min^{-1} for microscopy analysis at room temperature.

4.3.6. Optical Microscopy (OM)

Samples were placed on a glass slide under a coverslip for imaging on an Axio Scope A1 optical microscope (Zeiss, Jena, Germany) equipped with AxioCam 1Cm1 monochrome and AxioCam 105 colour cameras. All images were collected and processed using Zen lite 2014 software supplied with the microscope.

4.3.7. Scanning Electron Microscopy (SEM)

SEM images were recorded by Mr. D. H. H. Chan using a field emission FEI Inspect-F instrument at an accelerating voltage of 10 kV. Samples were allowed to dry overnight on silicon wafers and then sputter-coated with a thin overlayer of gold prior to imaging. Where specified, ImageJ software was used to determine crystal dimensions (mean lengths and widths). A minimum of 50 crystals were counted across multiple images recorded for each sample on the same day.

4.4. Results and Discussion

4.4.1. Synthesis of PLMA macro-CTA

A $PLMA_{98}$ macro-CTA was prepared via RAFT solution polymerisation of LMA in toluene at 70 °C using PETTC as a RAFT chain transfer agent (CTA) (see **Scheme 4.2**). This polymerisation was quenched at 57 % conversion to produce a mean DP of 98. Quenching the polymerisation well below full conversion avoids monomer-starved conditions and hence aids retention of the trithiocarbonate end-groups.[39,40] This is usually considered to be desirable for ensuring high blocking efficiencies for the subsequent synthesis of PLMA-PBeMA diblock copolymers. Analysis by THF GPC indicated an M_n of 18.0 kg mol^{-1} and a relatively narrow molecular weight distribution ($Đ$ = 1.20).

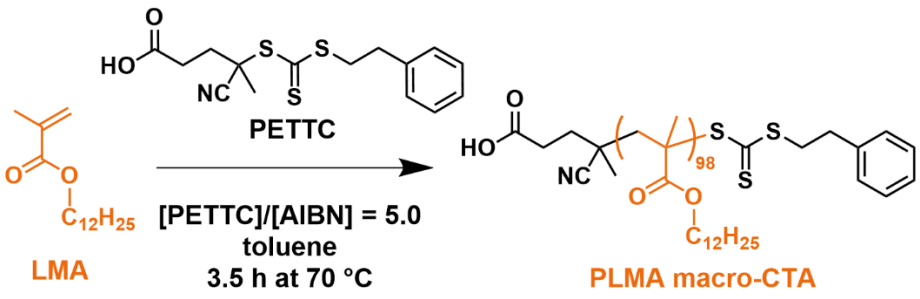

Scheme 4.2. Synthesis of a poly(lauryl methacrylate) (PLMA) macro-CTA by RAFT solution polymerisation of LMA at 50% w/w solids in toluene at 70 °C.

4.4.2. Synthesis of PLMA-PBeMA block and statistical copolymers

A series of four $PLMA_{98}$-$PBeMA_x$ diblock copolymers and four P(LMA_{100}-*stat*-$BeMA_x$) statistical copolymers, where x = 10, 20, 40 and 60, were prepared by RAFT solution polymerisation at 80 % w/w solids in *n*-dodecane (see **Scheme 4.1**). Given its relatively high molar mass (395 g mol^{-1}), BeMA monomer has a relatively low molar concentration for a given weight percent concentration compared to most common methacrylic monomers, e.g. methyl methacrylate (100 g mol^{-1}). Thus, 80 % w/w solids was selected to ensure that a high BeMA conversion could be obtained, whilst still maintaining sufficient stirring at the reaction temperature. All copolymerisations were initiated using the organic peroxide T21s at 90 °C using either a [mCTA]/[I] molar ratio or [CTA]/[I] molar ratio of 3.0.

After 16 h, ≥ 98% BeMA conversion was achieved for all four diblock copolymers, as determined by ^{1}H NMR spectroscopy (see **Table 4.1**). THF GPC analysis indicated M_n values of between 21.4 kg mol^{-1} and 33.2 kg mol^{-1} and relatively narrow MWDs ($Đ \leq 1.25$), which suggested good RAFT control. Comparison with the GPC curve obtained for the PLMA mCTA confirmed relatively high blocking efficiencies, although a low molecular weight shoulder is evident when targeting a PBeMA DP of 40 or 60 (see **Figure 4.7a**). Reaction times were increased to 64 h for the synthesis of the statistical copolymers to ensure ≥ 99% comonomer conversion (see **Table 4.1**). THF GPC analysis indicated copolymer M_n values of between 24.4 kg mol^{-1} and 39.6 kg mol^{-1} and relatively narrow MWDs ($Đ \leq 1.24$) (see **Figure 4.7b**).

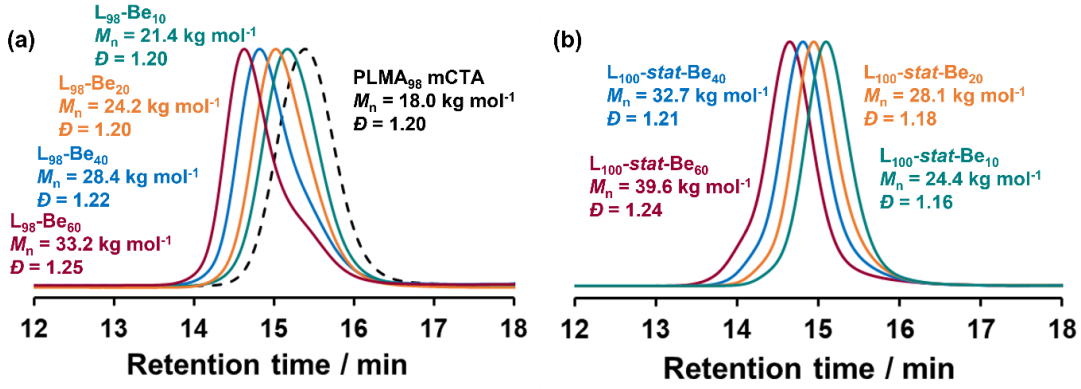

Figure 4.7. GPC curves recorded for **(a)** a $PLMA_{98}$ macro-CTA and the corresponding $PLMA_{98}$-$PBeMA_x$ diblock copolymers and **(b)** P(LMA_{100}-*stat*-$BeMA_x$) statistical copolymers (all copolymers are analysed prior to their purification by precipitation in ethanol).

Prior to their examination as wax crystal modifiers, all copolymers were purified to remove residual BeMA monomer by precipitation (twice) into excess ethanol at 35 °C. ^{1}H NMR spectroscopy confirmed the disappearance of the vinyl signals between 5.5 and 6.1 ppm, indicating the complete removal of unreacted monomer(s) Comparison of GPC curves recorded for diblock copolymers before and after such purification indicated only a modest difference between the initial and final M_n in each case, along with a marginally narrower MWD (see **Figure 4.8**).

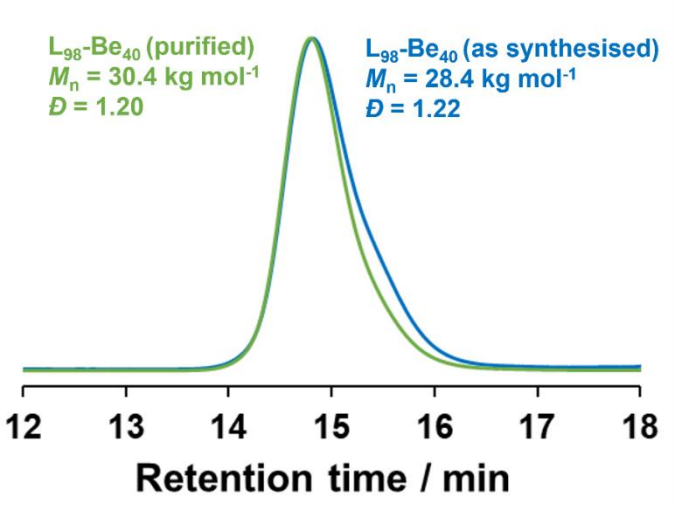

Figure 4.8. GPC curves recorded for a $PLMA_{98}$-$PBeMA_{40}$ diblock copolymer before and after its purification *via* precipitation into excess ethanol at 35 °C.

A summary of the THF GPC and DSC data obtained for all eight purified copolymers and also the reference $PLMA_{98}$ and $PBeMA_{37}$ homopolymers is provided in **Table 4.1**. The $PBeMA_{37}$ homopolymer was prepared by Derry *et al.*[41] All eight copolymers reported in **Table 4.1** have M_n values ranging between 21.1 kg mol^{-1} and 39.4 kg mol^{-1} and relatively narrow MWDs ($Đ \leq 1.23$). DSC was used to determine the crystallisation temperature (T_c) and melting temperature (T_m) for the semi-crystalline PBeMA chains in the $PBeMA_{37}$ homopolymer and the eight copolymers. [N.B. These two characteristic temperatures correspond to when the amorphous PBeMA phase becomes crystalline and the crystalline PBeMA phase becomes amorphous, respectively].[42,43]

Table 4.1. Summary of (co)polymer compositions, BeMA conversions, GPC molecular weights and dispersities, and T_c and T_m values determined by DSC for two series of BeMA-based diblock and statistical copolymers.

Polymer composition	BeMA conversion[a] / %	M_n[b] / kg mol^{-1}	$Đ$[b]	T_c[c] / °C	T_m[c] / °C
L_{98}	-	18.0	1.20	-44.3	-36.8
L_{100}-*stat*-Be_{10}	>99	26.1	1.15	-34.6	-27.1
L_{100}-*stat*-Be_{20}	>99	28.1	1.18	-16.8	-1.4
L_{100}-*stat*-Be_{40}	99	32.1	1.21	0.5	16.9
L_{100}-*stat*-Be_{60}	99	39.1	1.23	11.0	26.1
L_{98}-Be_{10}	99	21.1	1.18	28.7	45.1
L_{98}-Be_{20}	>99	24.3	1.19	39.3	50.5
L_{98}-Be_{40}	99	30.4	1.20	41.7	53.5
L_{98}-Be_{60}	98	39.4	1.17	43.9	54.4
Be_{37}	-	12.5	1.14	48.3	60.0

[a]Determined by ^{1}H NMR spectroscopy.
[b]Determined by THF GPC and expressed relative to a series of poly(methyl methacrylate) standards.
[c]Determined by DSC (all copolymers were subjected to two thermal cycles to remove any hysteresis effects).

Both PBeMA and PLMA are semi-crystalline polymers. T_m values of 60.0 °C and -36.8 °C were measured for PBeMA and PLMA, respectively. These compare well to the literature.[41,44] Notably, PLMA exhibits relatively subtle melting and crystallisation transitions compared to PBeMA (because the latter homopolymer is much more crystalline), see **Figure 4.9**. According to the literature, PLMA exhibits a T_g of -65 °C.[45,46] It is likely that this transition is obscured by the broad T_m peak for the $PLMA_{98}$ homopolymer in **Figure 4.9**.[44] The four diblock copolymers exhibit well-defined peaks for crystallisation and melting, with both T_c and T_m lying above ambient temperature (25 °C). Both transition temperatures increase as the DP of the PBeMA

block is raised and approach the T_c and T_m values observed for the PBeMA homopolymer (T_c = 48.3 °C; T_m = 60.0 °C). Such thermal transitions are attributed to crystallisation of the PBeMA blocks. However, no separate T_c and T_m values for the less crystalline PLMA block within the diblock copolymers could be observed under the experimental procedure used (*e.g.* 10 °C min^{-1}). The four statistical copolymers displayed broader, more subtle thermal transitions, with most T_c and T_m values occurring below 25 °C. In this case, crystallisation arises from self-organisiation of the pendent behenyl groups randomly located along the methacrylic backbone. This clear difference is reflected in the differing physical appearance of these copolymers. At ambient temperature, the four statistical copolymers form viscous fluids while the four diblock copolymers are solids.

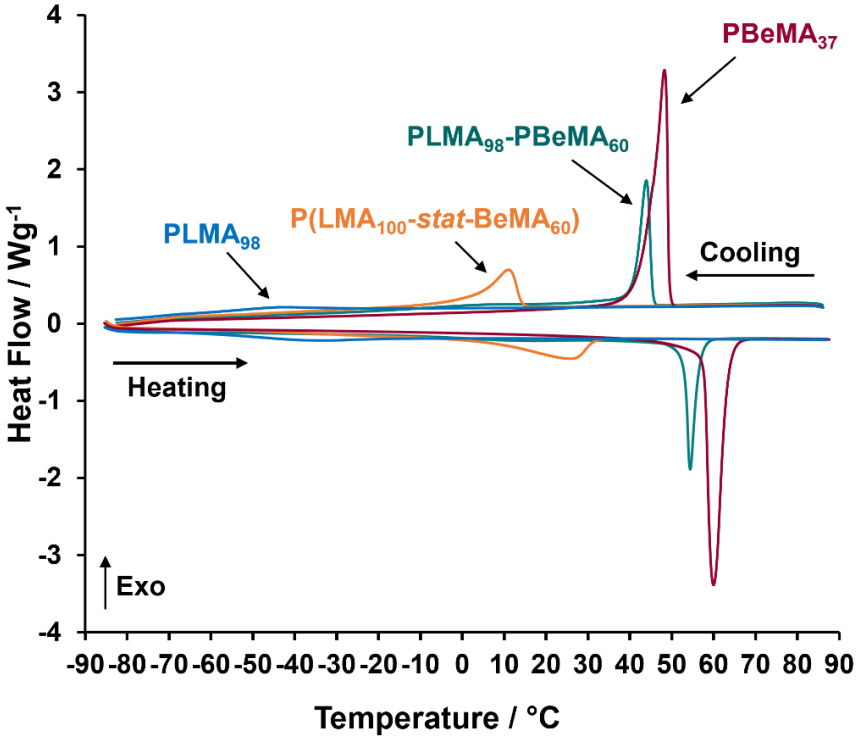

Figure 4.9. DSC traces conducted at a cooling/heating rate of 10 °C min^{-1} showing T_c values (exothermic) and T_m values (endothermic) for PLMA$_{98}$-PBeMA$_{60}$ and P(LMA$_{100}$-*stat*-BeMA$_{60}$) copolymers as well as the PBeMA$_{37}$ and PLMA$_{98}$ reference homopolymers.

4.4.3. Application of PLMA-PBeMA copolymers as wax crystal modifiers at a fixed copolymer concentration

n-Octacosane ($C_{28}H_{58}$) was selected as a single-component model wax and used at 5.0% w/w solids in *n*-dodecane. This concentration is at the lower end of the typical wax content in crude oils (5-30% w/w)[12], but such conditions produced sufficient wax crystals for characterisation by optical microscopy and SEM. Moreover, Ashbaugh *et al.*[19] and Kurniawan *et al.*[47] used comparable wax concentrations in their studies. Macrocrystalline paraffin wax comprises mainly low molecular weight *n*-alkanes (C_{16}-C_{40}) and generally crystallises in the form of either needles or platelets.[12] Indeed, wax crystal platelets are observed on cooling a 5.0% w/w solution of *n*-octacosane dissolved in *n*-dodecane in the present study (see **Figure 4.10**). Prior literature studies suggested that an initial copolymer concentration of 1.0% w/w should be selected for initial experiments.[37,48] 1.0% w/w $PLMA_{98}$-$PBeMA_{10}$ is equivalent to a copolymer concentration of 0.26 mM. This *molar* concentration was held constant for all copolymers to ensure that the number of chains remained the same in each experiment (*i.e.* 2.1 x 10^{17} chains per gram of solution) when varying the copolymer composition.

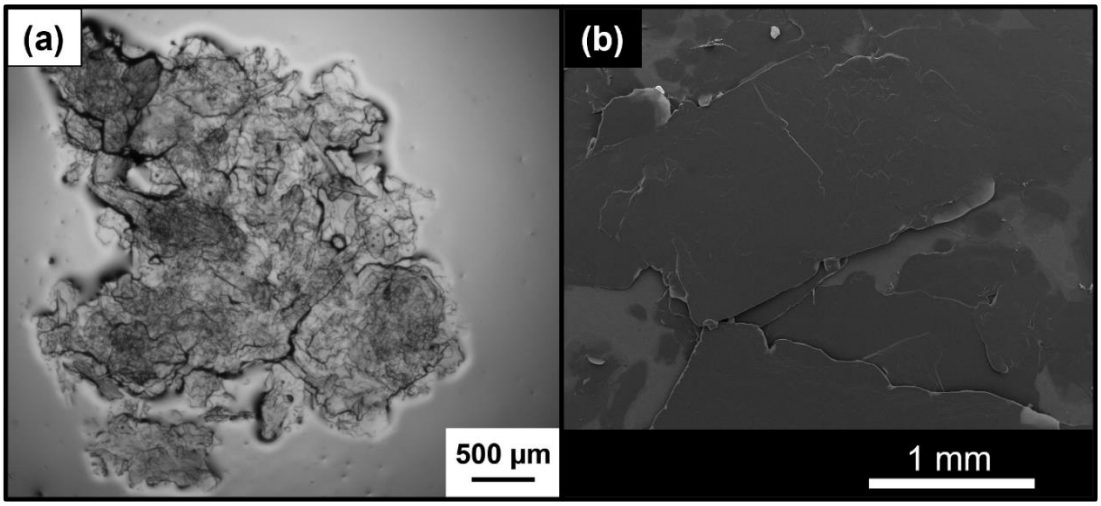

Figure 4.10. Images recorded for pure *n*-octacosane ($C_{28}H_{58}$) wax crystals prepared in the absence of any copolymer additive at 20 °C: **(a)** as a 5.0% w/w suspension in *n*-dodecane using bright field optical microscopy and **(b)** dried crystals examined by SEM.

4.4.3.1. Turbidimetry studies

Effective wax crystal modifiers act by lowering the temperature for the onset of crystallisation of paraffin wax, which is known as the wax appearance temperature (WAT).[6] To examine how the present copolymers influence the WAT of a model wax, turbidimetry measurements were conducted using 5.0% w/w *n*-octacosane dissolved in *n*-dodecane. Initial experiments were performed at a copolymer concentration of 0.26 mM. Thermal cycles (50 °C to 0 °C to 50 °C) were carried out three times at a cooling/heating rate of 1.0 °C min^{-1}. Data obtained for one such thermal cycle performed in the absence of any copolymer are presented in **Figure 4.11**, along with digital photographs of the physical appearance of the *n*-octacosane/*n*-dodecane mixture recorded at 50 °C and 0 °C. Wang and co-workers reported using a similar light transmittance method to evaluate WATs for model paraffin waxes in *n*-decane in the presence and absence of wax inhibitors.[35]

The *n*-octacosane/*n*-dodecane mixture is a highly transparent solution at 50 °C (100 % transmittance) but becomes opaque (0 % transmittance) on cooling owing to wax

crystallisation. A WAT occurs at around 23 °C, below which a sharp reduction in transmittance is observed. T_{cool} is taken to be the temperature required for 0% transmittance on cooling, *i.e.* the temperature at which crystallisation is judged to be complete (see **Figure 4.11**). T_{cool} occurs at around 19 °C, which is a few degrees below the WAT. The former parameter was used to compare various wax-copolymer mixtures as it can be readily identified from transmittance *vs.* temperature plots. On reheating to 50 °C, a transparent solution (100% transmittance) is obtained. The minimum temperature corresponding to 100% transmittance on heating is denoted as T_{heat}. As anticipated for a first-order phase transition, some thermal hysteresis is observed: the sharp increase in transmittance on heating occurs approximately 10 °C higher than the corresponding reduction in transmittance during cooling. This is because there is a kinetic energy barrier associated with the formation of wax crystals on cooling, whereas the corresponding melting event involves no such barrier. Similar behaviour has been reported in the literature.[37,41]

Turbidimetry data for a series of eleven experiments conducted using 5.0% w/w *n*-octacosane in *n*-dodecane in the presence or absence of copolymer are presented in **Table 4.2**. The T_{cool} values are calculated from the three consecutive cooling ramps, with the standard deviation quoted as the error. In all cases, the T_{cool} value was a few degrees below the WAT. The *n*-octacosane wax in *n*-dodecane has a T_{cool} of 19.3 ± 0.5 °C in the absence of any (co)polymer. This T_{cool} value remains unchanged (within experimental error) in the presence of the $PBeMA_{37}$ homopolymer. However, addition of $PLMA_{98}$ homopolymer reduces T_{cool} to 16.8 ± 0.1 °C. However, the greatest reduction in T_{cool} is achieved by using PBeMA-based diblock or statistical copolymers, with the copolymer architecture making surprisingly little difference. BeMA-rich

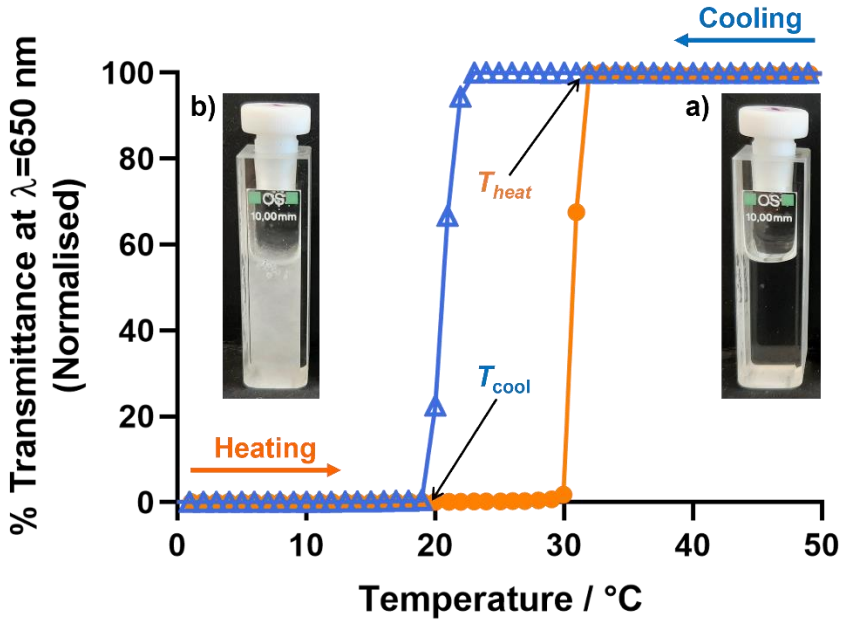

Figure 4.11. Normalised transmittance (%) at λ = 650 nm *vs.* temperature plot for 5.0 % w/w *n*-octacosane in *n*-dodecane on cooling from 50 °C to 0 °C (blue empty triangles) and on heating from 0 °C to 50 °C (orange filled circles) at a cooling/heating rate of 1.0 °C min^{-1}. The temperatures required for zero transmittance on cooling (T_{cool}) and 100% transmittance on heating (T_{heat}) are labelled. Digital photograph **(a)** shows a transparent solution at 50 °C and **(b)** shows the same sample after cooling to 0 °C.

diblock or statistical copolymers can reduce T_{cool} by approximately 5 °C compared to that observed for the pure wax in *n*-dodecane in the absence of any copolymer. Other workers have reported similar observations for effective wax crystal modifiers.[33–35] For example, Sjöblom and co-workers reported WAT reductions of between 1.4 and 5.5 °C for 5.0% w/w macrocrystalline wax in toluene in the presence of a range of both commercial and putative PPDs.[25] It is generally accepted that polymers reduce the WAT of a wax by changing the solubility equilibrium.[6,25,27,36] Polymers interact with (or become incorporated into) the precipitating wax crystals, which results in changes in the kinetics of crystal growth on cooling and changes in the kinetics of dissolution on heating.[35]

Table 4.2. Composition of (co)polymer additive and mean T_{cool} for wax-polymer mixtures as determined by turbidimetry studies. Wax-polymer mixtures contain 5.0% w/w C_{28} in *n*-dodecane with 0.26 mM (co)polymer additive.

Polymer composition	T_{cool} **wax + polymer**[a] **/ °C**
none	19.3 ± 0.5
L_{98}	16.8 ± 0.1
Be_{37}	18.9 ± 0.1
L_{98}-Be_{10}	15.7 ± 0.1
L_{98}-Be_{20}	15.6 ± 0.1
L_{98}-Be_{40}	14.1 ± 0.5
L_{98}-Be_{60}	14.7 ± 0.1
L_{100}-*stat*-Be_{10}	15.0 ± 0.1
L_{100}-*stat*-Be_{20}	16.2 ± 0.5
L_{100}-*stat*-Be_{40}	13.7 ± 1.2
L_{100}-*stat*-Be_{60}	14.0 ± 0.5

[a]Mean value calculated from three consecutive cooling cycles in turbidimetry studies and the standard deviation quoted as error.

4.4.3.2. Optical Microscopy and Scanning Electron Microscopy studies

It is well-established that wax inhibitors and PPDs can alter the morphology of wax crystals.[6] Such polymeric additives are believed to delay nucleation, and either adsorb onto, or co-crystallise with, paraffin waxes.[12,49]

In order to ensure the same cooling rate for all the wax-copolymer mixtures, optical microscopy and SEM images were always recorded after performing turbidimetry measurements at a cooling rate of 1.0 °C min^{-1}. After the third cooling sweep from 50 °C to 0 °C, each sample was returned to 20 °C at a heating rate of 1.0 °C min^{-1}. Turbidimetry studies confirm that 20 °C is a sufficiently low temperature to maintain crystals, *i.e.* it is just below T_{heat} for the wax-copolymer mixtures. Optical microscopy was employed to determine the wax crystal size and morphology in solution, whereas high resolution SEM images were recorded for the dried wax crystals. The former

technique shows that wax crystals are formed as large clumps of platelets (mean length, $l \approx 0.5 - 2.5$ mm) when cooling a 5.0% w/w solution of *n*-octacosane in *n*-dodecane from 50 °C to 0 °C (see **Figure 4.10a**). Large platelets, up to 2 mm in length, are also discernible in SEM images obtained for dried wax crystals (see **Figure 4.12a**). Binks and co-workers reported the formation of similar irregularly-shaped thin platelets when cooling solutions of either a $C_{24}H_{50}$ wax in toluene or a $C_{36}H_{74}$ wax in heptane in the absence of any copolymer additive.[37] Fetters and co-workers reported a 3D 'house of cards' structure when using optical microscopy to characterise wax crystals when cooling a 4% w/w solution of similar *n*-paraffins in *n*-decane to 0 °C.[8,14]

The effect of using a copolymer concentration of 0.26 mM on the wax crystal size and morphology was also studied by SEM (see **Figure 4.12**). Addition of a $PLMA_{98}$ homopolymer has minimal effect on *n*-octacosane crystals prepared in the absence of any copolymer additive (see **Figure 4.12b)**. More specifically, large, irregular platelets are observed which are similar to those shown in **Figure 4.12a**. Similar platelets are also obtained for wax crystals prepared in the presence of a $PBeMA_{37}$ homopolymer (see **Figure 4.12c**), but small clumps of approximately 5 μm diameter are also visible. Interestingly, addition of a $PLMA_{98}$-$PBeMA_x$ diblock copolymer results in significantly smaller wax crystals. All four diblock copolymer compositions examined (*i.e.* x = 10, 20, 40 or 60) produced similar crystal morphologies; a mixture of irregular-shaped clumps (~2-10 μm) and needle-like crystals [$l = 25 \pm 17$ μm (averaged over 175 crystals); width, $w = 0.7 \pm 0.3$ μm (averaged over 50 crystals); mean aspect ratio, $l/w = 31$] are represented in **Figures Figure 4.12(d)-(g).**

There are many literature examples of polymeric wax crystal modifiers producing smaller wax crystals.[19,25–29] This is considered to be useful because it can improve

crude oil flowability. Fewer contacts between neighbouring crystals leads to weaker gel networks, so the removal of waxy deposits is easier.[7,28] In principle, increasing the anisotropy of wax crystals to produce elongated needle-like structures should also reduce gel strength relative to that for 'house of cards' networks formed by large platelets.[8,50]

In contrast to the four PLMA-PBeMA diblock copolymers, the BeMA content of the four P(LMA_{100}-*stat*-$BeMA_x$) statistical copolymers has a discernible effect on their wax crystal modifier performance. Thus, adding the P(LMA_{100}-*stat*-$BeMA_{10}$) statistical copolymer mainly results in large platelets (see **Figure 4.12h**), although some smaller (< 200 μm) and more elongated crystals are also present. However, a strikingly different wax crystal morphology is obtained when using P(LMA_{100}-*stat*-$BeMA_{20}$): large needle-like crystals [l = 280 ± 136 μm (averaged over 80 crystals); w = 13 ± 3 μm (averaged over 50 crystals); l/w = 22] are observed almost exclusively (see **Figure 4.12i**).

Fetters and co-workers observed a similar crystal morphology when investigating the influence of semi-crystalline poly(ethylene-*stat*-butene) (PEB) statistical copolymers on the crystallisation of *n*-octacosane.[14] On cooling this model wax (4 wt% in *n*-decane) to 0 °C in the presence of 0.05-0.3 wt% PEB7.5, crystals described as 'long sticks' ($l \approx$ 50-100 μm) were observed by optical microscopy. According to Zhang and co-workers, such rod-like crystals provide fewer opportunities for inter-particle interactions than platelets, resulting in significantly weaker crystal−crystal interactions.[50]

Increasing the mean number of BeMA repeat units per copolymer chain up to 40 or 60 results in much smaller crystals (see **Figure 4.12**). Mixtures of small platelets

($l \approx$ 5-10 μm) and a few needle-like crystals ($l \approx$ 50 μm) are visible in **Figure 4.12j** and small platelets co-existing with smaller needle-like crystals can be observed in **Figure 4.12k**. Fetters and co-workers also reported the formation of smaller *n*-octacosane wax crystals ('short bars') in the presence of a higher PEB concentration (0.8 wt%), as opposed to the 'long sticks' that are generated at lower copolymer concentrations.[14] The effect of varying the total copolymer concentration of the copolymers studied herein is investigated in **Section 4.4.4**.

In summary, the presence of various BeMA-based diblock or statistical copolymers at a fixed copolymer concentration of 0.26 mM affects the morphology of the wax crystals formed when cooling a 5.0% w/w solution of *n*-octacosane in *n*-dodecane. In some cases, a significant reduction in the crystal dimensions and/or an increase in the crystal aspect ratio was observed. For the diblock copolymers, increasing the mean DP of the PBeMA had relatively little effect on the wax crystal morphology. Smaller wax crystals (< 50 μm) were observed by SEM for all four diblock copolymers. In striking contrast, large needle-like crystals were obtained when increasing the BeMA content of the statistical copolymers from ten to twenty repeat units per copolymer chain, while relatively small wax crystals were formed at BeMA contents of forty and sixty repeat units per copolymer chain. Yao *et al.* found that the addition of EVA resulted in a reduction in the wax precipitation temperature and concluded that co-crystallisation was the dominant wax-copolymer interaction.[51] The dominant interaction mechanism for the copolymers studied herein is likely to be co-crystallisation of the pendent behenyl groups with the *n*-octacosane wax crystals. This interpretation is supported by the reduction in T_{cool} indicated by turbidimetry studies and the resulting changes in crystal morphology observed by OM and SEM.

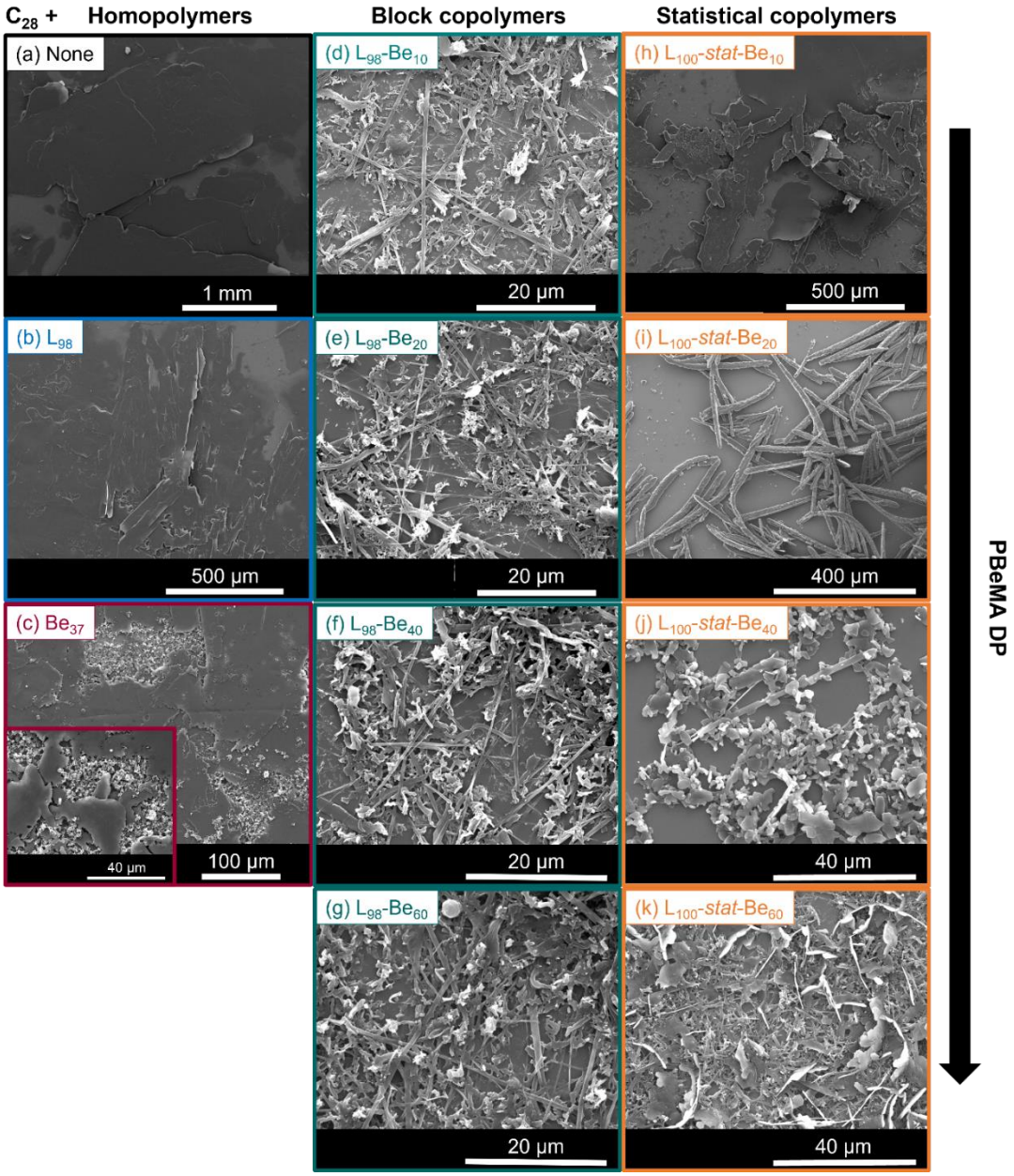

Figure 4.12. SEM images recorded for wax crystals formed by cooling solutions of 5.0% w/w *n*-octacosane in *n*-dodecane in the presence of various (co)polymers at a constant (co)polymer concentration of 0.26 mM.

4.4.4. The effect of varying copolymer concentration

The effect of varying the copolymer concentration on the T_{cool} values identified by turbidimetry studies and the wax crystal morphology was investigated for selected copolymers. $PLMA_{98}$-$PBeMA_{40}$ and $P(LMA_{100}$-*stat*-$BeMA_{40})$ were chosen to compare the diblock and statistical copolymer architecture because this pair produced

the lowest T_{cool} values by turbidimetry and also some of the smallest crystals when used at 0.26 mM. The copolymer concentration was systematically varied from 0.06 to 1.03 mM (or from one-quarter to four-fold the initial concentration of 0.26 mM) and turbidimetry studies were used to identify T_{cool} for wax-copolymer mixtures at each concentration. For 5.0% w/w *n*-octacosane in *n*-dodecane, T_{cool} is reduced from 17.5 °C to 14.0 °C when increasing the $PLMA_{98}$-$PBeMA_{40}$ concentration from 0.06 to 0.26 mM (see **Figure 4.13a**). However, higher concentrations produce an increase in T_{cool} up to 16.0 °C. A similar concentration dependence is observed for $P(LMA_{100}$-*stat*-$BeMA_{40})$: a minimum T_{cool} value of 12.9 °C is observed at a copolymer concentration of 0.51 mM (see **Figure 4.13b**). Such behaviour suggests two competing effects, but it is not clear why the initial interaction between the copolymer chains and the wax crystals should be reduced at higher copolymer concentration.

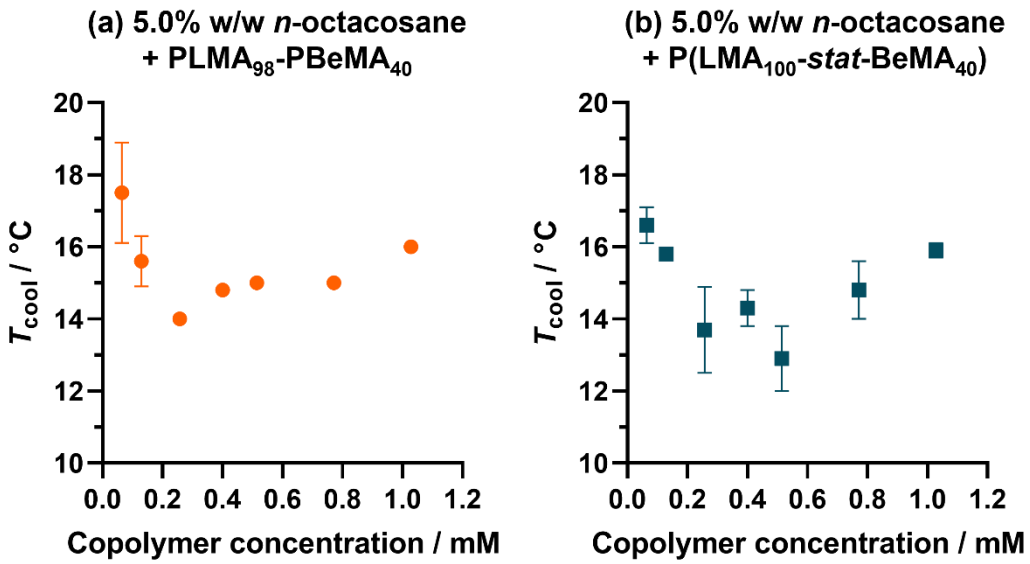

Figure 4.13. T_{cool} vs. copolymer concentration plots for 5.0% w/w *n*-octacosane in *n*-dodecane for **(a)** $PLMA_{98}$-$PBeMA_{40}$ diblock copolymer and **(b)** $P(LMA_{100}$-*stat*-$BeMA_{40})$ statistical copolymer.

The *n*-octacosane crystals obtained in the presence of the $PLMA_{98}$-$PBeMA_{40}$ diblock copolymer were imaged at 20 °C by optical microscopy (see **Figure 4.14**). Larger wax crystals are formed at lower copolymer concentrations (≤ 0.26mM), with a mixture of irregular-shaped and needle-like crystals being observed in **Figure 4.14(a)**-(**c)**. The smaller crystals observed above 0.51mM, seen in **Figure 4.14(a), (b), (c) and (e)**, were also examined by SEM to obtain higher resolution images, see **Figure 4.14(h)-(k)**. **Figure 4.14h** shows platelets prepared at a copolymer concentration of 0.06 mM, while mixtures of irregular-shaped and needle-like crystals obtained at copolymer concentrations of 0.13 mM, 0.26 mM and 0.51 mM are shown in **Figure 4.14(i)-(k)**.

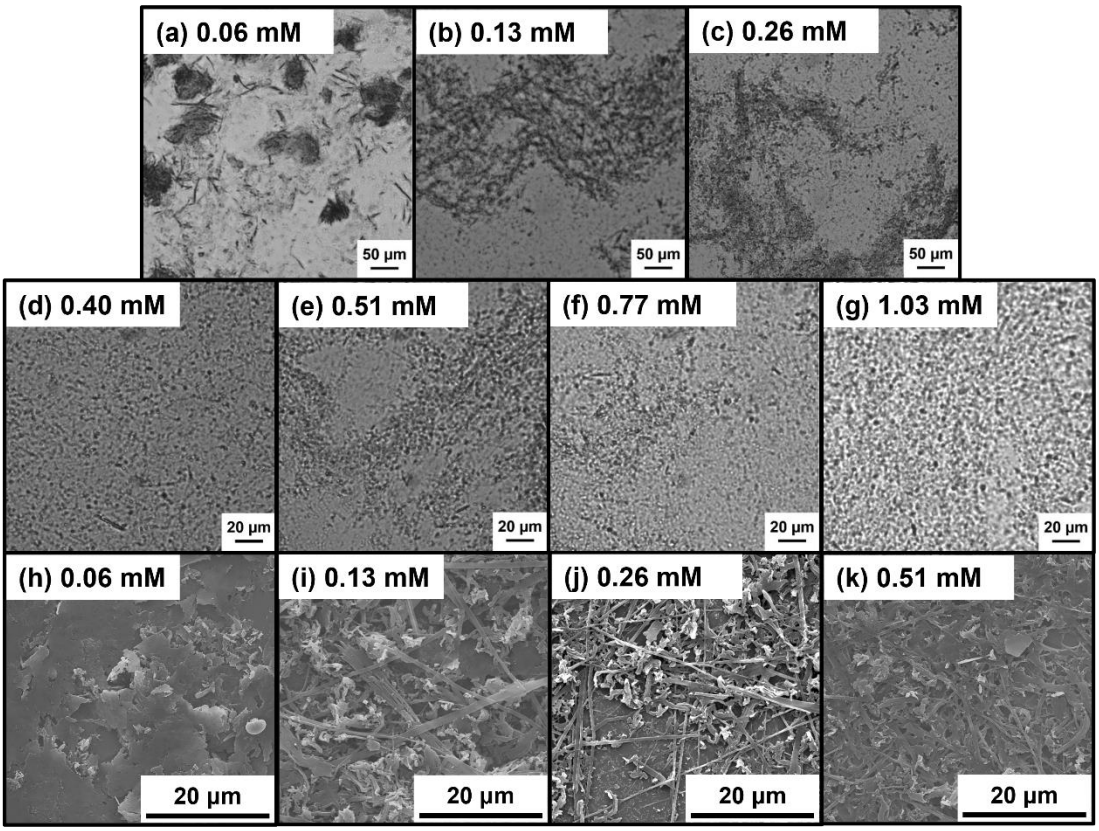

Figure 4.14. Representative images of wax crystals formed on cooling 5.0% w/w *n*-octacosane in *n*-dodecane in the presence of $PLMA_{98}$-$PBeMA_{40}$ at various copolymer concentrations obtained by **(a)-(g)** optical microscopy and **(h)-(k)** SEM.

A series of *n*-octacosane crystals formed in the presence of P(LMA_{100}-*stat*-$BeMA_{40}$) were imaged in solution at 20 °C by optical microscopy and after drying by SEM (see **Figure 4.15**). Large needle-like structures [l = 77 ± 28 μm (averaged over 50 crystals); width, w = 3.3 ± 0.8 μm (averaged over 50 crystals); mean aspect ratio, l/w = 23] are obtained at a copolymer concentration of 0.06 mM (see **Figure 4.15a** and **Figure 4.15h**). These wax crystals are smaller but have a comparable mean aspect ratio to the needles formed in the presence of P(LMA_{100}-*stat*-$BeMA_{20}$) at 0.26 mM (see **Figure 4.12i**). Large, relatively thick needles (l ≈ 100-300 μm; w ≈ 10-20 μm), plus a population of much smaller crystals, are obtained at 0.13 mM (see **Figure 4.15b** and **Figure 4.15i**). For copolymer concentrations at or above 0.26 mM, irregular-shaped wax crystals of less than 50 μm are observed by optical microscopy [see **Figure 4.15(c)-(g)]** and SEM [see **Figure 4.15(j)-(k)**].

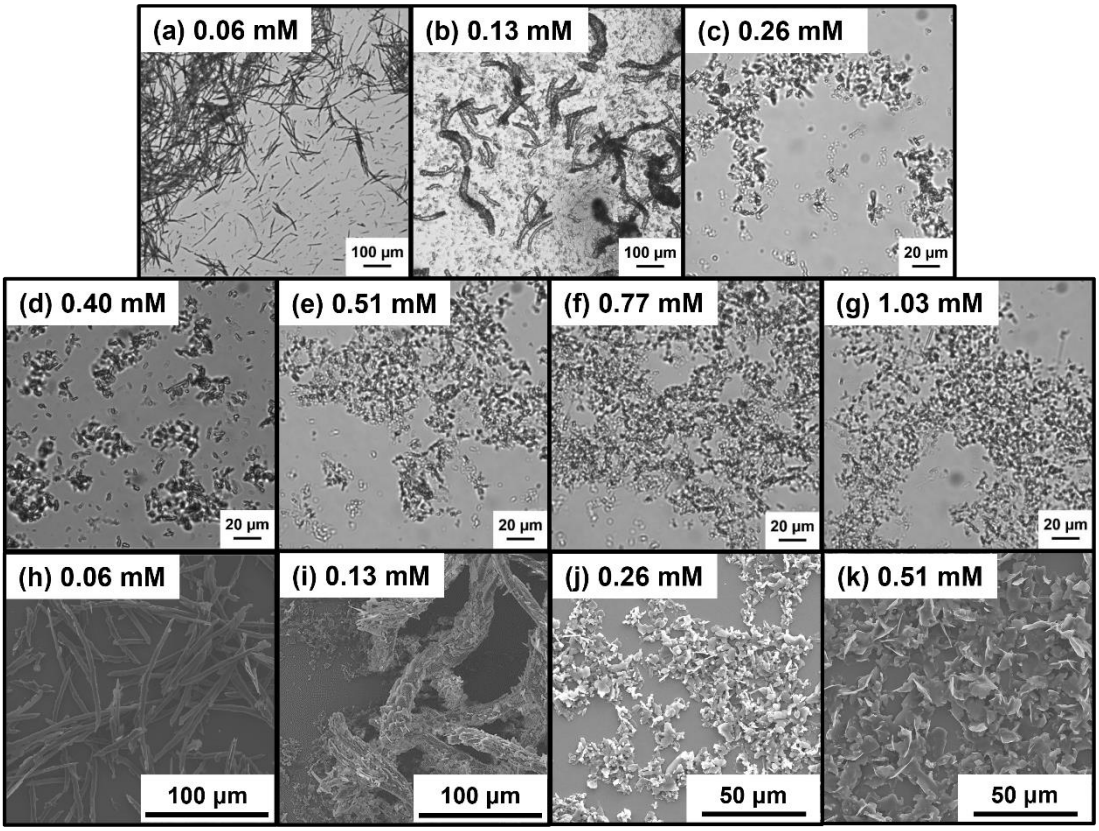

Figure 4.15. Representative images of wax crystals formed on cooling 5.0% w/w *n*-octacosane in *n*-dodecane in the presence of P(LMA_{100}-*stat*-$BeMA_{40}$) at various copolymer concentrations obtained by **(a)-(g)** optical microscopy and **(h)-(k)** SEM.

A morphology map, similar to pseudo-phase diagrams constructed for diblock copolymer nano-objects,[52] is used to illustrate the effect of varying copolymer composition and concentration on the wax crystal morphology when using P(LMA_{100}-*stat*-$BeMA_x$), see **Figure 4.16**. For the copolymer with the lowest BeMA content, relatively large crystals are formed at all copolymer concentrations. For P(LMA_{100}-*stat*-$BeMA_{20}$), the large platelets produced at a copolymer concentration of 0.06 mM are replaced by needle-like crystals at higher copolymer concentrations. For the copolymer with the highest BeMA content, relatively fine needles are produced at 0.06 mM, with much smaller, irregular crystals being formed at higher concentrations. These observations suggest that statistical copolymers with higher BeMA contents (*i.e.*, x = 50 or 60) may promote the formation of relatively small crystals at copolymer

concentrations at or below 0.06 mM. This hypothesis warrants further experiments but unfortunately this is beyond the scope of the current study owing to time constraints.

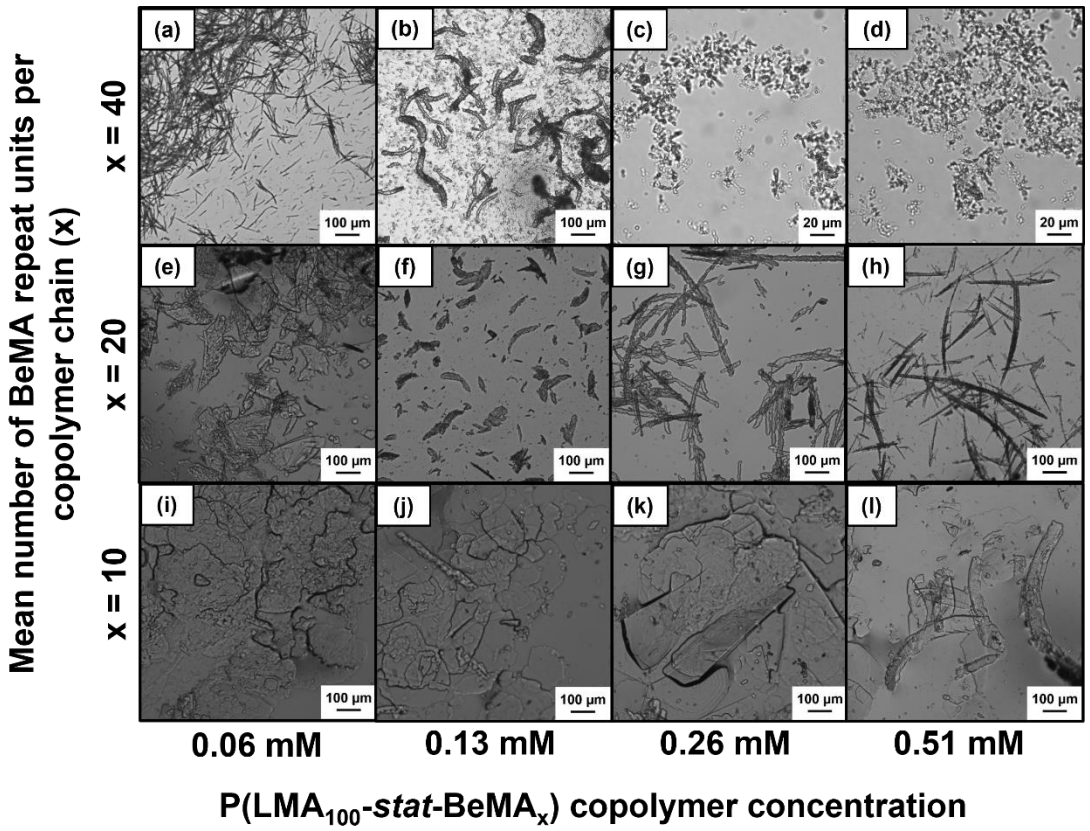

Figure 4.16. Optical microscopy images obtained for wax crystals formed by a 5.0% w/w dispersion of *n*-octacosane in *n*-dodecane in the presence of various concentrations of P(LMA$_{100}$-*stat*-BeMA$_x$), where x = 10, 20 or 40

4.5. Conclusions

Two series of PLMA-PBeMA diblock and P(LMA-*stat*-PBeMA) statistical copolymers have been prepared by RAFT solution polymerisation at 80% w/w solids in *n*-dodecane. High monomer conversions (≥ 98%) and narrow MWDs ($Đ \leq 1.25$) were obtained for all copolymers, which were purified by precipitation into excess ethanol at 35 °C. DSC studies confirmed that the P(LMA-*stat*-PBeMA) statistical copolymers exhibited significantly lower crystallisation and melting temperatures than PLMA-PBeMA diblock copolymers of almost identical overall composition.

All eight copolymers were evaluated as potential wax crystal modifiers for a 5.0% w/w dispersion of a model C_{28} wax in *n*-dodecane, with PLMA and PBeMA homopolymers also being examined as reference materials. Temperature-dependent turbidimetry studies were conducted to determine T_{cool}, the temperature at which zero transmittance is first recorded owing to wax crystallisation. Typically, T_{cool} was a few degrees below the wax appearance temperature (WAT) observed. At a constant molar copolymer concentration of 0.26 mM, there is little difference between the T_{cool} values obtained by turbidimetry studies for the various wax-copolymer mixtures. Each of the eight copolymers produced a modest reduction in T_{cool} of approximately 3-5 °C. Similar reductions in WAT have been reported in the literature for effective wax crystal modifiers.[33–35]

SEM studies confirm that the presence of such copolymers leads to significant changes in the morphology of the wax crystals. Using either diblock or statistical copolymers at 0.26 mM produced a reduction in the overall size and/or an increase in the crystal aspect ratio. In principle, smaller crystals should improve the flow properties of crude oil because the wax crystals have a lower propensity to interact with each other and therefore form weaker gels.[7,25,28]

For the PLMA-PBeMA diblock copolymer series, increasing the mean DP of the PBeMA block from 10 to 60 has no significant effect on the wax crystal morphology. Relatively small crystals of less than 50 μm are observed by SEM for all four diblock copolymers. In contrast, strikingly different needle-like crystals are obtained simply by increasing the BeMA content of the statistical copolymers.

The optimum copolymer concentration for the lowest wax crystallisation temperature (T_{cool}) is 0.26 mM for the $PLMA_{98}$-$PBeMA_{40}$ diblock copolymer and 0.51 mM for the

P(LMA_{100}-*stat*-$BeMA_{40}$) statistical copolymer. The wax crystals formed under these conditions appear small (< 50 μm) by optical microscopy and SEM studies. Larger wax crystals are formed at lower copolymer concentrations for both the diblock and statistical copolymers, as indicated by optical microscopy and SEM studies. For the P(LMA_{100}-*stat*-$BeMA_x$) series, increasing either the copolymer concentration or the mean number of BeMA repeat units per copolymer chain (x) causes the elongation of the initial platelets to form needle-like structures, with the subsequent formation of relatively small, irregular crystals. These observations suggest that statistical copolymers with higher BeMA contents (*i.e.*, x = 50 or 60) may promote the formation of relatively small crystals at copolymer concentrations at or below 0.06 mM. This hypothesis warrants further experiments.

We hypothesise that the dominant interaction mechanism for the copolymers studied herein is co-crystallisation of the wax with the pendent behenyl chains in the BeMA repeat units, thus altering the size and shape of the growing wax crystals. This is supported by the reduction in T_{cool} for a 5.0% w/w wax dispersion in *n*-dodecane in the presence of such copolymers, as indicated by turbidimetry studies.

In summary, the PLMA-PBeMA diblock and statistical copolymers studied herein appear to offer some potential as new wax crystal modifiers. The diblock and statistical copolymers studied are essentially equivalent in their performance. However, the statistical copolymers may offer an advantage as they are easier to synthesise than the diblock copolymers and do not suffer from any homopolymer contamination. Investigating the effect of such copolymers on T_{cool} provides valuable information and the literature suggests that smaller wax crystals produce weaker gels. However, the

effect on the pour point temperature and the gel strength should also be examined to assess the performance of these copolymers as putative PPDs.

4.6. References

1 C. Chang, Q. D. Nguyen and H. P. Rønningsen, *J. Nonnewton. Fluid Mech.*, 1999, **87**, 127–154.

2 P. Singh, R. Venkatesan, H. S. Fogler and N. Nagarajan, *AIChE J.*, 2000, **46**, 1059–1074.

3 H. P. Roenningsen, B. Bjoerndal, A. Baltzer Hansen and W. Batsberg Pedersen, *Energy & Fuels*, 1991, **5**, 895–908.

4 A. M. Al-Sabagh, M. R. Noor El-Din, R. E. Morsi and M. Z. Elsabee, *J. Pet. Sci. Eng.*, 2009, **65**, 139–146.

5 Y. Wu, G. Ni, F. Yang, C. Li and G. Dong, *Energy & Fuels*, 2012, **26**, 995–1001.

6 Y. Chi, J. Yang, C. Sarica and N. Daraboina, *Energy and Fuels*, 2019, **33**, 2797–2809.

7 M. Senra, T. Scholand, C. Maxey and H. S. Fogler, *Energy and Fuels*, 2009, **23**, 5947–5957.

8 H. S. Ashbaugh, A. Radulescu, R. K. Prud'homme, D. Schwahn, D. Richter and L. J. Fetters, *Macromolecules*, 2002, **35**, 7044–7053.

9 G. A. Holder and J. Winkler, *J. Inst. Petrol.*, 1965, **51**, 235–242.

10 P. Singh, H. S. Fogler and N. Nagarajan, *J. Rheol.*, 1999, **43**, 1437–1459.

11 R. Venkatesan, P. Singh and H. S. Fogler, *SPE J.*, 2002, **7**, 349–352.

12 F. Yang, Y. Zhao, J. Sjöblom, C. Li and K. G. Paso, *J. Dispers. Sci. Technol.*, 2015, **36**, 213–225.

13 D. Schwahn, D. Richter, M. Lin and L. J. Fetters, *Macromolecules*, 2002, **35**, 3762–3768.

14 X. Guo, B. A. Pethica, J. S. Huang, R. K. Prud'homme, D. H. Adamson and L. J. Fetters, *Energy and Fuels*, 2004, **18**, 930–937.

15 A. Radulescu, D. Schwahn, J. Stellbrink, E. Kentzinger, M. Heiderich, D. Richter and L. J. Fetters, *Macromolecules*, 2006, **39**, 6142–6151.

16 W. Leube, M. Monkenbusch, D. Schneiders, D. Richter, D. Adamson, L. Fetters, P. Dounis and R. Lovegrove, *Energy and Fuels*, 2000, **14**, 419–430.

17 H. S. Ashbaugh, L. J. Fetters, D. H. Adamson and R. K. Prud'homme, *J. Rheol.*, 2002, **46**, 763–776.

18 A. L. . Machado, E. F. Lucas and G. González, *J. Pet. Sci. Eng.*, 2001, **32**, 159–165.

19 H. S. Ashbaugh, X. Guo, D. Schwahn, R. K. Prud'homme, D. Richter and L. J. Fetters, *Energy and Fuels*, 2005, **19**, 138–144.

20 E. Marie, Y. Chevalier, F. Eydoux, L. Germanaud and P. Flores, *J. Colloid Interface Sci.*, 2005, **290**, 406–418.

21 J. B. Taraneh, G. Rahmatollah, A. Hassan and D. Alireza, *Fuel Process. Technol.*, 2008, **89**, 973–977.

22 R. A. Soldi, A. R. S. Oliveira, R. V. Barbosa and M. A. F. César-Oliveira, *Eur. Polym. J.*, 2007, **43**, 3671–3678.

23 Y. Song, S. Han and T. Ren, *Pet. Sci. Technol.*, 2010, **28**, 860–867.

24 G. Moriceau, D. Lester, G. S. Pappas, P. O'Hora, J. Winn, T. Smith and S. Perrier, *Energy and Fuels*, 2019, **33**, 7257–7264.

25 J. Ruwoldt, S. Simon, J. Norrman, H. J. Oschmann and J. Sjöblom, *Energy and Fuels*, 2017, **31**, 6838–6847.

26 K. Cao, Q. J. Zhu, X. X. Wei and Z. Yao, *Energy and Fuels*, 2015, **29**, 993–1000.

27 K. G. Paso, K. K. Krückert, H. J. Oschmann, H. Ali and J. Sjöblom, *J. Pet. Sci. Eng.*, 2014, **115**, 38–49.

28 H. R. Jafari Ansaroudi, M. Vafaie-Sefti, S. Masoudi, T. J. Behbahani and H. Jafari, *Pet. Sci. Technol.*, 2013, **31**, 643–651.

29 X. Guo, B. A. Pethica, J. S. Huang, D. H. Adamson and R. K. Prud'homme, *Energy and Fuels*, 2006, **20**, 250–256.

30 K. S. Pedersen and H. P. Rønningsen, *Energy and Fuels*, 2003, **17**, 321–328.

31 L. Fang, X. Zhang, J. Ma and B. Zhang, *Ind. Eng. Chem. Res.*, 2012, **51**, 11605–11612.

32 B. Coto, C. Martos, J. J. Espada, M. D. Robustillo and J. L. Peña, *Energy Sci. Eng.*, 2014, **2**, 196–203.

33 T. Wang, J. Xu, M. Wang, X. Wei, M. Shen, J. Huang, R. Zhang, L. Li and X. Guo, *J. Appl. Polym. Sci.*, 2015, **132**, 41660.

34 J. Xu, H. Jiang, T. Li, X. Wei, T. Wang, J. Huang, W. Wang, A. L. Smith, J. Wang, R. Zhang, Y. Xu, L. Li, R. K. Prud'Homme and X. Guo, *Ind. Eng. Chem.*

Res., 2015, **54**, 5204–5212.

35 K.-S. Wang, C.-H. Wu, J. L. Creek, P. J. Shuler and Y. Tang, *Pet. Sci. Technol.*, 2003, **21**, 359–368.

36 P. Claudy, J. M. Létoffé, B. Bonardi, D. Vassilakis and B. Damin, *Fuel*, 1993, **72**, 821–827.

37 B. P. Binks, P. D. I. Fletcher, N. A. Roberts, J. Dunkerley, H. Greenfield, A. Mastrangelo and K. Trickett, *Phys. Chem. Chem. Phys.*, 2015, **17**, 4107–4117.

38 M. J. Rymaruk, K. L. Thompson, M. J. Derry, N. J. Warren, L. P. D. Ratcliffe, C. N. Williams, S. L. Brown and S. P. Armes, *Nanoscale*, 2016, **8**, 14497–14506.

39 P. Cacioli, D. G. Hawthorne, R. L. Laslett, E. Rizzardo and D. H. Solomon, *J. Macromol. Sci. Part A - Chem.*, 1986, **23**, 839–852.

40 M. Rodlert, E. Harth, I. Rees and C. J. Hawker, *J. Polym. Sci. Part A Polym. Chem.*, 2000, **38**, 4749–4763.

41 M. J. Derry, O. O. Mykhaylyk, A. J. Ryan and S. P. Armes, *Chem. Sci.*, 2018, **9**, 4071–4082.

42 F. Fleischhaker, A. P. Haehnel, A. M. Misske, M. Blanchot, S. Haremza and C. Barner-Kowollik, *Macromol. Chem. Phys.*, 2014, **215**, 1192–1200.

43 M. Semsarilar, N. J. W. Penfold, E. R. Jones and S. P. Armes, *Polym. Chem.*, 2015, **6**, 1751–1757.

44 U. N. Arua and F. D. Blum, *J. Polym. Sci. Part B Polym. Phys.*, 2018, **56**, 89–96.

45 S. S. Rogers and L. Mandelkern, *J. Phys. Chem.*, 1957, **61**, 985–990.

46 H. A. Schneider, *Polymer*, 2005, **46**, 2230–2237.

47 M. Kurniawan, J. Ruwoldt, J. Norrman and K. G. Paso, *Energy and Fuels*, 2021, **35**, 7666–7680.

48 J. Jennings, M. F. Butler, M. McLeod, E. Csányi, A. J. Ryan and O. O. Mykhaylyk, *Cryst. Growth Des.*, 2018, **18**, 7094–7105.

49 Y. H. Jang, M. Blanco, J. Creek, Y. Tang and W. A. Goddard, *J. Phys. Chem. B*, 2007, **111**, 13173–13179.

50 C. Bai and J. Zhang, *Ind. Eng. Chem. Res.*, 2013, **52**, 2732–2739.

51 B. Yao, C. Li, F. Yang, X. Zhang, Z. Mu, G. Sun and Y. Zhao, *Energy and Fuels*, 2018, **32**, 1567–1578.

52 S. L. Canning, G. N. Smith and S. P. Armes, *Macromolecules*, 2016, **49**, 1985–2001.

Chapter 5. Conclusions and Future Work

5.1. Conclusions and Future Work

RAFT enables the convenient polymerisation of vinyl monomers and remains an attractive synthesis technique for industrial scale-up, with several examples of RAFT polymerisation being employed on an industrial scale. For example, Lubrizol produce a range of star polymers that act as viscosity modifiers for engine oils.[1,2] The synthesis, characterisation and potential applications of diblock and statistical copolymers prepared by RAFT polymerisation in non-polar media have been explored in this Thesis. More specifically, oil-soluble polymethacrylate precursors (PSMA and PLMA) have been synthesised and subsequently chain-extended with methacrylic monomers (BzMA, BuMA and BeMA) in either *n*-dodecane or mineral oil. In the literature, well-established block copolymer self-assembly techniques such as PISA and PI-CDSA have enabled the convenient preparation of many examples of well-defined diblock copolymer nano-objects using a wide range of monomers. Such diblock copolymer nanoparticles offer a wide range of potential applications, including biocompatible hydrogels for either 3D cell culture[3] or stem cell storage,[4] nanoparticle lubricants for automotive engine oils,[5] novel dispersants for agrochemical formulations,[6] or as novel Pickering emulsifiers.[7] In this Thesis, well-defined diblock copolymer nano-objects prepared by PISA and diblock and statistical copolymers prepared by RAFT solution polymerisation are considered for oil-thickening or wax crystal modification applications, respectively.

Chapter 2 builds on a previous study by Derry *et al.*, whereby a vesicle-to-worm thermal transition was induced by heating a dispersion of $PSMA_{13}$-$PBzMA_{96}$ vesicles in mineral oil.[8] The significant increase in viscosity (*G'* increased by five orders of magnitude) caused by the change in morphology provided a novel high-temperature oil-thickening mechanism, which offers a potential application for viscosity

modification in automotive engine oils. In **Chapter 2**, this PSMA-PBzMA formulation was revisited to examine what happens on heating well above the critical transition temperature required for the vesicle-to-worm transition. Interestingly, temperature-dependent rheology studies indicated a sharp reduction in the dispersion viscosity at such elevated temperatures. This was attributed to a subsequent worm-to-sphere transition owing to further surface plasticisation of the structure-directing PBzMA block, which was supported by TEM observation of spherical nanoparticles on drying this copolymer dispersion at 180 °C. This dual thermal transition for this PISA formulation in non-polar media is consistent with recent literature examples of a single thermoresponsive diblock copolymer switching reversibly between spheres, worms or vesicles on varying the (aqueous) solution temperature.[9–13] A similar observation of a vesicle-to-cylinder-to-sphere transition on heating has also been reported by Lodge and co-workers.[14] The dilute dispersion (1% w/w) of diblock copolymer vesicles was initially prepared by dissolving polystyrene-polydimethylsiloxane (PS-PDMS) in diethyl phthalate (a selective solvent for polystyrene).

The work presented in **Chapter 2** also set out to investigate whether statistical incorporation of an appropriate comonomer (BuMA) into the membrane-forming block would enable tuning of the critical onset temperature required for a vesicle-to-worm transition. In principle, lowering this critical transition temperature to, say, 60 °C should enable thickening of oil-based cosmetic formulations. Indeed, introducing up to 50 mol% BuMA comonomer within the membrane-forming block systematically lowered the critical transition temperature required to induce a vesicle-to-worm transition, from 167 °C (with no BuMA comonomer) to 109 °C (with 50 mol% BuMA), as determined by oscillatory rheology. Moreover, a five-fold

increase in *G'* was observed above the critical temperature, which is comparable to that previously reported for $PSMA_{13}$-$PBzMA_{96}$ vesicles.[8] Thus, the work presented in **Chapter 2** provides a useful proof of concept for tuning the critical onset temperature required for a vesicle-to-worm transition by statistical incorporation of a suitable comonomer within the membrane-forming block. In practice, there remains further scope to optimise such formulations if they are to become commercially viable. In particular, higher final comonomer conversions are required and alternative comonomers such as 2-ethylhexyl methacrylate should be investigated to examine whether the critical transition temperature can be lowered further.

Furthermore, the thermal transitions reported in **Chapter 2** proved to be irreversible on cooling within normal experimental timescales (hours). A mixture of worms and vesicles was confirmed by TEM studies of the dried 10% w/w $PSMA_{14}$-P(0.5BzMA-*stat*-0.5BuMA)$_{130}$ dispersion after cooling to 20 °C. Interestingly, this differs from observations made by Byard *et al.* for aqueous dispersions of 'shape-shifting' diblock copolymer nano-objects, whereby the sphere-to-worm-to-vesicle transitions observed on *heating* proved to be fully reversible on cooling.[10] It seems likely that the sphere-to-worm and worm-to-vesicle transitions that should occur on *cooling* for the $PSMA_{14}$-P(0.5BzMA-*stat*-0.5BuMA)$_{130}$ nano-objects are disfavoured simply because this pathway involves highly cooperative transitions (*e.g.* worms are formed via the stochastic 1D fusion of multiple spheres). Thus, much longer time scales (days or weeks) may be required to access the equilibrium vesicle morphology at 20 °C. Further experiments would be required to test this hypothesis but unfortunately this is beyond the scope of this Thesis.

Lodge and co-workers reported polystyrene-polydimethylsiloxane vesicles in diethyl phthalate were converted on heating into cylinders at 110 °C and spheres at 170 °C.

In this case, each thermal transition proved to be reversible on cooling on the time scale of the experiment (minutes). Such reversibility was attributed to the unusually low T_g of the insoluble PDMS block.[14]

Chapter 3 investigates whether PLMA-PBeMA diblock copolymer cylinders could be prepared *via* PI-CDSA. In contrast to a prior study by Derry and co-workers,[15] PBeMA was used as the semi-crystalline core-forming block, rather than the steric stabiliser block. Bearing in mind the relevant CDSA literature,[16–20] cylindrical rods were targeted by preparing highly asymmetric diblock copolymers comprising a relatively long corona-forming block and a relatively short core-forming block. It was hypothesised that melting of the crystalline core-forming block cores within the 20-50 °C range should cause the rods to become much more flexible, with the resulting significant reduction in their mean persistence length leading to a significant change in the rheology of such dispersions.

In **Chapter 3**, it is shown that BeMA monomer prepared in-house by reacting behenyl alcohol with methacrylic acid is of comparable purity to that of the original Lubrizol-supplied batch employed by Derry and co-workers (and far superior to the isomeric mixture supplied by BASF).[15] The former batch of BeMA monomer was used to prepare $PLMA_{102}$-$PBeMA_{20}$ diblock copolymers at 30% w/w solids in mineral oil by thermally-initiated RAFT solution polymerisation of BeMA at 90 °C. Alternatively, photoiniferter RAFT polymerisation of BeMA was conducted using blue light irradiation at either 32 or 15 °C, with the latter temperature lying below the T_c of $PLMA_{102}$-$PBeMA_{20}$, as determined by DSC. Such $PLMA_{102}$-$PBeMA_{20}$ diblock copolymers exhibited reversible thermoresponsive behaviour: relatively transparent free-standing gels were formed at or below 20 °C, whereas free-flowing fluids were obtained at higher temperatures. In principle, such behaviour is consistent with the

formation of PBeMA-core cylinders or rods. However, TEM, DLS and SIPLI studies did not provide any evidence for the presence of such highly anisotropic nanoparticles. Instead, only ill-defined colloidal aggregates were observed. It remains unclear why no self-assembly occurs for such diblock copolymers in mineral oil. In principle, replacing BeMA with behenyl acrylate (BeA) should lower the T_g of the core-forming block and this enhanced chain mobility might lead to CDSA. Alternatively, investigating alternative (polar) non-solvents for the PBeMA block might promote self-assembly.

Although not reported in this Thesis, preliminary experiments were conducted to examine this hypothesis. More specifically, the RAFT dispersion polymerisation of BeMA using a poly(2-(dimethylamino)ethyl methacrylate) (PDMA) precursor was conducted in *iso*-propyl alcohol (IPA) at 70 °C. A series of PDMA-PBeMA nano-objects were obtained at 20-30% w/w solids, with TEM studies confirming the presence of spheres, worms or a mixed phase comprising a vesicle population (see **Figure 5.0.1**). Bearing in mind the prior study by Semsarilar *et al.* on PDMA-PSMA worms,[21] it would be interesting to investigate whether the higher crystallinity of PBeMA relative to PSMA enables the preparation of relatively stiff rods whose rigidity can be tuned by increasing the temperature above the T_m for the PBeMA block. Unfortunately, such additional experiments are beyond the scope of this Thesis.

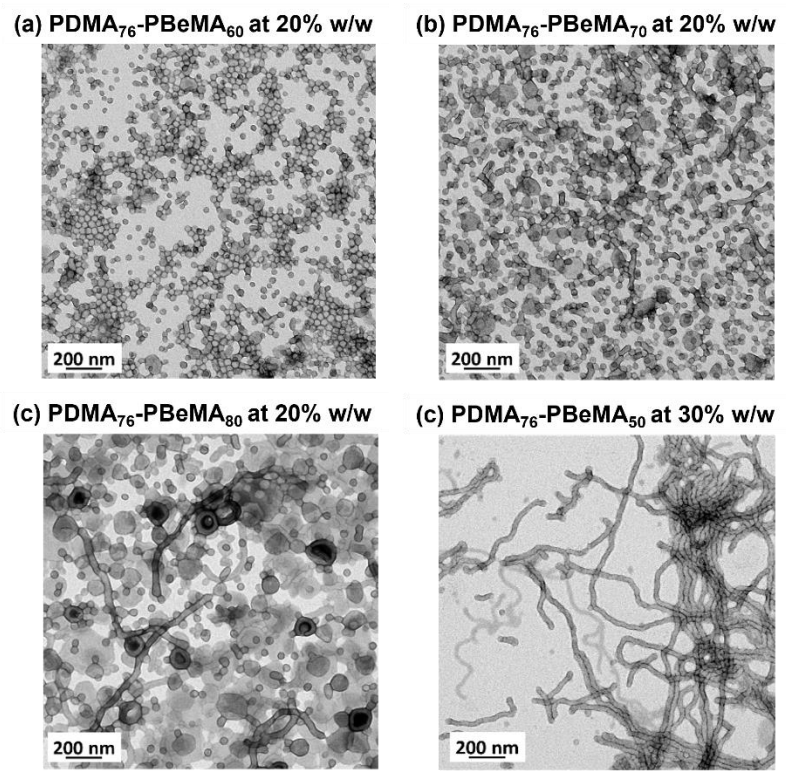

Figure 5.0.1. TEM images recorded for various $PDMA_{76}$-$PBeMA_x$ nano-objects in IPA: **(a)** $PDMA_{76}$-$PBeMA_{60}$ spheres synthesised at 20% w/w solids, **(b)** $PDMA_{76}$-$PBeMA_{70}$ spheres and short worms synthesised at 20% w/w solids, **(c)** $PDMA_{76}$-$PBeMA_{80}$ spheres, worms and vesicles synthesised at 20% w/w solids and **(d)** $PDMA_{76}$-$PBeMA_{50}$ worms synthesised at 30% w/w solids.

Chapter 4 investigates whether similar PLMA-PBeMA diblock copolymers to those reported in **Chapter 3**, as well as the analogous statistical copolymers, can modify the crystallisation of a model wax (*n*-octacosane) in *n*-dodecane. At a constant copolymer concentration of 0.26 mM, each of the eight copolymers produced a modest reduction in T_{cool} of approximately 3-5 °C. Similar reductions have been reported in the literature for effective wax crystal modifiers.[22–24] SEM studies confirmed that the presence of such copolymers led to significant changes in the morphology of the resulting wax crystals. Using either diblock or statistical copolymers at 0.26 mM produced a reduction in the overall size and/or an increase in the crystal aspect ratio. In principle, smaller crystals should improve the flow properties of crude oil by reducing its propensity to form gels at sub-ambient temperature.[25–27] We hypothesise that the

copolymers undergo co-crystallisation with the wax via the pendent behenyl chains in the BeMA repeat units. In principle, X-ray diffraction (XRD) or WAXS studies could be conducted to examine this hypothesis. Based on the analysis conducted in **Chapter 4**, the PLMA-PBeMA diblock and statistical copolymers studied are essentially equivalent in their performance as potential wax crystal modifiers. The statistical copolymers are easier to make than the diblock copolymers and do not suffer from any homopolymer contamination.

In summary, these new PLMA-PBeMA diblock and statistical copolymers appear to offer some potential as wax crystal modifiers. This work could be extended to investigate the effect of such copolymers on the pour point temperature and the gel strength of the model wax, as described in the literature.[28,29] In particular, temperature-dependent rheology studies and yield stress measurements should provide valuable information and enable a more nuanced assessment of the performance of these copolymers as putative PPDs.

The findings from **Chapter 4** provide insight into the behaviour observed in **Chapter 3**. More specifically, results suggest that PLMA homopolymer interacts with *n*-octacosane model wax in *n*-dodecane, as seen by a change in crystal morphology by SEM and a small reduction in T_{cool} in the presence of this homopolymer (T_{cool} = 16.8 °C). This is likely to be caused by co-crystallisation between the PLMA and the model wax. Therefore, PLMA is also likely to interact with PBeMA in the PLMA-PBeMA diblock copolymer studied in **Chapter 3**. Co-crystallisation of both blocks could explain the ill-defined aggregate structures observed by TEM, rather than exclusively the crystallisation of PBeMA driving self-assembly, as desired. Thus, making PLMA an ineffective stabiliser block for PI-CDSA of PLMA-PBeMA.

Using the techniques in **Chapter 4** to investigate the interactions of alternative homopolymers with model wax could be used as a scoping study to find a polymer to act as an effective stabiliser block in a diblock copolymer with the potential to undergo PI-CDSA. As previously stated, further studies to optimise this self-assembly behaviour involve changing parameters, such as the DP of each block, temperature, and solvent media.

5.2. References

1 D. Visger, M. Davies, D. Price, M. Baum and B. J. Schober, Star Polymers and Compositions Thereof, WO2006047398A3, 2005.

2 B. J. Schober, M. C. Davies, M. R. Sutton, M. Baum, D. C. Visger, D. Price, B. R. Dohner and M. F. Wilkes, Star Polymer Lubricating Composition, US9006159B2, 2012.

3 K. A. Simon, N. J. Warren, B. Mosadegh, M. R. Mohammady, G. M. Whitesides and S. P. Armes, *Biomacromolecules*, 2015, **16**, 3952–3958.

4 I. Canton, N. J. Warren, A. Chahal, K. Amps, A. Wood, R. Weightman, E. Wang, H. Moore and S. P. Armes, *ACS Cent. Sci.*, 2016, **2**, 65–74.

5 M. J. Derry, T. Smith, P. S. O'Hora and S. P. Armes, *ACS Appl. Mater. Interfaces*, 2019, **11**, 33364–33369.

6 D. H. H. Chan, E. L. Kynaston, C. Lindsay, P. Taylor and S. P. Armes, *ACS Appl. Mater. Interfaces*, 2021, **13**, 30235–30243.

7 S. J. Hunter and S. P. Armes, *Langmuir*, 2020, **36**, 15463–15484.

8 M. J. Derry, O. O. Mykhaylyk and S. P. Armes, *Angew. Chemie - Int. Ed.*, 2017, **56**, 1746–1750.

9 L. P. D. Ratcliffe, M. J. Derry, A. Ianiro, R. Tuinier and S. P. Armes, *Angew. Chemie Int. Ed.*, 2019, **58**, 18964–18970.

10 S. J. Byard, C. T. O'Brien, M. J. Derry, M. Williams, O. O. Mykhaylyk, A. Blanazs and S. P. Armes, *Chem. Sci.*, 2020, **11**, 396–402.

11 O. J. Deane, J. Jennings and S. P. Armes, *Chem. Sci.*, 2021, **12**, 13719–13729.

12 O. J. Deane, J. Jennings, T. J. Neal, O. M. Musa, A. Fernyhough and S. P. Armes, *Chem. Mater.*, 2021, **33**, 7767–7779.

13 D. L. Beattie, O. J. Deane, O. O. Mykhaylyk and S. P. Armes, *Polym. Chem.*, 2022, **13**, 655–667.

14 S. Abbas, Z. Li, H. Hassan and T. P. Lodge, *Macromolecules*, 2007, **40**, 4048–4052.

15 M. J. Derry, O. O. Mykhaylyk, A. J. Ryan and S. P. Armes, *Chem. Sci.*, 2018, **9**, 4071–4082.

16 J. Massey, K. Nicole Power, I. Manners and M. A. Winnik, *J. Am. Chem. Soc.*, 1998, **120**, 9533–9540.

17 J. A. Massey, K. Temple, L. Cao, Y. Rharbi, J. Raez, M. A. Winnik and I. Manners, *J. Am. Chem. Soc.*, 2000, **122**, 11577–11584.

18 L. Cao, I. Manners and M. A. Winnik, *Macromolecules*, 2002, **35**, 8258–8260.

19 I. Korczagin, M. A. Hempenius, R. G. Fokkink, M. A. Cohen Stuart, M. Al-Hussein, P. H. H. Bomans, P. M. Frederik and G. Julius Vancso, *Macromolecules*, 2006, **39**, 2306–2315.

20 D. A. Rider and I. Manners, *Polym. Rev.*, 2007, **47**, 165–195.

21 M. Semsarilar, N. J. W. Penfold, E. R. Jones and S. P. Armes, *Polym. Chem.*, 2015, **6**, 1751–1757.

22 K.-S. Wang, C.-H. Wu, J. L. Creek, P. J. Shuler and Y. Tang, *Pet. Sci. Technol.*, 2003, **21**, 359–368.

23 T. Wang, J. Xu, M. Wang, X. Wei, M. Shen, J. Huang, R. Zhang, L. Li and X. Guo, *J. Appl. Polym. Sci.*, 2015, **132**, 41660.

24 J. Xu, H. Jiang, T. Li, X. Wei, T. Wang, J. Huang, W. Wang, A. L. Smith, J. Wang, R. Zhang, Y. Xu, L. Li, R. K. Prud'Homme and X. Guo, *Ind. Eng. Chem. Res.*, 2015, **54**, 5204–5212.

25 M. Senra, T. Scholand, C. Maxey and H. S. Fogler, *Energy and Fuels*, 2009, **23**, 5947–5957.

26 H. R. Jafari Ansaroudi, M. Vafaie-Sefti, S. Masoudi, T. J. Behbahani and H. Jafari, *Pet. Sci. Technol.*, 2013, **31**, 643–651.

27 J. Ruwoldt, S. Simon, J. Norrman, H. J. Oschmann and J. Sjöblom, *Energy and Fuels*, 2017, **31**, 6838–6847.

28 B. P. Binks, P. D. I. Fletcher, N. A. Roberts, J. Dunkerley, H. Greenfield, A. Mastrangelo and K. Trickett, *Phys. Chem. Chem. Phys.*, 2015, **17**, 4107–4117.

29 Y. Chi, J. Yang, C. Sarica and N. Daraboina, *Energy and Fuels*, 2019, **33**, 2797–2809.